ANALYSIS OF DYNAMIC BEHAVIOR OF VARIABLE SPEED PUMP STORAGE UNITS UNDER CONVERTER FAULTS

Ph.D. THESIS

by

ANTO. J

DEPARTMENT OF WATER RESOURCES DEVELOPMENT & MANAGEMENT
INDIAN INSTITUTE OF TECHNOLOGY ROORKEE
ROORKEE -247 667 (INDIA)
JULY, 2018

ANALYSIS OF DYNAMIC BEHAVIOR OF VARIABLE SPEED PUMP STORAGE UNITS UNDER CONVERTER FAULTS

A THESIS

Submitted in partial fulfilment of the requirements for the award of the degree

of

DOCTOR OF PHILOSOPHY

in

WATER RESOURCES DEVELOPMENT AND MANAGEMENT

by

ANTO. J

DEPARTMENT OF WATER RESOURCES DEVELOPMENT & MANAGEMENT
INDIAN INSTITUTE OF TECHNOLOGY ROORKEE
ROORKEE -247 667 (INDIA)
JULY, 2018

INDIAN INSTITUTE OF TECHNOLOGY ROORKEE
ROORKEE

CANDIDATE'S DECLARATION

I hereby certify that the work which is being presented in the thesis entitled "**ANALYSIS OF DYNAMIC BEHAVIOR OF VARIABLE SPEED PUMP STORAGE UNITS UNDER CONVERTER FAULTS**" in partial fulfillment of the requirements for the award of the Degree of Doctor of Philosophy and submitted in the Department of Water Resources Development and Management of the Indian Institute of Technology Roorkee, Roorkee is an authentic record of my own work carried out during a period from December, 2014 to July, 2018 under the supervision of Dr. Thanga Raj Chelliah, Asst. Professor, Department of Water Resources Development and Management, Indian Institute of Technology Roorkee, Roorkee.

The matter presented in the thesis has not been submitted by me for the award of any other degree of this or any other Institution.

(Anto. J)

This is to certify that the above statement made by the candidate is correct to the best of my knowledge.

(Thanga Raj Chelliah)
Supervisor

The Ph.D. Viva-Voce Examination of ……., Research Scholar, has been held on ……..

Chairman, SRC **Signature of External Examiner**

This is to certify that the student has made all the corrections in the thesis.

Signature of Supervisor **Head of the Department**

Date: 06.07.2018

ABSTRACT

Several possible technologies for electricity storage are developed including high energy batteries, flywheels, superconducting magnetics, compressed air, and Pumped Storage Power Plants (PSPP). Among the mentioned technologies, PSPP is considered as reliable and bulk energy storage system. The PSPP's that are constructed in the beginning of the 20th century in the European continent were of fixed speed type employing synchronous machine and the same were continually established in Asian and American continents also. The total installed capacity of fixed speed PSPP in India is 4804 MW out of worldwide capacity of 140 GW. However, the fixed speed PSPP suffers from major drawbacks including: (i) inability to generate power over full range of water head, (ii) reduced efficiency during partial generation/pumping modes of operation. The aforementioned drawbacks can be overcome by the transformation of PSPP from fixed speed mode to variable speed mode. In order to enable variable speed operation, synchronous machines of fixed speed PSPP need to be driven by power electronic converters with a rating equivalent to the rating of machine. Such design of high capacity power electronic converter is not economical. Furthermore, these full size converters (> 200 MW) are very challenging in size, cost and site clearance in case of underground power houses. Therefore, variable speed PSPP employing Doubly Fed Induction Machine (DFIM) is an acceptable option for the sites with wide variation in water head since they provide variable speed operation with reduced power converter rating and high dynamic stability. In India, the first variable speed PSPP (with 3-level VSI) having 4 nos. of 250 MW DFIM totaling to a capacity of 1000 MW is under construction at the Tehri dam of Uttarakhand state.

In DFIM, rotor side power converters act as excitation system and control the real and reactive powers of the machine based on set points (reference) and feedback signals from various sensors. A comprehensive literature survey is carried out in the area of power converter topology, modulation techniques, parallel converter schemes, circulating current reduction techniques, machine control, grid disturbances, protection of power converter, fault analysis, fault tolerant control and power converter redundancy techniques. In addition, operational challenges for the power converter redundancy and the protection circuit is studied through simulation and experimental tests.

Smooth starting/regenerative braking of the DFIM unit is discussed with real and reactive power consumption/delivery. Time required during smooth starting and regenerative

braking of large rated DFIM unit plays an important role in transition from generating to pumping mode and vice versa. Furthermore, it is beneficial for the better management of grid operation and energy balancing. An Energy efficient method for starting of DFIM fed pump turbine is discussed. Variable voltage/frequency applied in rotor side and fixed dc supply provided in stator circuit during starting, saves considerable amount of energy compared to conventional smooth starting. It is observed that 35% of electrical energy shall be conserved in comparison with conventional method during starting.

Dynamic behavior of power and control circuit (excitation system) faults of a 250 MW DFIM hydrogenerating unit, to be commissioned in 1000 MW Tehri PSPP, operating at generation, pumping and condenser modes are discussed. In addition, survivability status of power and control circuit faults of DFIM at said modes are assessed based on performance measures. Further, Economic analysis of 1000 MW PSPP under power and control failures are also investigated. The present work also investigates fault tolerant operation of 250 MW DFIM unit at open switch fault in converters to increase the continuity of the unit operation, where power electronic converter redundancy is not available in large rated DFIM unit. Open switch fault is detected through Park's vector phase currents technique and variation in dc link voltage. An experimental set-up with 2.2 kW DFIM is developed in the laboratory to support the simulation results. Overall, the present research work shall be helpful to the project authorities/policy makers in hydropower engineering during the design stage of their future projects.

ACKNOWLEDGMENTS

I wish to acknowledge my deep sense of gratitude and indebtedness to Dr. Thanga Raj Chelliah, Asst. Professor, Department of Water Resources Development and Management, Indian Institute of Technology Roorkee, for his invaluable guidance, sincere advice and encouragement throughout the completion of this research work. I feel highly privileged to have worked under him during the course of this work.

My heartily gratitude to Prof. Deepak Khare, DRC Chairman and Internal Expert of my SRC, Department of Water Resources Development and Management, IIT Roorkee, whose humanistic and warm personal approach always helped me from beginning to end of my work.

I intend to record my gratitude to Dr. Dheeraj. K. Khatod, External Expert of my SRC, Associate Professor, Department of Electrical Engineering, IIT Roorkee for providing constructive comments during my presentations.

I am extremely thankful to Prof. S.K. Mishra, Head of Department, Water Resources Development and Management Department, IIT Roorkee and Prof. N.P. Padhy, Dean Academics, IIT Roorkee for their moral support and humanitarian support during this period.

I am very indebted to Mr. Pradeep Loyola, Asst. Prof, St. Joseph University in Tanzania, Dr. Raja Singh R., Asst. Prof, VIT University, Dr. Arun Dominic, Asst. Prof, NIT Jalandhar, Mr. R.R. Semwal, DGM (O&M), THDC India Ltd., and Mr. S.V. Appa Sarma, Consultant, THDC India Ltd., for their encouragement and support during this period.

I acknowledge all the teaching and non-teaching faculties of Water Resources Development and Management Department for their support and making my stay pleasant during this period.

I express my sincere thanks to THDC India Ltd, Uttarakhand, India for providing financial support.

I would like to thank my fellow colleagues Mr. Birudula Anil Kumar, Mr. Carunai Selvane, Mr. Raghu Selvaraj, Mr. Chandra Seker and Mrs. Rupesh Kumari for their positive attitude and cooperation that always encouraged me to accomplish my research work. Special thanks to Mr. Karthik Desingu, for his contribution in laboratory experimentation and proof reading of my entire thesis.

I would heart fully thank Mr. Deepak Murugan, Mr. Kalai Vanan, Mr. Deepan, Mr. Krishna Prasath, Mr. Vignesh G, Mr. Gowtham Raj Sampath, and Mr. Simbu Arasan for being a good friend in all kind of situations along with me during my stay in IIT Roorkee.

I gratefully acknowledge the moral support and encouragement of my grandmother Mrs. Maria Savariai, my mother Mrs. D. Mary Rajammal, my dear brother J. Raja Simmon & family. I salute you all for the selfless love, care, pain and sacrifice you did to shape my life. Although you hardly understood what I researched on, you were willing to support any decision I made. I would never be able to pay back the love and affection showered upon by my mother and brother.

Thanks to my mentor Fr. Augustine P, my father-in-law Mr. M. Yesudhason, my mother-in-law Mrs. Mary Judit, Mr. Antony Arul Dhas & family, Mr. Bruno Premson & family, Mr. Saldin Pratheesh & family, whose blessings have helped me throughout the research work.

I appreciate and feel proud to always have helping hands and patience from my wife Y. Angel Salvini. I greatly value her contribution and deeply appreciate her belief in me. I appreciate our cute angels, R. Noa Senorina and A. Vian de Mario, for abiding my ignorance and the patience they showed during my thesis writing. Words would never say how grateful I am to both of you.

I am proud to humbly dedicate this research work to my family.

May all praises be to Almighty, the most beneficent, the most merciful.

(ANTO. J)

CONTENTS

This page is intentionally left blank

LIST OF FIGURES

This page is intentionally left blank

LIST OF TABLES

This page is intentionally left blank

LIST OF ACRONYMS

ACS	Active Current Sharing
ANSI	American National Standards Institute
CCC	Circular Chain Control
CHB	Cascaded H-Bridge
CLC	Central Limit Control
DCSC	DC Link Short Circuit
DFIG	Doubly-Fed Induction Generator
DFIM	Doubly Fed Induction Machine
DLC	Distributed Logical Control
FC-MLC	Flying Capacitor Multilevel Converters
GCT	Gate Commutated Thyristor
GSC	Grid Side Converter
GTO	Gate Turn Off Thyristor
HVDC	High-Voltage Direct Current
IEC	International Electro-technical Commission
IEEE	Institute of Electrical and Electronics Engineers
IEGT	Injection Enhanced Gate Transistor
IGBT	Insulated Gate Bipolar Transistor
LCI	Load Commutated Inverters
MCM	Million Cubic Meter
MIV	Main Inlet Valve
NPC	Neutral Point Diode Clamped VSC
OCF	Open Circuit Fault
PGSC	Phase to Ground SC
PPSC	Phase to Phase SC
PSPP	Pumped Storage Power Plant
PWM	Pulse Width Modulation
QEP	Quadrature Encoder Pulse
RMS	Root Mean Square
RSC	Rotor Side Converter

SC	Short Circuit
SDOC	Single Device Open Circuit Fault
SDSC	Single Device Short Circuit
SFC	Static Frequency Converter
SHE	Selective Harmonic Elimination
SLOC	Single Leg Open Circuit Fault
SPWM	Sinusoidal PWM
SSC	Stator Short Circuit
STATCOM	Static Synchronous Compensator
SVM	Space Vector Modulation
THD	Total Harmonic Distortion
VSI	Voltage Source Inverter

LIST OF SYMBOLS

A, B, C	Stator phases
a, b, c	Rotor phases
v_a, v_b, v_c	Phase voltages
v_{ab}, v_{bc}, v_{ca}	Line voltages
v_s	Stator phases voltage
v_r	Rotor phases voltage
V_g	Grid voltage
i_s	Stator current
i_r	Rotor current
v_{DC}	DC-link voltage
P_s	Stator side real power
Q_s	Stator side reactive power
P_r	Rotor side real power
Q_r	Rotor side reactive power
P_{mec}	Mechanical power
R_s, R_r	Stator and rotor winding resistances/phase
L_s, L_r	Stator and rotor winding inductances/phase
L_m	Magnetizing inductance
$L_{s\sigma}, L_{r\sigma}$	Stator and rotor winding leakage inductances/phase
Ψ	Flux
i_{ms}	Stator flux magnetizing current
p	No of poles
ω_s	Stator flux angular frequency
ω_e	Rotor flux angular frequency
ω_r	Rotor angular speed (electrical)
f_s	Stator frequency
f_e	Rotor frequency
θ_s	Angle between αβ and dq reference frames
θ_r	Angle between αβ and DQ reference frames

θ_e	Angle between dq and DQ reference frames
T_{em}	Electromagnetic torque
T_{load}	Load torque
e	Induced emf
s	Slip
J	Moment of inertia
B	Friction coefficient
ω_e	Rotor flux angular frequency
η	Efficiency
σ	Leakage coefficient
H	Head
pu	Per unit
Subscript	
d	Direct component
q	Quadrature component
s	Stator quantity
r	Rotor Quantity
Superscript	
s	Stationary reference frame
r	Rotor reference frame
a	Synchronously rotating reference frame
*	Reference quantity
→	Vector quantity
→ a	Complex conjugate of vector quantity

Chapter I

Introduction and Literature Review

[This chapter summarizes the present research work and expounds the power converter topologies in large rated variable speed pumped storage power plant (PSPP), suitability of converter topology, modulation techniques, and parallel converter schemes in PSPP is discussed. Also, it presents operational issues of parallel converter system fed variable speed hydrogenerating unit such as converter redundancy and fault tolerant control schemes, power outage due to the inadequacy of converter protection system, and unbalanced power sharing due to circulating current. Further, it describes the importance of present work and discusses the benefits to the project authorities of large variable speed PSPP.]

1.1 Introduction

In hydroelectric energy systems, pumped storage power plant is adopted in view of, (i) bulk energy storage, (ii) ability to provide flexibility to the power system, and (iii) load balancing [1]. Since 1900's, synchronous machine based fixed speed PSPP has been installed in the European, American and Asian continents, and now more than 140 GW fixed speed PSPP operating in the world. In India, 4804 MW of fixed speed PSPP are installed and presently only about 2600 MW are being operated under pumping mode [2]. Nowadays, variable speed PSPP is an emerging technology in a pumped storage system where it has several benefits, specifically: (i) increased efficiency in generation/pumping mode with respect to the varying water level in the dam, (ii) taking minimum time during mode transition from pumping to generation and vice versa, (iii) high dynamic stability during grid voltage and speed perturbations, (iv) high ramp rate in generation/pumping compared to fixed speed unit, etc. [3]. The first variable speed PSPP was commissioned in the early 1990's and till now 18 nos. of such power plants are installed/under construction all over the world with a total capacity of 9425 MW. Large variable speed PSPP (>200 MW) employing synchronous machines is not viable due to: (i) the requirement of power converters of higher rating corresponding to the rating of the machine, (ii) full size converter is challengeable in cost, size and site clearance in case of underground power houses, (iii) rotating over full range of speed in hydrogenerating unit is not given much difference in efficiency compared to 10-15% speed variation in the unit [4], [5]. Therefore, variable speed PSPPs with doubly fed induction machine (DFIM) have gained prominence all over the world since they

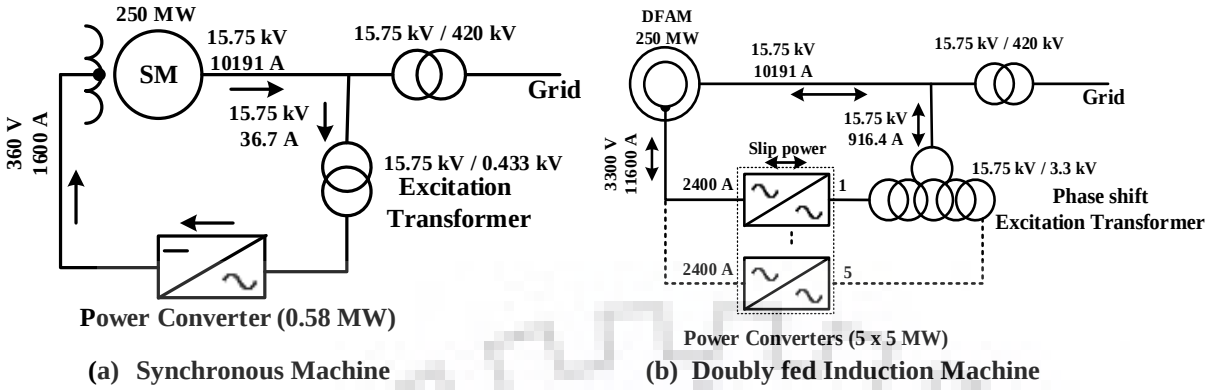

Fig. 1.1 Machines serving to a typical 250MW hydro generating unit

provide variable speed operation with reduced power converter rating and high dynamic stability [6], [7]. In India, four DFIM units with a unit capacity of 250 MW with the speed variation of -10.73% to +8.33% is under construction at Tehri dam of Uttarakhand state. The speed of machine (250 MW DFIM) was fixed at 230.77 rpm based on hydraulic studies conducted in Tehri pumped storage plant. Therefore, the design team has gone for DFIM with 26 poles to meet grid frequency. It is noted that a DFIM with 18 poles is serving in Goldisthal PSPP (Germany) at the rotational synchronous speed of 333 rpm [4]. In addition, brushless DFIM is not preferred for large rated PSPP in view of quick voltage regulation and large amount of reactive power support. As far as author's knowledge, brushless DFIM is not yet installed or planned for large rated PSPP in any part of the world [8] – [10]. High amount of current in rotor circuit of DFIM through brushes and slip rings seems to be challengeable due to: (i) operating temperature, and (ii) brush voltage drop. However, it is practically acceptable in presently available technology, e.g. a 400 MW Ohkawachi (Japan) hydrogenerating unit with rotor currents of 12670A and a 300 MW Goldisthal (Germany) hydrogenerating unit with rotor currents of 8970A are currently in operation [6], [11].

The schematic diagram of doubly fed induction machine fed variable speed PSPP is shown in Fig 1.1b. The power electronic converters are connected in rotor circuit of the DFIM, there by acting as AC excitation system of the machine. The main advantage of such scheme is the requirement of the power electronic converter with rating equivalent to slip power, normally, will be a fraction of the machine rating [12] - [18]. The rating of the rotor side power converter in DFIM is chosen based on required speed variation of the unit. In general, the rotor side power converters are chosen at 10 to 15% of the rated capacity of the machine (e.g. 72 MVA cycloconverter is chosen with a current rating of 8760 A for a 400 MW DFIM unit, Ohkawachi,

Japan; 45 MVA three level back-to-back power converter is chosen with a current rating of 11600A for a 250 MW DFIM unit, Tehri, India) [19] – [20]. In a situation where in the semiconductor devices ratings are limited, it is preferred to employ parallel converters to share the rotor circuit current [21]. Under the availability of water head and grid supply, the power electronic converters primarily dictate the continuity of operation of the DFIM fed variable speed PSPP. This type of plants helps in improving power controllability, grid balancing, increase energy efficiency and power quality in grid networks [22].

The application of semiconductor devices in DFIM fed variable speed PSPP ranges from naturally commutated devices (Thyristor) to self-commutated devices (IGBT, IEGT, etc.,) depending on the requirements such as switching characteristics, ease of gate control, reliability, low on state power losses and voltage drop, etc. [18], [19]. During these modes of operation, bi-directional power flow is achieved through the rotor side power converters. Therefore, HV-IGBT/IEGT device is selected for the rotor side converters. In Tehri variable speed PSPP (India), IEGT (Injection Enhanced Gate Transistor) is selected for handling large currents in rotor circuit in view of low on state voltage drop and lower conduction losses, etc. compare to IGBT. In a similar way, the advancement in power converter topology ranges from cycloconverter to multi-level voltage source converters to achieve rotor current harmonic distortion reduction, pure sinusoidal supply, etc. [23], [24]. The usage of cycloconverter in variable speed PSPP were prominent in the past and it has been started by using external static frequency converters (SFC) during pumping mode (e.g. 400 MW DFIM PSPP, Ohkawachi (Japan); 300MW DFIM PSPP, Goldisthal (Germany)). However, presently cycloconverters are not preferred in PSPP applications as with advancement in power electronics technology, now back-to-back voltage source converter (VSC) gives better current waveform and lesser THD. In addition, this converter is used for smooth starting and dynamic/regenerative braking of unit in pumping mode and there is no requirement of SFC (e.g. 380 MW Frades II DFIM PSPP, Portugal employed with 2 level back-to-back VSC; 250 MW Linthal DFIM PSPP, Switzerland employed with 3 level back-to-back VSC).

1.2 Power Converters Employed in DFIM Fed Variable Speed PSPP

Power converters play an important role in DFIM fed variable speed PSPP by facilitating variable speed operation, smooth starting, braking (regenerative & dynamic), reactive power compensation and also acting as active power filters. Moreover, the converters are also responsible for achieving real & reactive power control in generation mode and speed & reactive

power control in the pumping mode [25]. The different power electronic converters that are employed in PSPP are presented below.

1.2.1 Load Commutated Inverters

Load commutated inverters (LCI) are employed in the fixed pumped storage plants driven by synchronous machines are in operation with the rating of 50MW to 100MW range [26], [27]. Due to lack of reactive power control, current distortion, and low power factor, these inverters are not recommended for DFIM fed variable speed PSPP [28] – [30]. It is also to mention that the installation of LCI fed DFIM in variable speed PSPP is not yet adopted in any of commissioned PSPP.

1.2.2 Matrix Converter

Matrix converter fed DFIM used in wind power system is discussed in [31], [32]. However, back-to-back converter topologies are preferred in such systems than matrix converters due to: (i) output voltage step-up capability, (ii) unconstrained reactive power compensation, (iii) simple feedback control of the input currents independent of the output currents, (iv) single phase operation capability [33]. In addition, considering the system operation under faulty conditions (open circuit fault), back -to- back converter seems to be a preferred option in industrial drives as it allows the process to continue even at open circuit faults in rectifier side i.e. ac- dc conversion stage [34]. Also, high power density and power -to- mass ratio are questionable in large rated, low switching frequency applications equipped with matrix converter. In view of this, matrix converters fed large rated DFIM is not yet adopted in any of commissioned PSPP [35].

1.2.3 Cycloconverters

Cycloconverter (shown in Fig. 1.2a) is a type of power electronic converter which provides variable AC voltage of variable frequency without DC link. Such type of converter employing GTO (Gate Turn Off thyristors) was adopted in the hydroelectric variable speed plants at Ohkawachi power station in Japan [6] and Goldisthal power plant in Germany [11]. The merits of cycloconverter over LCI is: (i) generation of low frequency AC voltage, (ii) Instantaneous real and reactive power control, (iii) low on state power losses. However, the cycloconverters suffers from demerits including: (i) inability to generate output voltage with a frequency greater than input frequency, (ii) requirement of additional static frequency converter (SFC) during starting in pump mode, (iii) high distorted rotor current in DFIM, thereby introducing the large size of filters compare to VSC's, (iv) reactive power absorption from grid in rotor side [11], [36]. The

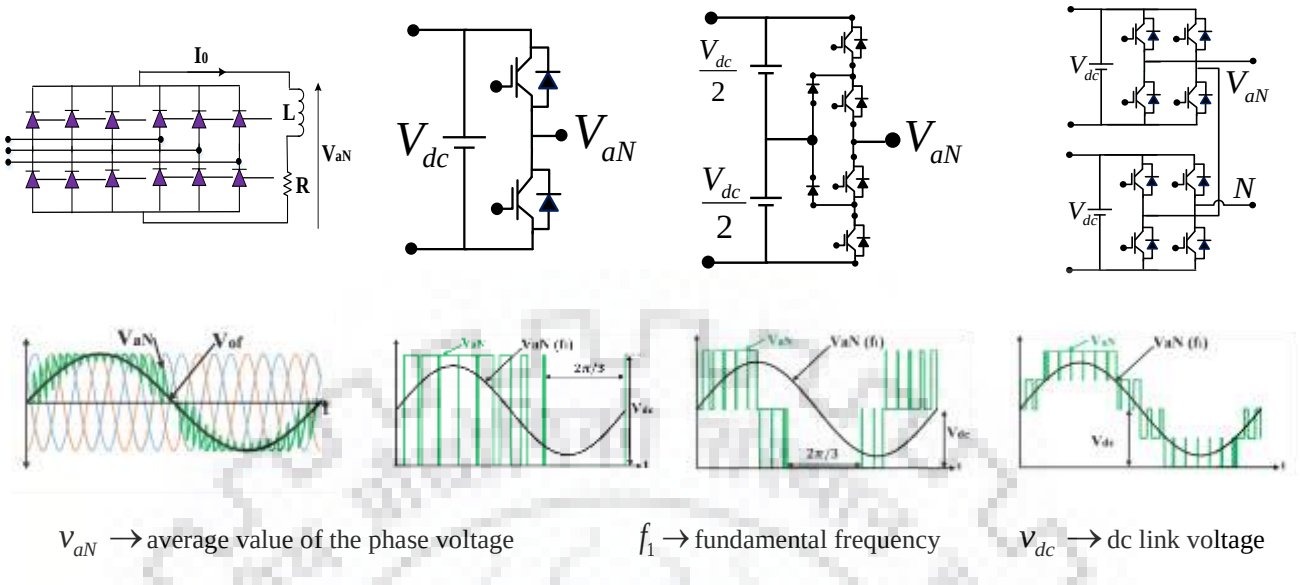

v_{aN} → average value of the phase voltage f_1 → fundamental frequency v_{dc} → dc link voltage

(a) Cycloconverter **(b) 2L- VSC** **(c) 3L-NPC VSC** **(d) 5L-CHB VSC**

Fig. 1.2. Power converter topologies and their voltage waveforms

preferable number of switching devices used in cycloconverter is seventy two (Conventional 12-pulse cyclo-converter cascade) [37], [38] for the minimum distorted required rotor current waveform (adopted in Ohkawachi power station, Japan), however, the number of switching devices shall be increased as per the higher pulse-numbers to achieve better quality of rotor current, which leads to increase in size and cost of the converter.

1.2.4 Back-to-Back Voltage Source Converters

Back-to-back Voltage Source Converters are the converters which has widespread applications including the control of DFIM based variable speed PSPP. Such converters have an ability to provide variable voltage and variable frequency supply during starting of the machine resulting the reduction of start-up transients and energy losses [39] - [41]. Also, VSC with suitable control technique finds applications in power conditioning circuits such as STATCOM (reactive power compensation) and active power filters (elimination of harmonics). The main advantage of VSC is its ability to offer decoupled control of real and reactive power with a significant reduction of load current harmonics [42] - [45]. The following are different types of VSC that are used DFIM fed variable speed PSPP.

1.2.4.1 Two Level Voltage Source Converter (2L-VSC)

This converter (shown in Fig. 1.2b) comprises six nos. of (3-phase) IGBT or GCT switch with a freewheeling diode across each switch [46]. The merits of this converter are: (i) simple converter topology and control scheme, (ii) active and reactive power control, (iii) independent

control of grid-side and machine-side converter, (iv) no need of auxiliary devices for start-up application in pumping mode, (v) unity power factor at grid side. The demerits are: (i) due to cross-influence of d- and q-axis, multi variable controllers are required for grid-side and machine-side converter, (ii) high THD, high dv/dt, high harmonic losses compare to multilevel VSC's, (iii) possibility of predominant harmonic injection into the grid depending on the PWM carrier frequency [47], [48]. The Frades II variable speed pumped storage hydropower plant (Portugal) has employed 2L-VSC [49].

1.2.4.2 Three Level Neutral Point Diode Clamped VSC (3L-NPC)

This type (shown in Fig. 1.2c) of VSC belongs to multi-level converter family, in which odd no.of levels are achieved due to the availability of the neutral clamp structure. This converter is maturely applied in large rating drives due to the lesser voltage stress on devices, resulting in the reduction of failure rate in semiconductor devices and generation of resultant waveform with better spectral performance [50]. Further, THD in rotor current is lesser than cycloconverter and 2L-VSC which leads reduction of filter size in 3L-NPC [51]. The drawbacks of this converter type of VSC are: (i) requirement of additional clamping diodes which increase the size and cost of the system, (ii) Non uniform power loss distribution among switches due to switching logic, (iii) complex control system compared to that of 2L-VSC, (iv) voltage imbalance problem in dc link capacitor due to clamping diodes [52]- [54]. This type of VSC is employed in variable speed PSPP at Linthal, Switzerland. Also, Tehri Hydropower Development and Corporation (THDC India Ltd) is planning to install 3L-NPC in stage III project of Tehri dam.

1.2.4.3 Cascaded H-Bridge Multilevel Converter (CHB)

This converter (shown in Fig. 1.2d) circuit is having a special arrangement with phase shift transformers (phase angle 15°) employed for the input line current/voltage THD improvement and common mode voltage mitigation [55]. The major advantages of such converter include: (i) very low rotor current THD, thereby requiring lesser cost and small size rotor side filters compare to 3L-NPC's, (ii) identical phase connections leading to optimized circuit layout, (iii) elimination of clamping diodes, (iv) the output voltage waveform nearer to sinusoidal. However, the cost of this converter is very high due to the requirement of phase shift transformer and associated cabling needs [56], [57]. In China at Xiang Hong PSPP, CHB is adopted in start-up applications of the synchronous machines fed pumped storage plant [58].

Table 1.1 Comparison of converter topologies (used in DFIM based PSPP)

	Cycloconverter [11],[36]-[38]	2L – VSC [46]- [49]	3L – NPC [50]- [54]	CHB [55], [56]	FC – MLC [47],[59]
No.of power Switches (IGBT + Diode)	72 *	12 +12	24 + 36	24 + 24	24 +24
dv/dt voltage stress	Very high	high	low	Very low	Very low
THD in rotor current**	0.582 %	0.482 %	0.449%	0.283 %	~0.3%
Size of filters	Very high	High	Moderate	Compact	Compact
Cost of filter	Very High	High	Reasonable	Low cost	Low cost
Fault tolerant capability	No	No	No	Yes	Yes
Advantages	No intermediate DC link required	Simple structure Few no.of power devices	High efficiency at increased switching frequency	Equal loss distribution, Less common mode voltage	good performance for high and low modulation index
Disadvantages	requirement of additional SFC during starting in pump mode, reactive power absorption from rotor side grid	High switching losses, Efficiency and technical requirements are difficult to fulfill	Clamping diodes requirement, unequal power loss distribution in switches, DC-link balancing	More DC sources required	The increase in capacitors leads to more costs and space
Employed	Ohkawachi power station, Japan	Frades II variable speed pumped storage hydropower plant, Portugal	Linthal variable speed pumped storage plant, Switzerland	Xiang Hong PSPP, China	Used as static compensators

* Conventional 12-pulse Cyclo-converter cascade.

** based on the simulation of 230MVA DFIM in SIMSEN software [29].

1.2.4.4 Flying Capacitor Multilevel Converters (FC-MLC)

The number of switching devices used in this topology is reasonable and the use of dc link capacitors provide more flexibility [59]. The voltage imbalance problem can be reduced by selecting proper switching technique of charging and discharging of capacitors. The most

important advantage of FC-MLC is low rotor current THD, improved power quality, and capacitor voltage balance. In addition, pre-charging of capacitors are necessary and sometimes it is difficult [60]. These converters are mostly used in static compensators and active filters in PSPP's. The summary of different types of voltage source converters is also presented in Table 1.1.

1.3 Converter Modulation Techniques for Variable Speed PSPP

The key factors to be considered while formulating the modulation technique in power converters are: (i) minimization of utility line harmonics, (ii) minimization of load current harmonics, (iii) good utilization of dc link voltage, (iv) minimization of switching frequency and losses, (v) uniform switching losses, (vi) uniform switching frequency for all switching devices, and (vii) voltage balance in dc link capacitor [61] – [71]. The following are the different modulation techniques adopted in variable speed PSPP applications.

1.3.1 Sinusoidal PWM (SPWM)

In electric drives, SPWM is the widespread modulation scheme used in power converter control [72]. In this technique, the low frequency modulating signal (sinusoidal wave) is compared with the high frequency (switching frequency) carrier signal (triangular wave) in a logic device that provides PWM pulses, which in turn control the switching devices. The amplitude and frequency of converter output voltage depend on the modulating wave amplitude and frequency respectively [73]. The output voltage waveforms and equation are shown in Fig.1.3a. The maximum value of modulation index selected for SPWM in large rated electric drives is 0.7885 and the value of switching frequency is limited to less than 1.5 kHz [74] considering semiconductor losses and filter requirements for the large rated converters. However, the third harmonic injection in the modulating wave can be utilized to ensure better utilization of dc link voltage in the high rated plant. SPWM strategy is commonly used in starting of the DFIM fed variable speed PSPP (pumping mode) [75], [76].

The selection of dc link voltage for SPWM, $V_{bus} = V_{out} / \left(\sqrt{\left(\frac{2}{3}\right)}.2.M \right)$ (1.1)

M → modulation index

1.3.2 Space Vector PWM (SVM)

SVM technique is derived from space vector theory and generates modulation signal according to the switching sector and angle [77]. Basically, it produces the acting and null vectors based on the level of converters, which decide the switching of power devices [78], [79]. The

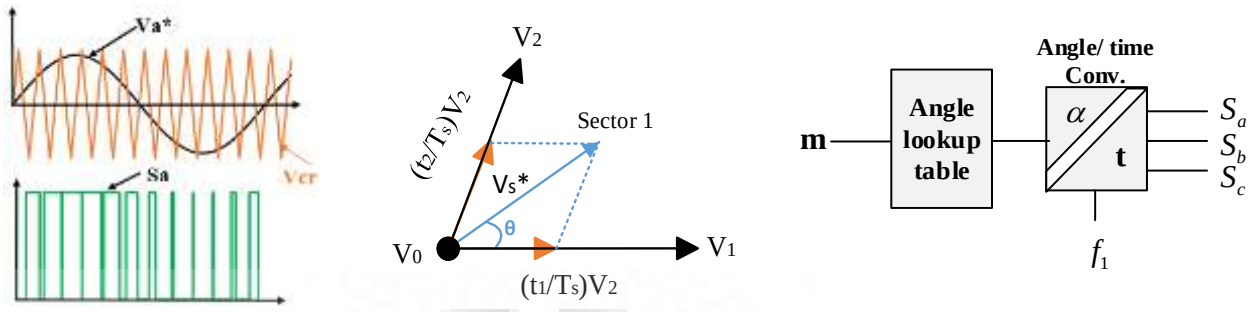

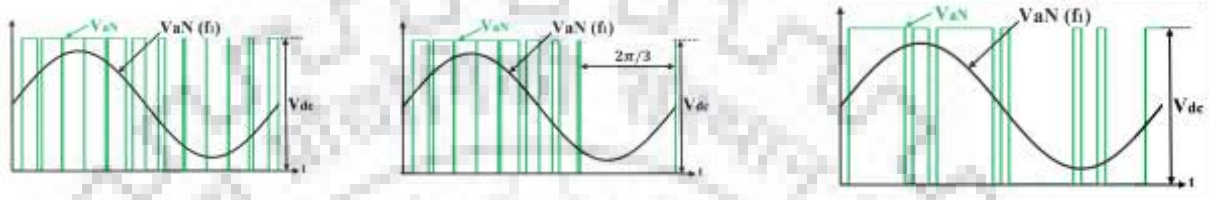

$V_{aN} = M\sqrt{3}V_{dc}$ $\qquad$ $V_{aN} = \frac{t_1}{T_s}V_1 + \frac{t_2}{T_s}V_2 + \frac{t_0}{T_s}V_0$ $\qquad$ $m = \frac{4}{\Pi}\sum_{i=0}^{k-1}\left[(-1)^i \sin(\alpha_i)\right]$

$0 = \frac{4}{j\Pi}\sum_{i=0}^{k-1}\left[(-1)^i \sin(j\alpha_i)\right]$

Where $j = 5, 7, 11, ..., q$

$M \rightarrow$ modulation index $\quad v_{aN} \rightarrow$ average value of the phase voltage

$f_1 \rightarrow$ fundamental frequency $\quad v_{dc} \rightarrow$ dc link voltage

(a) SPWM **(b) SVM** **(c) SHE-PWM**

Fig. 1.3. Operating waveform for modulation techniques for two level VSC [39]

output voltage waveforms and equation are shown in Fig. 1.3b. Compared to universal SPWM, space vector modulation utilizes 15.4 % additional dc supply. In addition, SVM fired converters generate waveforms with less THD in rotor current and also suitable for fast dynamic response application. Moreover, it can accommodate maximum modulation index (0.907) and provide less switching losses [80] - [82]. The dynamic control of real and reactive power in variable speed PSPP is desirable through SVM for low switching frequency operation. e.g., Linthal variable speed PSPP, Switzerland.

The selection of dc link voltage for SVM, $V_{bus} = V_{out} / \left(\sqrt{\left(\frac{2}{3}\right)}.\sqrt{3}.M\right)$ (1.2)

1.3.3 Selective Harmonic Elimination PWM (SHE-PWM)

This PWM technique is framed based on frequency switching theory. The main advantage of this technique is that the harmonics of higher order (e.g. 11, 13, 17, etc.) can be eliminated by selecting the switching angle corresponding to the harmonic order as per pre-determined look-up table [83], [84]. The output voltage waveforms and equation are shown in Fig. 1.3c. In general Newton-Raphson iteration method is used to formulate the look-up table. Due to the elimination of higher order harmonics it is possible to obtain superior sinusoidal output waveform with a

Table 1.2 Comparison of modulation techniques (used in DFIM based PSPP)

	Third Order Injection SPWM [72] - [76]	SVC [77] – [82]	SHE – PWM [83] - [86]
Modulation Index	0.7855	0.907	0.83
Engaged	Smooth starting	Real and reactive power control	Active power filters
DC bus utilization	86.6%	86.6 %	86.6%
Maximum line-line voltage	0.707 Vdc	0.707 Vdc	0.707 Vdc
Switching frequency	~ 1.5 kHz	250 Hz to 500 Hz	< 1kHz
Principle	Carrier based Sine-triangle modulation	Space vector theory	Frequency switching theory
Switching losses	high	moderate	less
Dynamic control response	moderate	high	low
Advantages	Easy implementation	precise control of the dc and ac current magnitude and phase	superior sinusoidal current waveform with a lower value of switching frequency
Disadvantages	Low output voltage	high level computational works required	Low dynamic response

lower value of switching frequency comparatively. This technique is widely used in active power filters. However, the dynamic response of the converter in closed loop control is low due to the pre-specified values [85], [86]. Due to selective harmonic elimination capability, this PWM technique finds application as active power filters in variable speed PSPP. The summary of different types of modulation techniques is also presented in Table 1.2.

1.4 Parallel Operation of Converters in Variable Speed PSPP

Due to the limitation in the semiconductor device rating, it becomes difficult to design a single converter for large power ratings. In such a situation parallel converters can be adopted to share high power in rotor circuit of the machine. The main criteria for the parallel operation of converters are that the output voltage of all converters connected in parallel should be equal in amplitude, frequency and phase. In such a configuration it is possible to have equal/unequal power sharing depending on the power rating of each converter. The application of parallel converter results in improvement of reliability, flexibility, and power quality of the plant. Further, the parallel converter operation increases the efficiency of the plant as the participation of each

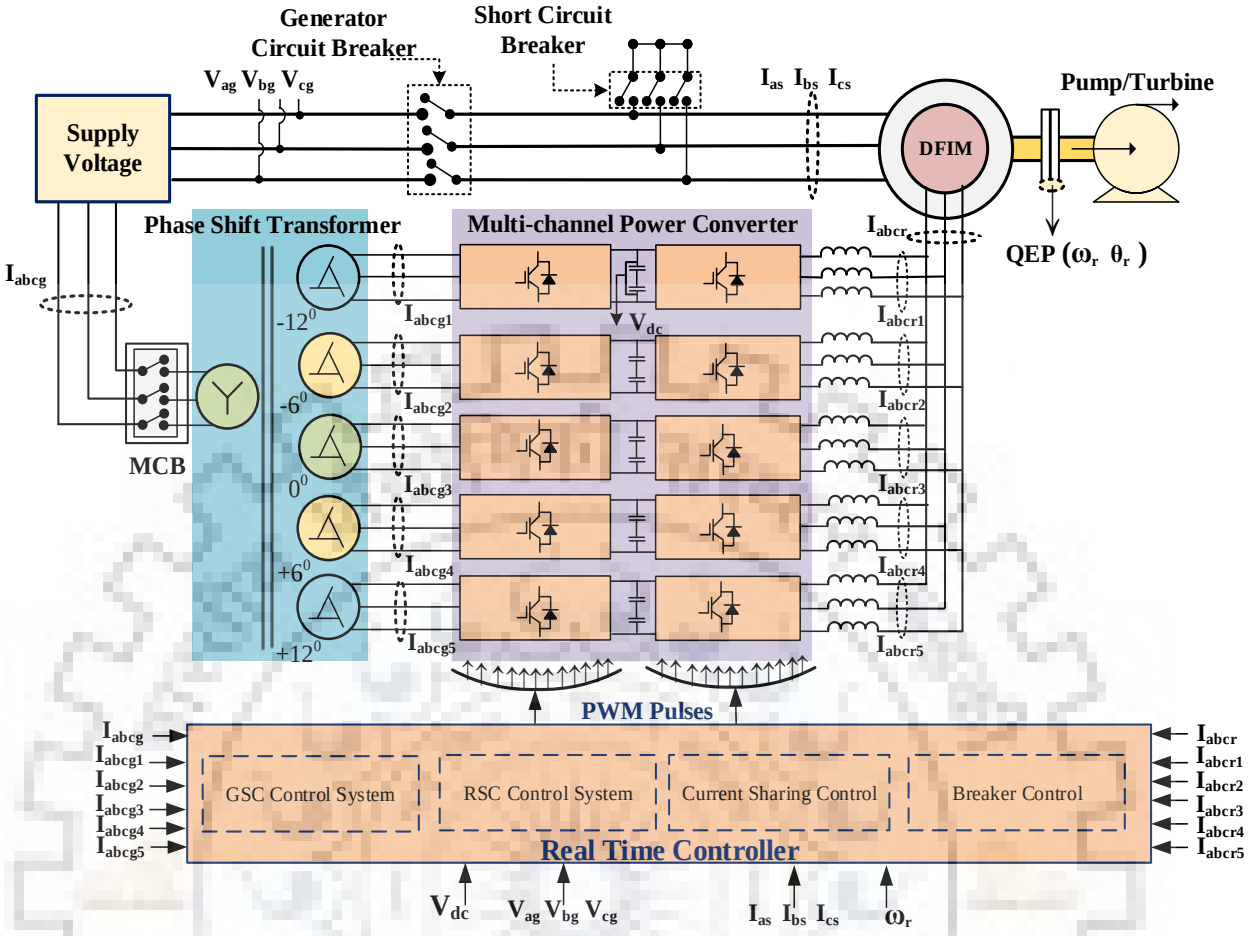

Fig. 1.4. Parallel converters serving to DFIM fed variable speed PSPP

converter can be controlled depending upon the output requirements [87]-[91]. Parallel converters serving to DFIM fed variable speed PSPP is shown in Fig. 1.4. From figure, it is inferred that the rotor circuit is connected to the grid through phase shift transformers (it is designed with phase shifts in secondary windings for harmonics reduction (Yd1 (-12^0) d1 (-6^0) d1 (0^0) d1 ($+6^0$) d1 ($+12^0$)) and five back-to-back converters are connected in parallel.

1.4.1 Power Sharing in Parallel Converters

In general: (i) Passive current sharing, (ii) Droop control method, and (iii) Active current sharing methods are utilized for the effective power/current sharing in parallel converters. Passive current sharing and droop control methods deal with low power circuits including uninterruptable power supplies (UPS) and islanded micro grid applications. Master-slave control used in active current sharing method is also preferable for UPS applications [92]-[105]. Hence, these methods are not discussed in this thesis as it focuses on large rated power converters serving in variable speed PSPP.

The active current sharing method is most suitable for the parallel converters in large rated variable speed PSPP. In active current sharing method, each converter to be connected in parallel is connected by wired communication [106]. A control system is developed to generate the reference current for power sharing, thereby eliminating the need of large impendence for current sharing. Depending upon the control the following are the different types of active current sharing methods.

1.4.1.1 Central Limit Control (CLC)

In this configuration (Fig.1.5a), the number of converters is pre-known and each converter is of same rating/topologies. Depending upon the load current requirement, the central control system sends a signal to each converter for sharing the load current. However, such scheme is less reliable due to the fact that the failure of any one converter renders the system to a standstill [107], [108].

1.4.1.2 Circular Chain Control (CCC)

In this method (Fig.1.5b), the converter controls are formulated in the circular configuration, wherein, each converter tracks the power of the preceding converter to achieve equal current sharing of the load [109]. This chain control requires more communication wires in between the converters and hence making the control complex. In addition, the implementation of redundant converter operation is not easy [110].

1.4.1.3 Active Current Distributed Logical Control (DLC)

In this method (Fig.1.5c), there are two types of controllers are employed namely, individual controller and coordinated controller. Coordinated control systems track the load current and give the reference current to the individual controller of each converter, which in turns regulates the sharing of load current. In addition, the individual controller is designed with

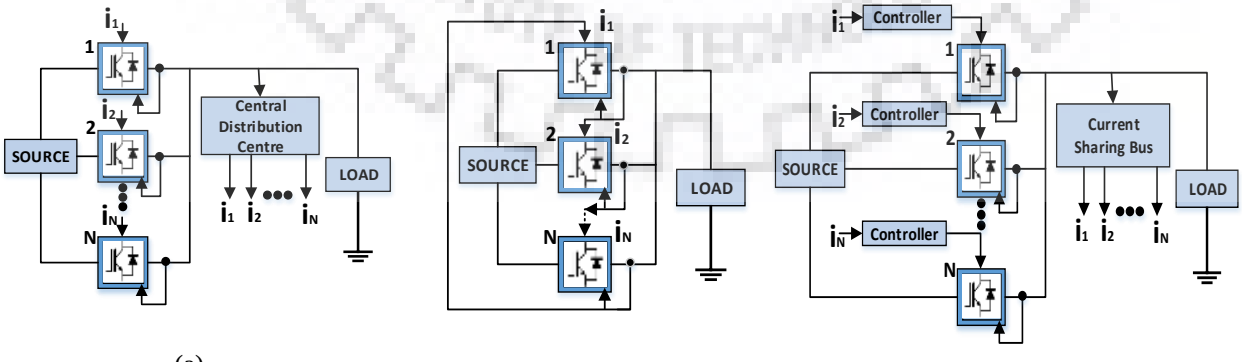

(a) **(b)** **(c)**

Fig. 1.5. Parallel converters control strategies: (a) central limit control [64], (b) circular chain control [66], (c) active current distributed logical control [67]

a capability to limit the circulating and harmonic currents in parallel converter configuration [111]. The merits of this method are: (i) the converter of different rating and topologies can be connected in parallel, (ii) extension of parallel converter is simple, (iii) isolated/redundant operation of converters are possible, (iv) for low power application it is possible to select the required number of converters in parallel configuration, (v) no need of external fault monitoring and detection schemes as in-build controller can identify defective converter [112] – [113].

1.4.2 Circulating Current in Parallel Converters

Circulating current is an important issue in the parallel connected converters during the sharing of current between them. These circulating currents are formed due to: (i) unbalance impedance in phases of the converter, (ii) characteristic of the converter components, and (iii) asynchronous switching operations [114] - [118]. The following are the schemes used to reduce the circulating currents in parallel converters.

1.4.2.1 Phase Shift Transformers

The provision of phase shift transformer (PST) in parallel converters are used to prevent the common mode over voltage and suppressing the circulating current by designing with certain turn's ratio and phase shift [119], [120]. These PST's are also used to reduce the line current harmonics e.g. Linthal variable speed PSPP, Switzerland (2011), PST vector group is Yd1 (-12^0) d1 (-6^0) d1 (0^0) d1 ($+6^0$) d1 ($+12^0$). In olden days (1995's), dc choke had been used to suppress the circulating current in variable speed PSPP instead of PST's. e.g. 300 MW Goldisthal variable speed PSPP, Germany.

1.4.2.2 Space Vector Modulation

The interleaved PWM with discontinuous space-vector modulation techniques can be used to reduce circulating currents. The interleaving techniques, maximizes the cancelation of harmonics between parallel modules, thereby reducing the filtering requirements [121].

1.4.2.3 Individual Voltage Oriented Control

This techniques can be used to eliminate the circulating current in the respective power converter module. An each module having its own modulator and controller with the closed loop system [122]. This independent regulation of each parallel module is adjusted the zero-sequence voltage to restrain the circulating current [123], [124]. Each power module has its own modulator and controller which makes system expandable to any number of modules in parallel.

In summary, phase shift transformers with multi-channel voltage source converters are preferable in rotor circuit of DFIM in variable speed PSPP (shown in Fig 1.4). This set-up offers

reduction in line current harmonics and maintain unity power factor of the system. Starting of pump turbine at motoring mode of operation is done by energizing rotor circuit through power converters. The stator circuit is short circuited while starting. Active current sharing method is desirable in multi-channel power electronic converter fed large rated hydrogenerating unit. Space vector modulation with less switching frequency (300Hz - 500Hz) is widely used in such units for real and reactive power control.

1.5 Operational Issues of Power Converters in Variable Speed PSPP

In fixed speed pumped storage plants, thyristor-based power electronic converters are used in the excitation system (DC) having a lower power rating in comparison with machine rating (e.g. for a typical 250MW synchronous machine, the excitation system needs around 0.58MW of power, i.e. 0.23% of the machine capacity). In addition, the failure rate of the thyristor is low and it can handle high power compared to self-commutated power semiconductor devices. Moreover, the power converters are not much affected by the stator side grid disturbances (voltage drop, short circuit, and frequency drop) due to the design of the synchronous machine. Therefore, the protection of the converter is not much complicated and the ability to fault ride through in plant is easy-going. Furthermore, providing redundancy in both power and control circuits is also easy in case of a fault in converter module, as the power handling of the converter is less. In Tehri (India) hydropower plant (Phase I), redundancy is ensured by means of two fully automatic power converter units with independent control.

On the other hand, the rating of excitation system (AC) equipped with power electronic converter is quite large in DFIM fed variable speed PSPP which handles slip power of the machine (Ex: For a typical 250MW doubly fed induction machine with the target of -10.73% to +8.33% speed variation, power converters need to handle 25MW (slip power) of power with the current rating of 11,600A). Due to the high power rating requirement there is a critical necessary to opt for the parallel operation of converters in DFIM fed variable speed PSPP. The operational issues associated with the power converters serving DFIM fed variable speed PSPP's are:

- Power Redundancy during the Converter Fault
  - Contactor used in series with each power converters in parallel converter system
  - Detection of dc component during a fault
- Control Redundancy
- Deficiency in the Protection of Power Converter
- Circulating Current in Parallel Converters

- Operating at Synchronous Speed.

Each operational issues are presented in detail below.

1.5.1 Power Redundancy during the Converter Fault

Around 38% of failure in an electric drive is due to the faults occurred in power converters which includes power devices failure, dc link capacitor failure, and driver circuit failure [125]. In power converters, open and short circuit faults are due to: (i) electromagnetic interference, (ii) malfunction in the driver circuit, (iii) rapid voltage dip/swell, (iv) auxiliary power supply failure, (v) avalanche stress, and temperature overshoot in power devices [126], [127]. Moreover, if any disturbances (voltage drop, short circuit) occur in the stator circuit, results in higher current/voltage in the rotor circuit, which easily affects the power converter connected in the rotor circuit of the machine.

In addition, a typical fault in converter circuit (without redundant converters) employed in variable speed PSPP may result in stopping of the plant for more than 8 hours, leading to huge financial losses. To illustrate, consider a plant having 5 units with each unit rated at 300 MW. If a converter fault at any one unit results in stopping of a unit for 8 hours, the estimated financial losses will be $176,560/fault/unit (considering $ 0.07/kWh). Further, if it is assumed that every unit encounters a fault per year, the estimated financial losses of the plant will be $882,800/plant/year. The assumption of one fault per year was taken by considering: (i) IGBT triggering circuit failure rate is 0.96 failure per year (i.e., 1 failure occurs at 1.04 years) [128], (ii) Motor drive failure rate is 0.27 failure per year (i.e., 1 failure occurs at 3.7 years) [129], (iii) IGBT failure rate is 500 FIT (1 FIT equals 10^{-9} failures per hour) [130], [131]. It is noted that the probability of failure of power converter serving in PSPP is high as it has more than 300 power devices (IGBT & Diode) [32].

In order to overcome the power converter failure, redundancy phenomena need to be incorporated so as to allow for the sustained operation of the plant. In India, the Central Electricity Authority (CEA) has mandated that all the hydropower plants having rating more than 100 MW must have power and control redundancy in excitation circuit [132]. However, there is no redundancy in any of the practical parallel converter system fed DFIM based variable speed PSPP in the world [133]. Generally, providing contactors/mechanical breaker connected in series with each converter is a solution to have redundancy. This contactor can be connected in either DC side or AC side of the converter. The following issues are identified when contactors are considered for the isolation of converters in the high rating plant.

1.5.1.1 Contactor used in series with each power converters in parallel converter system

The contactors connected in series with the power converter produces triangular transient recovery voltage (high amplitude and high frequency of short duration) during interruption of the fault current in the high power rated circuit [134], [135]. This very high steep voltage causes the insulation of the rotor winding of the DFIM to be stressed and can result in breakdown. This rapid change in the voltage have deleterious effects on the power devices and sometimes this will also affect the healthy converters that are in service. The developed transient voltage is given by the eqn. 1.3. Moreover, provision of contactors increases the risk and maintenance related issues in the high rated plant [136], [137]. Hence, this contactor configuration is not preferred for redundant operation of the converter.

$$V_{TRV} = \sqrt{2} I_f \omega L_{eq} \left[\left(1 - e^{-\alpha t}\right) \left(\cosh \beta t + \frac{\alpha}{\beta} \sinh \beta t \right) \right] \tag{1.3}$$

$$\alpha = \frac{1}{2 Z_{eq} C_{eq}} \qquad \beta = \sqrt{\alpha^2 - \frac{1}{L_{eq} C_{eq}}} \qquad \omega = 2\pi f$$

V_{TRV} → transient recovery voltage across the breaker contacts

I_f → fault current magnitude (in kA rms)

Z_{eq} → equivalent source impedance in ohms

L_{eq} → equivalent source inductance in henrys

C_{eq} → equivalent source capacitance in farads

As per the standard ANSI/IEEE C37.013-1993, the acceptable level of transient recovery voltages (TRV) for 10 to 50MVA generator is 1.5kV/μs during the interruption of circuit breaker and the production of peak voltage is 1.84 times rms value of maximum input voltage . However, the maximum permissible rotor voltage is limited to 1.34 times rms value of the rotor voltage and the TRV rate is limited to 0.6kV/μs for considering the insulation of the rotor winding of a DFIM based variable speed unit [138]. Hence, the interruption of circuit breaker will definitely cause overburden to insulation used in rotor winding of DFIM and converter redundancy is challengeable.

In order to investigate the effect of this option, a contactor is connected in series with each converter (Fig. 1.4). The simulation is carried out by introducing a single leg open circuit fault within any one of the main converter at 125s and the fault is detected by the Park's vector phase currents technique and variation in dc link voltage. The faulty converter is isolated from

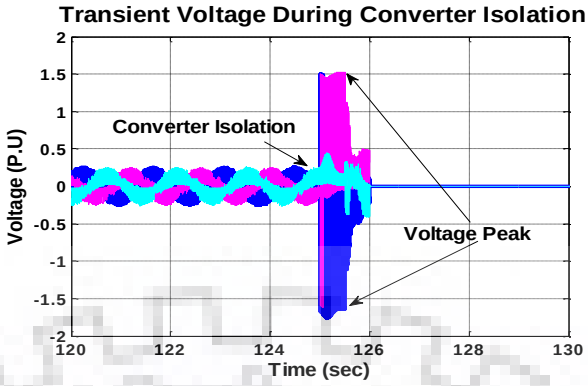

Fig. 1.6 Response of contactor used isolation - 250MW DFIM

the system by contactor as well as redundant converter comes to the action for continuous operation of the plant. It is observed that phase voltage in rotor winding reaches to 1.75 p.u, (shown in Fig. 1.6) during isolation of faulty converter. Over voltage in rotor windings leads to deteriorate the life of insulation.

1.5.1.2 Detection of dc component during a fault

During faults in the converter, due to the large time constants (high X/R) a current of high amplitude and very low frequency is produced, typically with the absence of zero crossing. The magnitude of DC component depends on fault current and fault inception in the cycle [139]. This high DC component can pose problems/challenges in diagnosis of fault current and interrupt difficulties. According to the standards IEC 62271-100 and IEEE C37.013-1997 that the interruption of current by a high speed circuit breaker should be completed in not more than 40ms, otherwise results in serious damage to the contactors and equipment [140], [141]. The detection of DC component and to break such a current during this fault by contactors is very difficult, prolonging the fault isolation process resulting in the damage of other converter modules due to the fault current. Moreover, a suitable circuit breaker break such a high DC component in power converter circuits is high challengeable [142] - [144].

ALSTOM jointly with EPFL, Switcherland suggested a possible solution for detecting DC component or extremely low frequency rotor current by using digital substation technology which incorporates Rogowski current transformers and resistive voltage dividers with IEC 61850-9-2 LE [133]. Nevertheless, the solution of these findings are not yet adopted in any of variable speed PSPP.

Rotor side short circuit faults (phase-phase and single leg) are injected at 125s. During faults, high magnitude (about 1.85 p.u) and very low-frequency (< 0.5 Hz) rotor phase currents

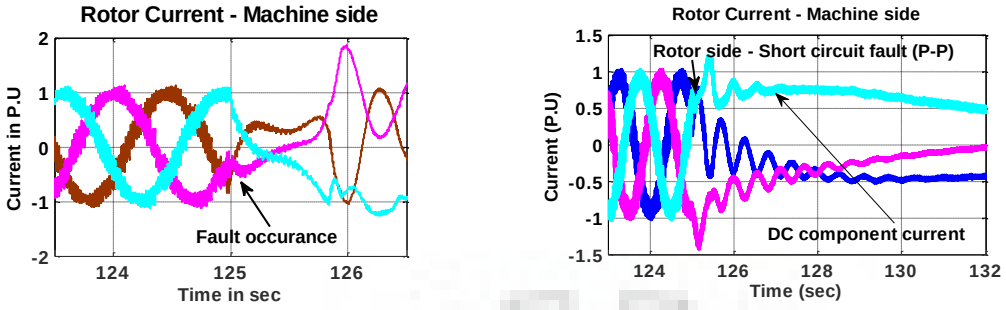

(a) (b)

(a) Response of rotor side short circuit fault (Phase - Phase)
(b) Response of rotor side short circuit fault (IGBT - single leg)
Fig. 1.7 DC component current

are produced as shown in Fig. 1.7a and Fig.1.7b. High magnitude and dynamic variation of frequency in rotor fault currents are challengeable in detection. Further, high DC or extremely low frequency fault currents are also challengeable in disruption by contactors. Experimental results reported in [144] validate the simulation results obtained.

1.5.2 Control Redundancy

Field oriented vector control provides the good dynamic performance of the doubly fed induction machine. This dynamic control works with the aid of controllers, sensors (speed, voltage, current, etc.), and accessories. These sensors and controllers can be affected by electromagnetic interferences, internal and external faults. Moreover, the complexity of the control circuit involving parallel converters, sensors, controllers, etc. will increase the chance of failure. Any failure in sensors at DFIM drive results to current transients in rotor winding, produces grid disturbance in higher magnitude and decisively process of the machine is interrupted. In variable speed drives, 53% of faults [125] are due to control circuit failure, therefore, much attention needs to be given to the control circuit faults and provide possible redundancy/fault tolerance in the control circuit of large rated variable speed pumped storage plant. Furthermore, the power converters are precisely controlled with the suitable modulation techniques by the use of driver circuit. If any faults occur in driver circuit leads to open circuit fault in the converter, which in turn produces non-sinusoidal current waveforms. These waveforms introduce the thermal overstress on the power semiconductor devices resulting in a short-circuit fault [127], [131].

Closed loop vector control system to facilitate desired dynamic performance of DFIM fed variable speed PSPP requires encoder, dc link voltage, grid voltage, grid current, stator current and rotor current sensors. The encoder omission fault is injected in the closed loop control

system and observe the performance of the drive (omission fault is modeled by setting the sensor output to zero). The performance measures are set for speed, dc link voltage, current and settling time. The performance bounds are considered as follows, (i) speed variation is ± 0.05p.u rpm (ii) dc link voltage variation is ± 0.1p.u (iii) current is acceptable up to 1.2p.u (iv) controller settling time is less than 250ms.

The encoder fault is injected at 125s and the results are shown in Fig. 1.8. During fault, speed controller reads input as zero and increases proportional gain of the controller which increases the speed of machine. Consequently, frequency of rotor current increases, shown in Fig. 1.8a, until the speed gets saturated (shown in Fig. 1.8c). From the test results, it is summarized as: (i) speed of the machine increases until the q-axis rotor current (Iqr) gets saturated and consequently magnitude of rotor voltage gets increased as shown in Fig. 1.8b, (ii) increase in I_{dg} (direct axis current - grid) to maintain the dc link voltage, (iii) reactive power delivery/consumption during encoder fault is unchanged. The probability of the survival of DFIM under the said fault is analyzed with the performance bounds. Results show that the unit fails to continue its operation under encoder omission faults, hence control redundancy is necessary to increase the continuity of operation of hydrogenerating units.

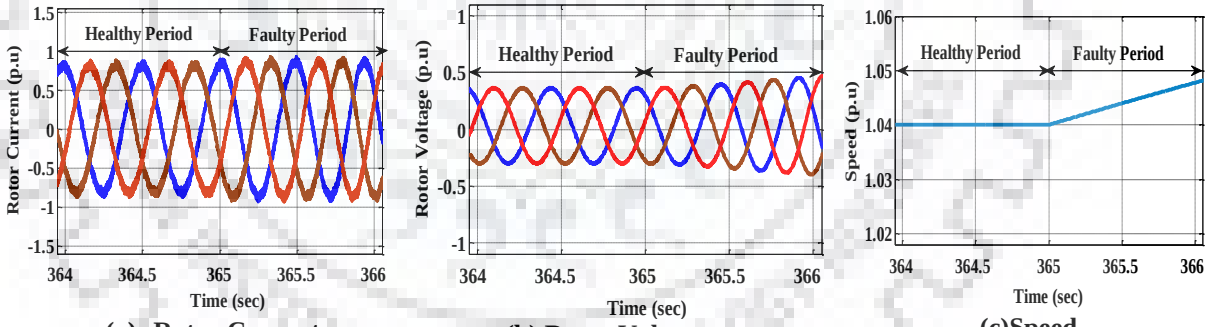

(a) Rotor Current (b) Rotor Voltage (c)Speed

Fig. 1.8 Response of encoder fault

1.5.3 Deficiency in Protection of Power Converter

Rotor side power converter facilitates real and reactive power control in DFIM fed variable speed PSPP. These converters are easily affected by grid disturbances and external faults. In general crowbar protection circuit is used for the protection of power converters and it is enabled based on the threshold value of dc link voltage [145]. This circuit is connected in rotor terminals of the machine in parallel with power converters. It consists of resistors and power switching devices to offer short circuited rotor at the time overvoltage experience by grid

disturbances. The value of resistance is selected based on the dc link clamp effect and this resistance should be sufficiently high to limit the short circuit current and low enough to avoid the high voltage while in operation [146], [147]. If any disturbances occur in the grid, then the value of dc link voltage will increase and crowbar protection circuit will come to operate. The crowbar circuit should not be turned on for the transient faults (short term faults, switch on/off of electrical equipment) and if it is triggered, the circuit gets to turn off when the transient is reduced. Hence, the self-commutating device (e.g. IGBT) is a better solution for the power devices in crowbar circuit [148].

Nowadays, crowbar protection is the only protection available for converters in variable speed PSPP. Once the crowbar protection is enabled, DFIM acts as the conventional induction machine (squirrel cage induction machine) and draws more reactive power from the grid causing voltage instability in the weak grid [149]. Therefore, the controller is instructed to stop the machine by enabling shutdown procedure in hydropower plants. To illustrate, consider a machine operating in generation mode at sub-synchronous speed, during which compensation frequency is supplied by the power converter to get the synchronization frequency for the delivering power to the grid. The sudden removal of the power converter in this situation leads to the cutoff of compensation frequency, end up in delivering power with a different frequency in reference to grid frequency which results to instability in the machine. Hence, it is clear that the plant will get shut down as soon as crowbar protection acts. The aforementioned consequences do happen for even a small disturbances occur in the grid (i.e. 0.05 p.u depth voltage sag) and stoppage of the plant further increases. However, once the plant is shut down, it will take several minutes to get restarted leading again to high economic losses. In addition, the fault ride-through capability of the plant is a major problem in the aforementioned situations. Hence, additional protection is needed for the plant to increases the fault ride-through capability and thereby ensuring the continuity of plant operation.

Single stage protection (crowbar protection) of the power converter in doubly fed induction machine is continuously disturbed the service of the plant even the fault is not severe. Momentary voltage sag of 0.5 p.u depth is applied between 150s and 151s (duration of 5 cycles) and results are shown in Fig. 1.9. Performance bounds are considered as discussed in test 4. Results shows (Fig. 1.9) that the parameter measures are near or slightly above the performance bounds, the crowbar protection is activated for this disturbance and the plant gets shut down. But if we are adjusting the parameter limits with the consideration of modest performance degrades

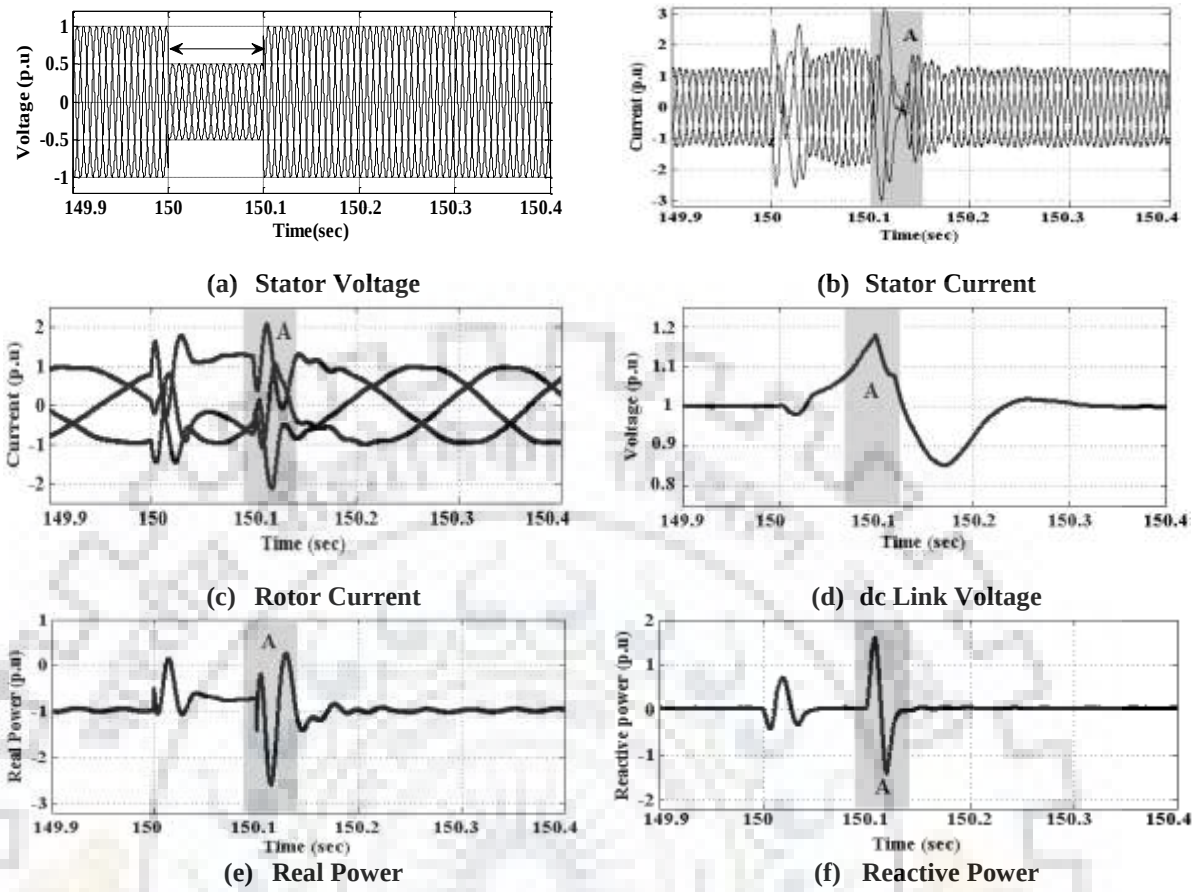

Fig. 1.9. Momentary grid voltage sag fault for a 250 MW DFIM (A- Crowbar protection)

will increase the survival of the plant under this fault. Otherwise, the suitable circuit is required to suppress the rotor current with the considerable limit helps to continuous operation of the plant of the disturbance.

Experimental results reported in [150] validate the simulation results obtained. It was observed that dc link voltage of the back-to-back voltage source converter rises up to 1.3 p.u and consequently crowbar protection is activated during the grid disturbances (voltage sag).

1.5.4 Circulating Current in Parallel Converters

Circulating current is an important issue in the parallel connected converters. These circulating currents are more vulnerable to the high rated parallel power converters in large rated variable speed PSPP. Such circulating currents will distort the current waveforms, increase the losses and introduced unbalance currents in rotor side of the machine. DC chokes are employed in 300 MW Goldisthal Variable speed PSPP to suppress the circulating current [11]. In addition, circulating current controller is also enabled in the vector control structure of the power converters. Also, it is to mention that the research has been continuously carried out to eliminate

circulating current in large rated parallel power converters with better robust characteristics [151], [152].

1.5.5 Operating at Synchronous Speed

When DFIM is operated at synchronous speed, due to the low frequency of the rotor currents, unbalanced thermal heating (unequal distribution of losses among the power devices) is produced in power converters [153]. In addition, it is noted that the junction temperature in power semiconductor devices (IGBT) during low frequency rotor voltage is higher which results high junction temperature swings [154]. Hence, the large rated doubly fed induction machines are not preferred to operate at synchronous speed and it is considered as an insensitive band. However, the research has been continuously undertaken to reduce the dead band around the synchronous speed [155]. In practice, three level VSC fed DFIM based variable speed PSPP is not designed to operate within the band of ± 0.33 Hz with reference to its synchronous speed.

In summary, power converter redundancy and protection of power converter connected in rotor circuit are considered the most important operational challenges in DFIM fed variable speed PSPP [133]. However, HVDC - VSC stations rated about 500MW (between Ireland and Great Britain, operating at +/- 200kV, 2012) are in action and redundancy in these power converter station is not an immense issue [156]. But, it is experimented/noted that multi-channel power converters connected in rotor circuit of DFIM produce over voltage in rotor windings during the operation of breakers/contactors, placed in each channel of converters, which causes insulation failure. Also it is known that, voltage rating of DFIM rotor circuit is much lesser than stator due to the usage of slip rings (typical 250MW DFIM rotor windings are ~ 4.8 times lesser voltage handling capabilities than stator).

DFIM is also widely used in wind power generating systems (WPGS) [157] - [159]. Issues on power redundancies (possibilities of overvoltage in rotor windings), protection of power converters (dynamic variation of rotor frequency and detection of dc component rotor current) are also applicable to WPGS [133]. However, the rating of DFIM used in WPGS (maximum of 8MW [110]) is much lesser in comparison with variable speed PSPP (e.g. 400MW). In addition, stoppage of one machine in wind farm does not make any impact on the stability of power grid. Furthermore, it is mandatory to have power and control redundancies in large rated hydro power plants (> 100MW) according to the country's electricity authority e.g., Central Electricity Authority (India) [132]. Unlike WPGS, DFIM is operated as motor in variable speed PSPP which has a dedicated control system for starting of pump turbine.

Energy conservation is the substantial factor to expand the growth of energy sector. Further, energy conservation is indirectly protecting the environment for future generations. According to WEC (world energy council, 2009), electrical motors are consuming 45% of countries electricity, predominantly asynchronous (induction) machines [160] - [161]. Energy conservation during starting period of large rated DFIM (> 100 MW) is worthy to attention since it consumes considerable amount of electrical energy [6], [162]. For example, a typical 250 MW DFIM consumes 540 kWh/start of electrical energy during conventional V/f smooth starting, reported at Tehri PSPP, India.

In 2011, Xibo Yuan et al. published a V/f smooth starting method for DFIM in centrifugal pump applications and the procedure for starting and grid synchronization. In addition, it is suggested that the stator is short-circuited during starting and rotor is energized through V/f control [25]. During V/f smooth starting, power consumption of the machine mainly depends on reactive component current (magnetization) and torque component current (acceleration). If stator is short circuited, both aforesaid currents are supplied by rotor side converters. This method is extensively used in all large rated DFIM (e.g. 250 MW DFIM variable speed PSPP, Linthal, Switcherland (2015)) [163]. In 2017, Rajasingh et al. published an energy efficient smooth starting of doubly fed induction machine [164]. In which, FDC is applied in stator winding where as it is short circuited in conventional smooth starting. However, it did not discuss the interplay of key factors such as selection of FDC and the value of rotor speed at which FDC applied to stator circuit. Therefore this thesis addresses the selection of key factors and their consequences in the performance of machine. Further, it analyses the dynamic behavior of the machine during energy efficient smooth starting subjected to various faults.

1.6 Problem Description and Importance of Present Work

From a study (discussed in Chapter IV and Chapter V), a 250 MW variable speed hydrogenerating unit provides additional generation of 6.1% per year and additional energy storage of 7.87% per year in generation mode and pumping mode respectively in comparison with synchronous machine based fixed speed PSPP with the speed variation of -10.73% to +8.33% (Tehri variable speed PSPP, India).

Application of doubly fed induction machine for pumped storage of this magnitude is a recent development considering the fact that only one more such project has been commissioned in Linthal, Switzerland (4 x 250 MW DFIM with the speed variation of ± 6% synchronous speed (500 rpm)). Problems associated with power part redundancy in excitation system of DFIM unit

is challengeable due to: (i) over voltages in rotor windings on opening of contactors/ breakers in converter redundant process, (ii) detection of DC component in rotor current and dynamic variation of rotor frequency during converter short circuit fault. Till date, there is no full converter redundancy available in any of the operational DFIM based variable speed PSPP in the world with parallel converter system.

However, in variable speed drives, around 90% of failure occurs due to the faults in converter's power and control circuits which includes power devices failure, driver circuit failure, failure of capacitor dc link, sensor failure and controller failure. The probability of a back-to-back power converter not having redundancy to be in operational state per year is 96.10%. In addition, Table 1.3 shows that the number of failures occurred in back-to-back power converter including GSC, RSC, and DC Link [165], [166]. Open switch fault in three level back-to-back converter is analyzed in [167]. Authors of [168] investigated the effects of short circuit faults in back-to-back power converter fed doubly fed induction generator. Different techniques for fault detection and isolation during speed sensor faults in electric drives are discussed in

Table 1.3.Power and control circuit failures in back-to-back VSC [165], [166]

System		Faults	No.of Failures/year
Power Converter	RSC	Open Circuit Fault (SDOC, SLOC)	1.9940
		Short Circuit Fault (SDSC,PPSC,PGSC)	0.6646
	GSC	Open Circuit Fault (SDOC, SLOC)	0.3025
		Short Circuit Fault (SDSC,DCSC,PPSC,PGSC)	0.1008
	DC Link	Open circuit/Short circuit	0.007
Control Circuits		Omission/Saturation	0.247
		Gain	0.355

SDOC - single device open circuit fault
SLOC - single leg open circuit fault
SDSC- Single device short circuit
DCSC - DC link short circuit
PPSC - Phase to phase SC
PGSC - Phase to ground SC
S - Survived
F - Failed

[169] – [173]. Several publications were discussed the detection of open switch faults in three level converters [174] – [180]. In which, Gaillard et al. had presented the open switch fault detection using voltage based approach [174]. Fault detection based on current distortion approach was discussed in [177], [178] which requires high computational efforts. Ref [181] reviewed fault-tolerant techniques in electric drives and categorized into: (i) switch-level redundancy, (ii) leg-level redundancy, (iii) module-level redundancy, and (iv) system level

redundancy. However, fault tolerant operation of parallel converters fed doubly fed induction machine is not yet available in any of the commissioned hydrogenerating unit. In addition, no literature is available in view of survivability status of the unit subjected to power converter and sensor failures during generation, pumping and condenser modes of operation.

Any failure in power converter and sensors at DFIM drive results to current/voltage transients in rotor winding, produces grid disturbance in higher magnitude and decisively operation of the machine is interrupted. Therefore, the overall benefit of the DFIM fed variable speed PSPP at generation mode is reduced to 1.7% from 6.1% due to the inadequate power converter and control circuit redundancy (discussed in Chapter IV). In addition, the overall benefit of the DFIM fed variable speed PSPP at pumping mode is reduced to 3.66% from 7.87% due to the inadequate power converter and control circuit redundancy (discussed in Chapter V).

The above challenge motivates the present research which shall be helpful to the project authorities during the design stage of their future projects. This thesis provides survivability status of the DFIM unit during power and control circuit faults operating at generation mode, pumping mode and condenser modes of operation. It shall be helpful to the plant authorities to drive the machine continuously during few faults identified in this research, which will not be a problem to the unit and increases the benefit to the plant.

When assessing fault rate in power converter, converter open circuit failure rate is 3 times higher than the other circuit failures as more failures occur in device triggering circuits. Considering this fault rate, this thesis investigates fault tolerant operation of a 250 MW DFIM unit at open circuit fault in converters, which helps to increase the continuity of the operation of generation unit with reduced power delivery. Further, the proposed fault tolerance method brings additional generation of 1.93% electrical energy (generation mode) compared to the DFIM without power redundancy operation. In addition, it brings additional energy storage of 2.49% electrical energy (pumping mode) compared to the DFIM without power redundancy operation at pumping mode of operation. Open switch fault is detected through rotor phase currents and variation in dc link voltage which reduce the computational efforts during fault diagnosis. Further, this paper provides the importance of power converter redundancy through an economic analysis. Hence, technical experts may give full consideration for resolving power converter redundancy issue.

Thus the main contributions of the author can be summarized as follows:

1. Comprehensive literature review on power electronic converters, modulation techniques, parallel converter schemes and circulating current reduction techniques used in DFIM based variable speed PSPP.
2. Find the key parameters that affect the design of power converter redundancy in large rated DFIM fed variable speed PSPP.
3. Smooth starting and regenerative braking of the large rated DFIM unit which is much useful for the grid operators for planning the grid operation.
4. Energy efficient starting of doubly fed induction machine fed pump turbine which conserve about 35% electrical energy compared to the conventional smooth starting. The proposed starting method saves about 230 kWhr/start-up for a 250 MW unit.
5. Exhaustive simulations (250 MW DFIM) and experiments on 2.2 kW proto-type are carried out to evaluate the performance of the DFIM during power converter faults and control circuit faults operating starting, condenser, generation, and pumping modes with given load.
   - The effect of power converter faults are analyzed on test parameters of unbalance in grid and stator currents, variation in real and reactive power consumption, overall grid side power factor, rotor current transients, speed and torque oscillations.
   - Fault diagnosis of open switch converter fault is presented for the grid side and machine side converters.
   - Fault tolerant operation of DFIM with reduced power delivery is proposed to continue the operation of the large rated unit in generation, pumping and condenser modes of operation.

1.7 Thesis Organization

The thesis is divided into seven chapters and the chapter-wise brief summary is given below:

Chapter 1: Introduction and Literature Review

This chapter summarizes the present research work and provides comprehensive literature review on power converter topologies serving to large rated variable speed PSPP. Further, it discusses the operational issues of the multichannel converter fed DFIM in variable speed PSPP.

Chapter 2: Dynamic Modelling of DFIM with Back-to-Back Power Converter

This chapter deals with the mathematical modelling of DFIM with power and control circuits. The control equations are explained in a lucid way. Modelling of power and control circuit faults, importance of test platform to analyse the survivability status of hydrogenerating unit are described at the end of the chapter.

Chapter 3: Starting and Braking of a Large Variable Speed PSPP

This chapters presents the procedure for smooth starting and regenerative braking of a large rated DFIM pump turbine unit, to be commissioned in Tehri PSPP. In addition, starting and braking behaviors of DFIM unit are assessed under power converter and control circuit faults. Further, it discusses the interplay of key elements in the challenging energy efficient starting of pump turbine.

Chapter 4: Dynamic Performance of Generation Mode of a Large Variable Speed PSPP

This chapter discusses the expected benefits of generation mode of DFIM based variable speed PSPP in comparison with fixed speed PSPP in consideration of water head variation. In addition, dynamic behavior of a hydrogenerating unit subjected to power converter and control circuit faults are analyzed. Also, it discusses the fault tolerant operation during single converter open switch fault to increase the continuity of operation of the unit.

Chapter 5: Dynamic Performance of Pumping Mode of a Large Variable Speed PSPP

Dynamic behavior of a large rated DFIM hydrogenerating unit operating in pumping mode subjected to power converter and control circuit faults are discussed. Survivability status of DFIM operating in pumping mode during excitation faults is also assessed. Also, it discusses the fault tolerant operation of hydrogenerating unit during single converter open switch fault.

Chapter 6: Dynamic Performance of Condenser Mode of a Large Variable Speed PSPP

This chapter presents the dynamic behavior of DFIM at variable speed condenser mode under normal and abnormal (faults in power and control circuit) operating conditions.

Chapter 7: Conclusion and Future Scope

This chapter addresses the concluding remarks of present work with future research scopes of large rated variable speed hydrogenerating unit.

1.8 Conclusion of the Chapter

This chapter has reviewed the power converter topologies, modulation techniques, and their suitability in DFIM fed variable speed PSPP. In addition, it is clearly presented the operational issues of the parallel converter in large rated variable speed PSPP with the simulation and experimental results. The importance of converter redundancy is presented with economic benefits, hence, the converter redundancy in parallel converter system is essential for the continuous operation of the plant which increases the reliability and provides more economical benefits. Also, the status of the protection circuit is analyzed and it is to be noted that the plant should have an additional protection circuit for converters with crowbar protection and improves fault ride through capability. In view of operational issues, it is concluded that the suitable parallel converter scheme should be utilized for the proper power sharing with converter redundancy and the accurate control system is to be implemented for mitigating the circulating current. Furthermore, it is decided that the importance and increasing technical requirements of the converter in variable speed PSPP drives will require substantial efforts and research in the future.

Chapter II

Dynamic Modelling of DFIM with Back-to- Back Power Converter

[This chapter deals with the mathematical modelling of DFIM with power and control circuit faults. Voltage source back-to-back power converters are connected in rotor circuit of the machine is responsible for starting/braking, controlling speed (real power) and reactive power of the machine through grid voltage oriented vector control and stator flux oriented vector control. The control equations are explained in a lucid way. Modelling of power and control circuit faults, importance of test platform to analyse the survivability status of the unit and simulation and experimental set-up parameters are described at the end of the chapter.]

2.1 Introduction

Stator circuit of DFIM is directly connected to grid and rotor circuit (three phase cylindrical winding) is also connected to the grid through power converters and excitation transformer which is designed with phase shifts in secondary windings for harmonics reduction. Voltage source back-to-back power converters are preferred in rotor circuit since it provides better rotor current profile and facilitate smooth starting, braking (regenerative) of the DFIM. The principle of operation of DFIM based PSPP is depicted in Table 2.1 and Fig. 2.1, which is similar to the wound rotor induction machine (mutual induction principle). Magnitude and frequency of rotor currents are controlled for adjustable real (speed) and reactive power delivery. The plant is able to operate in two modes namely supersynchronous and subsynchronous allowing the optimum energy transfer from source to load (motoring) and vice-versa (generating).

Table 2.1.Principle of operation of DFIM

Mode of Operation	Speed	Stator Power	Rotor Power	Frequency
Subsynchronous Motoring	$\omega_s > \omega_r$	Positive	Negative	$F_s = \frac{\omega_r * p}{120} + F_r$
Supersynchronous Motoring	$\omega_s < \omega_r$	Positive	Positive	$F_s = \frac{\omega_r * p}{120} - F_r$
Subsynchronous Generation	$\omega_s > \omega_r$	Negative	Positive	$F_s = \frac{\omega_r * p}{120} + F_r$
Supersynchronous Generation	$\omega_s < \omega_r$	Negative	Negative	$F_s = \frac{\omega_r * p}{120} - F_r$

Positive – Power Flow From Grid To Machine

Negative – Power Flow From Machine To Grid

F_s – Stator frequency F_r – Rotor frequency

ω_s - Synchronous speed

ω_r - Rotor speed

p – no.of poles

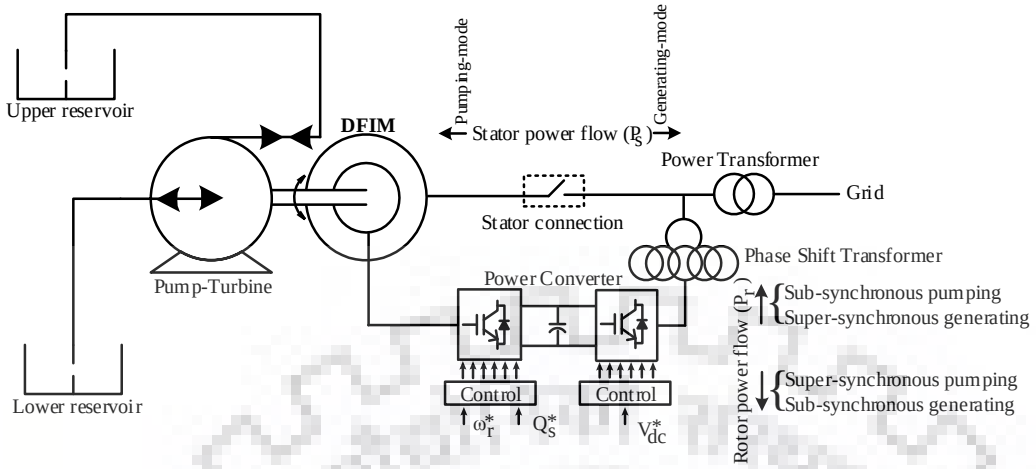

Fig. 2.1. DFIM operation in generation/pumping mode

2.2 Dynamic Modelling of DFIM

Dynamic modelling (direct -quadrature axis mathematical model) of DFIM simplifies the control of real power (speed) and reactive power of the machine. Direct (d) and quadrature (q) axis mathematical model is derived using space vector theory in which three phase quantities (phase 'a_r', phase 'b_r', and phase 'c_r') rotating in a plane with 120^0 phase differences are converted into two phase quantities (phase 'α' and phase 'β') with a phase difference of 90^0. Consider the three phase voltage quantities V_{ar} , V_{br} & V_{cr} as shown in Fig. 2.2. It is converted into two phase quantities $V_{\alpha r}$, $V_{\beta r}$ in a stationary reference frame. The equations are given below:

$$V_{\alpha r} = V_{ar}\cos 0^{o} + V_{br}\cos 120^{o} + V_{cr}\cos 240^{o} \quad (2.1)$$

$$V_{\alpha r} = V_{ar} - \frac{1}{2}V_{br} - \frac{1}{2}V_{cr} \quad (2.2)$$

$$V_{\beta r} = V_{ar}\cos 90^{o} + V_{br}\cos 30^{o} + V_{cr}\cos 150^{o} \quad (2.3)$$

$$V_{\beta r} = \frac{\sqrt{3}}{2}V_{br} - \frac{\sqrt{3}}{2}V_{cr} \quad (2.4)$$

$$\begin{bmatrix} V_{\alpha r} \\ V_{\beta r} \end{bmatrix} = \frac{2}{3}\begin{bmatrix} 1 & -\frac{1}{2} & -\frac{1}{2} \\ 0 & \frac{\sqrt{3}}{2} & -\frac{\sqrt{3}}{2} \end{bmatrix}\begin{bmatrix} V_{ar} \\ V_{br} \\ V_{cr} \end{bmatrix} \quad (2.5)$$

Similarly $$\begin{bmatrix} I_{\alpha r} \\ I_{\beta r} \end{bmatrix} = \frac{2}{3}\begin{bmatrix} 1 & -\frac{1}{2} & -\frac{1}{2} \\ 0 & \frac{\sqrt{3}}{2} & -\frac{\sqrt{3}}{2} \end{bmatrix}\begin{bmatrix} I_{ar} \\ I_{br} \\ I_{cr} \end{bmatrix} \quad (2.6)$$

Term $\left(\frac{2}{3}\right)$ is used for scaling the magnitude.

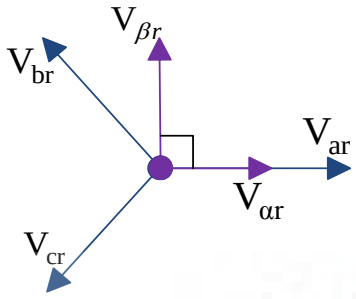

Fig. 2.2. Voltage quantities in stationary reference frame

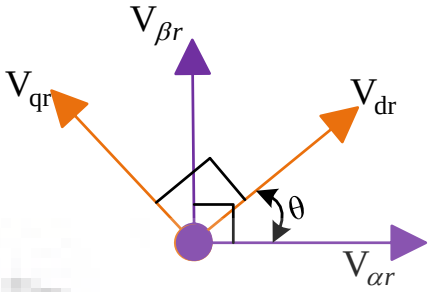

Fig. 2.3. Voltage quantities in rotating reference frame

Consider Fig. 2.3 and convert stationary two phase quantities (phase ‘α’ and phase ‘β’) into variable two phase quantities (phase ‘d’ and phase ‘q’) in a rotating reference frame with space vector at an angle ‘θ’.

$$V_{dr} = V_{\alpha r}\cos\theta + V_{\beta r}\cos(90\text{-}\theta) \tag{2.7}$$

$$V_{dr} = V_{\alpha r}\cos\theta + V_{\beta r}\sin\theta \tag{2.8}$$

$$V_{qr} = V_{\alpha r}\cos(270-\theta) + V_{\beta r}\cos\theta \tag{2.9}$$

$$V_{qr} = -V_{\alpha r}\sin\theta + V_{\beta r}\cos\theta \tag{2.10}$$

$$\text{where } \theta = \tan^{-1}\left[\frac{V_{\beta r}}{V_{\alpha r}}\right] \tag{2.11}$$

$$\text{From that, } \begin{bmatrix} V_{dr} \\ V_{qr} \end{bmatrix} = \begin{bmatrix} \cos\theta & \sin\theta \\ -\sin\theta & \cos\theta \end{bmatrix} \begin{bmatrix} V_{\alpha r} \\ V_{\beta r} \end{bmatrix} \tag{2.12}$$

Similarly, current and flux equations are given below,

$$\begin{bmatrix} I_{dr} \\ I_{qr} \end{bmatrix} = \begin{bmatrix} \cos\theta & \sin\theta \\ -\sin\theta & \cos\theta \end{bmatrix} \begin{bmatrix} I_{\alpha r} \\ I_{\beta r} \end{bmatrix} \tag{2.13}$$

$$\begin{bmatrix} \psi_{dr} \\ \psi_{qr} \end{bmatrix} = \begin{bmatrix} \cos\theta & \sin\theta \\ -\sin\theta & \cos\theta \end{bmatrix} \begin{bmatrix} \psi_{\alpha r} \\ \psi_{\beta r} \end{bmatrix} \tag{2.14}$$

Induced emf in stator and rotor windings can be obtained through the generalized model theory and Kroon’s primitive machine model (shown in Fig.2.4). From figure,

In stator side,

$$\vec{V}_{ds}^{a} = R_s \vec{I}_{ds}^{a} + \frac{d}{dt}(\vec{\psi}_{ds}^{a}) \tag{2.15}$$

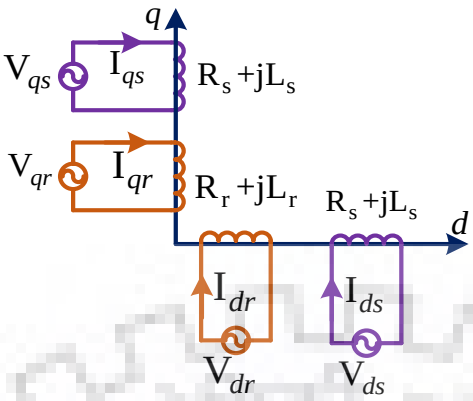

Fig. 2.4. Kroon's primitive machine model

$$\vec{V}_{qs}^{a} = R_s \vec{I}_{qs}^{a} + \frac{d}{dt}(\vec{\psi}_{qs}^{a}) \tag{2.16}$$

In rotor side,

$$\vec{V}_{dr}^{a} = R_r \vec{I}_{dr}^{a} + \frac{d\vec{\psi}_{dr}^{a}}{dt} \pm \omega_r \vec{\psi}_{qr}^{a} \tag{2.17}$$

$$\vec{V}_{qr}^{a} = R_r \vec{I}_{qr}^{a} + \frac{d\vec{\psi}_{qr}^{a}}{dt} \pm \omega_s \vec{\psi}_{dr}^{a} \tag{2.18}$$

In this system, q-axis rotor flux is helping the rotor voltage/induced emf and d-axis rotor flux is opposing the rotor voltage/induced emf. Therefore eqn. (2.17) and (2.18) can be rearranged as

$$\vec{V}_{dr}^{a} = R_r \vec{I}_{dr}^{a} + \frac{d\vec{\psi}_{dr}^{a}}{dt} - \omega_r \vec{\psi}_{qr}^{a} \tag{2.19}$$

$$\vec{V}_{qr}^{a} = R_r \vec{I}_{qr}^{a} + \frac{d\vec{\psi}_{qr}^{a}}{dt} + \omega_s \vec{\psi}_{dr}^{a} \tag{2.20}$$

Flux linkage produced in the stator and rotor windings are given by,

$$\vec{\psi}_{ds}^{a} = L_s \vec{I}_{ds}^{a} + L_m \vec{I}_{dr}^{a} \tag{2.21}$$

$$\vec{\psi}_{qs}^{a} = L_s \vec{I}_{qs}^{a} + L_m \vec{I}_{qr}^{a} \tag{2.22}$$

$$\vec{\psi}_{dr}^{a} = L_r \vec{I}_{dr}^{a} + L_m \vec{I}_{ds}^{a} \tag{2.23}$$

$$\vec{\psi}_{qr}^{a} = L_s \vec{I}_{qr}^{a} + L_m \vec{I}_{qs}^{a} \tag{2.24}$$

whereas, $L_s = L_m + L_{\sigma s}$ $\qquad$ $L_r = L_m + L_{\sigma r}$

Equations (2.15) to (2.24) are the generalized model equations of the induction machine.

In DFIM, synchronous rotating reference frame is used for the better dynamic control and the equations are rearranged as per the equivalent circuit (shown in Fig. 2.5) and it is given below,

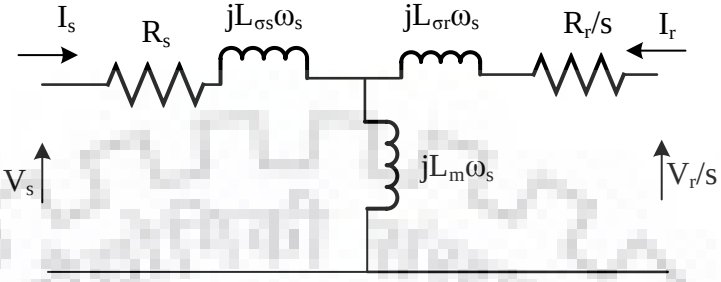

Fig. 2.5. One phase equivalent circuit of DFIM referred to stator

$$\vec{V}_{ds}^{a} = R_s \vec{I}_{ds}^{a} + \frac{d\vec{\psi}_{ds}^{a}}{dt} - \omega_s \vec{\psi}_{qs}^{a} \tag{2.25}$$

$$\vec{V}_{qs}^{a} = R_s \vec{I}_{qs}^{a} + \frac{d\vec{\psi}_{qs}^{a}}{dt} + \omega_s \vec{\psi}_{ds}^{a} \tag{2.26}$$

$$\vec{V}_{dr}^{a} = R_r \vec{I}_{dr}^{a} + \frac{d\vec{\psi}_{dr}^{a}}{dt} + \omega_r \vec{\psi}_{qr}^{a} - \omega_s \vec{\psi}_{qr}^{a} \tag{2.27}$$

$$\vec{V}_{qr}^{a} = R_r \vec{I}_{qr}^{a} + \frac{d\vec{\psi}_{qr}^{a}}{dt} - \omega_r \vec{\psi}_{dr}^{a} + \omega_s \vec{\psi}_{dr}^{a} \tag{2.28}$$

Flux linkages can be rewritten as

$$\vec{\psi}_{ds}^{a} = L_s \vec{I}_{ds}^{a} + L_m \vec{I}_{dr}^{a} \tag{2.29}$$

$$\vec{\psi}_{qs}^{a} = L_s \vec{I}_{qs}^{a} + L_m \vec{I}_{qr}^{a} \tag{2.30}$$

$$\vec{\psi}_{dr}^{a} = \sigma L_r \vec{I}_{dr}^{a} + \frac{L_m}{L_s} \vec{\psi}_{ds}^{a} \tag{2.31}$$

$$\vec{\psi}_{qr}^{a} = \sigma L_r \vec{I}_{qr}^{a} \quad 2.32)$$

$$\sigma = 1 - \left(\frac{L_m^{\,2}}{L_s L_r} \right)$$

By using the equations, stator and rotor power can be calculated as,

$$P_s = \frac{3}{2}\left(\vec{V}_{ds}^{a}\, \vec{I}_{ds}^{a} + \vec{V}_{qs}^{a}\, \vec{I}_{qs}^{a} \right) \tag{2.33}$$

$$Q_s = \frac{3}{2}\left(-\vec{V}_{ds}^{a}\, \vec{I}_{qs}^{a} + \vec{V}_{qs}^{a}\, \vec{I}_{ds}^{a} \right) \tag{2.34}$$

$$P_r = \frac{3}{2}\left(\vec{V}_{dr}^{a}\, \vec{I}_{dr}^{a} + \vec{V}_{qr}^{a}\, \vec{I}_{qr}^{a} \right) \tag{2.35}$$

$$Q_r = \frac{3}{2}\left(-\vec{V}_{dr}^{a}\, \vec{I}_{qr}^{a} + \vec{V}_{qr}^{a}\, \vec{I}_{dr}^{a} \right) \tag{2.36}$$

Electro-magnetic torque can be written as

$$T_{em} = \frac{3}{2}\, p \frac{L_m}{L_s}\left(-\vec{\psi}_{ds}^{a}\, \vec{I}_{qs}^{a} + \vec{\psi}_{qs}^{a}\, \vec{I}_{ds}^{a} \right) \tag{2.37}$$

And $T_L - T_e = J \dfrac{d\Omega_m}{dt}$ (2.38)

$$\int \frac{T_L - T_e}{J} = \Omega_m \tag{2.39}$$

And we know, $\Omega_m \times p = \omega_m$ (2.40)

$$\int \omega_m = \theta_e \tag{2.41}$$

$\theta_e \rightarrow$ Rotor position of machine.

When T_e is positive, it shows that the machine is in pumping mode and when T_e is negative it notices that the machine is operating under generation mode. Blcok diagram of the DFIM with input and ouput equations are shown in Fig. 2.6.

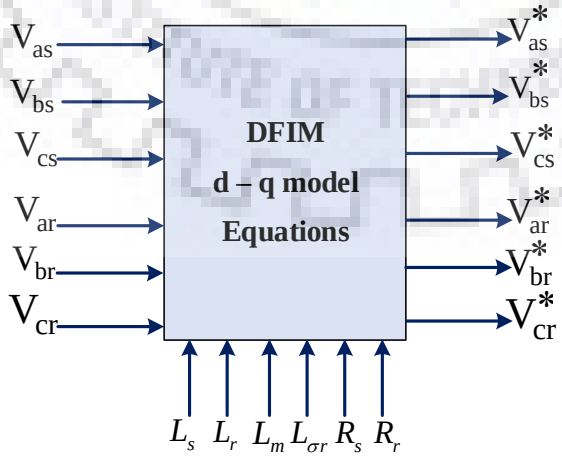

Fig. 2.6. Block diagram of d-q model of DFIM with input and output equations

2.3 Modelling of Back-to-Back Voltage Source Power Converter

2.3.1 Two Level VSC

Back-to-back voltage source converter are preferable in industrial applications since it provides flexible operation and lower harmonics. Fig. 2.7 shows the two level VSC topology. The generation of voltage in the converter are refereed to 'zero point' of the DC bus.

$$V_{jo} = V_{bus} S_{jg} \text{ with } S_{jg} \varepsilon (0,1) \text{ and } j=a,b,c \quad (2.42)$$

$$V_{ao} = V_{bus} S_{ag} \quad (2.43)$$

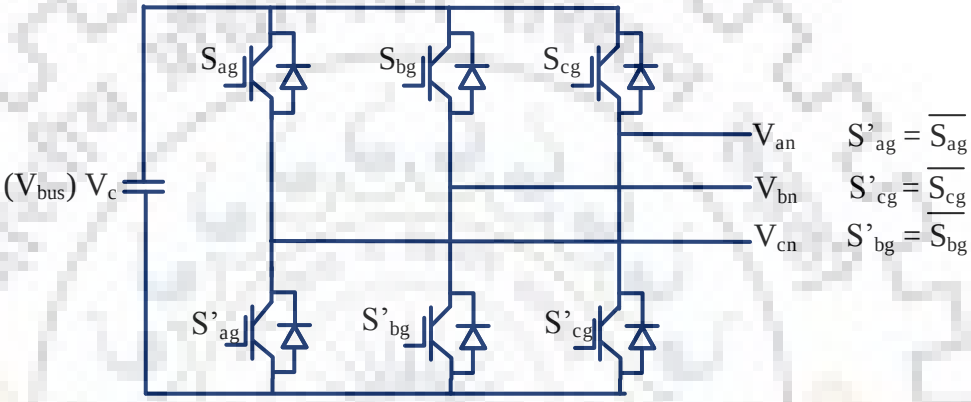

FIG. 2.7. Two level voltage source converter

Different combinations of S_{ag}, S_{bg}, S_{cg} create the output voltage with different amplitude and frequency. For the modelling purpose the converter output voltages referred to the neutral point of the grid three phase system.

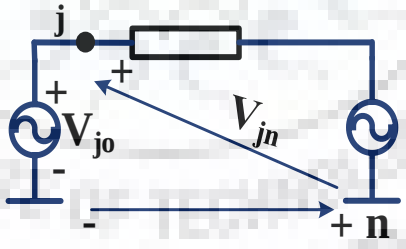

Fig.2.8. Equivalent circuit of single phase grid circuit

From the equivalent circuit (Fig. 2.8),

$$V_{jn} = V_{jo} - V_{no} \; ; \; j=a,b,c \quad (2.44)$$

$$V_{an} = V_{ao} - V_{no} \quad (2.45)$$

$$V_{bn} = V_{bo} - V_{no} \quad (2.46)$$

$$V_{cn} = V_{co} - V_{no} \quad (2.47)$$

Add eqn (45) to (47).

$$V_{ao} - V_{no} + V_{bo} - V_{no} + V_{co} - V_{no} = V_{an} + V_{bn} + V_{cn} \quad (2.48)$$

Assume as the balanced system, $V_{an} + V_{bn} + V_{cn} = 0$ (2.49)

$$V_{ao} + V_{bo} + V_{co} - 3V_{no} = 0 \quad (2.50)$$

$$V_{no} = \frac{V_{ao} + V_{bo} + V_{co}}{3} \quad (2.51)$$

Eqn (2.45) can be rewritten as

$$V_{an} = V_{ao} - \frac{V_{ao} + V_{bo} + V_{co}}{3} \quad (2.52)$$

$$V_{an} = \frac{2}{3} V_{ao} - \frac{1}{3}(V_{bo} + V_{co}) \quad (2.53)$$

Similarly,

$$V_{bn} = \frac{2}{3} V_{bo} - \frac{1}{3}(V_{ao} + V_{co}) \quad (2.54)$$

$$V_{cn} = \frac{2}{3} V_{co} - \frac{1}{3}(V_{bo} + V_{ao}) \quad (2.55)$$

Further the equations (2.53) to (2.55) can be simplified into

$$V_{an} = \frac{V_{bus}}{3}\left[2S_{ag} - S_{bg} - S_{cg}\right] \quad (2.56)$$

$$V_{bn} = \frac{V_{bus}}{3}\left[2S_{bg} - S_{ag} - S_{cg}\right] \quad (2.57)$$

$$V_{cn} = \frac{V_{bus}}{3}\left[2S_{cg} - S_{ag} - S_{bg}\right] \quad (2.58)$$

By applying the Fourier series the amplitude of the voltage is,

$$V_{an} = V_{bn} = V_{cn} = \frac{2V_{bus}}{3\pi x}\left[2 + \cos\left(x\frac{\pi}{3}\right) - \cos\left(x\frac{2\pi}{3}\right)\right] \quad (2.59)$$

Where $x = 1, 5, 7, 11, 13, \ldots$

With constant dc bus voltage, the fixed fundamental component is $\left(\frac{2V_{bus}}{\pi}\right)$. The amplitude and frequency can be modified with the help of pulses.

V_{ao} (pole voltage) **V_{ab} (line to line voltage)** **V_{an} (phase to neutral voltage)**

Fig.2.9. Output voltages of two level VSC

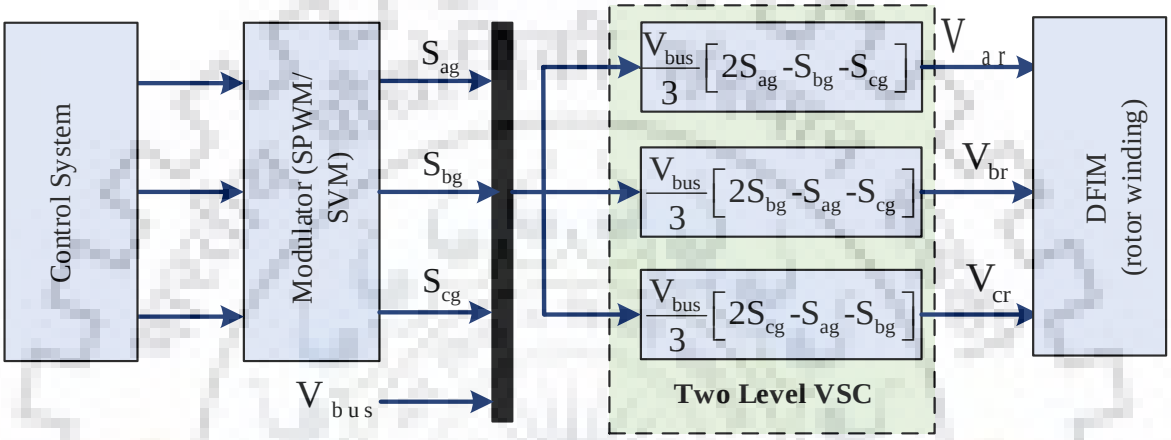

Fig.2.10. Simplified two level VSC model

Table 2.2.Output voltage combinations of two level VSC

S_{ag}	S_{bg}	S_{cg}	V_{ao}	V_{bo}	V_{co}	V_{an}	V_{bn}	V_{cn}
0	0	0	0	0	0	0	0	0
0	0	1	0	0	V_{bus}	$-\left(\frac{V_{bus}}{3}\right)$	$-\left(\frac{V_{bus}}{3}\right)$	$\left(\frac{2V_{bus}}{3}\right)$
0	1	0	0	V_{bus}	0	$-\left(\frac{V_{bus}}{3}\right)$	$\left(\frac{2V_{bus}}{3}\right)$	$-\left(\frac{V_{bus}}{3}\right)$
0	1	1	0	V_{bus}	V_{bus}	$-\left(\frac{2V_{bus}}{3}\right)$	$\left(\frac{V_{bus}}{3}\right)$	$\left(\frac{V_{bus}}{3}\right)$
1	0	0	V_{bus}	0	0	$\left(\frac{2V_{bus}}{3}\right)$	$-\left(\frac{V_{bus}}{3}\right)$	$-\left(\frac{V_{bus}}{3}\right)$
1	0	1	V_{bus}	0	V_{bus}	$\left(\frac{V_{bus}}{3}\right)$	$-\left(\frac{2V_{bus}}{3}\right)$	$\left(\frac{V_{bus}}{3}\right)$
1	1	0	V_{bus}	V_{bus}	0	$\left(\frac{V_{bus}}{3}\right)$	$\left(\frac{V_{bus}}{3}\right)$	$-\left(\frac{2V_{bus}}{3}\right)$
1	1	1	V_{bus}	V_{bus}	V_{bus}	0	0	0

The output voltages of V_{ao}, V_{bo}, V_{co} only take two different voltage level '0' and 'V_{bus}'. But the output voltages V_{an}, V_{bn}, V_{cn} takes the different voltage levels $-\frac{2V_{bus}}{3}, -\frac{V_{bus}}{3}, 0, \frac{V_{bus}}{3}, \frac{2V_{bus}}{3}$.

2.3.2 Three Level VSC

Three level VSC topologies are handling high power with accessible power semiconductor devices and desirable in high power applications. Further, it improves the quality of the output power and voltage. It generates output phase voltage waveforms V_{ao}, V_{bo}, V_{co} comprising three switching levels of amplitude $\left(0, \frac{V_{bus}}{2}, V_{bus}\right)$.

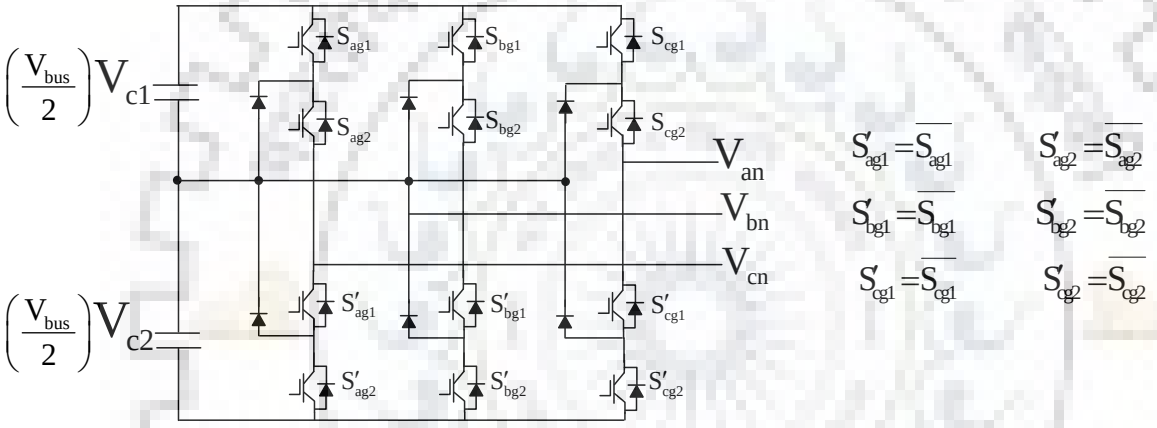

Fig.2.11. Three Level VSC

The output AC voltages of the 3LNPC referred to as the zero of the DC bus can be expressed as follows:

$$V_{ao} = V_{c1}S_{ag1} + V_{c2}S_{ag2} \quad (2.60)$$

$$V_{bo} = V_{c1}S_{bg1} + V_{c2}S_{bg2} \quad (2.61)$$

$$V_{co} = V_{c1}S_{cg1} + V_{c2}S_{cg2} \quad (2.62)$$

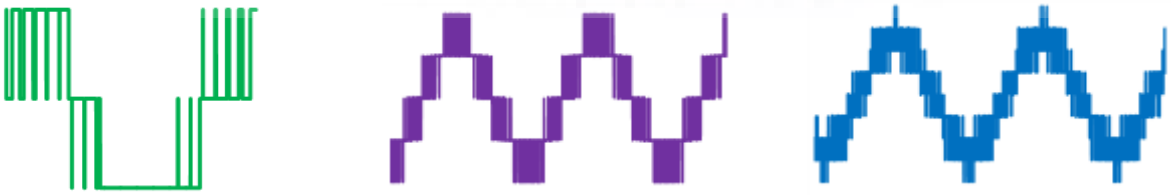

V_{ao}(pole voltage) **V_{ab}(line to line voltage)** **V_{an} (phase to neutral voltage)**

Fig.2.12. Output voltages of three level VSC

Further, phase voltage (V_{an}, V_{bn}, V_{cn}) of the three level VSC can be obtained as

$$V_{an} = \frac{V_{c1}}{3}\left[2S_{ag1}\text{-}S_{bg1}\text{-}S_{cg1}\right] + \frac{V_{c2}}{3}\left[2S_{ag2}\text{-}S_{bg2}\text{-}S_{cg2}\right] \quad (2.63)$$

$$V_{bn} = \frac{V_{c1}}{3}\left[2S_{bg1}\text{-}S_{ag1}\text{-}S_{cg1}\right] + \frac{V_{c2}}{3}\left[2S_{bg2}\text{-}S_{ag2}\text{-}S_{cg2}\right] \quad (2.64)$$

$$V_{cn} = \frac{V_{c1}}{3}\left[2S_{cg1}\text{-}S_{ag1}\text{-}S_{bg1}\right] + \frac{V_{c2}}{3}\left[2S_{cg2}\text{-}S_{ag2}\text{-}S_{bg2}\right] \quad (2.65)$$

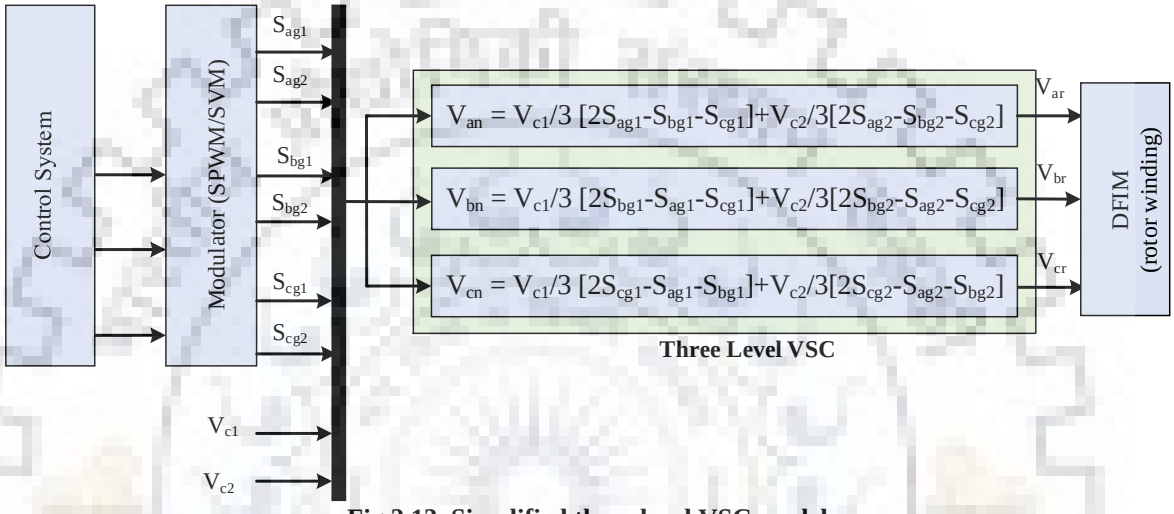

Fig.2.13. Simplified three level VSC model

2.3.3 Modulation Issues

A modulation technique generates gate signal for the power semiconductor of a converter and control the process fed by the converter. In this thesis, sinusoidal pulse width modulation (SPWM) scheme is implemented for controlling voltage source converters, since it is very simple and easy to implement by using digital technique in view of multi-channel converter fed large asynchronous machine drives. Modulation techniques have to deal with issues, such as maximum power-conversion efficiency, minimum harmonic distortion, costly efficient filters, and auxiliary control- tracking (dc-voltage-imbalance reduction, equalization of power losses, and equal power distribution). Since, switching frequency of converter is very low (300 Hz), phase shift transformer (five shifts) is adopted for harmonic reduction.

The voltage unbalance between the upper and lower capacitors is an important problem in the three-level PWM converter system. It is noted that zero sequence voltage injection technique is employed in SPWM for balancing dc link capacitor voltages.

DC link voltage balancing of the back-back NPC's are connected in parallel is also considered. The demagnetization current control technique is used to balance the DC link voltage in parallel converter during power switch failures.

As real time controller (DS1202) set-up is not supporting two carrier signals at a time. Therefore, modulating wave is splitted into two signals and it is used for controlling three level NPC with single carrier signal during experimentation.

2.3.4 DC Link Model

DC link is connected between grid side and rotor side converter. Energy stored in a capacitor tries to maintain the constant voltage in a dc link. DC link model can be derived based on dc bus voltage which depends on current flow through the capacitor.

$$V_{bus} = \frac{1}{C_{bus}} \int i_c dt \tag{2.66}$$

$$i_c = i_{rotor\_dc} - i_{grid\_dc} - i_{resistance} \tag{2.67}$$

$$i_{grid\_dc} = S_{a\_grid} i_{a\_grid} + S_{b\_grid} i_{b\_grid} + S_{c\_grid} i_{c\_grid} \tag{2.68}$$

$$i_{rotor\_dc} = -S_{a\_rotor} i_{a\_rotor} - S_{b\_rotor} i_{b\_rotor} - S_{c\_rotor} i_{c\_rotor} \tag{2.69}$$

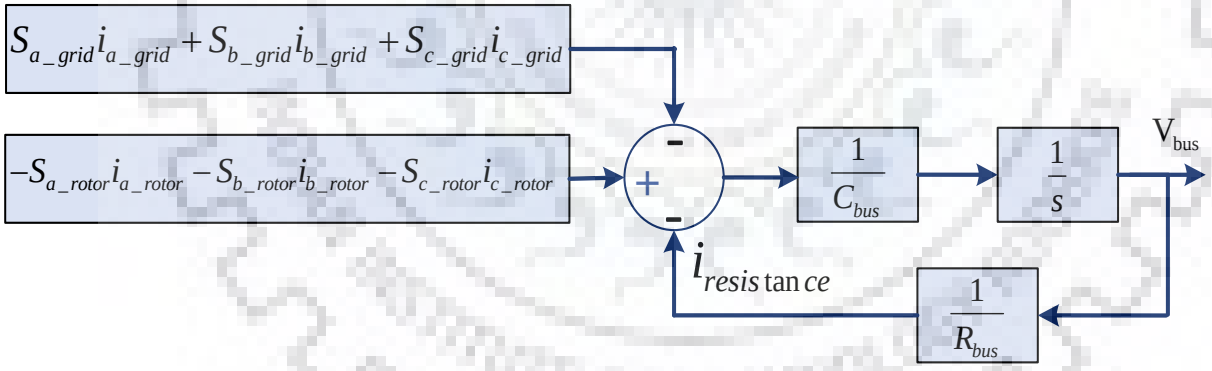

Fig.2.14. DC link model

2.3.5 Selection of Power converter rating

Back-to-back power converter rating is selected based on speed variation, rotor current and voltage of the machine. Moreover, excitation transformer is to be added in the rotor circuit is to reduce the size and rating of the converter. The rated voltage of the converter depends on slip (s) and it is calculated by,

$$V_{r\_c} = (\omega_s - \omega_r)\psi_{ds} \tag{2.70}$$

Converter power rating, $P_c = s\left(\frac{P_{load}}{1-s}\right)$ (2.71)

2.3.6 DC Link Voltage Selection

The selection of dc link voltage is based on the grid voltage, power factor and current rating of the rotor side machine. It is calculated by,

$$V_{bus} = 1.1\sqrt{3}V_{af} \quad (2.72)$$

$$V_{af} = \sqrt{\left(V_{ag} \pm R_f I_{ag}\right)^2 + \left(L_f \omega_s I_{ag}\right)^2} \quad (2.73)$$

In eqn. (2.72), constant term 1.1 is taken for the consideration of switching and conduction losses in power converters. The term (R_f.Iag) is addictive for the converter is delivering power to grid and it is subtracted for grid delivering power to converter.

2.3.7 DC Link Capacitance Selection

The selection of dc link capacitance is based on switching frequency, allowable ripple voltage in the dc link, dc link voltage, rating of the power converter and grid voltage. The selection of dc link capacitance (C) is estimated as given below,

$$C = \left[\frac{T_{SW}.P_{Converter}}{\Delta V_{dc}.V_{dc}}\right]\left[1 - \frac{V_{max(grid)}}{V_{dc}}\right]$$

2.4 Modelling of Sinusoidal Pulse Width Modulation

2.4.1 SPWM for Two Level VSC

SPWM technique is extensively used in voltage source converters. Low frequency (grid frequency) modulating signal (sinusoidal wave) is compared with the high frequency (switching frequency) carrier signal (triangular wave) in a logic device that provides PWM pulses, which in turn control the switching devices.

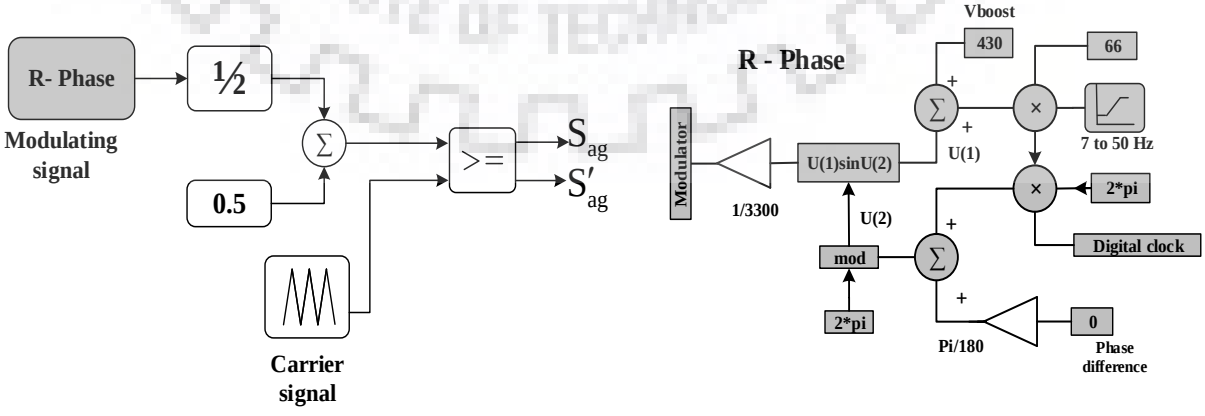

Fig. 2.15. SPWM for two level VSC

S_{jg} =1; if $V_{a\_modulatind\ signal} \geq V_{carrier\ signal}$ with j=a,b,c

2.4.2 SPWM for Three Level VSC

Sinusoidal PWM for three level is similar to the two level VSC. The modulating signal both upper and lower half cycle is distinctly compared with the carrier signal and produce the PWM pulses. The activation of switches are given below (S_{ag}=1 means device is ON).

S_{ag1}=1 if $V_{a\_modulating(upper)} \geq V_{carrier}$; S_{ag1}=0 if $V_{a\_modulating(upper)} \leq V_{carrier}$

S_{ag2}=1 if $V_{a\_modulating(lower)} \geq V_{carrier}$; S_{ag1}=0 if $V_{a\_modulating(lower)} \leq V_{carrier}$

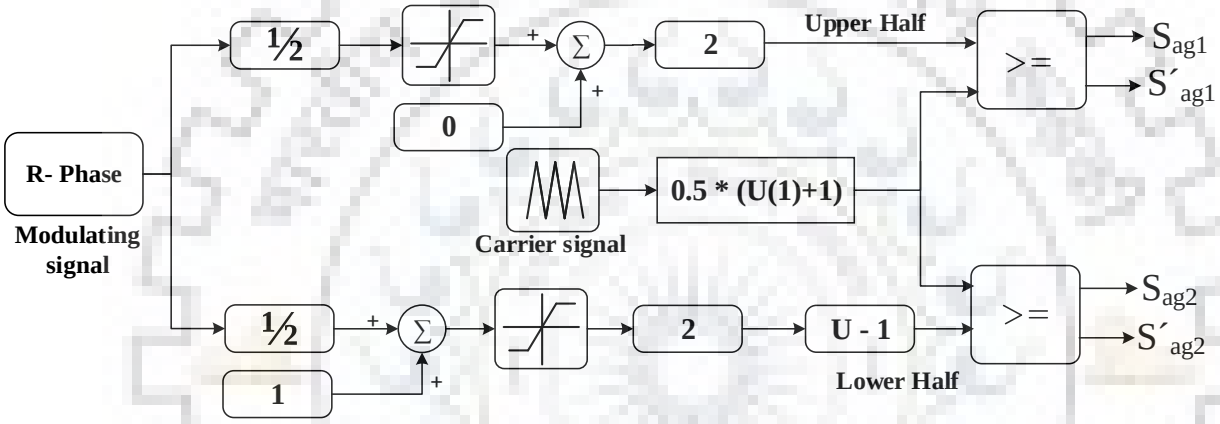

Fig. 2.16. SPWM for three level VSC

2.5 Grid Voltage Oriented Vector Control

Grid voltage oriented vector control in GSC ensure the decoupled control of DC link voltage (dc bus) and unity power factor [182]. Sinusoidal PWM/space vector modulation strategy can be used as modulation techniques in GSC. The three phase grid (a, b, c) vector quantities are converted into two phase (d-q) vector quantities by space vector theory; d-axis grid current control the active power flow to the DC bus through GSC which indirectly regulate the DC link voltage and q-axis grid current control the transfer of reactive power from grid to converter and vice-versa.

Space vector representation allows the derivation of the dynamic model of the grid side system. From simplified grid model diagram, three phase converter output voltage is given by,

$$\overrightarrow{V_{az}} = R_f \overrightarrow{I_{ag}} + L_f . \frac{d\overrightarrow{I_{ag}}}{dt} + \overrightarrow{V_{ag}} \qquad (2.74)$$

$$\overrightarrow{V_{bz}} = R_f \overrightarrow{I_{bg}} + L_f . \frac{d\overrightarrow{I_{bg}}}{dt} + \overrightarrow{V_{bg}} \quad (2.75)$$

$$\overrightarrow{V_{cz}} = R_f \overrightarrow{I_{cg}} + L_f . \frac{d\overrightarrow{I_{cg}}}{dt} + \overrightarrow{V_{cg}} \quad (2.76)$$

Convert three phase quantities into two phase quantities in a stationary reference frame by using Clarke transformation and is given by,

$$\overrightarrow{V_{\alpha z}}^{s} = R_f \overrightarrow{I_{\alpha g}}^{s} + L_f . \frac{d\overrightarrow{I_{\alpha g}}^{s}}{dt} + \overrightarrow{V_{\alpha g}}^{s} \quad (2.77)$$

$$\overrightarrow{V_{\beta z}}^{s} = R_f \overrightarrow{I_{\beta g}}^{s} + L_f . \frac{d\overrightarrow{I_{\beta g}}^{s}}{dt} + \overrightarrow{V_{\beta g}}^{s} \quad (2.78)$$

$(\rightarrow s)$ denotes space vectors referred to stationary reference frame.

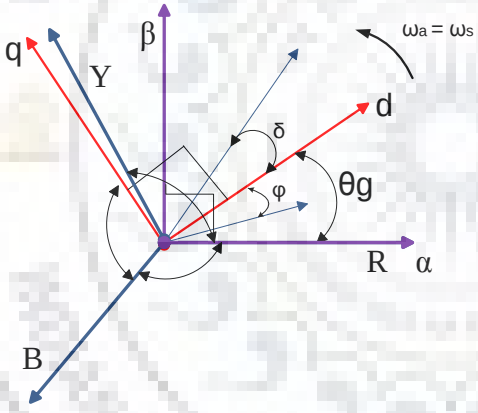

Fig. 2.17. Vector diagram of grid voltage oriented control

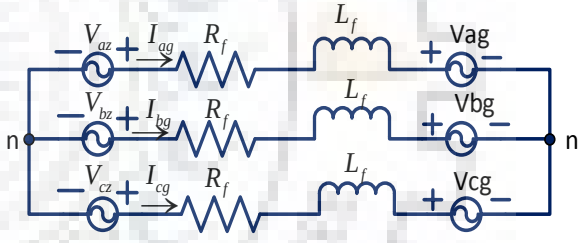

Fig.2.18. One phase equivalent circuit of DFIM referred to stator

Stationary two phase quantities are converting into rotating two phase quantities by using Park transformation referred to synchronous rotating frame with angular speed of ω_a and is given by

$$\overrightarrow{V_{dz}}^{a} = R_f \overrightarrow{I_{dg}}^{a} + L_f . \frac{d\overrightarrow{I_{dg}}^{a}}{dt} + \overrightarrow{V_{dg}}^{a} - \omega_a L_f \overrightarrow{I_{qg}}^{a} \quad (2.79)$$

$$\overrightarrow{V_{qz}}^{a} = R_f \overrightarrow{I_{qg}}^{a} + L_f . \frac{d\overrightarrow{I_{qg}}^{a}}{dt} + \overrightarrow{V_{qg}}^{a} + \omega_a L_f \overrightarrow{I_{dg}}^{a} \quad (2.80)$$

$(\rightarrow a)$ denotes space vectors referred to synchronously rotating reference frame.

In grid side system, synchronous rotating reference frame with angular speed ω_a is chosen during conversion of three phase quantities into rotating two phase quantity. In grid voltage oriented control (shown in Fig. 2.19): (i) angular speed of ω_a is chosen as angular speed of the grid voltage ω_s, (ii) d-axis rotating frame is aligning with grid voltage space vector. Hence,

$$\vec{V}_g^{\,a}\,\vec{V}_{dg}^{\,a} = \left|\vec{V}_g^{\,a}\right| \qquad \vec{V}_{qg}^{\,a} = 0; \qquad \omega_a = \omega_s \tag{2.81}$$

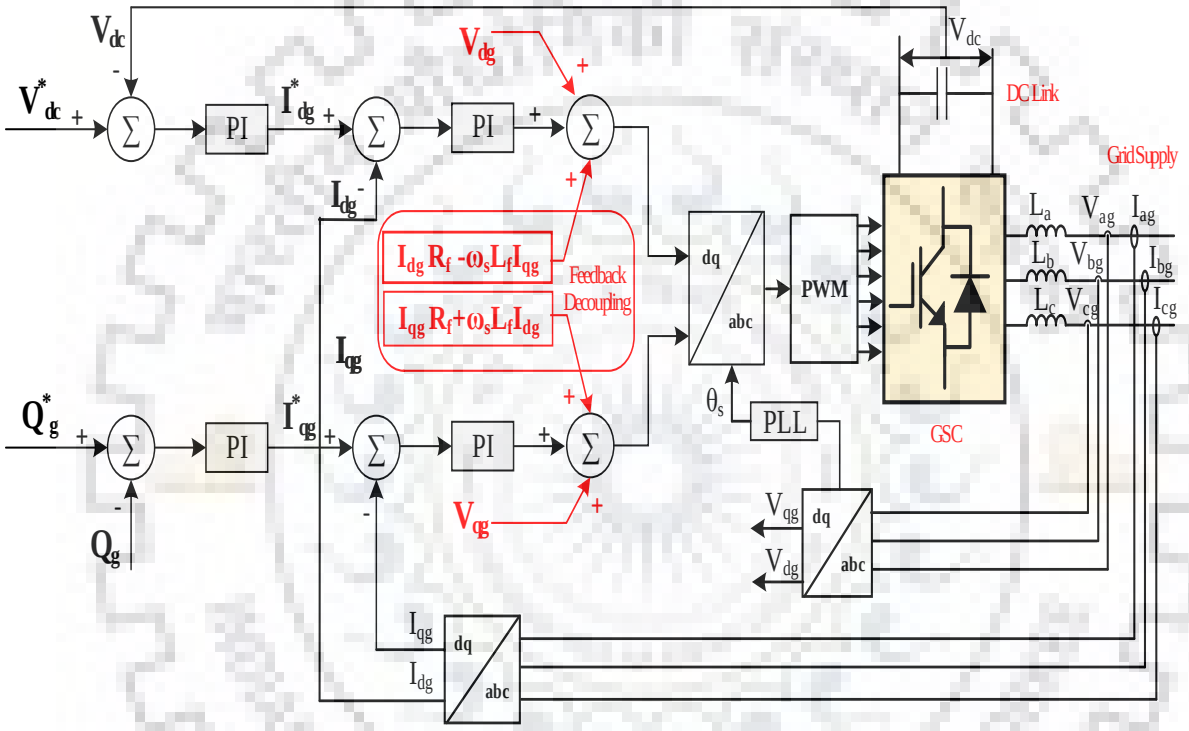

Fig. 2.19. Grid voltage oriented vector control for grid side converter

The converter output voltage equations are given as

$$\vec{V}_{dz}^{\,a} = R_f\,\vec{I}_{dg}^{\,a} + L_f.\frac{d\,\vec{I}_{dg}^{\,a}}{dt} + \vec{V}_{dg}^{\,a} - \omega_s L_f\,\vec{I}_{qg}^{\,a} \tag{2.82}$$

$$\vec{V}_{qz}^{\,a} = R_f\,\vec{I}_{qg}^{\,a} + L_f.\frac{d\,\vec{I}_{qg}^{\,a}}{dt} + \omega_s L_f\,\vec{I}_{dg}^{\,a} \tag{2.83}$$

Active and reactive power are calculated as

$$P_g = \frac{3}{2}.\left|\vec{V}_g^{\,a}\right|.\vec{I}_{dg}^{\,a} \tag{2.84}$$

$$Q_g = -\frac{3}{2}.\left|\vec{V}_g\right|.\vec{I}_{qg} \tag{2.85}$$

Eqn. (2.84) and eqn. (2.85) indicates that the d-axis grid current ($\vec{I}_{dg}$) controls the active power flow to the dc link which indirectly regulates dc link voltage and q-axis grid current ($\vec{I}_{qg}$) maintains rotor side input power factor at unity respectively. To maintain unity power factor at input of grid side converter, reference current of $\vec{I}_{qg}$ is chosen as zero. The reference d-axis and q-axis currents are obtained as below.

$$\vec{I}_{dg}^{\,*} = K_{p(V_{bus})}(V_{bus\_ref} - V_{bus}) - K_{I(V_{bus})}\int(V_{bus\_ref} - V_{bus}) \tag{2.86}$$

$$\vec{I}_{qg}^{\,*} = 0 \tag{2.87}$$

Inner current controller system used to derive d-axis and q-axis grid voltages from d-axis and q-axis grid currents reference, respectively. The generated d- axis and q-axis grid voltages are thereby transformed into three phase quantitates by inverse Park and Clarke transformation. Controlled three phase quantities are given to modulator to provide corresponding PWM pulses to control GSC, hence desired unity power factor and constant dc link linkage are achieved. The controlled d-axis and q-axis converter output voltage are as follows,

$$\left.\begin{aligned}\vec{V}_{dz}^{\,*} &= K_{p(i)}(\vec{I}_{dg}^{\,*} - \vec{I}_{dg}) - K_{I(i)}\int(\vec{I}_{dg}^{\,*} - \vec{I}_{dg}) - \omega_s L_f \vec{I}_{qg} \\ \vec{V}_{qz}^{\,*} &= K_{p(i)}(\vec{I}_{qg}^{\,*} - \vec{I}_{qg}) - K_{I(i)}\int(\vec{I}_{qg}^{\,*} - \vec{I}_{qg}) + \omega_s L_f \vec{I}_{dg}\end{aligned}\right\} \tag{2.88}$$

2.6 Stator Flux Oriented Vector Control

With the stator flux orientation, decoupled control between electro-magnetic torque and stator reactive power control is achieved. In stator flux oriented vector control (shown in Fig. 2.20), d-axis stator flux is aligning with stator flux space vector $\vec{\psi}_s$ in a synchronously rotating reference frame [14], [183 - 188].

$$\vec{\psi}_{ds} = \vec{\psi}_s \qquad \vec{\psi}_{qs} = 0 \qquad \vec{\psi}_s = L_m.\vec{I}_{ms} \tag{2.89}$$

Also, stator flux is proportional to grid voltage, therefore

$$\vec{V}_{ds}^{\,*} = 0 \qquad \vec{V}_{ds}^{\,*} = \vec{V}_s^{\,*} = \omega_s \vec{\psi}_{ds} \tag{2.90}$$

Stator and rotor voltage equations are given as,

$$\vec{V}_{ds}^{a\,*} = R_s \vec{I}_{ds}^{a} + L_m \frac{d\vec{I}_{ms}^{a}}{dt}\;; \qquad \vec{V}_{qs}^{a\,*} = R_s \vec{I}_{qs}^{a} + \omega_s L_m . \vec{I}_{ms}^{a} \tag{2.91}$$

$$\left.\begin{aligned} \vec{V}_{dr}^{a\,*} &= R_r \vec{I}_{dr}^{a} + \sigma L_r \frac{d\vec{I}_{dr}^{a}}{dt} - \omega_{sl}\sigma L_r \vec{I}_{qr}^{a} \\ \vec{V}_{qr}^{a\,*} &= R_r \vec{I}_{qr}^{a} + \sigma L_r \frac{d\vec{I}_{qr}^{a}}{dt} + \omega_{sl}\frac{L_m^{\,2}}{L_s}\vec{I}_{ms}^{a} + \omega_{sl}\sigma \vec{I}_{dr}^{a} \end{aligned}\right\} \tag{2.92}$$

Similarly, the expression of electro-magnetic torque and reactive power can be derived as

$$T_{em} = -\frac{3}{2}.p.\frac{L_m}{L_s}\frac{\vec{V}_s^{a}}{\omega_s}\vec{I}_{qr}^{a} \tag{2.93}$$

$$Q_s = \frac{3}{2}\left(\frac{\vec{V}_s^{a\,2}}{\omega_s L_s} - \vec{V}_s^{a}\frac{L_m}{L_s}\vec{I}_{dr}^{a}\right) \tag{2.94}$$

Eqn. (2.92) and eqn. (2.93) indicates that q-axis rotor current ($\vec{I}_{qr}^{a}$) allows to control the electro-magnetic torque which indirectly regulates speed and d-axis rotor current ($\vec{I}_{dr}^{a}$) controls the stator reactive power respectively. Further, cross coupling terms (shown in Eqn.2.92) in rotor voltage equations are enhancing the dynamic performance of controllers.

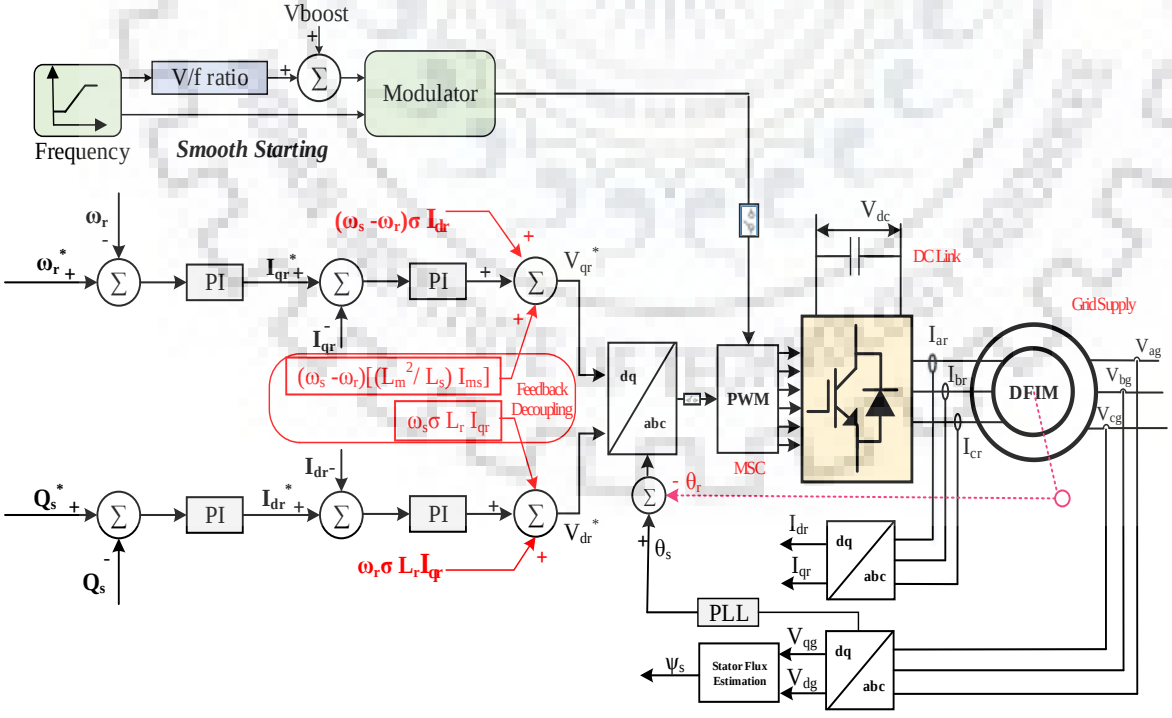

Fig. 2.20. Stator flux oriented vector control for DFIM

RSC control involves four control loops: two inner current control loops and two outer loops for controlling speed and reactive power. The outer control loops are deriving reference d-axis and q-axis rotor currents corresponding to the speed and reactive power reference, respectively. These reference currents are given as input to inner current controllers. The reference d-axis and q-axis currents are derived as,

$$\left\{\begin{array}{l} \vec{I}_{qr}^{a\,*} = K_{p(\omega_r)}(\omega_{r\_ref} - \omega_r) - K_{I(\omega_r)}\int(\omega_{r\_ref} - \omega_r) \\ \vec{I}_{dr}^{a\,*} = K_{p(Q_s)}(Q_{s\_ref} - Q_s) - K_{I(Q_s)}\int(Q_{s\_ref} - Q_s) \end{array}\right\} \quad (2.95)$$

Afterward, inner current controller generates d-axis and q-axis rotor voltages, transformed into three phase quantities by inverse Park and Clarke transformation. Controlled three phase quantities are given to modulator to provide corresponding PWM pulses to control RSC, hence desired speed and reactive power are attained. The controlled d-axis and q-axis rotor voltage are generated as,

$$\left\{\begin{array}{l} \vec{V}_{dr\_new}^{a\,*} = K_{p(i)}(\vec{I}_{dr}^{a\,*} - \vec{I}_{dr}^{a}) - K_{I(i)}\int(\vec{I}_{dr}^{a\,*} - \vec{I}_{dr}^{a}) - \omega_{sl}\sigma L_r \vec{I}_{qr}^{a} \\ \vec{V}_{qr\_new}^{a\,*} = K_{p(i)}(\vec{I}_{qr}^{a\,*} - \vec{I}_{qr}^{a}) - K_{I(i)}\int(\vec{I}_{qr}^{a\,*} - \vec{I}_{qr}^{a}) + \omega_{sl}\frac{L_m^{\,2}}{L_s}\vec{I}_{ms}^{a} + \omega_{sl}\sigma\vec{I}_{dr}^{a} \end{array}\right\} \quad (2.96)$$

2.7 Volts/hertz Control

The energy consumption, maximum torque and inrush current during starting of the machine depends on flux developed and is control based on the ratio of voltage and frequency as shown in eqn. (2.98) & eqn. (2.99). In V/f control, selection of: (i) voltage boost, (ii) frequency start-up, (iii) v/f ratio, are the important considerations for maintaining a constant torque and to reduce inrush current during starting. The desired V/f control reference signal is generated by voltage/angle ramp method. The reference signal is compared with a carrier signal for generating PWM pulses for RSC results to smooth starting/regenerative braking of the machine.

$$F_{start-up} = \left[\frac{T_{e\_start}}{T_{e\_rated}}\right] * f_{sl(rated)} \quad (2.97)$$

$$T_{e(\max)} = \left(\frac{V_r}{f_r}\right)^2 \quad (2.98)$$

$$\left(\frac{V_r}{f_r}\right) = \varphi_r \quad (2.99)$$

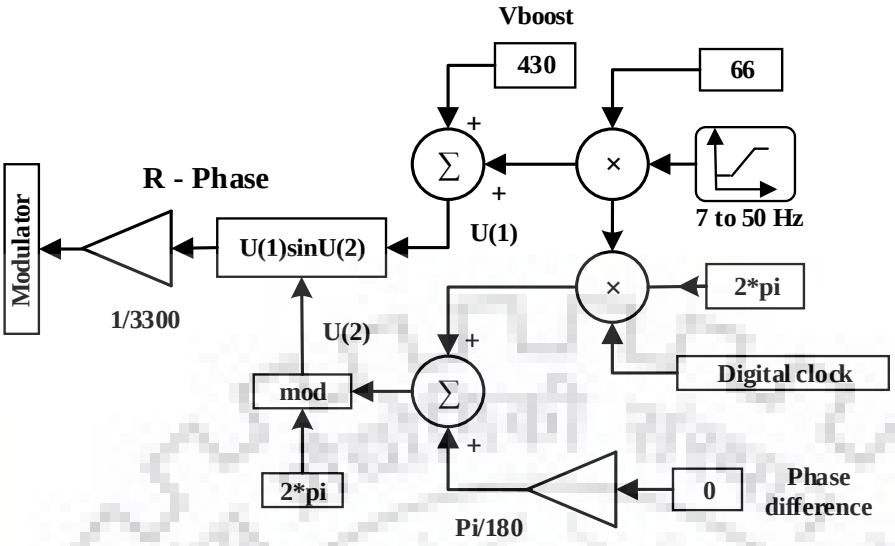

Fig.2.21. V/f control diagram

2.8 Active Current Sharing Control for Parallel Converters

Active Current Sharing (ACS) method is well suited to parallel converters power sharing in large rated variable speed PSPP. Combination of current sharing control system and individual control system in each converter provides better current/power sharing among converters. In which, (i) current sharing control system collects current from the load and share the equal current to the converters, (ii) individual control system precisely control the shared current in each converter and it consists of three control loops namely voltage control loop, current control loop and inner current sharing control loop. Compared to the single converter vector control, parallel converters vector control additionally have inner current sharing control loop which precisely control the shared current among converter.

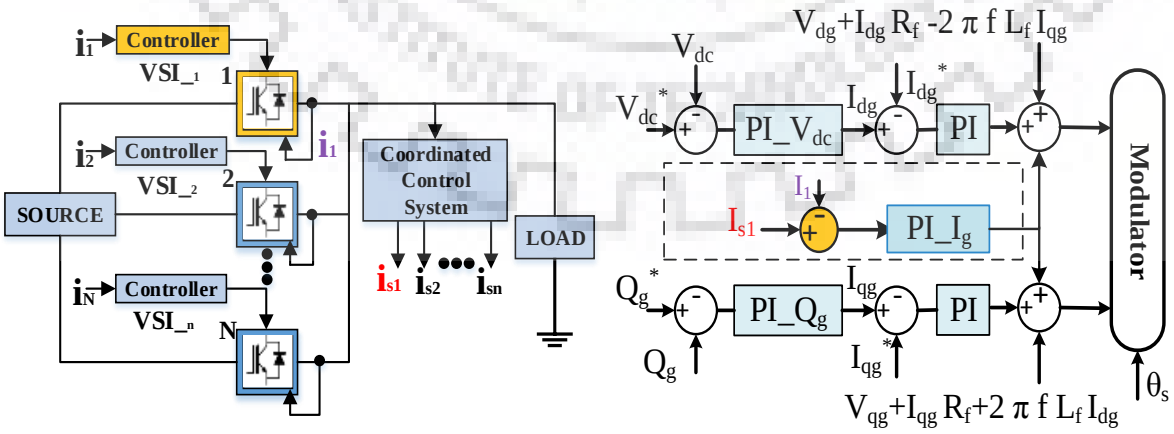

Fig.2.22. Active current sharing control

2.9 Modelling of Power and Control Circuit Faults

Faults in RSC (single device/single leg open), PWM pulses to the converter, and sensors (current, voltage, and speed), are considered. Converter faults include open circuit, short circuit, and dc link short circuit. Sensor faults are referred to rotor current sensors, encoder and reactive power signal. These sensor faults includes open circuit/omission (loss of signal), incorrect gain, constant value/saturation (unresponsive signal) and bias. The faults are summarized in Table 2.3.

Table 2.3. Leading faults in DFIM drive under converter and sensors

	Rotor current sensor	Reactive Power signal	Speed sensor	RSC
Fault Types	Omission	Omission	Omission	Open circuit
	Gain	Gain	Gain	Short circuit (SC)
	Saturation	Saturation	Saturation	DC link SC
	Bias	-	-	Phase to ground

Open circuit fault in a power device (switch) is modelled by removing gate signal in a particular device by an external control switch. Likewise, short circuit fault is modelled by creating a short circuit across the device. In sensor faults, omission fault is modelled by interrupting sensor feedback signal.

Table 2.4. Values used with sensor faults

Sensor Fault Type	Reactive power signal	Rotor current sensor	Speed sensor
Gain	$1.5\,Q_{ref}$	$1.5\,I_r$	$1.5\,\omega_r$
Saturation	$0.6\,Q_{ref}$	$0.6\,I_r$	$0.6\,\omega_r$
Bias	-	$0.05\,I_r + I_r$	-

The gain fault is modelled by connecting a gain block in series with sensor signal. Saturation fault is modelled by assigning a constant block in sensor signal. Bias fault is modelled by adding an addition/subtraction block in series with sensor signal. Table 2.4 shows the values of gain, saturation, and bias used in the present studies.

DFIM drive performance is assessed based on performance bounds. These bounds should consider the safety of the machine drive, energy consumption and transient of voltage/current, etc. Performance bounds include the acceptable limits of rotor current, stator current, machine speed and settling time of controllers. After every fault, continuity of operation of machine drive is assessed based on performance bounds. The performance bounds are considered in accordance with machine rating and its operating characteristics.

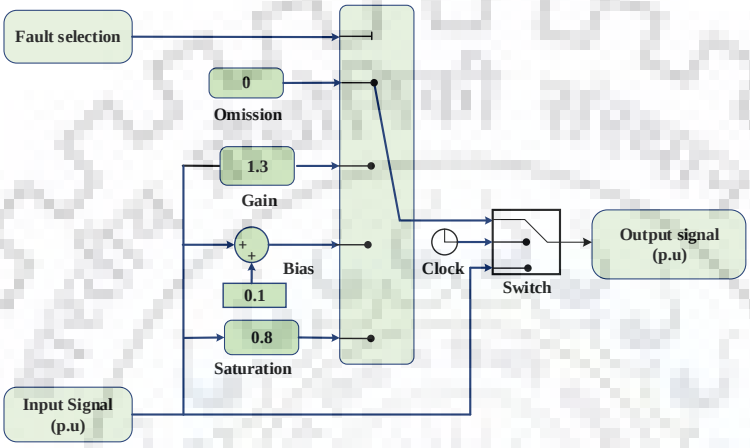

Fig.2.23. Modeling of sensor fault type

Test platform is developed to analyze the dynamic behavior of faults and their effects in the machine drive. Performance related parameters are measured and compared with their acceptable limits because of: (i) increase in current and dc link voltage of power converter above the rated value affects the safety and longtime availability of the converter, (ii) increase in speed of the machine takes more power from the grid. It is not acceptable since consuming more than surplus power is not reliable to the power grid, (iii) increase in current of the machine above the rated value affects the safety and longtime availability of the windings. If all parameters are within the limit then the machine drive is considered as survived state; otherwise, it is assumed as failed.

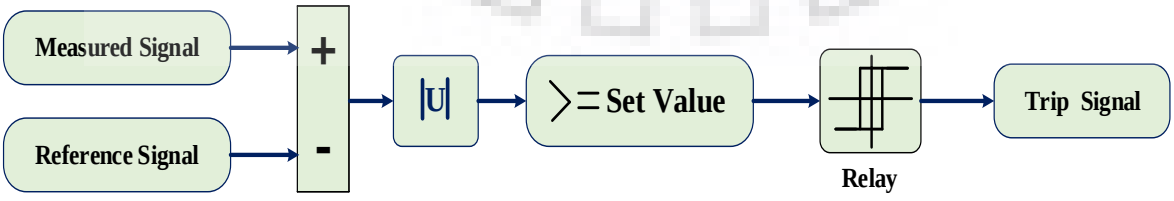

Fig.2.24. Modeling of test platform

2.10 Simulation Model

In order to demonstrate the power converter and control circuit failure, a 250 MW DFIM is simulated in MATLAB/Simulink environment. 400 kV, 50Hz ac source is considered as the grid and it is stepped down to 15.75 kV through power transformer. In rotor side, excitation transformer is used to step down the voltage from 15.75 kV to 3.3 kV and secondary is connected to the back-to-back voltage source power converter. In the simulation, the machine is controlled to operate at rated power generation (250 MW) and energy storage (250 MW) at generation and pumping mode respectively. The switching frequency of RSC is selected as 300Hz; dc link voltage of the two level back-to-back voltage source converter is maintained at 5000V by GSC with the switching frequency of 500Hz. The sampling time is selected as 5e-4s. The value of dc link capacitance is selected as 18000μF to withstand the rotor currents. Voltage source back-to-back converter connected to rotor side provides smooth starting of the machine. Maximum voltage (P-P) applied to the rotor winding during starting is 3080 volts, in view of acceleration and no-load losses.

Table. 2.5. Machine parameters of 250 MW DFIM (26 poles, 230.77 rpm, 50 Hz)

Stator voltage	15.75 kV	Rotor inductance	5.07 mH
Stator current	11.25 kA	Stator leakage inductance	0.38 mH
Rotor voltage	3.3 kV	Rotor leakage inductance	0.52 mH
Rotor current	11.6 kA	Magnetizing inductance	4.55 mH
Stator resistance	2.52 mΩ	Moment of Inertia	4.6 e^6 kgm^2
Rotor resistance	1.04 mΩ	Friction of coefficient	0.006kgm^2/s
Stator inductance	4.94 mH	Sampling Time	0.1 ms
AC excitation system for 250 MW DFIM			
AC Excitation VSI Transformer			
Nominal power	25 MVA	Primary Voltage	15.75 kV
Secondary Voltage	5X 3AC 3050 V	Grid Frequency	50 Hz
Vector Group	Yd1 (-12 ^{0}) d1 (-6^0) d1 (0^0) d1 (+6^0) d1 (+12^0)).		
5 Channel-Three level VSI Back-to-Back Power module (GE MV7311)			
Output Voltage	3 AC/ (0-3.3) kV	Frequency	0 to 90 Hz
V_{dc}	5000 V (18000 μF)	GSC/RSC	30-Pulse
GSC switching Frequency	500 Hz	RSC switching Frequency	300 Hz
Semiconductor Switch	Toshiba IEGT (ST2100GXH24A)		

The performance bounds of the 250MW DFIM drive is considered as follows: (i) allowable reactive power variation is ± 0.05 p.u, (ii) allowable speed variation is ± 0.03 p.u, (iii) dc link voltage variation is ± 0.1 p.u, (iv) rotor side grid current variation up to 0.05 p.u, (v) stator current variation up to 0.05 p.u, (vi) machine rotor current variation up to 0.05 p.u (vii) controller settling time is less than 250ms. Machine and Excitation system Parameters are given in Table 2.5. Matlab/Simulink model created for this research is given between Fig. 2.25 and Fig. 2.26.

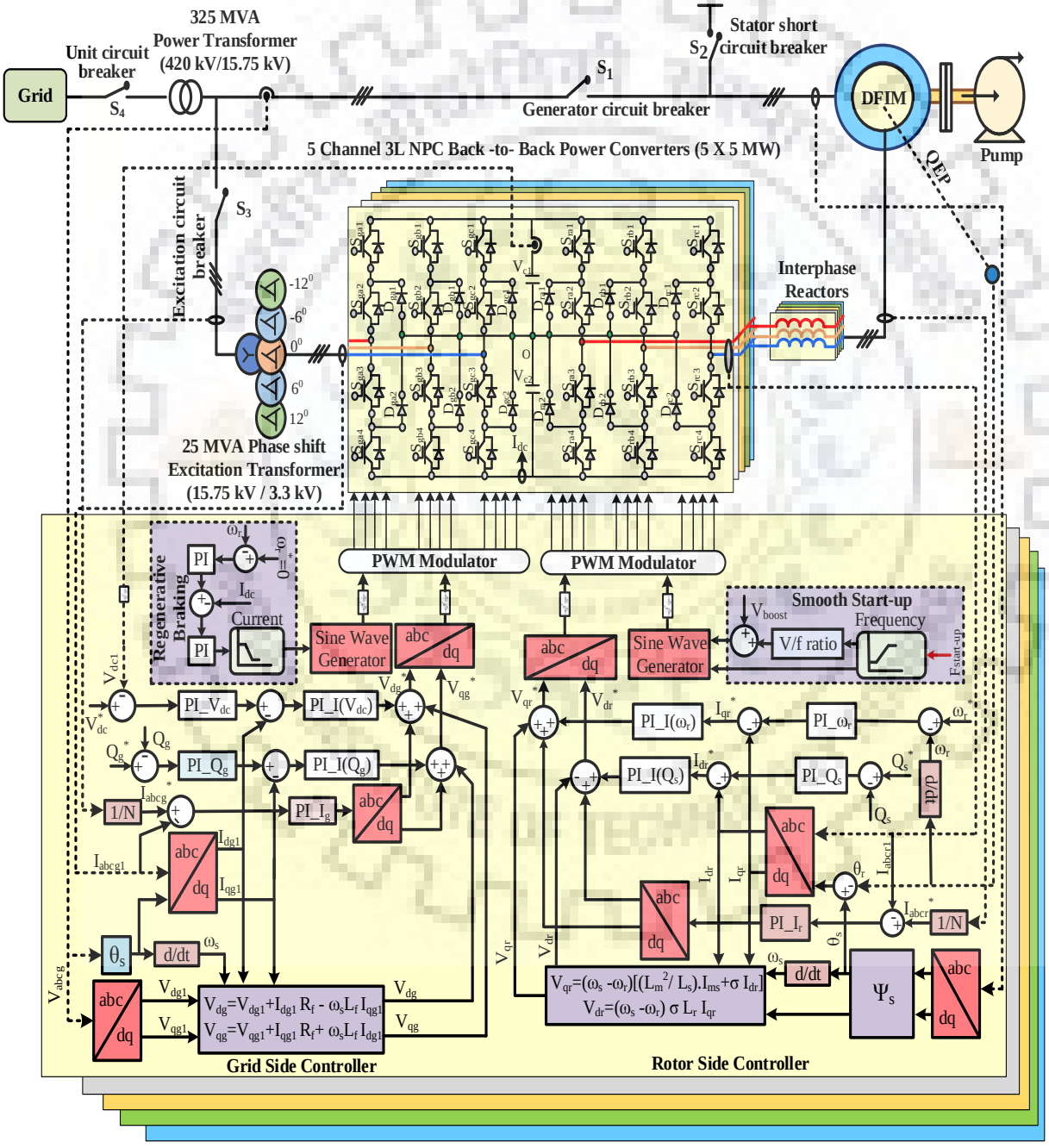

Fig.2.25. Control diagram of DFIM with parallel converters

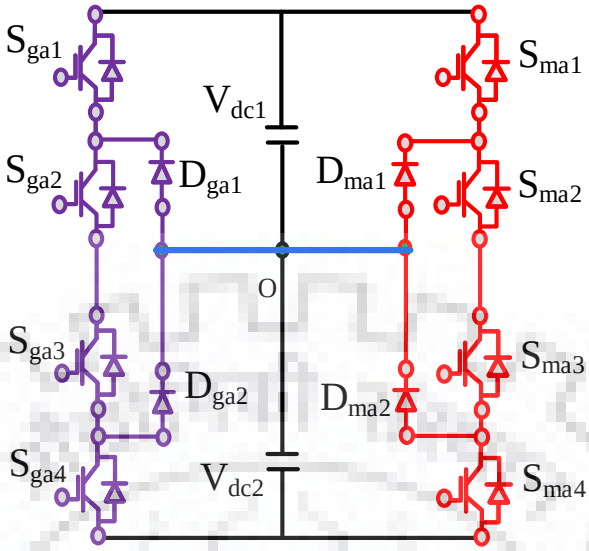

Fig.2.26. Three level back-to-back voltage source converter

2.11 Experimental Set-Up

A 2.2 kW DFIM is tested to validate the effectiveness of pumping, generation and condenser modes of DFIM with power and control circuit faults. The experiments are performed with two parallel connected three level neutral point clamped back-to-back voltage source converter (3L-NPC) with DFIM are shown in Fig. 2.27. The control actions are performed through DS1102 (dSPACE Microlab Box) real time controller. In addition, the prototype comprises of Hall Effect current sensor, voltage sensor, and Quadrature Encoder Pulse (QEP) type encoder (1024 pulses per revolution) for speed and position measurements, the feedbacks of which are integrated to ADC channel in real time controller. The control algorithm is designed in MATLAB/Simulink environment and it is dumped in real time controller. The proposed control algorithm generates Sine PWM with dead band of 6μs to drive both GSC and RSC. The stator short circuit breaker and generator circuit breaker are controlled by the real time controller.

The equal load current distribution among the parallel inverters are obtained through current sharing reactors $L_1 = L_2 = 2$ mH. In experimental validation, a separately excited dc machine (5 kW) is used as prime mover or load to DFIM. Hydro-turbine characteristics are matched by controlling the torque of the dc machine. The experimental set-up parameters are listed in Table 2.6. During super synchronous and sub-synchronous operation of DFIM at

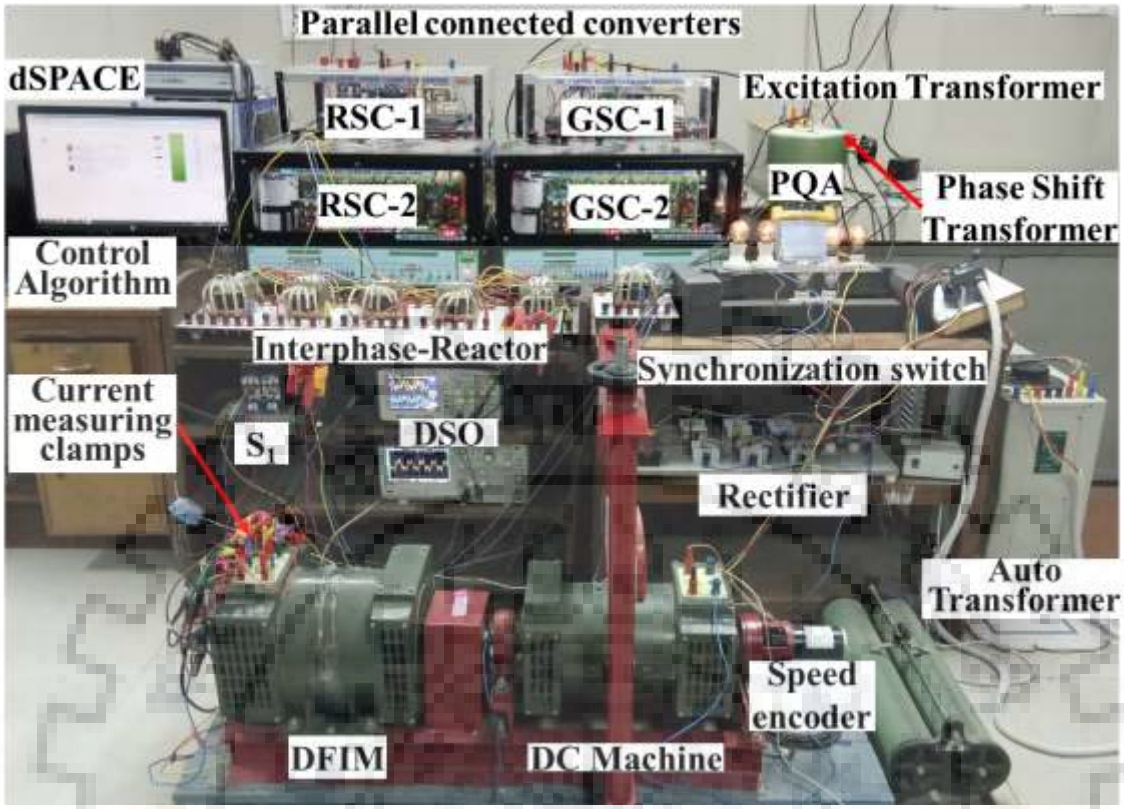

Fig. 2.27 (a) Experimental set-up

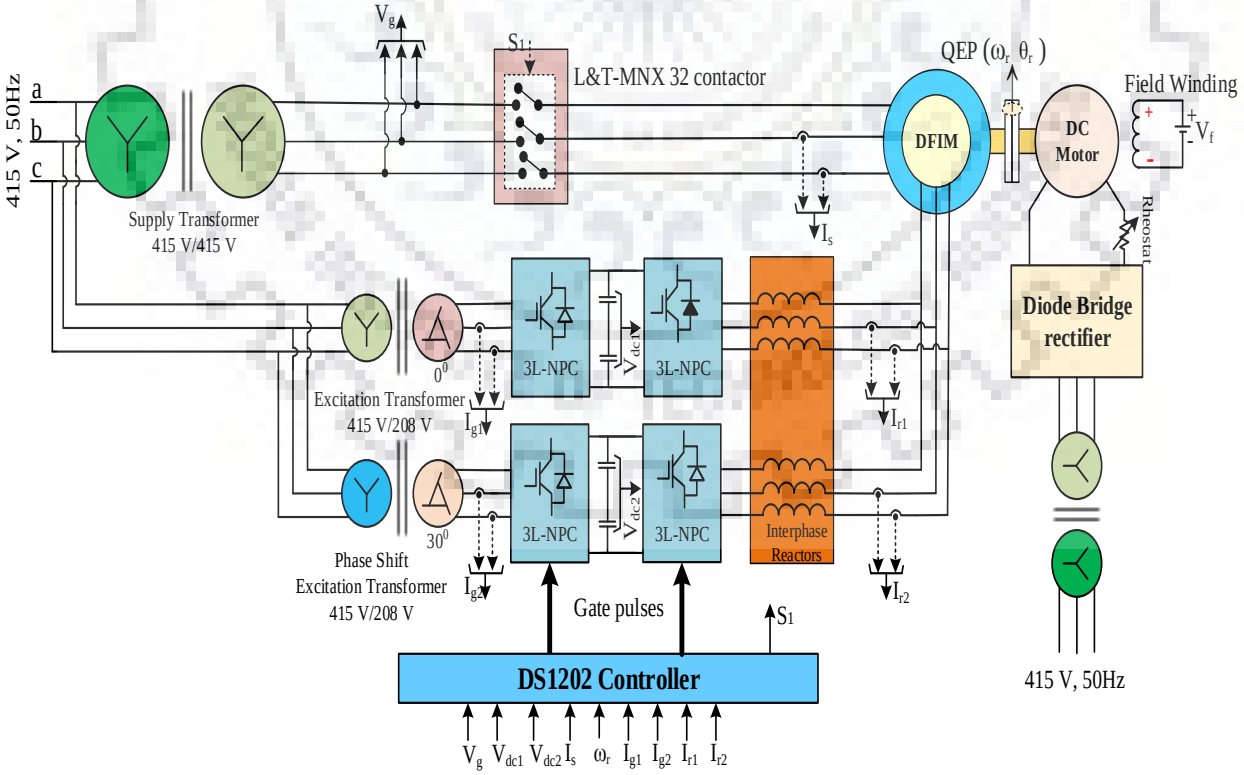

Fig. 2.28 (b) Experimental block-diagram

Table 2.6. Machine Parameters of 2.2 kW DFIM (4 poles, 1460 rpm)

Stator voltage	415 V	Rotor inductance	306.82 mH
Stator current	4.7 A	Stator leakage inductance	24.87 mH
Rotor voltage	185 V	Rotor leakage inductance	24.87 mH
Rotor current	7.5 A	Magnetizing inductance	281.96 mH
Stator resistance	3.678 Ω	Moment of Inertia	0.014 kgm^2
Rotor resistance	5.26 Ω	Friction of coefficient	0.03kg m^2/s
Stator inductance	306.82 mH	Sampling Time	0.001s
AC Excitation for 2.2 kW DFIM			
Nominal power	3 KVA	Primary Voltage	3 AC 415 V
Secondary Voltage	2X 3AC 185 V	Grid Frequency	50 Hz
Vector Group	YY (0^0) Yd1 ($+30^0$)		
2 Channel-Three level VSI Back to Back Power module			
Output Voltage	3 AC/ (0-185) V	Frequency	0 to 70 Hz
V_{dc}	450 V (4700 µF)	GSC/RSC	12-Pulse
GSC switching Frequency	5 kHz	RSC switching Frequency	3 kHz
Semiconductor Switch	SEMIKRON 2 IGBT (SKM100GB12T4)		

pumping, generation and condenser modes of operation, dc link voltage of back-to-back three level converter is maintained at 325 V and the sample time is selected 0.001 s. In consideration of machine rating, duration for smooth starting and regenerative braking are selected as 96 s.

2.12 Conclusion of the Chapter

Mathematical modelling of DFIM with power and control circuit faults is presented. Dynamic model is described in this chapter is one of the required background tool. Real and reactive power control of DFIM is explained with equations and control diagrams. Further, simulation and experimental test parameters are given.

This page is intentionally left blank

Chapter III

Starting and Braking of a Large Variable Speed PSPP

[This chapters presents the procedure for smooth starting and regenerative braking of a large rated DFIM pump turbine unit to be commissioned in Tehri PSPP. In addition, starting and braking behaviors of DFIM unit are assessed under power converter and control circuit faults. Survivability of the unit is analyzed based on: (i) current, (ii) speed, (iii) dc link voltage. Further it presents the total time required to changeover from generation to pumping mode for a 250 MW DFIM. This chapter also investigates fault tolerant operation of 250 MW DFIM pump turbine at converter fault in consideration of available water head. At the end of this chapter, it discussed the energy efficient smooth starting of DFIM fed pump-turbine, which shall be conserved 35% of the electrical energy in comparison with conventional smooth starting method]

3.1 Introduction

In DFIM, rotor side power converters act as excitation system and facilitate smooth starting and stopping of the unit. The usage of cycloconverter in DFIM unit was prominent in the past and it has been started by using external static frequency converters (SFC) during pumping mode. However, presently cycloconverters are not preferred in PSPP applications as with advancement in power electronics technology, now back-to-back voltage source converter gives better current waveform and lesser THD. In addition, this converter is used for smooth starting and dynamic/regenerative braking of unit in pumping mode and there is no requirement of SFC (Fig. 3.1).

Starting of small and medium rated DFIM during motoring mode is well known by the literature in a Ref [25]. However, this thesis discusses starting and braking of a large DFIM (250 MW) with 3-level VSC fed pump turbine in variable speed hydrogenerating unit which helps the project authorities to know the time required for smooth starting and braking for better management of grid operation and energy balancing. It may be noted that DFIM needs more attention during starting and braking (regenerative) as it is designed with more inertia than synchronous machines. Initial (boost) voltage is calculated based on torque-speed characteristics of DFIM for V/f control at rotor side. Transients in stator and rotor currents during opening of stator short circuit (SSC) and grid synchronization are investigated. Minimum rotational speed

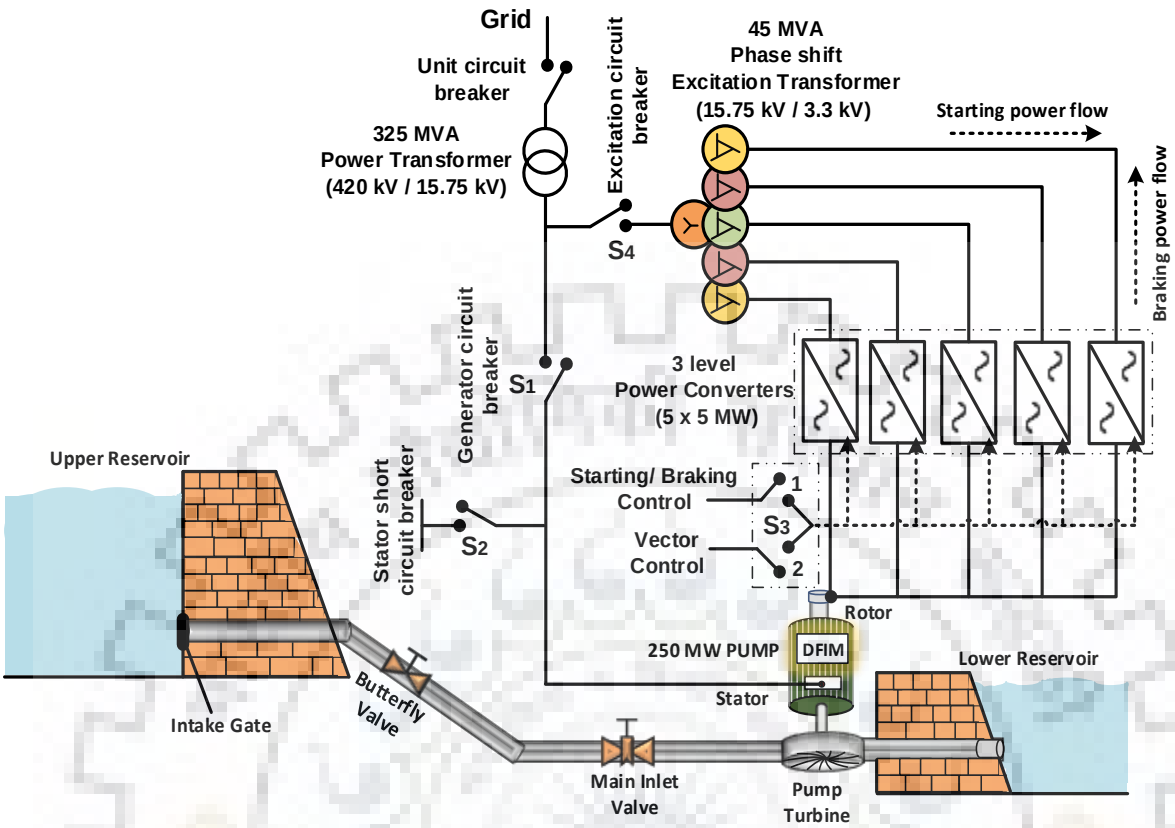

Fig.3.1. Hydrological and electrical depiction of a 250 MW variable speed hydrogenerating unit – Starting & Braking

of DFIM during synchronization process (removal of SSC and switch-in to grid) is estimated as 103% of synchronous speed.

3.2 Smooth Starting and Regenerative Braking of DFIM Hydrogenerating Unit

In India, grid operation is planned for every 15 minutes. Time required during smooth starting and regenerative braking of large rated DFIM unit plays an important role in transition from generating to pumping mode and vice versa. Hydraulic diagram with electrical circuit of a 250 MW variable speed hydrogenerating unit is shown in Fig. 3.1. A flowchart indicating starting and braking systems with timing diagram is shown in Fig. 3.2. From figures, it is inferred that the total time required to changeover from generation to pumping mode is about 11 minutes and 30 seconds (i.e. 40 seconds to reach minimum speed (206 rom) from the operating speed (234 rpm), 240 seconds to reach 5% of synchronous speed, 160 seconds for mechanical braking and 250 seconds for smooth starting).

3.2.1 Smooth Starting

Volts/hertz (V/f) smooth starting is preferable in large rated drives due to: (i) less torque pulsations, (ii) reduction in inrush current, (iii) less energy consumption.

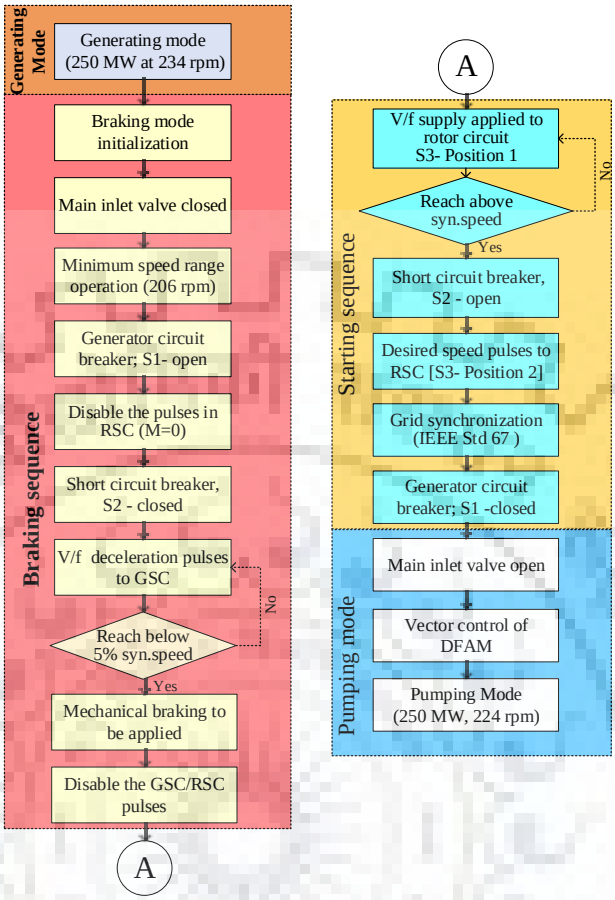

(a) Flowchart for starting and braking sequences

Fig. 3.2 Starting and braking of a 250 MW DFIM unit

The steps involved in smooth starting of hydrogenerating unit are given below.

Step 1: stator circuit of the machine is shorted (generator circuit breaker S1 is open & stator short circuit breaker S2 is closed) and the rotor is energized with V/f control by rotor side converters (RSC). During smooth starting, starting current should not be exceeded beyond the converters (RSC). During smooth starting, starting current should not be exceeded beyond the acceptable limit and maintain a constant torque. Hence, it is to consider, (i) *F_start-up*, is to limit the stator equivalent current during starting resulting in marginally reduced stator winding losses, (ii) *voltage boost*, to compensate the voltage drop across the rotor resistance in the initial stage of the starting of machine where starting frequency is low and inductance value is negligible. The boost voltage (initial voltage) keeps air-gap flux constant in the initial stage of starting for maintaining the constant torque. The value of voltage boost is selected based on rotor winding resistances

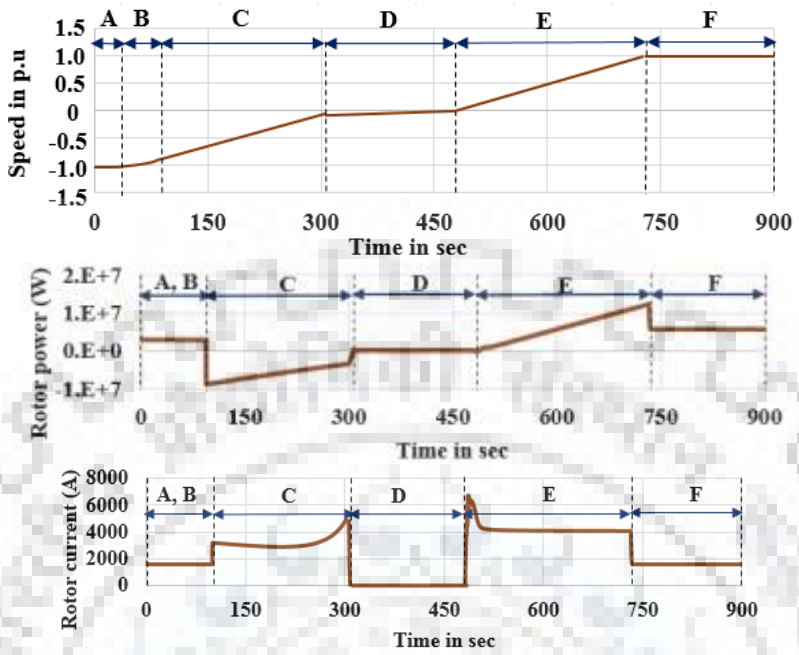

A - generation mode, B - minimum speed range at generation mode,
C- regenerative braking mode D - mechanical braking
E - smooth starting, F - pumping mode

(b) Timing diagram during mode changeovers

Fig. 3.2 Starting and braking of a 250 MW DFIM unit

and torque-speed characteristics of the unit. (iii) V/f ratio, the ratio of V/f should be constant for maintaining a constant torque and reduce the inrush current [185].

Step 2: Once the machine attains synchronous speed, frequency of the rotor voltage is increased to reach above the synchronous speed. After the machine reaches above the synchronous speed then the pulses in RSC are disabled to let the stator current reduce to zero (i.e. defluxing). During this period, machine speed gradually decreases on account of the machine's inertia.

Step 3: Open the stator of the machine which is shorted before (stator short circuit breaker S2 is open). The delay between the removal of pulses in RSC and opening stator circuit is based on time taken for stator current reduced to zero.

Step 4: Provide the PWM pulses in RSC (Transition breaker - S3 - position 2) to maintain desired frequency of rotor current. Monitor the voltage, phase, and frequency of the stator of DFIM and connect it to the grid when the parameters fulfill the requirements as per IEEE Standard 7 (angle ±10 degrees, voltage 0 to +5 %, slip frequency ±0.067 Hz).

Step 5: Main inlet valve is opened to discharge the water from lower to upper reservoir and pumping mode is in continuous operation.

3.2.2 Regenerative Braking

In fixed speed PSPP, dynamic braking is used to stop the synchronous unit and energy being wasted during braking. However, back-to-back converters available in rotor side of DFIM unit provides regenerative braking with the aid of V/f control strategy and energy is fed back to the grid through rotor side power converters. The steps involved in regenerative braking of hydrogenerating unit are given below.

Step 1: Main inlet valve is closed.

Step 2: Set the machine speed reaches to minimum operating speed (-10.73% synchronous speed in Tehri PSPP, India) through vector control system. Therefore rotor voltage reaches to maximum value which is required for achieving regenerative braking of the unit.

Step 3: Generator circuit breaker S1 is open and disable the pulses in RSC (i.e. modulating index (M) as zero).

Step 4: Short circuit the stator (stator short circuit breaker S2 is closed) and apply the V/f control strategy to GSC. The unit is decelerated smoothly and power is fed back to the grid.

Step 5: Once the machine reaches to 5% of the synchronous speed then mechanical braking is applied and V/f pulses are disabled in GSC/RSC.

3.3 Simulation Results (250 MW DFIM)

In order to demonstrate the power converter and control circuit failures at smooth starting and regenerative braking mode, a 250 MW, 0.95 power factor DFIM with 5 channel back -to-back IGBT based three level parallel converters (5 MW each) is simulated in MATLAB/Simulink environment. Each converter is carrying the current limit of 2400 A (1 p.u) and machine rotor current is rated at 11600 A. In addition, dc link voltage is maintained at 5000 V (1 p.u) with help of 18000 μF capacitors.

3.3.1 Smooth Starting Mode

Maximum voltage (L-L) applied to the rotor winding during starting is 3080 volts in view of acceleration and no-load losses. It is observed that: (i) the maximum real (P) and reactive power (Q) consumption are 8.6 MW and 11.8 MVAR respectively (shown in Fig.3.3b), (ii) Maximum power consumption during smooth starting of a 250 MW DFIM is 15. 3 MVA, (iii) RMS value of current flowing in rotor winding is 4200 A and each converter is carrying

current of 840 A, (iv) reactive component current (magnetization) and torque component current (acceleration) reaches 3127A (0.2896 p.u) and 2268A (0.210 p.u), respectively. Further, the duration for smooth starting is selected as 250s. Initial (boost) voltage is estimated as 430 volts and it is continuously applied till machine speed reaches 14% of synchronous speed. Minimum rotational speed of DFIM during synchronization process (removal of SSC and switch-in to grid) is estimated as 103% of synchronous speed. In addition, stator current transients reach about 0.6 p.u during the synchronization process.

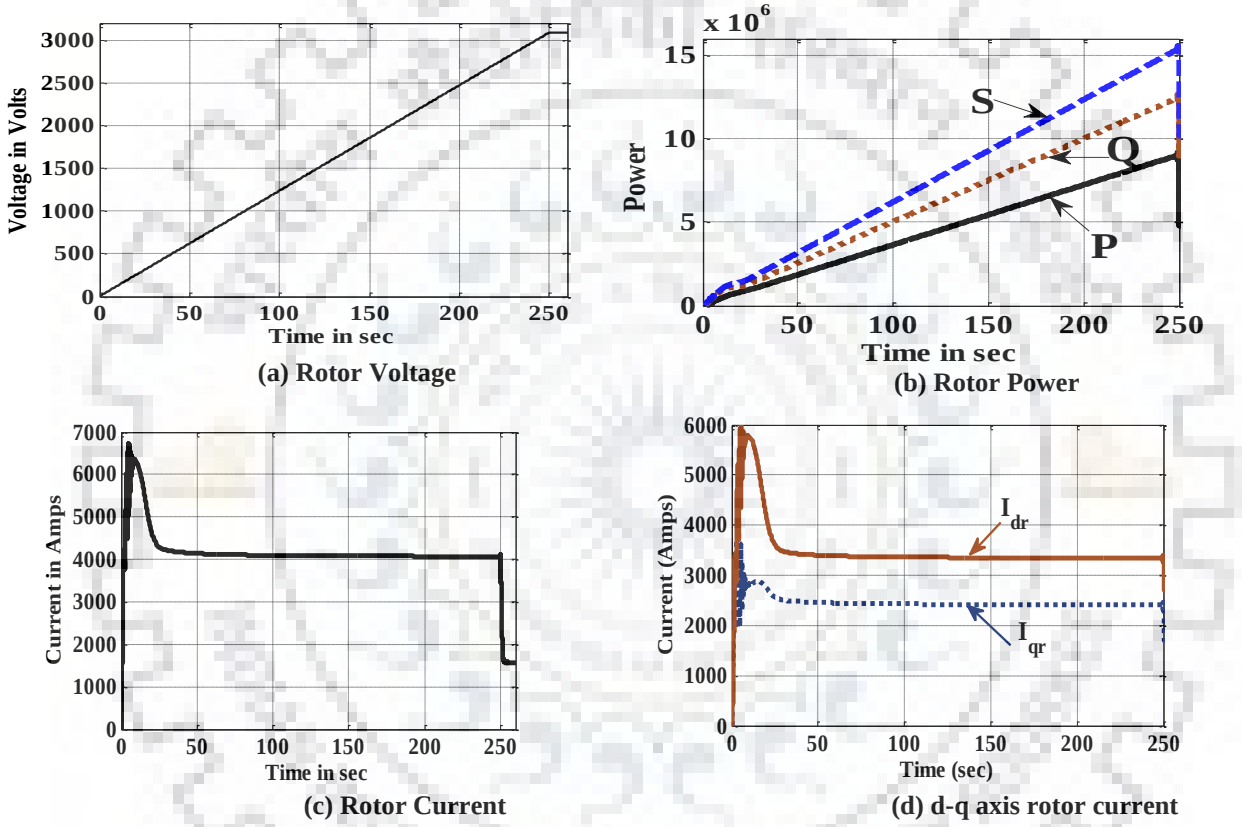

Fig. 3.3. Smooth starting of 250 MW DFIM

3.3.1.1 Power Converter Failure in a Single Converter

In a 250 MW DFIM, five channel three level power converters are connected in rotor side provides smooth starting of the DFIM. In this test case, faults are injected at 650 s at any one of the converter connected in parallel. During starting, grid side converters helps to maintain the unity power factor at grid side and maintain the dc link voltage as constant. Variable voltage/frequency supply is given to rotor of the machine for smooth starting with the help of the rotor side converters.

3.3.1.1.1 GSC Single Device (Upper Switch) Open Circuit Fault

During the fault, phase current corresponding to the switch is disturbed in upper half cycle and continually carrying uncontrollable current as shown in Fig. 3.4a (current flowing through diode) and leads to disturbs the other phase currents caused by dc link voltage controller regulating the dc link voltage by adjusting other phase currents. However, current flowing through the other healthy converters are not affected as shown in Fig. 3.4b. From the test results, it is observed that: (i) dc link voltage marginally fluctuated (oscillation in the rate of 50 Hz and increases only in upper half cycle above the set voltage) in the faulty converter as shown in Fig. 3.4c, (ii) variation in capacitor dc link voltages, faulty switch connected to the dc link capacitor voltage (V_{d1}) gets marginally reduced and other dc link capacitor voltage (V_{d2}) increases to

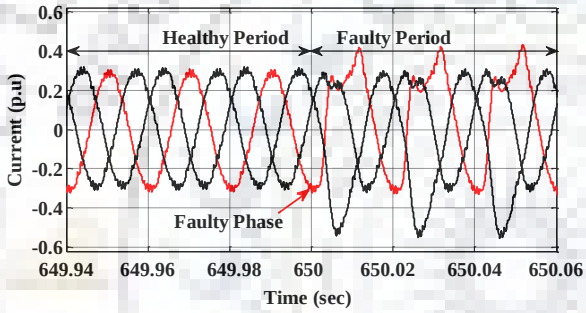

(a) Rotor Current (Grid Side) – Faulty Converter

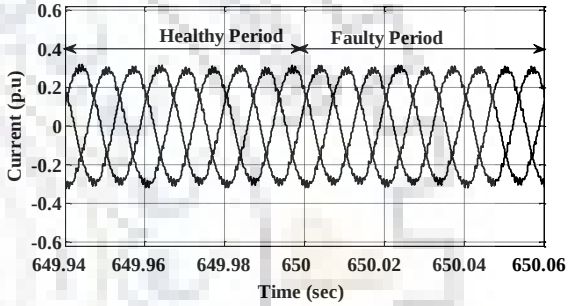

(b) Rotor Current (Grid Side) – Healthy Converter

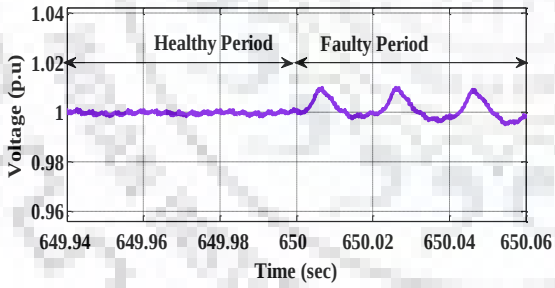

(c) DC Link Voltage – Faulty Converter

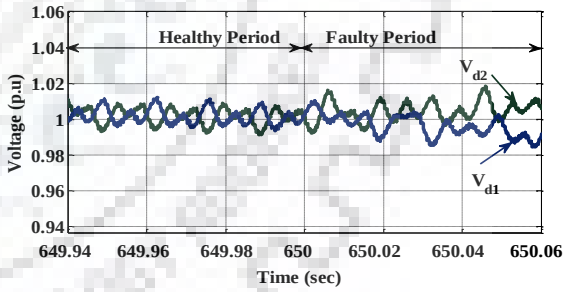

(d) Capacitor DC Link Voltage – Faulty Converter

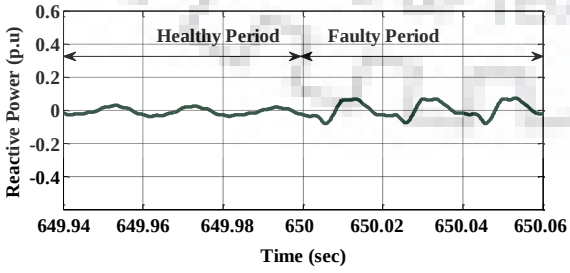

(e) Reactive Power

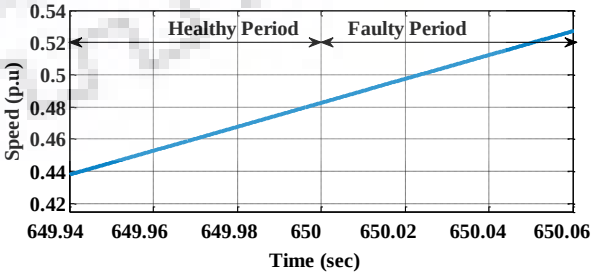

(f) Speed

Fig. 3.4. GSC single device (upper switch) OCF (250 MW DFIM) at starting

regulate the dc link voltage as shown in Fig. 3.4d, (iii) Fluctuation in reactive power consumption (shown in Fig. 3.4e) and leads to variation in power factor at grid side, (iv) speed of the machine is gradually increased as set by rotor side control system (shown in Fig. 3.4f). In case of lower switch open circuit fault, results are similar to the upper switch fault. However, it is observed that (i) phase current is disturbed in lower half cycle, (ii) variation in capacitor dc link voltages are reversed when compared to upper switch fault, (iii) dc link voltage variation is below the set voltage.

3.3.1.1.2 GSC Single Leg Open Circuit Fault

During the fault, phase current corresponding to the leg is uncontrolled (current flowing through diode across each switch) and other two phase currents are changes in phase and act

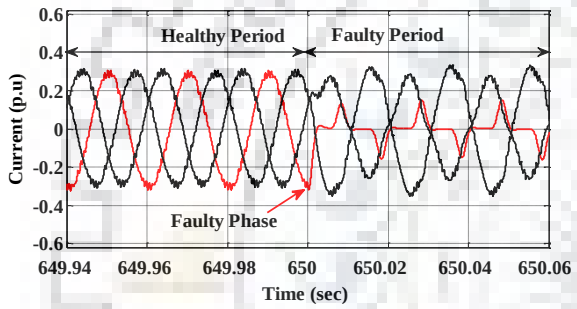

(a) Rotor Current (Grid Side) – Faulty Converter

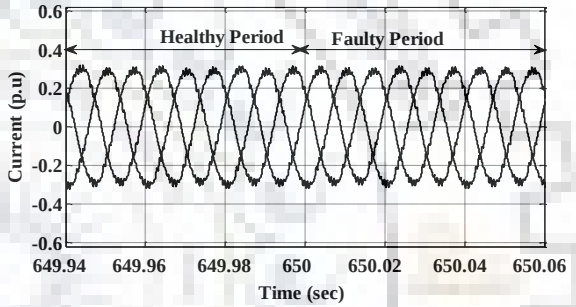

(b) Rotor Current (Grid Side) – Healthy Converter

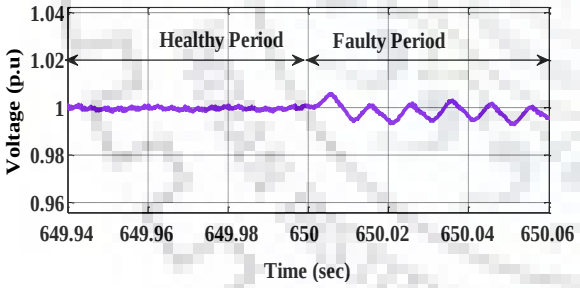

(c) DC Link Voltage – Faulty Converter

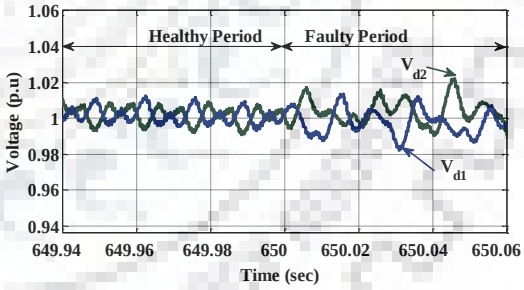

(d) Capacitor DC Link Voltage – Faulty Converter

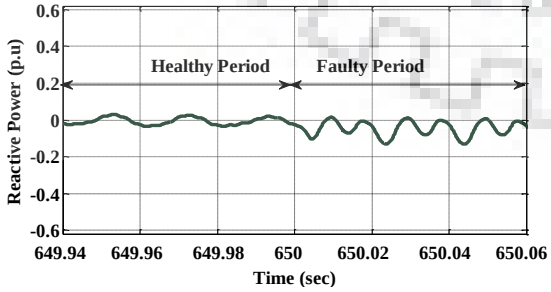

(e) Reactive Power

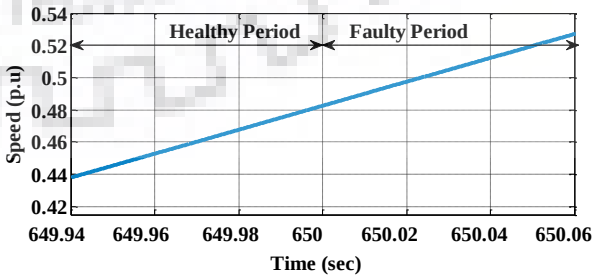

(f) Speed

Fig. 3.5. GSC single leg OCF (250 MW DFIM) at starting

similar to single phase rectifier as shown in Fig. 3.5a. From the test results, it is observed that: (i) it does not affects the other healthy converters connected in parallel (shown in Fig. 3.5b), (ii) dc link voltage of the faulty converter get fluctuated with the frequency of 100 Hz (both upper and lower part of the set voltage) as shown in Fig. 3.5c, (iii) marginal variation in capacitor dc link voltages, however both voltages are not varied oppositely (shown in Fig. 3.5d), (iv) variation in reactive power consumption of the grid and it is less compared to the single switch open circuit faults (shown in Fig. 3.5e), (v) speed of the machine is gradually increased as set by rotor side control system as shown in Fig. 3.5f.

3.3.1.1.3 GSC Short Circuit Fault (Upper Two Switches)

During the fault, phase current corresponding to the faulty leg is distorted in upper half cycle and negative half cycle is omitted as shown in Fig. 3.6a, results in variation in phase and

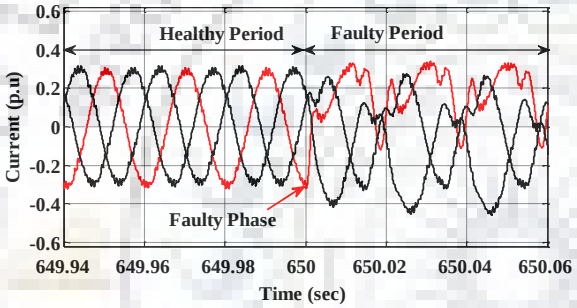

(a) Rotor Current (Grid Side) – Faulty Converter

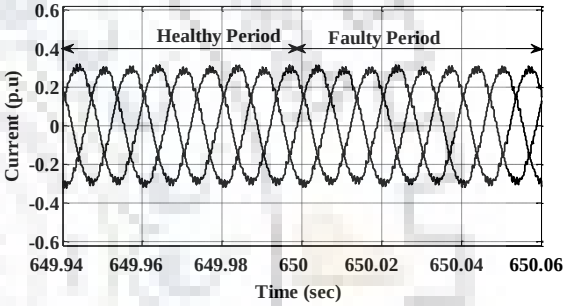

(b) Rotor Current (Grid Side) – Healthy Converter

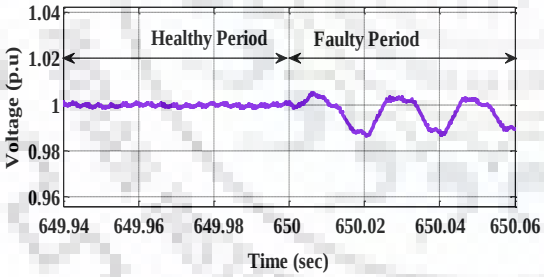

(c) DC Link Voltage – Faulty Converter

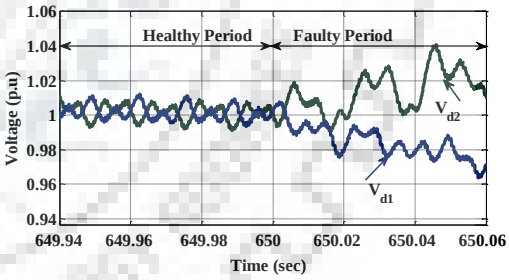

(d) Capacitor DC Link Voltage – Faulty Converter

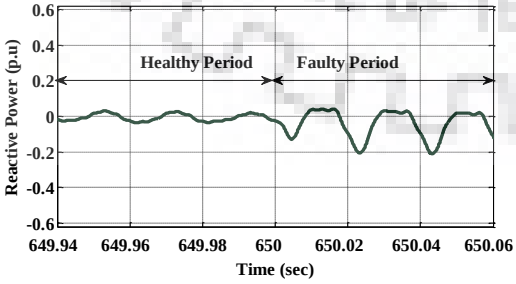

(e) Reactive Power

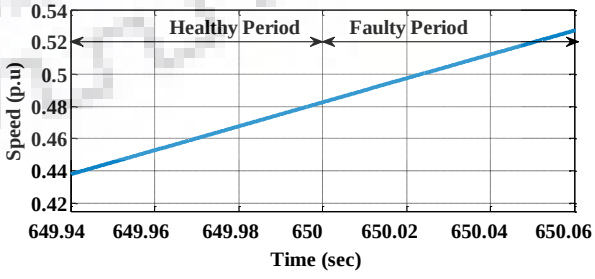

(f) Speed

Fig. 3.6. GSC upper two switches SCF (250 MW DFIM) at starting

magnitude of other phase currents. However, current flowing through the other healthy converters are not affected as shown in Fig. 3.6b. From the test results, it is observed that: (i) dc link voltage marginally fluctuated in the faulty converter (oscillation in the rate of 50 Hz and decreases only in lower part of the set voltage) and high compared to the open circuit switch faults (shown in Fig. 3.6c), (ii) variation in capacitor dc link voltages and highly varied when compared to the open circuit switch faults), faulty switch connected to the dc link capacitor voltage (V_{d1}) gets marginally reduced and other dc link capacitor voltage (V_{d2}) increases to regulate the dc link voltage as shown in Fig. 3.6d, (iii) High fluctuation in reactive power consumption (shown in Fig. 3.6e) when compared to the open circuit switch faults and leads to variation in power factor at grid side, (iv) speed of the machine is gradually increased as set by rotor side control system (shown in Fig. 3.6f). In case of short circuit fault in lower two switches, results are similar to the upper switch fault. However, it is observed that (i) Faulty leg phase current is disturbed in lower half cycle and it is omitted in upper half cycle, (ii) variation in capacitor dc link voltages are reversed when compared to upper switches short circuit fault, (iii) dc link voltage variation is above the set voltage.

3.3.1.1.4 GSC Single Leg Short Circuit Fault (DC Link Short Circuit Fault)

During the fault, phase current corresponding to the shorted leg increases in upper half cycle as it is allowed by the grid side controller, results to affects the other phase currents in magnitude and phase as shown in Fig. 3.7a. Further, single leg short circuit fault affects the other healthy converters connected in the system as shown in Fig. 3.7b. From the test results, it is observed that: (i) dc link voltage of the faulty converter get highly fluctuated as shown in Fig. 3.7c, (ii) capacitor dc link voltages are highly fluctuated as shown in Fig.3.7d, (iii) reactive power consumption from the grid is greatly increases as shown in Fig. 3.7e, (iv) speed of the machine has affected as shown in Fig. 3.7f.

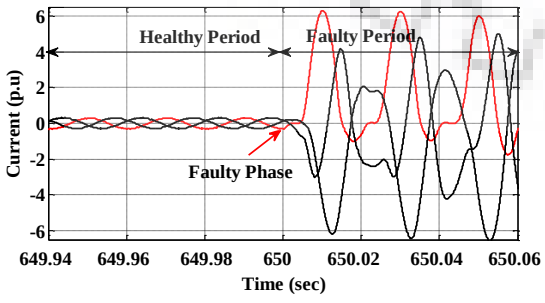

(a) Rotor Current (Grid Side) – Faulty Converter

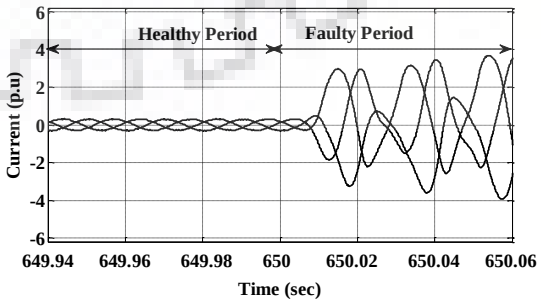

(b) Rotor Current (Grid Side) – Healthy Converter

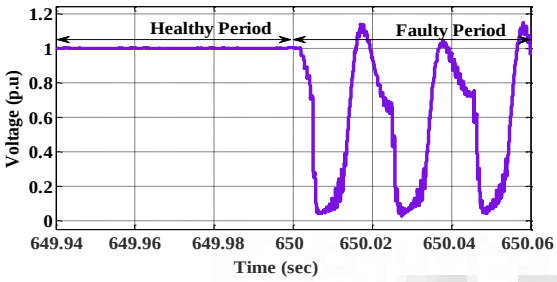

(c) DC Link Voltage – Faulty Converter

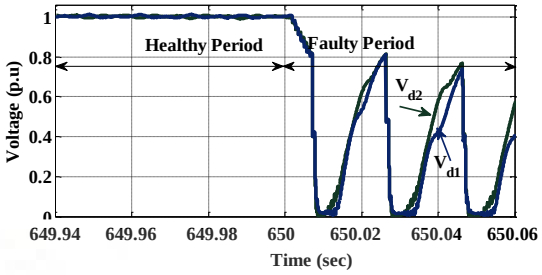

(d) Capacitor DC Link Voltage – Faulty Converter

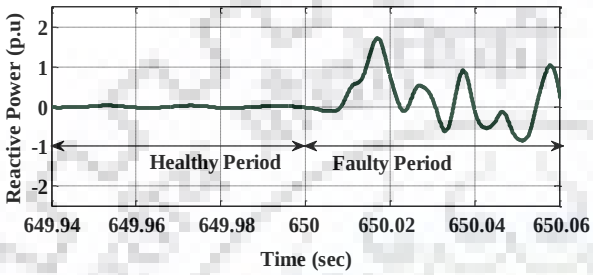

(e) Reactive Power

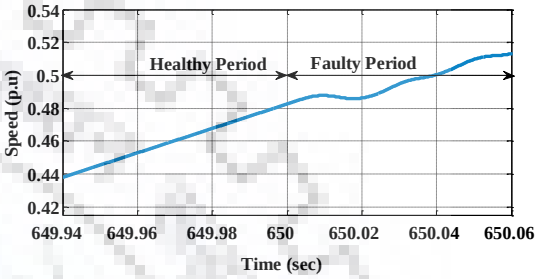

(f) Speed

Fig. 3.7. GSC single leg SCF (250 MW DFIM) at starting

3.3.1.1.5 RSC Upper Two Switches Open Circuit Fault

When the fault occurs, one of the rotor phase currents in the faulty converter is discontinuous (i.e. upper half is omitted, shown in Fig. 3.8a) in nature and other two phases are carrying currents as regular value. However, the same phase current in other parallel converters increases 1.2 times (upper half cycle) of regular value (Fig. 3.8b). From the test results, it is observed that: (i) dc link voltage of the faulty converter is marginally oscillated as shown in Fig. 3.8c and healthy converter dc link voltage also get minimum disturbance as compared to the faulty converter (shown in Fig. 3.8d), further, dc link voltage fluctuation only in above the dc link set voltage, (ii) it does not impact on overloading the power converter and starting of the

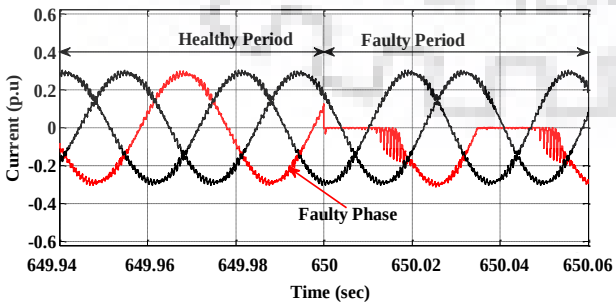

(a) Rotor Current (Machine Side) – Faulty Converter

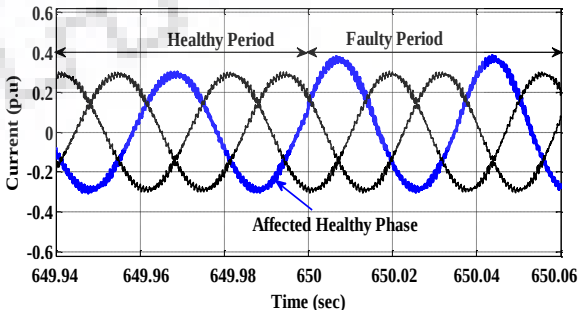

(b) Rotor Current (Machine Side) – Healthy Converter

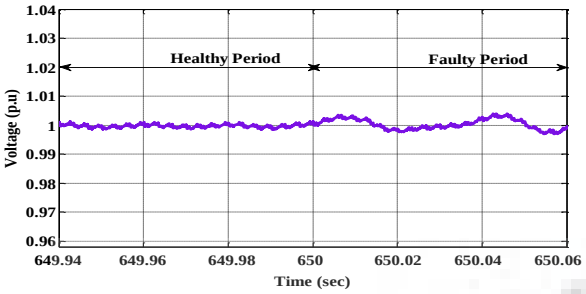

(c) DC Link Voltage – Faulty Converter

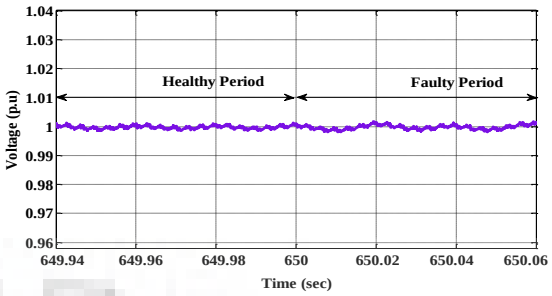

(d) DC Link Voltage – Healthy Converter

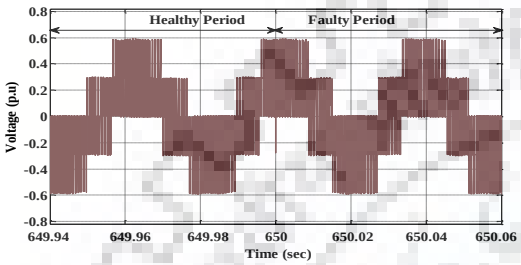

(e) Rotor Voltage – Machine Side

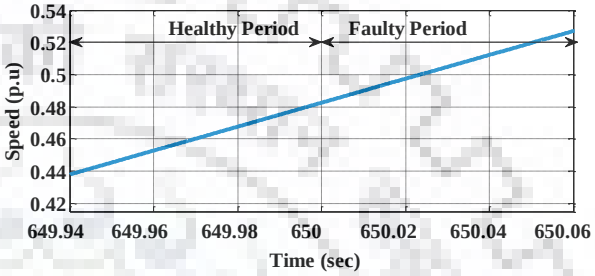

(f) Speed

Fig. 3.8. RSC upper two switches OCF (250 MW DFIM) at starting

machine as it rotates at no-load (Fig. 3.8f). In case of lower switches fault, lower half cycle is omitted and dc link voltages gets fluctuation at below the set voltage.

3.3.1.1.6 RSC Single Leg Open Circuit Fault

When fault occurs, one of the rotor phase current in faulty converter goes to zero (Fig. 3.9a) and the other two phases are carrying current as regular value. However, the same phase current in other parallel converters are increased about 1.2 times of regular value (Fig. 3.9b) to maintain required rotor phase current. From the test results, it is observed that: (i) dc link voltage of the converter is marginally oscillated as shown in Fig.3.9c, (ii) it does not impact on overloading the power converter and starting of the machine as it rotates at no-load (Fig. 3.5f).

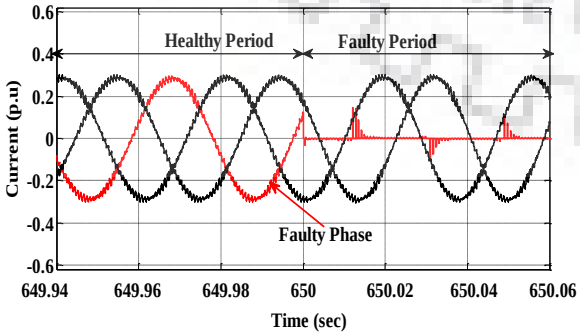

(a) Rotor Current (Machine Side) – Faulty Converter

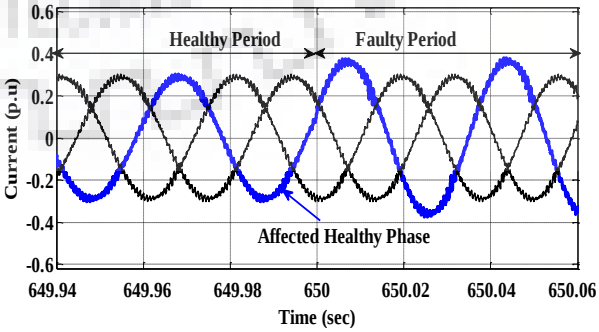

(b) Rotor Current (Machine Side) – Healthy Converter

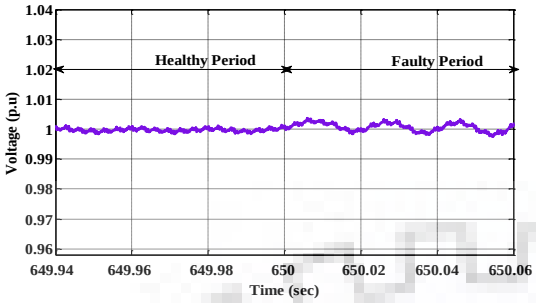

(c) DC Link Voltage – Faulty Converter

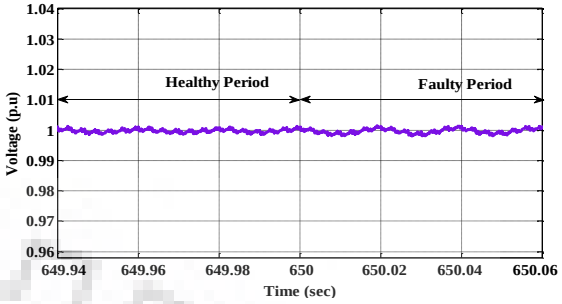

(d) DC Link Voltage – Healthy Converter

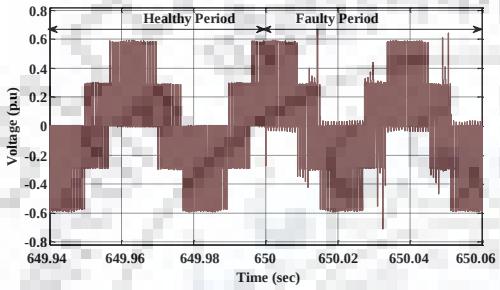

(e) Rotor Voltage – Machine Side

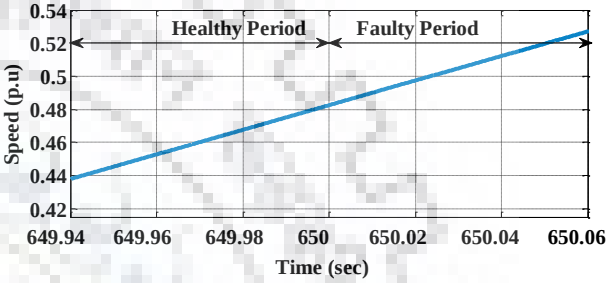

(f) Speed

Fig. 3.9. RSC single leg OCF (250 MW DFIM) at starting

3.3.1.1.7 RSC Short Circuit Fault (Upper Two Switches)

When the fault occurs, one of the rotor phase currents in the faulty converter is discontinuous (i.e. upper half is omitted, shown in Fig. 3.10a) and other two phases are carrying currents as regular value. However, the same phase current in other parallel converters increases 1.2 times (upper half cycle) of regular value (Fig. 3.10b). From the test results, it is observed that: (i) dc link voltage of the faulty converter is marginally oscillated as shown in Fig. 3.10c, (ii) it does not impact on overloading the power converter and starting of the machine as it rotates at no-load (Fig. 3.10f). In case of lower switches fault, lower half cycle is omitted. RSC single

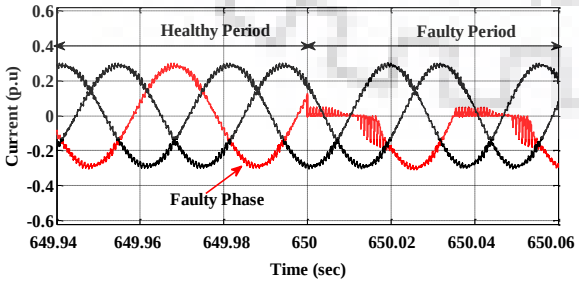

(a) Rotor Current (Machine side) – Faulty Converter

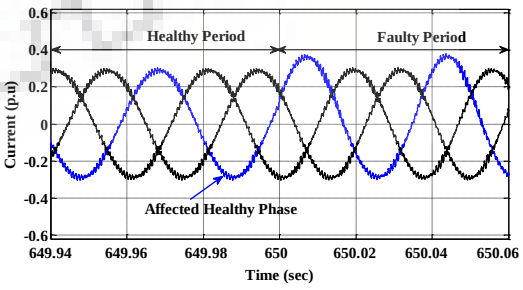

(b) Rotor Current (Machine Side) – Healthy Converter

leg short circuit fault leads to dc link short circuit fault of the corresponding converter. Results are similar to the GSC single leg short circuit fault.

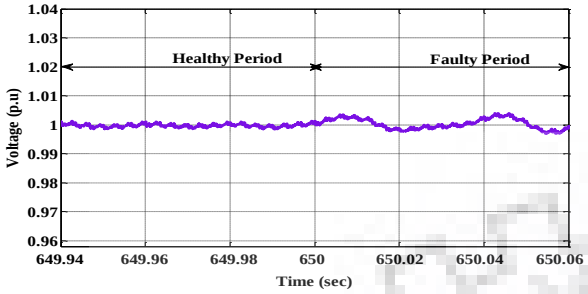

(c) DC Link Voltage – Faulty Converter

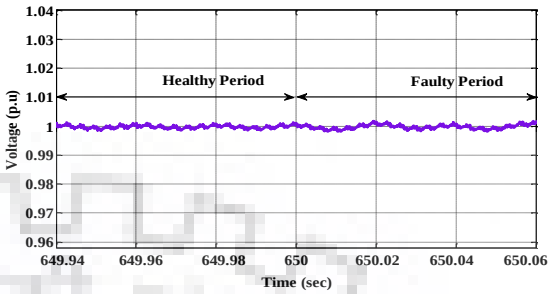

(d) DC Link Voltage – Healthy Converter

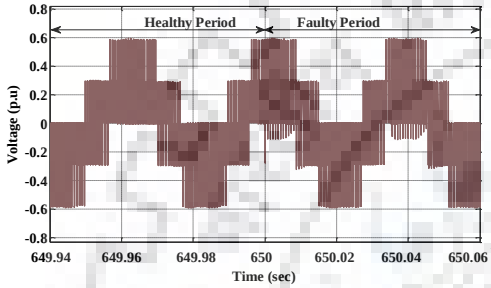

(e) Rotor Voltage – Machine Side

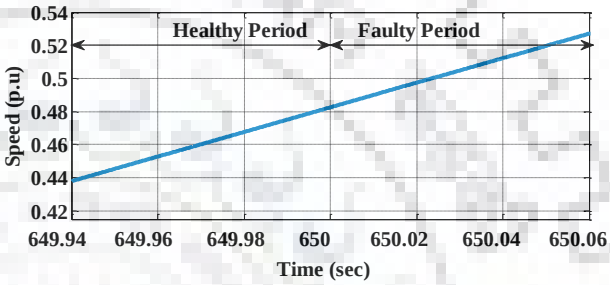

(f) Speed

Fig. 3.10. RSC upper two switches SCF (250 MW DFIM) at starting

3.3.1.2 Control Circuit (Sensor) Failure

Three sensors including dc link voltage sensor, grid voltage sensor and grid current sensor are required in the GSC control system for maintain unity power factor and dc link voltage. All the above said sensors, omission fault is injected and it is in 650s.

3.3.1.2.1 DC Link Voltage Sensor Omission Fault

During the fault, dc link voltage controller reads input as zero and increases proportional gain of the dc link voltage controller which increases the d-axis rotor side grid current, consequently, dc link voltage of the back-to-back power converter increases (shown in Fig. 3.11a) until the dc link voltage gets saturated. In addition, dc link voltage of the healthy converter also get marginally increased as shown in Fig. 3.11d. From the test results, it is summarized as: (i) grid side rotor currents increases in all phases (shown in Fig. 3.11b), (ii) dc link voltage of the back-to-back power converter increases until the d-axis grid rotor current (I_{dg}) gets saturated, (iii) power factor of the grid side system fluctuated initially and maintained unity after the interval period (shown in Fig. 3.11e) (iv) speed of the machine is unchanged as shown in Fig. 3.11f.

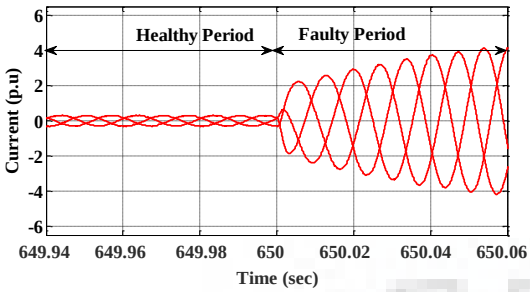

(a) Rotor Current (Grid Side) – Faulty Converter

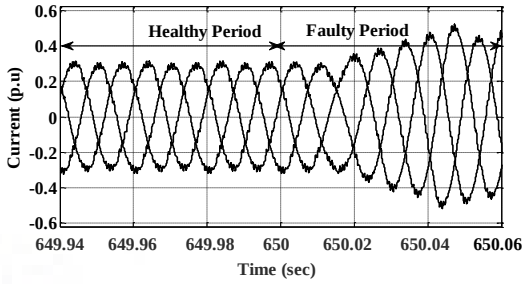

(b) Rotor Current (Grid Side) – Healthy Converter

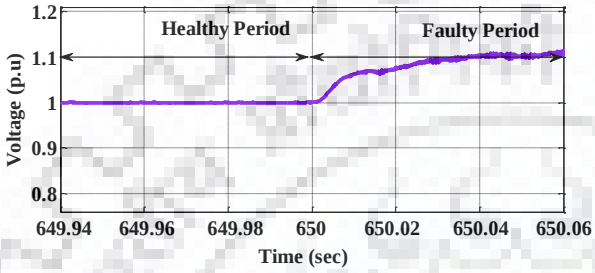

(c) DC Link Voltage – Faulty Converter

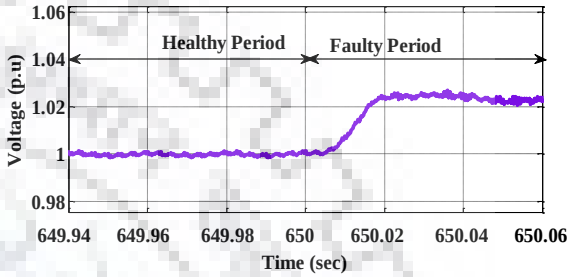

(d) DC Link Voltage – Healthy Converter

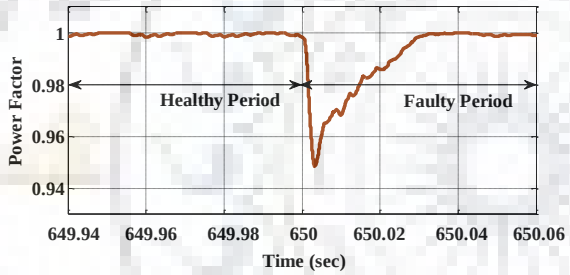

(e) Power Factor (Grid - Rotor side)

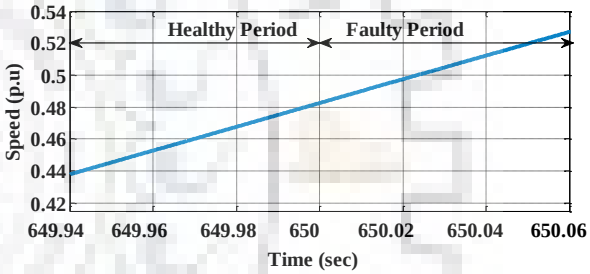

(f) Speed

Fig. 3.11. DC link voltage sensor omission fault (250 MW DFIM) at starting

3.3.1.2.2 Single Rotor Grid Current Sensor Omission Fault

During the fault, faulty sensor reads input as zero and changes in estimating the d-q axis rotor current. As an effect, one of the rotor phase current (faulty sensor phase) magnitude is

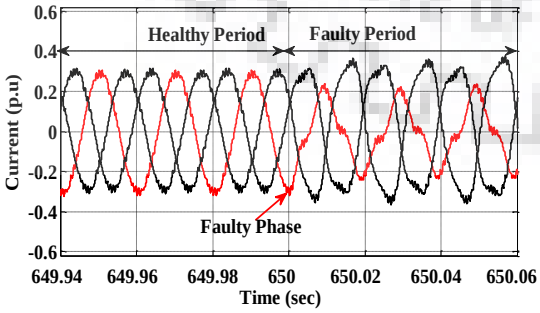

(a) Rotor Current (Grid Side) – Faulty Converter

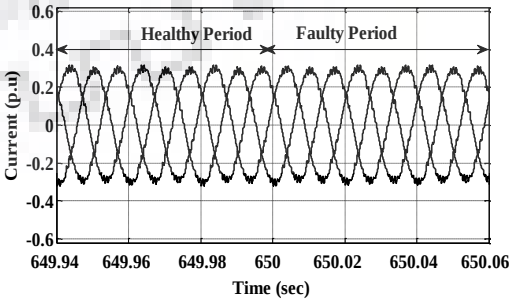

(b) Rotor Current (Grid Side) – Healthy Converter

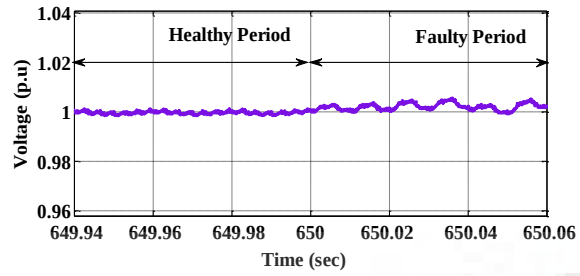

(c) DC Link Voltage – Faulty Converter

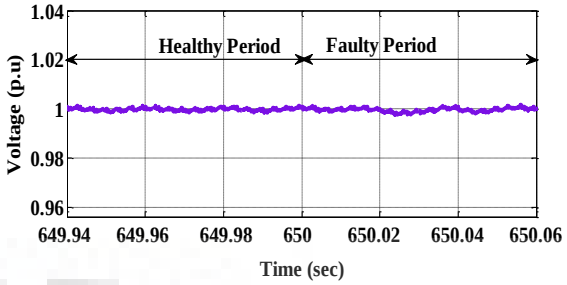

(d) DC Link Voltage – Healthy Converter

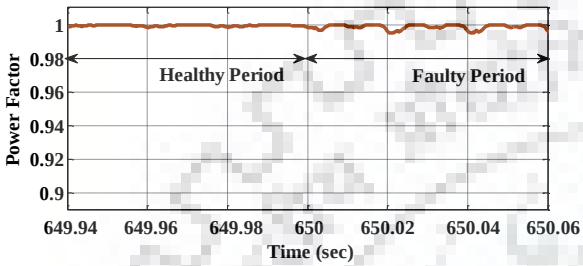

(e) Power Factor (Grid - Rotor side)

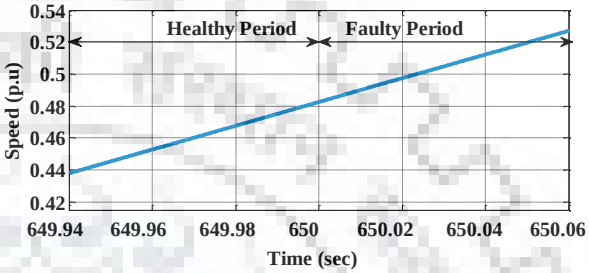

(f) Speed

Fig. 3.12. Single rotor grid current sensor omission fault (250 MW DFIM) at starting

reduced and results to increase in other two phase currents. Further, phase angle of other two phase currents also changed, like as a single phase operation (shown in Fig. 3.12a). However, it does not affects the healthy converters (Fig. 3.12b). From the test results, it is observed that: (i) dc link voltage of the fault converter is marginally fluctuated (oscillation at the rate of 100 Hz) as shown in Fig. 3.12c, (ii) power factor of the grid side system is fluctuated (shown in Fig. 3.12e), (iii) speed of the machine is gradually increased as set by rotor side control system as shown in Fig. 3.12f.

3.3.1..2.3 Single Rotor Grid Voltage Sensor Omission Fault

During the fault, faulty sensor reads input as zero and changes in estimating the d-q axis rotor voltage results in distortion of all phase currents (magnitude and phase) as shown in Fig.

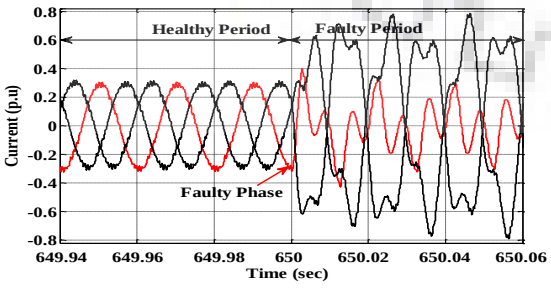

(a) Rotor Current (Grid Side) – Faulty Converter

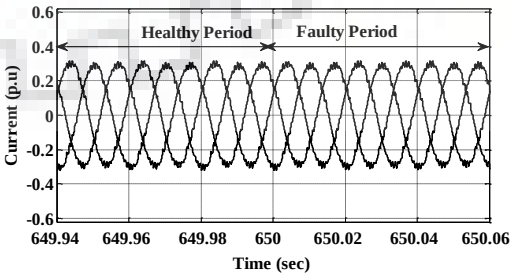

(b) Rotor Current (Grid Side) – Healthy Converter

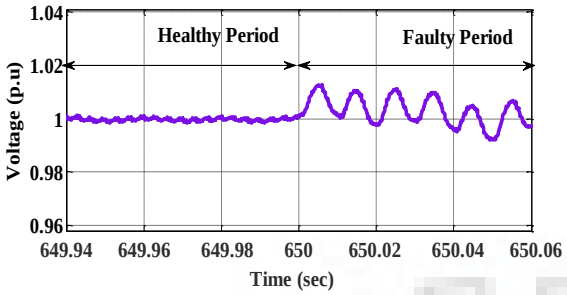

(c) DC Link Voltage – Faulty Converter

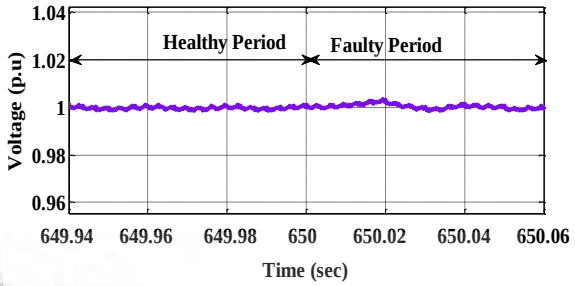

(d) DC Link Voltage – Healthy Converter

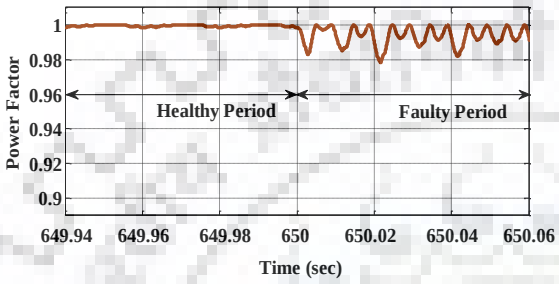

(e) Power Factor (Grid - Rotor side)

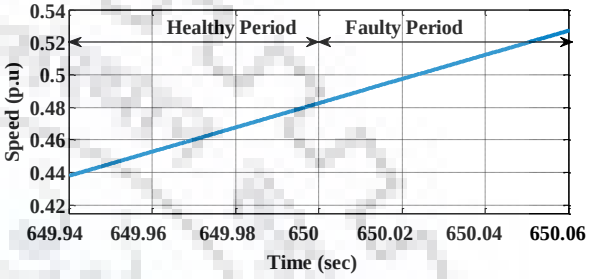

(f) Speed

Fig. 3.13. Single rotor grid voltage sensor omission fault (250 MW DFIM) at starting

3.13a. From the test results, it is observed that: (i) dc link voltage of the faulty converter is marginally fluctuated with the rate of 100 Hz, (ii) power factor of the grid side system is fluctuated as shown in Fig. 3.13e, (iii) speed of the machine is gradually increased as set by rotor side control system as shown in Fig. 3.13f.

3.3.1.3 Power Converter Failure in All Channels (Five Converters)

Power converter failure in all channels at same time is very rare. However, open/damages in rotor winding (i.e. slip rings open circuit) leads to open circuit fault in all rotor side converters. In a similar way, open circuit fault in grid or excitation transformer results in open circuit fault in grid side converter. Further, DFIM fed three level converter (single) is emerging in variable speed drives including wind, small hydro and marine applications. Open and short circuit failures in all grid side converters are similar to the faults in any one of the parallel connected grid side converters. Nonetheless, variation in dc link voltage, reactive power consumption from the grid and power factor variation is slightly higher than parallel connected converters. For example, RSC upper two switches open circuit fault is discussed here. In addition, Control circuit failures in grid side controller is similar to the parallel connected converters. But, failures

in a rotor side converter is entirely different and it is discussed below. The faults are injected at 650s.

3.3.1.3.1 GSC Upper Single Switch Open Circuit Fault

During the fault, phase current corresponding to the switch is disturbed in upper half cycle and continually carrying uncontrollable current as shown in Fig. 3.14a (current flowing through diode) and leads to disturbs the other phase currents. From the test results, it is observed that: (i) dc link voltage marginally fluctuated (oscillation in the rate of 50 Hz) in the faulty converter as shown in Fig. 3.14c, (ii) variation in capacitor dc link voltages, faulty switch connected to the dc link capacitor voltage (Vd1) gets marginally reduced and other dc link capacitor voltage (Vd2) increases to regulate the dc link voltage as shown in Fig. 3.14d, (iii) Fluctuation in reactive power consumption and leads to variation in power factor at grid side

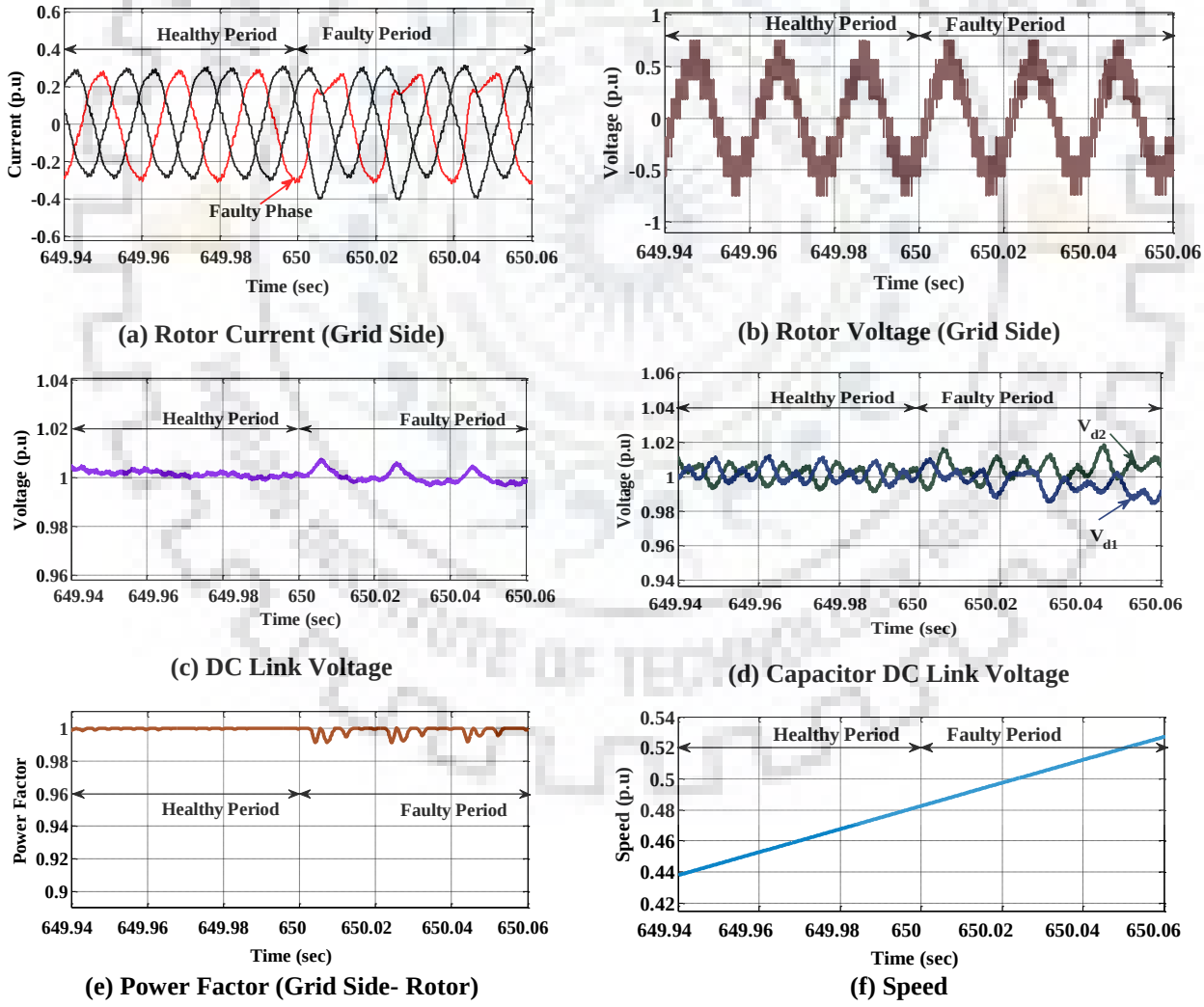

Fig. 3.14. GSC single device (upper switch) OCF (250 MW DFIM) at starting

(shown in Fig. 3.14e), (iv) speed of the machine is gradually increased as set by rotor side control system (shown in Fig. 3.14f). In case of lower switch open circuit fault, results are similar to the upper switch fault. However, it is observed that (i) phase current is disturbed in lower half cycle, (ii) variation in capacitor dc link voltages are reversed when compared to upper switch fault.

3.3.1.3.2 RSC Upper Two Switches Open Circuit Fault

When fault occurs, one of the rotor phase currents is discontinuous (upper half cycle) in nature and other two phases are carrying currents about 1.5 times of regular value also changes in phase (shown in Fig. 3.15a). During the fault, dc link voltage of the converter is fluctuated at a rate of 25 Hz frequency (shown in Fig. 3.15c) and also capacitor dc link voltages are varied. From the test results, it is observed that: (i) speed of the machine is gradually increased with marginal oscillation as shown in Fig. 3.15d, (ii) reactive power consumption of the machine increases leads to fluctuation in power factor of the grid side system. In addition, the results are similar for the RSC short circuit fault in upper two switches.

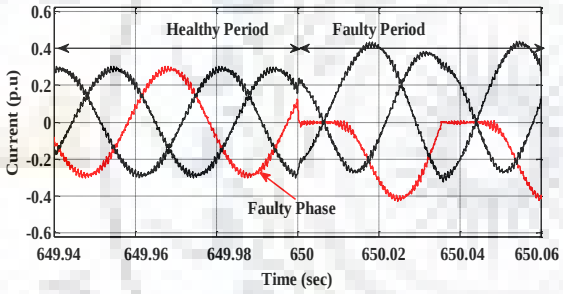

(a) Rotor Current (Machine Side)

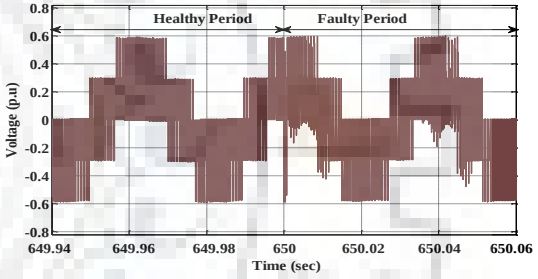

(b) Rotor Voltage (Machine Side)

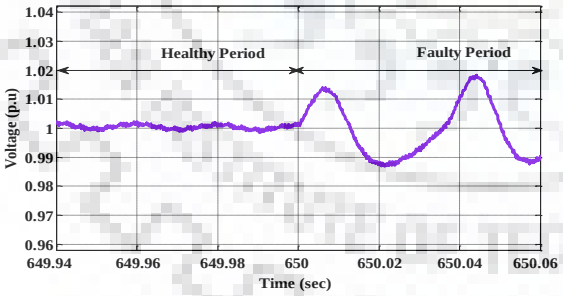

(c) DC Link Voltage

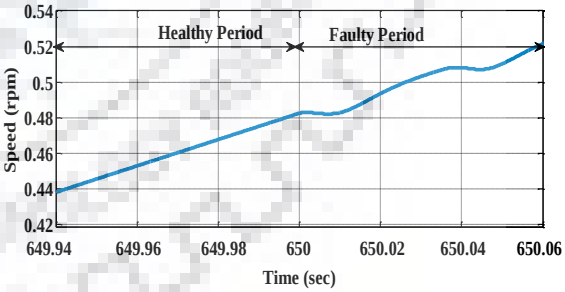

(d) Speed

Fig. 3.15. RSC upper two switches OCF (250 MW DFIM) at starting

3.3.1.3.3 RSC Single Leg Open Circuit Fault

When fault occurs, one of the rotor phase currents goes to zero and the conduction mode is equivalent to the single phase converter with other two healthy legs (Fig. 3.16a). During fault,

dc link voltage of the converter is fluctuated at a rate of 50 Hz frequency (shown in Fig. 3.16c) and also capacitor dc link voltages are varied. From the test results, it is observed that: (i) speed of the machine is gradually increased with marginal oscillation as shown in Fig. 3.16d, (ii) reactive power consumption of the machine increases leads to fluctuation in power factor of the grid side system, (iii) increase in apparent power consumption of the machine.

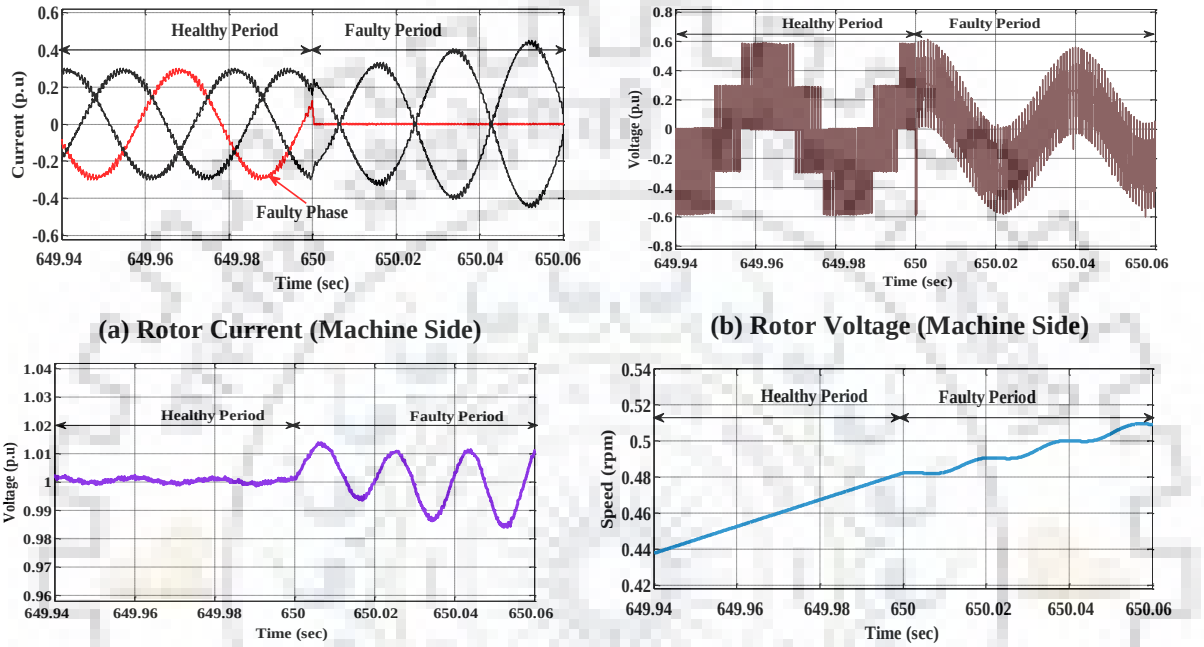

(a) Rotor Current (Machine Side)

(b) Rotor Voltage (Machine Side)

(c) DC Link Voltage

(d) Speed

Fig. 3.16. RSC single leg OCF (250 MW DFIM) at starting

3.3.2 Regenerative Braking Mode

In regenerative braking mode, (i) the maximum real power delivery to the grid is 8.25 MW, (ii) RMS value of current flowing in rotor winding is 3100A and each converter is carrying current of 620 A. Further, the duration for regenerative braking is selected as 250s. During the braking, RSC acts as rectifier, controls the dc link voltage of back-to-back converter and GSC acts as inverter and send back the real power to the grid from the machine. In case of starting, GSC acts as rectifier and RSC acts as inverter. The results of open and short circuit faults in rectifier and inverters are similar to the faults in starting mode. But, the speed is gradually reduced in braking mode and fluctuation is similar to the starting mode.

3.4 Experimental Validation (2.2 kW DFIM)

During smooth starting and regenerative braking, dc link voltage of back-to-back three level converter is maintained at 325 V and the sample time is selected 0.001 s. In consideration of machine rating and power consumption, duration for smooth starting and regenerative braking are selected as 96 s and voltage/frequency ratio is chosen as 3.7. Initially smooth starting of a DFIM under healthy condition are performed at no-load and results are shown in Fig. 3.17. From figure, it is inferred that: (i) rotor current initially go up to 0.75 p.u and once the rotor get acceleration then current reduced to 0.35 p.u and continued till machine reaches to synchronous speed as shown in Figure 3.17a (i), (ii) dc link voltage of the back-to-back converter is maintained constant at 1 p.u during starting period (iii) Maximum power consumed as 0.35 p.u at 0.95 p.u speed, (iv) speed is gradually increases as set by the rotor control system. Results are measured by power quality analyzers and recorded through dSPACE control desk 5.1 automation. Further, 2.2 kW simulation results (shown in Fig. 3.17 b) are also considered to support the 250 MW DFIM. The maximum current carrying of each power converter module is rated at 3.75 A (1 p.u) and machine rotor current is rated at 7.5 A (1 p.u).

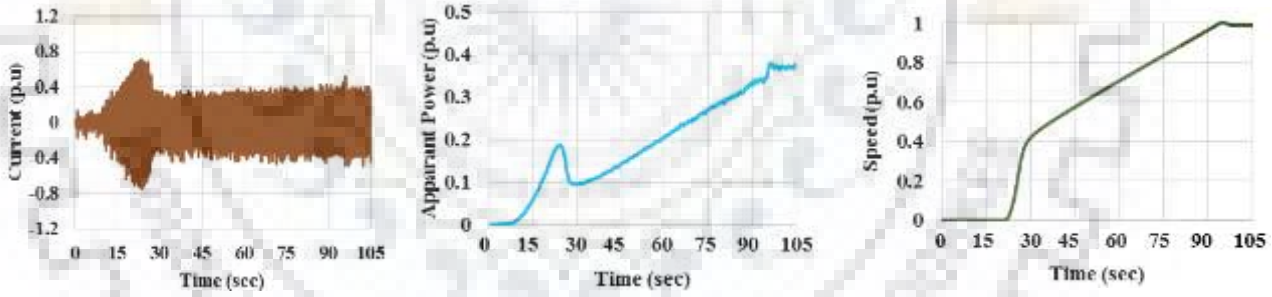

(i) Rotor Current **(ii) Apparent power** **(iii)Speed**

Fig. 3.17 (a) Experimental results of a 2.2 kW DFIM during starting

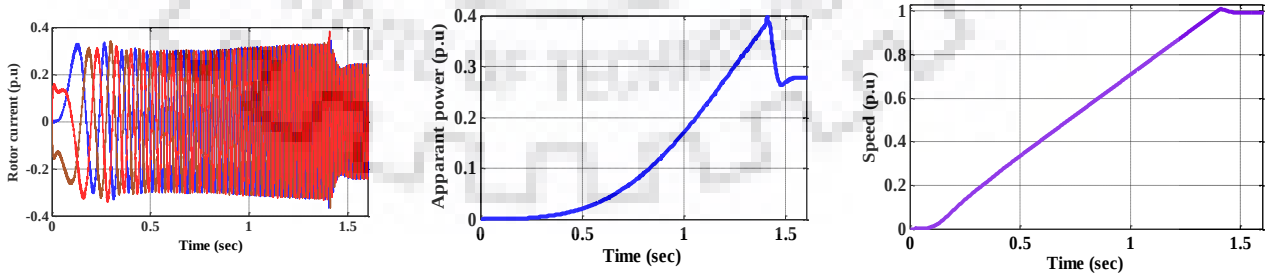

(i) Rotor Current **(ii) Apparent power** **(iii)Speed**

Fig. 3.17 (b) Simulation results of a 2.2 kW DFIM during starting

3.4.1 Power Converter Failure in All Channels (Five Converters)

3.4.1.1 RSC Single Device Open Circuit Fault

Single device gate drive open circuit fault is injected in RSC at 40.7 s and results are show in Fig. 3.18. During the fault, magnitude of rotor current in healthy phase (upper half cycle) increases to 1.35 times of regular value (shown in Fig. 3.18a (i)) and phase sequences are altered. The speed of the machine is marginally dipped at the time of fault and continue to accelerate as set by control system (shown in Fig. 3.18a (iii)). In addition, total power consumption of the machine is increased (shown in Fig. 3.18a (ii)). It is estimated that rise/reduction in rotor current, speed and apparent power is similar to simulation results obtained.

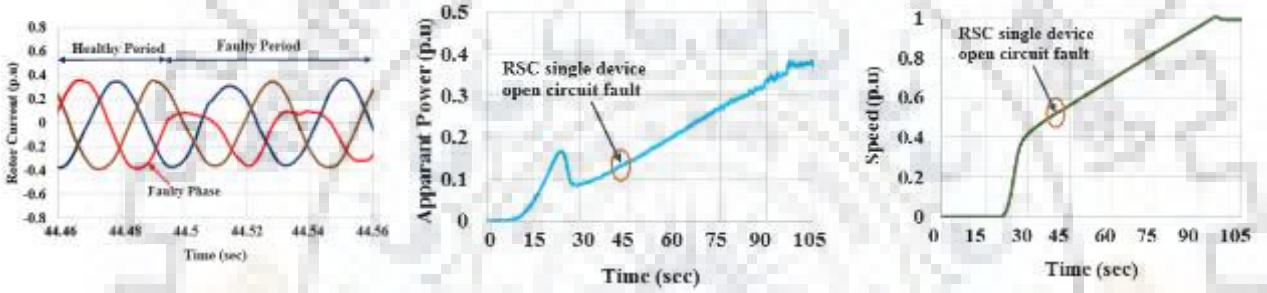

(i) Rotor Current **(ii) Apparent power** **(iii)Speed**

Fig. 3.18 (a) Experimental results of a 2.2 kW DFIM during starting at single device open circuit fault

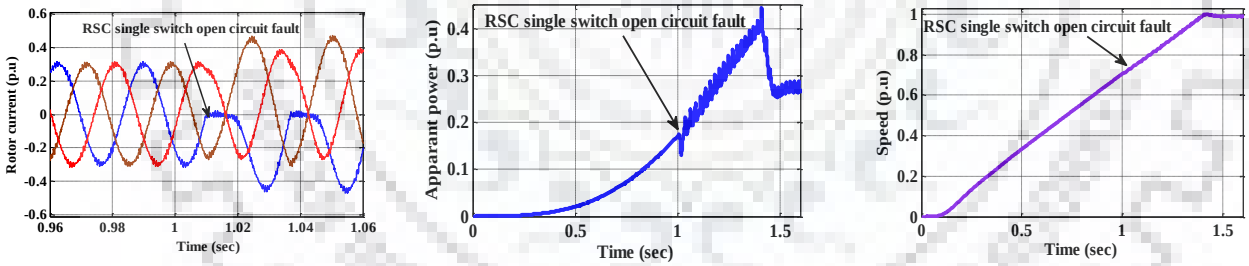

(i) Rotor Current **(ii) Apparent power** **(iii)Speed**

Fig. 3.18 (b) Simulation results of a 2.2 kW DFIM during starting at single device open circuit fault

3.4.1.2 RSC Single Leg Open Circuit Fault

RSC single leg gate drive open circuit fault is injected at 40.44 s and results are shown in Fig. 3.19. During the fault, the magnitude of rotor current in healthy legs reach to 2 times of regular value (shown in Fig. 3.19a (i)) and converter conduction mode is equivalent to the single phase converter with other two healthy legs. The speed of the machine is considerably affected

(shown in Fig. 3.19a (iii)) during the fault. It is estimated that rise/reduction in rotor current, speed and apparent power is similar to simulation results obtained.

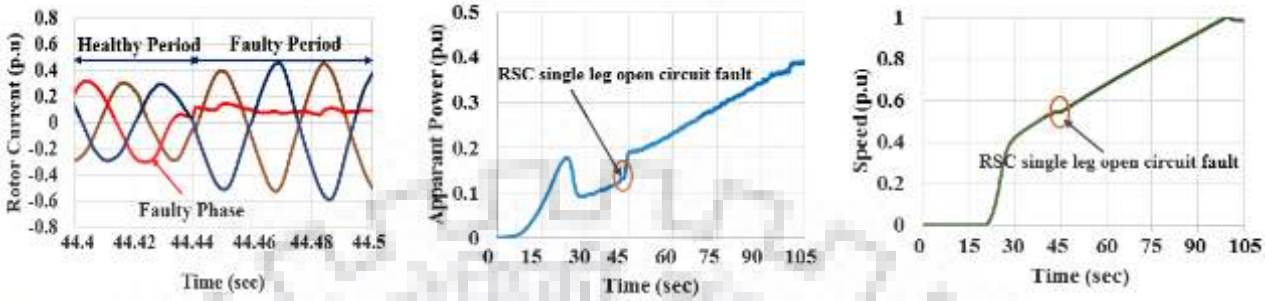

(i) Rotor Current **(ii) Apparent power** **(iii)Speed**

Fig. 3.19 (a) Experimental results of a 2.2 kW DFIM during starting at single leg open circuit fault

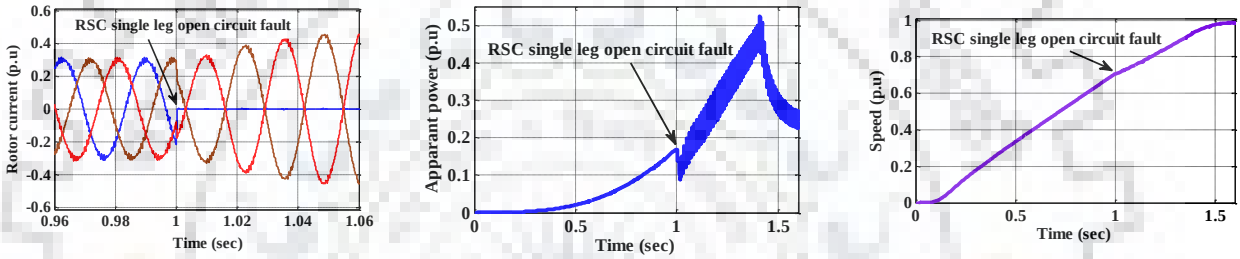

(i) Rotor Current **(ii) Apparent power** **(iii)Speed**

Fig. 3.19 (b) Simulation results of a 2.2 kW DFIM during starting at single leg open circuit fault

3.4.1.3 GSC Upper Two Switches Open Circuit Fault

GSC upper two switches fault is injected at 42.38 s and results are shown in Fig. 3.20. During the fault, phase current corresponding to the switch is disturbed in upper half cycle and continually carrying uncontrollable current as shown in Fig. 3.20a and leads to disturbs the other phase currents. In addition, dc link voltage marginally fluctuated as shown in Fig. 3.20b. Real and Reactive power consumption of the machine is severely affected as shown in Fig. 3.20c and

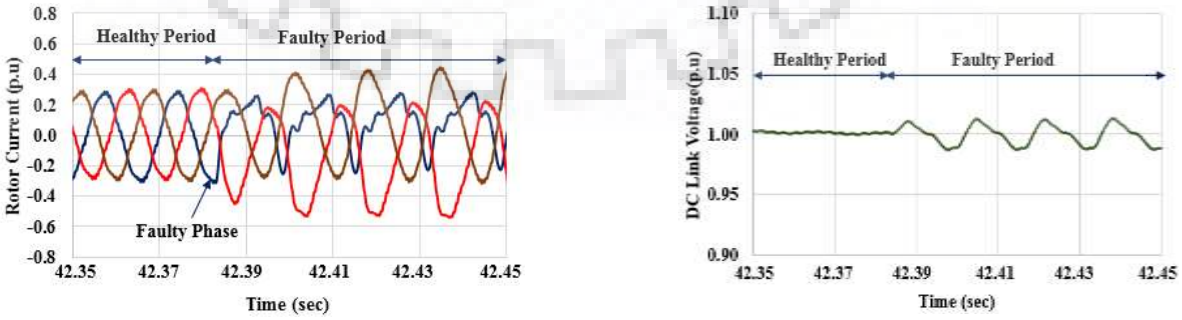

(a) Rotor Current –Grid Side **(b) DC Link voltage**

Fig.3.20d respectively. From the results, it is inferred that rise/reduction in rotor current, real and reactive power of the machine is similar to the simulation results obtained.

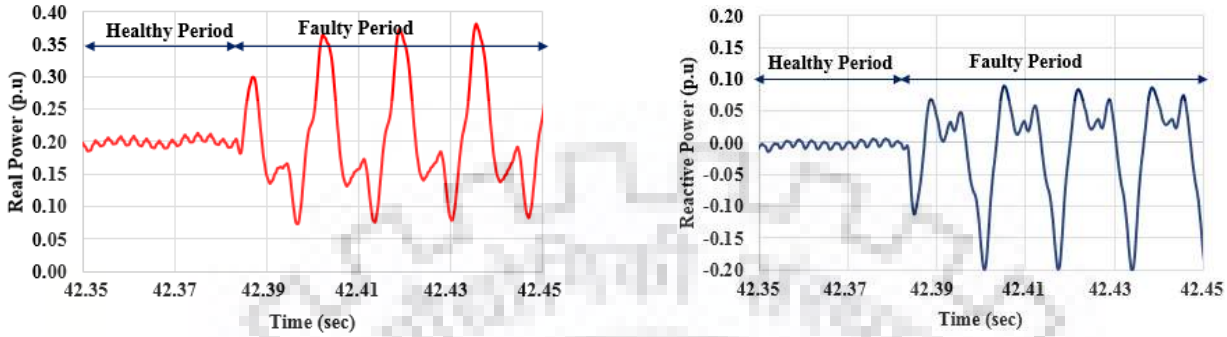

(c) Real Power (Rotor Side -Grid)

(d) Reactive Power (Rotor Side -Grid)

Fig. 3.20 . GSC upper two switches open circuit fault (2.2 kW DFIM) at starting

3.4.2 Power Converter Failure in a Single Converters

3.4.2.1 RSC Upper Two Switches Open Circuit Fault

Single device open circuit faults during starting have been injected at 43.78 s. During the fault, magnitude of one of the rotor current (upper half cycle) in parallel connected healthy

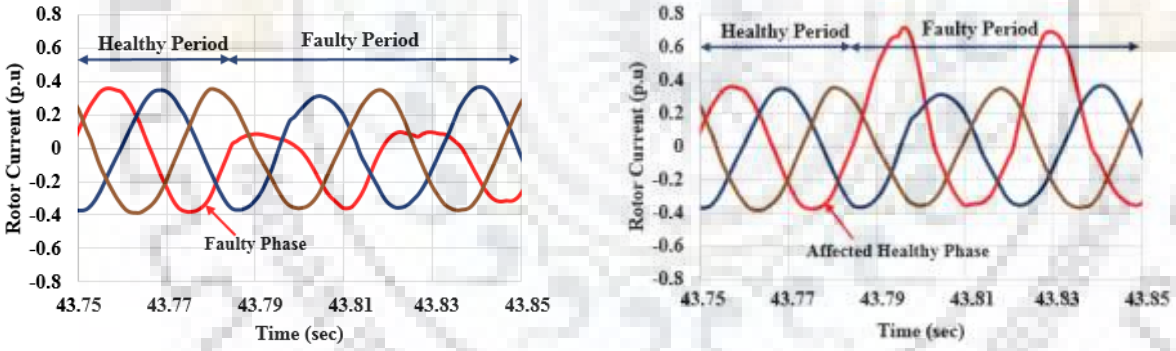

(a) Rotor Current - Faulty Converter

(b) Rotor Current - Healthy Converter

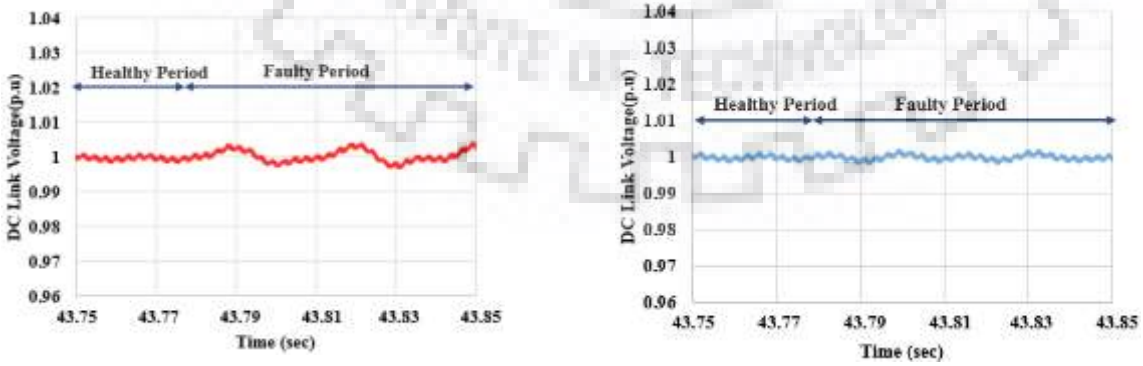

(c) DC Link Voltage - Faulty Converter

(d) DC Link Voltage - Healthy Converter

Fig. 3.21 . RSC upper two switches open circuit fault (2.2 kW DFIM) at starting

converters reach to 0.65 p.u (2.44 A) as shown in Fig 3.21b and other phases are carrying current as normal.

3.4.2.2 RSC Single Leg Open Circuit Fault

Single leg gate drive open circuit fault is injected at 46.48 s and results are shown in Fig.3.22. During the fault, magnitude of one of the rotor currents in parallel connected healthy converters increases two times (half cycle period) of regular value (shown in Fig. 3.22b). However, machine speed is not affected and gradually increases as set by the smooth starting control system. From Fig. 3.22c, it is inferred that fluctuation in dc link voltage in faulty converter is two times than open circuit fault in upper two switches. From the experimental results, it is estimated that rise in rotor current is similar to simulation results in consideration of number of power converters connected in parallel, turns ratio and inertia.

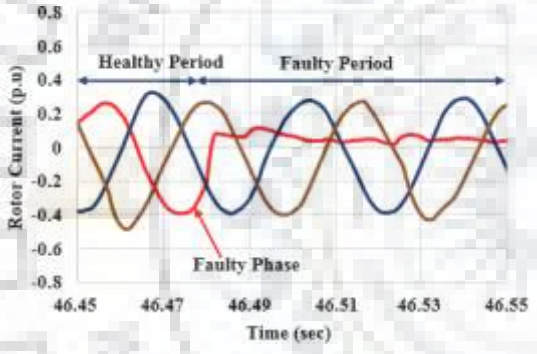

(a) Rotor Current - Faulty Converter

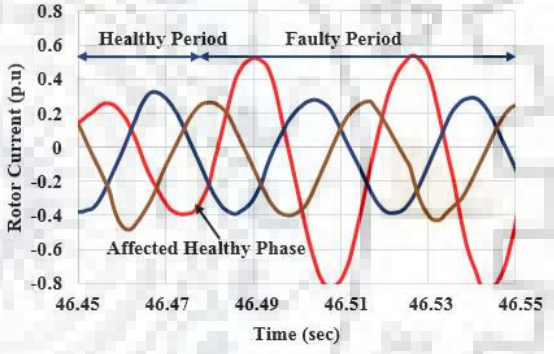

(a) Rotor Current - Healthy Converter

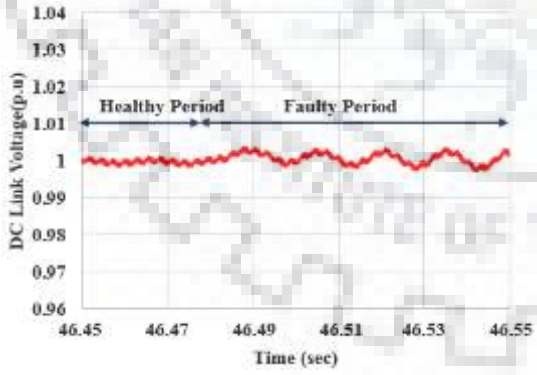

(c) DC Link Voltage - Faulty Converter

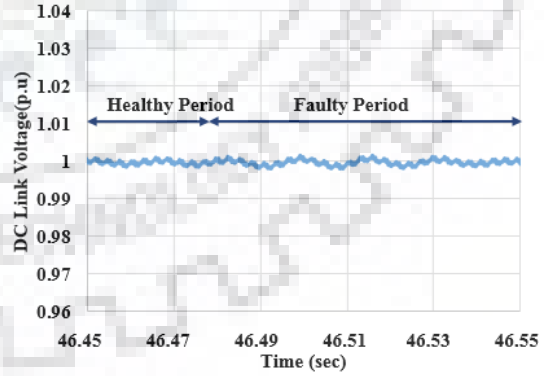

(d) DC Link Voltage - Healthy Converter

Fig. 3.22 . RSC single leg open circuit fault (2.2 kW DFIM) at starting

Likewise short circuit fault, dc link voltage sensor, single grid voltage sensor fault, and single grid current sensor fault are injected for both starting and braking mode and results are summarized in Table 3.1.

Table 3.1: DFIM drive status at converter and sensor failure during starting and braking

System		Faults	Fault Status
Power Converter	Rotor side converter	Open Circuit Fault (SDOC, SLOC)	S
		Short Circuit Fault (U/LTDSC)*	S
		Short Circuit Fault (PPSC,PGSC)	F
	Grid side converter	Open Circuit Fault (SDOC, SLOC)	S
		Short Circuit Fault (SDSC, U/LTDSC)	S
		Short Circuit Fault (DCSC,PPSC,PGSC)	F
Sensor	Omission/ saturation	DC link voltage sensor	F
		Single grid current sensor	S
		Single grid voltage sensor	F
	Gain	DC link voltage sensor	F
		Single grid current sensor	S
		Single grid voltage sensor	F

SDOC - single device open circuit fault
SLOC - single leg open circuit fault
U/LTDSC - upper/lower two devices short circuit fault
* short circuit through pulses
DCSC - DC link short circuit
PPSC - Phase to phase SC
PGSC - Phase to ground SC
S - Survived F- Failed

3.5 Fault Tolerant Operation in Power Converter Open Switch Fault

From the experimental results (shown in Table 3.1), open circuit fault in rotor side power converter during starting is not affected the continuity of operation of the unit. However, once the machine is started, power converters need to be handled more currents in accordance with power set points (e.g. 11600 A full load current in a 250 MW DFIM unit of Tehri PSPP, India). Therefore, open circuit fault in any one of the power converter results to stoppage of the machine. To continue the operation of the unit, power redundancy or fault tolerant operation needs to be provided in the parallel converters. However, there is no power redundancy in any of the commissioned variable speed PSPP unit. The issue of production of overvoltage in rotor windings is ducked by not providing any mechanical contactors in rotor side of the machine. Presently, resistive voltage dividers with IEC 61850-9-2 LE and rogowski current transformers are detecting extremely low frequency or dc component current [86].

The proposed fault tolerant system aims to design redundancy system in multichannel converter fed DFIM without the contactors connected in series with each channels. By doing so, risk of over voltages in rotor winding can be avoided during their operations (ON/OFF). Further,

it is planned to remove the PWM pulses from the faulty converters (open circuit and other faults except short circuit fault in a whole leg) and operate the machine with other healthy converters at reduced (partial) loads. It is noted that the fault is detected by de-saturation, circulating current fault detection techniques and the knowledge of open circuit fault in parallel power converters.

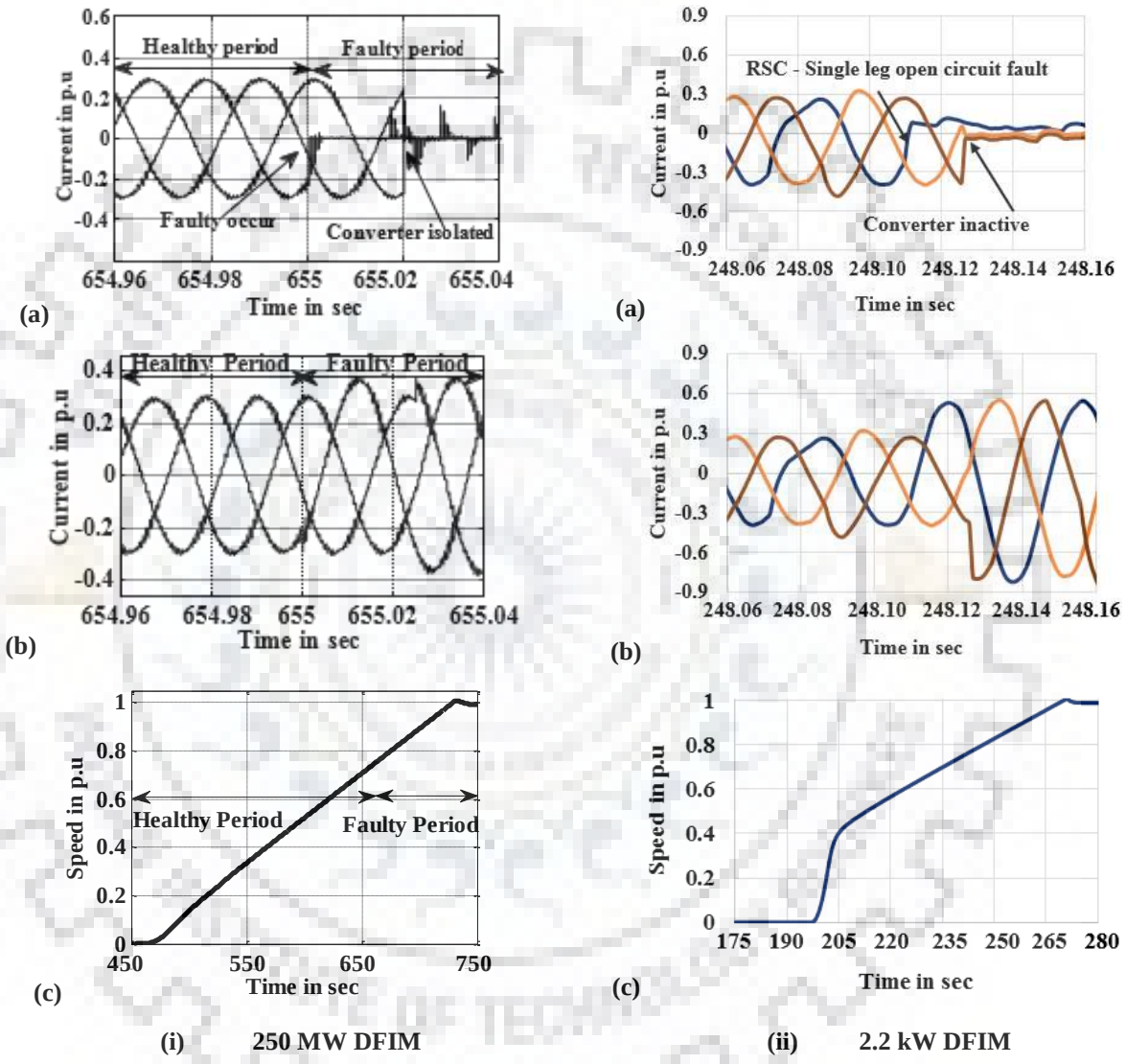

Fig. 3.23. RSC single leg open circuit fault tolerant operation: (a) Rotor Current-faulty converter, (b) Rotor current- healthy converter, (c) Speed

The simulation and experimental results are shown in Fig. 3.23 (i) and Fig. 3.23 (ii), respectively. It shows that when the fault (single leg OC fault) occurs, one of the faulty converter phase current goes to zero, then fault detection algorithm finds out the fault in the converter and inactivates the faulty converter by removing gate pulses (shown in Fig 3.23(i)a). The healthy

Table3.2. Economic analysis of fault tolerant operation of DFIM

Mode of operation	Power Converters Faults	Fault Status	No.of Failures/year	U Period/year	250 MW DFIM			Fault Tolerant		
					Energy Storage Losses* (MU)	Financial Losses**/year (M$)	P	Energy Storage Gained (MU)	Benefits/year (M$)
Pumping	RSC Open Circuit Fault (SDOC, SLOC)	F	1.9940	50.59	9.87	0.59	Yes	8.50	0.51***
	RSC Short Circuit Fault (SDSC,PPSC,PGSC)	F	0.6646	16.86	3.29	0.20	NA	-	-
	GSC Open Circuit Fault (SDOC, SLOC)	F	0.3025	11.83	2.31	0.14	Yes	1.99	0.12***
	GSC Short Circuit Fault (SDSC,DCSC,PPSC,PGSC)	F	0.1008	3.94	0.77	0.05	NA	-	-
	DC Link Open circuit/Short circuit	F	0.007	2.19	0.43	0.03	NA	-	-
				Total Energy Storage	16.67			10.49	

* Average energy storage is 195 MW/year/unit for a 250 MW DFIM
** Financial losses are considered as $ 0.06/kWh
*** Fault tolerant proposed in this paper with reduced power generation (168 MW)
U – unavailability
P – possibility
Total energy storage year is 427.37 MU (Considering 6 hours/day)
Total energy storage considering fault tolerant operation is 420.92 MU
Total energy storage considering power redundancy problem is 410.71 MU
Benefit of fault tolerant operation = $\frac{420.92 - 410.71}{410.71}$ =2.49 %

SDOC - single device open circuit fault SLOC - single leg open circuit fault SDSC - Single device short circuit DCSC - DC link short circuit
PPSC - Phase to phase SC PGSC - Phase to ground SC S - Survived F - Failed

converters are in operation and carry the current of 1.2 times of regular value during starting. Subsequently, pumping mode continues at part load operation of 0.672 p.u (168 MW) which is accepted by the other healthy converters. During fault tolerant operation, healthy converters are carrying current 0.85 p.u each. During experiment, current in healthy converters increases

2 times (shown in Fig. 3.23(ii) b) of their regular values since only two converters are connected in parallel.

3.5.1 Possible Pumping operation of 250MW DFIM during RSC - single leg/device Open Circuit Fault during Starting

The efficiency of pump turbine depends on water head level in the dam and volume of water pumped back to the upper reservoir from the lower reservoir. The requirement of input power of the machine depends on water head. i.e., availability of minimum water head level in dam requires less input power for the rated water discharge from lower to upper reservoir.

A typical 250 MW DFIM unit has been operated with five parallel three level back-to-back voltage source converters with a full load current rating of 11600 A. The rated current of the each power converter is 2400 A. During open circuit fault in a converter, the corresponding converter unit is isolated/inactivated from the parallel converter system and remaining four units are in continuous operation. However, power handling of the unit with the aid of four converter is limited to 168 MW. Therefore, shaft power of the unit is fixed at 168 MW during fault tolerant operation. Fig. 3.24b shows the amount of water discharge from lower to upper reservoir at fixed input power (168 MW) considering variable water heads (shown in Fig. 3.24a [192]). It is inferred that the water discharge varies with respect to variable water heads. In addition, it shows that the proposed fault tolerant operation in open circuit fault provides considerable amount of water pumped back to the upper reservoir through four parallel connected healthy converters. The probability of operational state of power converter without redundancy in variable speed PSPP per year is 96.10%. But, the incorporation of fault tolerant operation in power converter

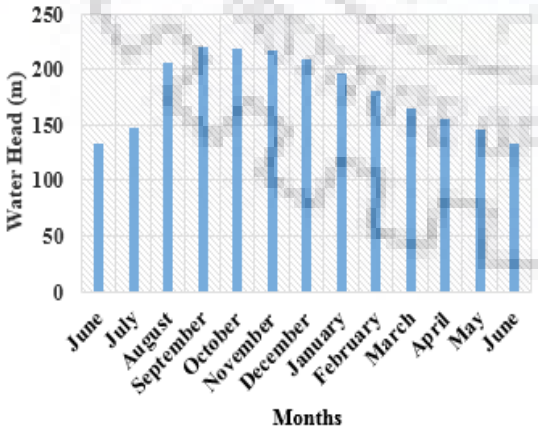

(a) Yearly water head variation

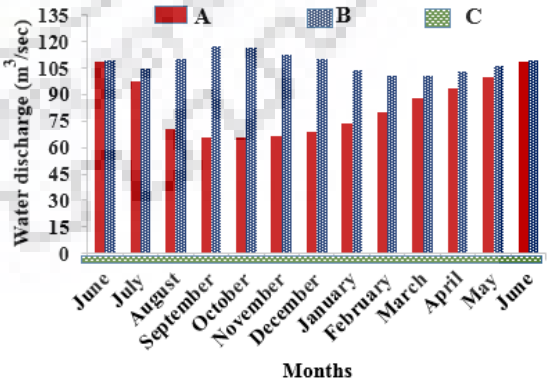

A – With fault tolerant operation B – Normal operation
C - Without power redundancy

(b) Discharge at various water heads at 168 MW input power

Fig. 3.24. Fault tolerant operation of a 250 MW DFIM variable speed PSPP

open circuit fault improves operational state of the power converter to 98.44%. It shows that the proposed fault tolerance during single leg/single device brings additionally 34.8 MCM (Million Cubic Meter) of water pumped back to the upper reservoir from lower reservoir which leads to an additional storage of 2.49% electrical energy compared to the operation of DFIM without power redundancy operation. Table 3.2 shows the outcomes of the fault tolerant operation.

3.6 Energy Efficient Start-up Control of DFIM Fed Large Pump Turbine

Energy efficient starting aims to eliminate the slip power losses and providing the reactive component current from stator dc source instead of rotor supply which results to reduction in no-load losses. Fixed dc voltage is applied to stator winding when the rotor started to rotate and continued till the machine synchronization with the grid.

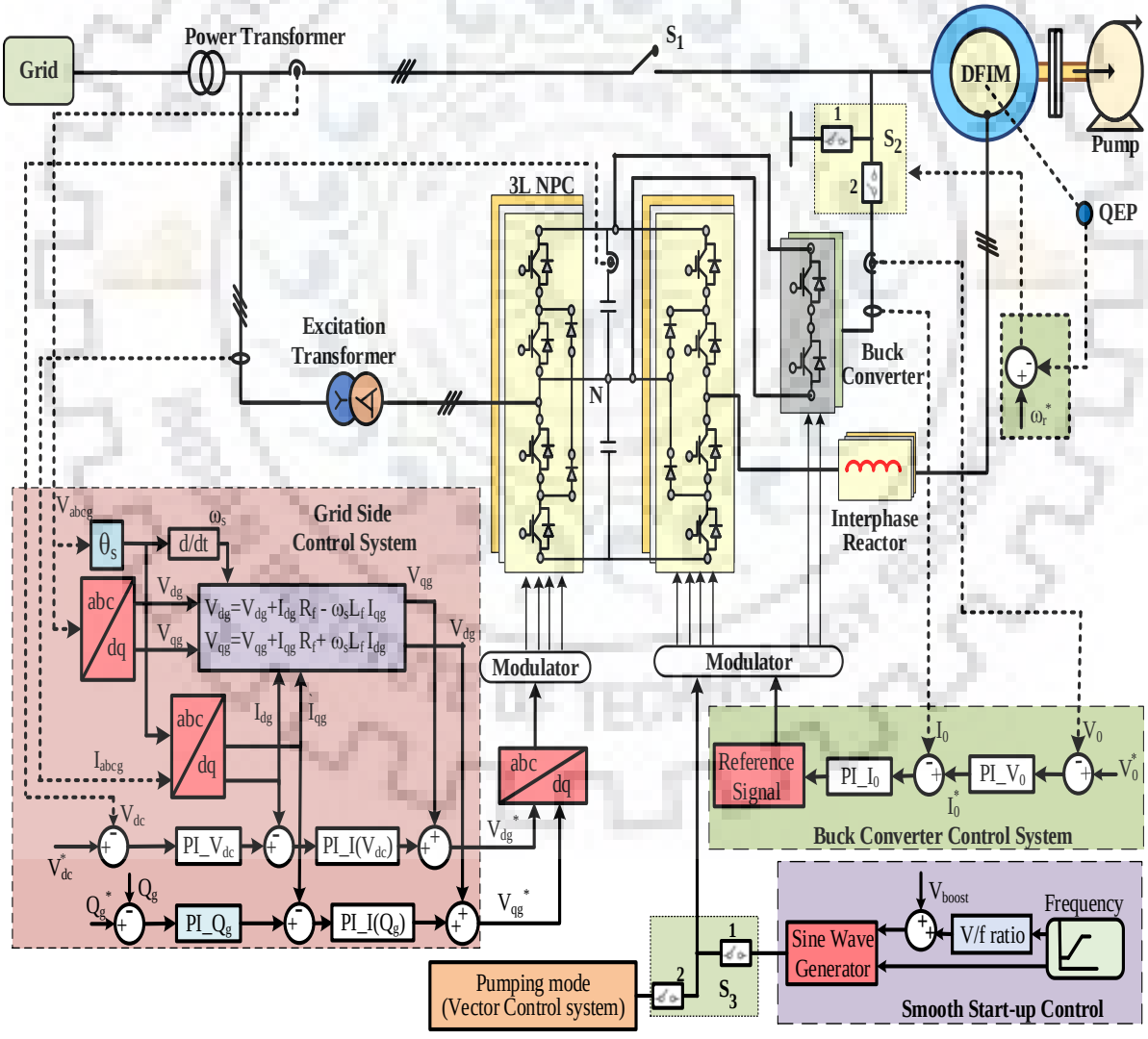

Fig. 3.25. Control diagram of energy efficient starting of DFIM

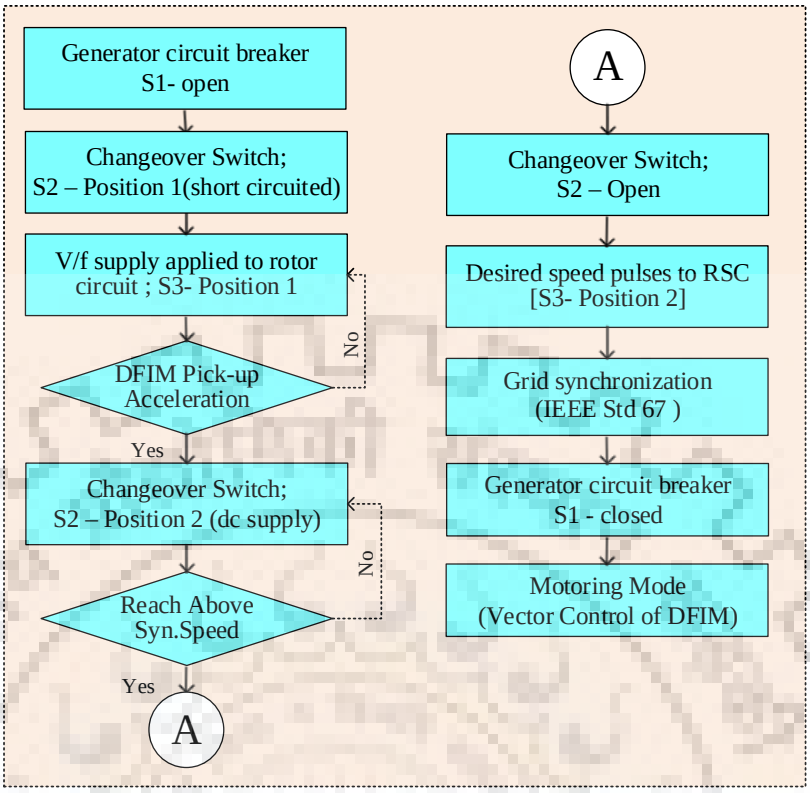

Fig. 3.26. Energy efficient starting sequences of DFIM

Control diagram and starting sequences for the proposed energy efficient starting are shown in Fig.3.25 and Fig.3.26, respectively. During starting, grid side converters help to maintain the unity power factor at grid side and maintain constant dc link voltage. Variable voltage/frequency supply is given to rotor of the machine with the help of rotor side converters (RSC). Changeover switch (S2) is placed in the stator circuit of the machine. Primarily, stator of the machine is short-circuited via changeover switch; V/f supply is applied to rotor circuit and the machine accelerates to pick up the speed. Encoder is sensing the speed and send a signal to changeover switch control section. Once the starting torque is established, changeover switch control section provides a signal to the changeover switch to change the stator terminal from short circuit to fixed dc supply. Fixed dc is applied till the machine is synchronized with the grid (no- load). The transition mode from stator short-circuited to dc supply is estimated through speed-torque characteristics. Step- down dc chopper is employed to provide the reduced dc voltage to stator circuit through a changeover switch. The input to the dc chopper is taken from the dc link voltage of the back-to-back voltage source converter. Chopper control system is designed in such a way that to maintain fixed dc voltage at the stator terminal.

3.6. 1 Simulation Results (250 MW DFIM)

In order to demonstrate the energy efficient starting, a 250 MW doubly fed induction machine is simulated in MATLAB/Simulink software and the control system is executed based on Fig. 3.25. The duration for smooth starting is selected as 250 seconds for starting and 60 seconds for additional operations till stator circuit is connected to grid. The voltage boost and frequency are selected as 430 volts and 7 Hz, respectively. Also voltage ratio is estimated as 66 considering rated rotor voltage and frequency. Machine is started by energizing the rotor with variable voltage variable frequency (VVVF) supply. Phase locked loop control (PLL) is used to estimate the angle (during smooth staring) of the machine from VVVF supply. Three current sensors used to sense the rotor currents. Afterward, torque component current and magnetization currents are splitted from the rotor current using Clarke and Park Transformations, which are calculated as 2268 A (I_{qr}) and 3128 A (I_{dr}), respectively. The fixed dc voltage is selected as 16.8 volts. Rotor speed at which the changeover switch is operated from stator short- circuited to fixed dc supply is 27% of the synchronous speed.

Energy consumption and performance related parameters of machine at stator short circuited and stator connected to fixed dc supply are given in Fig. 3.27. The estimation of energy consumption is calculated through the equation (3.1) & (3.2).

$$P_{Total} = \sum_{i=1}^{n} \left[\frac{\left(P(i) + p(i+1) \right)}{2} \right] * \left[T(i+1) - T(i) \right] \tag{3.1}$$

$$E_{Total} = \frac{P_{Total}}{3600 * 1000} \tag{3.2}$$

where, P → Power; T → Time; n → number of samples

In Fig. 3.27c, reactive and torque component current are stabilized at 40 s (i.e. 0.18 p.u speed). In conventional method, machine consumes about 0.2896 p.u (3128 A) reactive component current for magnetization and 0.210 p.u (2268 A) torque component current for acceleration as shown in Fig. 3.27c. In addition, the maximum power consumption for conventional start-up method (at 250s) is observed about 0.0506 p.u (15.484 MVA). In Fig. 3.27b, fixed dc supply is applied to the stator winding is about 66s (i.e. 0.27 p.u speed). During FDC to stator circuit, both reactive and torque component current produce acceptable transients of about 0.4742 p.u (5121 A) and then reactive component current reaches near to zero, torque component rises to 0.2554 p.u (2748 A), shown in Fig. 3.27d. At stator side, terminal A carries 0.308 p.u (3465 A),

terminal B carries -0.02 p.u (225 A) and terminal C carries -0.284 p.u (-3195 A) currents. It is noted that the power consumption at 250s is 0.0372 p.u (11.383 MVA) in case of proposed start-up method.

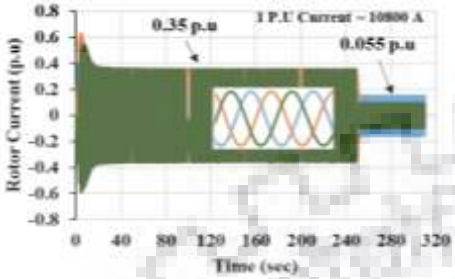

(a) Rotor Current – Conventional start-up

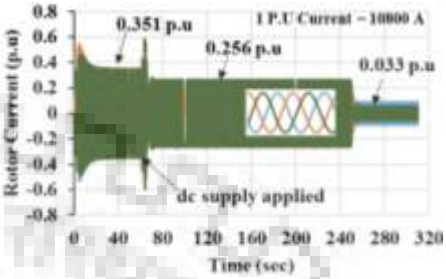

(b) Rotor Current – Proposed start-up

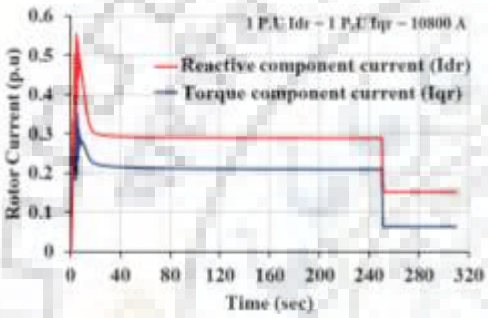

(c) d-q-axis Rotor Current – Conventional start-up

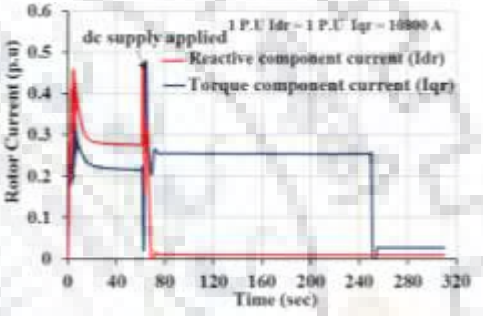

(d) d-q-axis Rotor Current – Proposed start-up

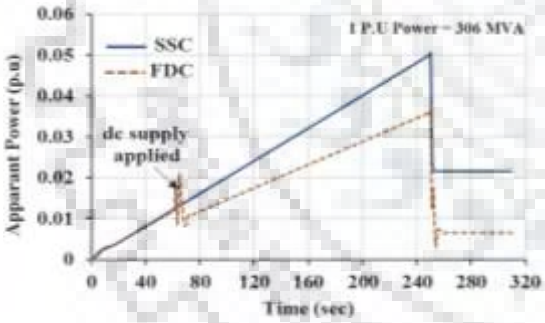

(e) Apparent Power Consumption

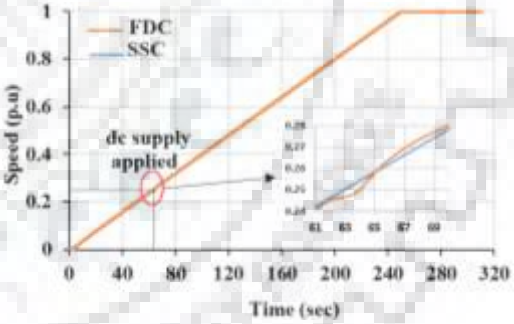

(f) Speed

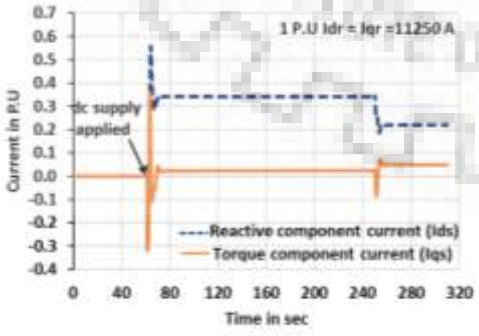

(g) Stator Current

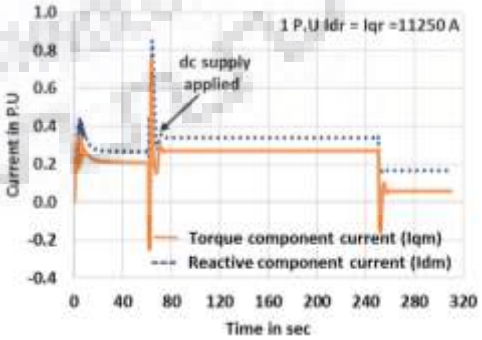

(h) Total Current (Stator + Rotor)

Fig. 3.27. Energy efficient starting of 250 MW DFIM

Table 3.3. Energy calculation of a 250 MW DFIM during starting

	Smooth starting stator short circuit (SSC)			Smooth starting with DC Excitation (FDC)				Comparison of SSC Vs FDC
	(a)	(b)	(c)	(d)	(e)	(f)	(g)	(h)
	zero - rated speed (0s -250 s)	rated speed - synchronization (250 s - 310 s)	Total (0 to 310 sec) (a+b)	zero - 27% speed* (0 s- 66 s)	27% - rated speed** (66 s - 250 s)	rated speed – synchronization (250 s - 310 s)	Total (0 s to 310 s) (d+e+f)	Total energy conserved/ unit (c-g)
Energy (kW-hr) consumption	537.79	113.37	651.16	85.14	321.73	14.09	420.96	230.20

*stator short circuit
**DC voltage injected in stator windings

% of Energy saving = $\left(\frac{c-g}{c}\right)$ X 100% = 35.35%

Fig. 3.27e shows the power consumption characteristics of conventional and proposed start-up method. During conventional start-up, the machine consumes 651.16 units (kW-hr) of energy whereas the proposed start-up strategy consumes only 420.96 units (Table 3.3). This energy consumption shows the proposed start-up saves about 35% energy from conventional starting.

Fig. 3.27f shows speed characteristics of conventional and proposed start-up method. In proposed method, the speed of the machine rotates at synchronous frequency after FDC applied to stator circuit. It conveys that the slip losses are neglected during the machine operate at synchronous speed.

Fig.3.27a and Fig. 3.27b show the rotor current (phases A, B, C) between conventional (Fig. 3.27a) and proposed (Fig.3.27b) start-up methods. In conventional starting, the rotor current reaches to 0.35 p.u (3780 A) and receives 0.055 (594 A) p.u at rated speed, whereas FDC applied to stator winding in proposed method, rotor current decreases to 0.256 p.u (2765 A).

In summary, the simulation results show that the rotor and stator current of the DFIM during transition period (SC to FDC) is below the name plate ratings (shown in Appendix) and are acceptable. Also it is observed that the proposed energy efficient smooth starting method saves about 35% energy from conventional stator short circuit based start-up of pump turbine.

3.6. 2 Experimental Validation (2.2 kW DFIM)

Smooth starting of DFIM is achieved through a three level back-to-back IGBT based converter module with dSPACE 1202 real time controller (shown in Fig. 3.28). GSC controls the dc link voltage and RSC ensures the smooth starting of the machine. In addition, transfer switch (Two contactors – MNX A1, 10A) is controlled by the real time controller through a

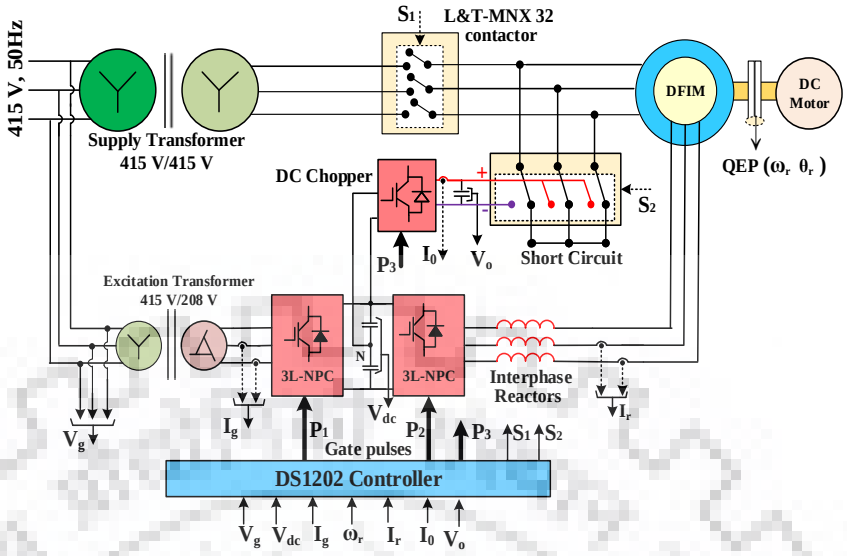

Fig. 3.28. Experimental block diagram of energy efficient starting

relay (SRD-5V-SL-C, 10A). SPWM pulses (carrier frequency of 1650 Hz and dead band of 6μs) generated in MATLAB Simulink are given to converters through the controller. The dc link voltage of back-to-back three level converter is maintained at 325 V and the sample time is 0.001s. The pedestal voltage (voltage boost) and frequency start-up is chosen as 36 volts and 5 Hz respectively. Also, voltage ratio is chosen as 3.7.

In experimental tests, duration for smooth starting is selected as 96 s. The speed at which the transfer switch is operated from stator short-circuited to fixed dc supply is 53% of the synchronous speed and the test results (2.2 kW) are shown in Fig. 3.29. At 90% of machine speed, during conventional smooth starting, it consumes 885 VAr (0.4025 p.u) reactive power

Table 3.4. Energy Calculation of a 2.2 kW DFIM during starting

	Smooth starting stator short circuit (SSC)			Smooth starting with DC Excitation (FDC)				Comparison of SSC Vs FDC
	(a)	(b)	(c)	(d)	(e)	(f)	(g)	(h)
	zero - rated speed (0s -96s)	rated speed - synchronization (96s - 120s)	Total (0 to 120 s) (a+b)	zero - 55% speed* (0s- 43 s)	55% - rated speed** (43s - 100s)	rated speed – synchronization (100s - 120 s)	Total (0 s to 120 s) (d+e+f)	Total energy conserved/ unit (c-g)
Energy (kW-hr) consumption	0.0108	0.004534	0.01534	0.00225	0.00519	0.00233	0.0098	0.00556

*stator short circuit

**DC voltage injected in stator windings

$$\% \text{ of Energy saving} = \left(\frac{c-g}{c}\right) X\ 100\% = 36.31\%$$

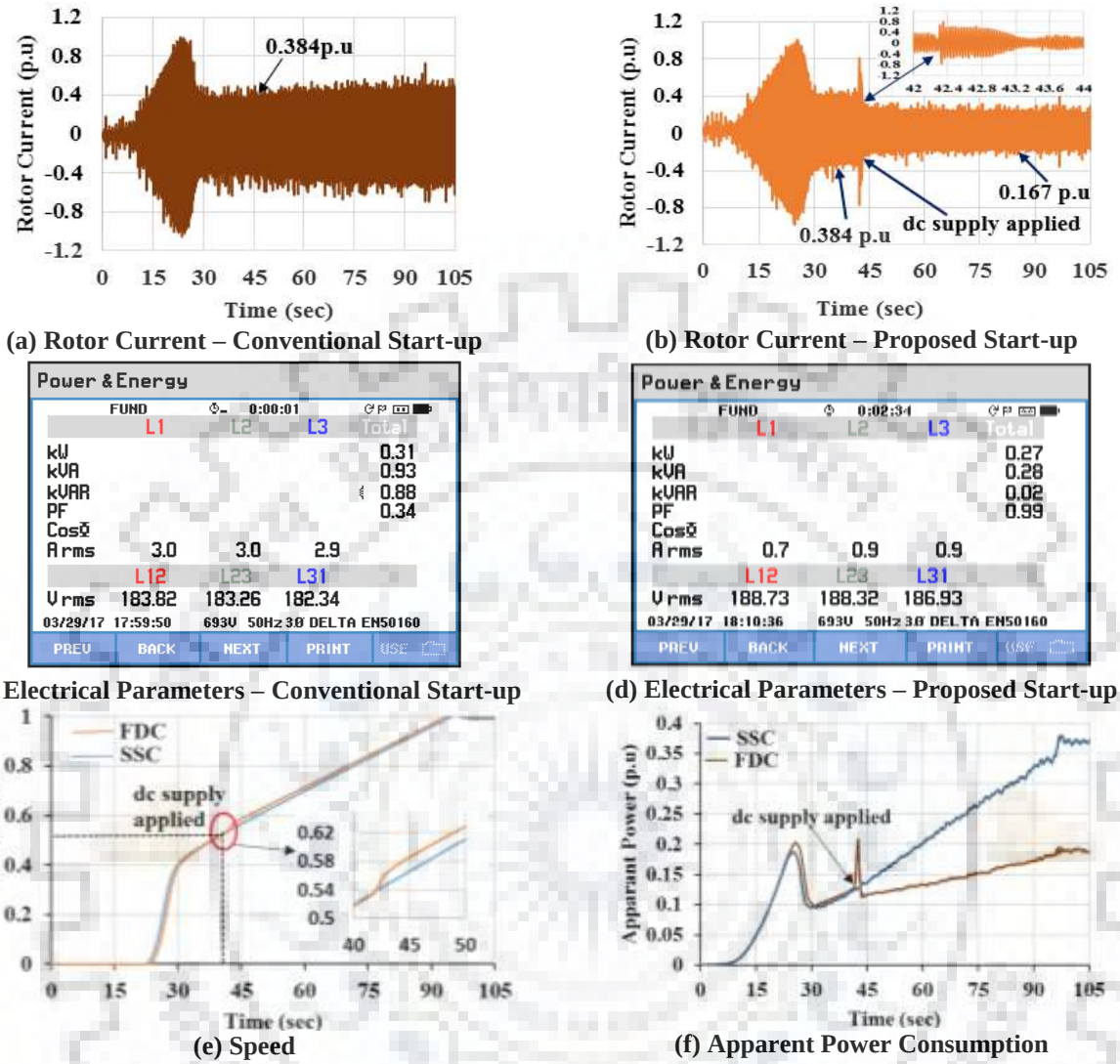

(a) Rotor Current – Conventional Start-up

(b) Rotor Current – Proposed Start-up

(c) Electrical Parameters – Conventional Start-up

(d) Electrical Parameters – Proposed Start-up

(e) Speed

(f) Apparent Power Consumption

Fig. 3.29. Energy efficient starting of 2.2 kW DFIM

and 204 watts (0.093 p.u) real power, respectively. Overall, it consumes about 924 VA (0.42 p.u) apparent power. Whereas in the proposed work, total power consumption is about 313 VA (0.142 p.u). During FDC to stator circuit, both reactive and torque component current produce transient currents of 0.798 p.u (5.985A) and the reactive component current reaches near to zero. In conventional starting (Fig. 3.29a), the rotor current reaches to 0.931 p.u (6.98 A) initially, once the machine pick-up the acceleration then the current is stabilized at 0.384 p.u (2.88 A). Whereas in proposed method (Fig. 3.29b), after applying FDC to stator circuit, rotor current decreases to 0.167 p.u (1.253 A).

Rotor side electrical quantities are shown in Fig. 3.29c (conventional method) and 3.29d (proposed start-up method). It is inferred that during proposed start-up method reactive power

of the machine at rotor side reaches to zero (about 0.02 kVar) whereas it is about 0.88 kVAr during conventional starting observed from Fig 3.29c and Fig. 3.29d. In summary, the total power consumption of the machine reduced to 0.28 KVA in proposed method, whereas it is about 0.93 KVA in conventional start-up method.

Fig. 3.29f shows the experimental results of energy consumption of conventional and proposed methods. The machine consumes 0.01534 units (kW-hr) of energy whereas it is reduced to 0.00977 units at proposed method. The estimation of energy consumption is calculated through the equation (3.1) and (3.2) and is tabulated in Table 3.4. The experimental results evidently prove that there is less transients (0.781 p.u =5.86 A) during transition period (SC to FDC) and also saves about 36.31% energy from conventional stator short circuit based start-up of pump turbine. Hence the simulation of 250 MW pump turbine at proposed start-up method is validated.

3.6. 3 Key Elements of Energy Efficient Starting

3.6. 3.1 Rotor speed at which the transfer switch is operated

Stator circuit of the doubly fed induction machine is switchover from short-circuited to dc supply is crucial during starting. During the transition, it is ensured that the swing in rotor and stator flux magnitude should be in acceptable limit, thereby it will not produce the undesirable electromagnetic torque and power disturbances. Speed versus torque characteristics of the induction machine (NEMA design standard) is shown in Fig. 3.30a. It shows that the machine pull-up acceleration is happened after 20% of the synchronous speed. Also, as per Allen Bradley, the chance of machine acceleration takes between 25% and 40% of the synchronous speed of the machine [189].

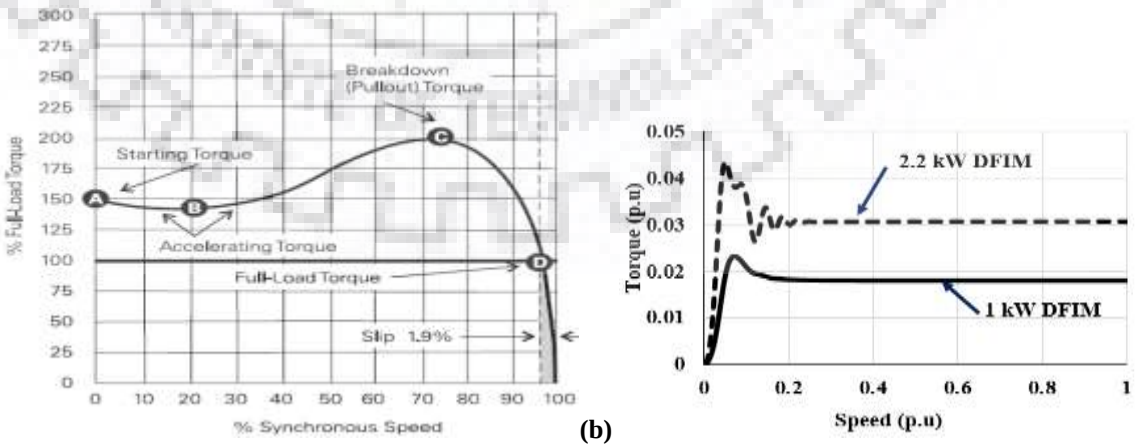

Fig. 3.30. Speed Vs Torque characteristics: (a) NEMA Design, (b) V/f smooth starting

During V/f control of machine, higher amount of electro-magnetic torque is produced at initial stage of starting and it is stabilized after the machine acceleration as shown in Fig. 3.30b. Further, it is noticed that the current and flux component of the machine are also stabilized after the acceleration. Therefore, it is decided to apply FDC to stator circuit after the stabilization of electro-magnetic torque provides less pulsations in speed and torque. The stabilizing point varies w.r.to power rating and inertia of the machine. Further, it is noticed from simulation and experimental tests conducted in the laboratory that the low rated machines require more speed for stabilizing electro-magnetic torque and rotor current as compared to large rated machines.

3.6. 3.2 Selection of Fixed DC voltage

Fixed dc voltage is selected in consideration of performance related parameters (stator and rotor currents of DFIM) should not be exceeded than nameplate ratings. The dynamic limit of stator and rotor currents are clarified through suitable equations given in (3.3) and (3.4), respectively.

$$I_s \geq \frac{1}{\sqrt{2}} I_{s(rated\_ac)} \tag{3.3}$$

$$I_r \geq \sqrt{\left(-\frac{L_s}{L_m} I_s \sin\delta\right)^2 + \left(\frac{\tau_{dc}}{L_m I_s \sin\delta} - \frac{L_s}{L_m} I_s\right)^2} \tag{3.4}$$

where, $\tau_{dc} = I_s \psi_{sdc} \sin\delta$

'δ' is the angle between stator flux and stator voltage (FDC). The fixed dc voltage is applied at no- load, therefore the machine does not produce much transients as compared to the loaded conditions. During conventional starting, magnetic flux of the machine is maintained by d-axis rotor current (magnetization current/reactive component current). However, in DFIM, the magnetic flux of the machine is associated with both rotor and stator d-axis currents as per eqn. (3.5).

$$\left\{\begin{array}{l} \vec{\psi}^{a}_{dr} = \sigma L_r \vec{I}^{a}_{dr} + \frac{L_m}{L_s} \vec{\psi}^{a}_{ds} \\ \vec{\psi}^{a}_{ds} = L_s \vec{I}^{a}_{ds} + L_m \vec{I}^{a}_{dr} \end{array}\right\} \tag{3.5}$$

Further, any one of the d-axis current (either d-axis stator current or d-axis rotor current) is enough to provide the required magnetic flux of the machine [190] - [192]. In proposed work,

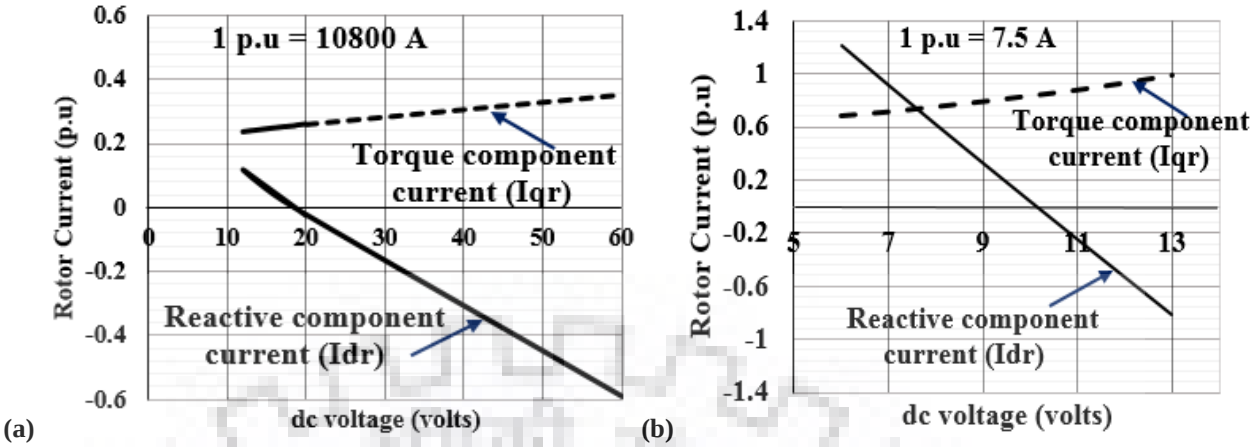

Fig. 3.31 DC link voltage source characteristics: (a) 250 MW, (b) 2.2 kW

required magnetic flux is provided by d-axis stator current through fixed dc supply. Magnitude of fixed dc voltage is estimated based on the requirement of reactive component current during starting and no-load torque requirements. The estimation of reactive component current (I_{dr}) is calculated from the rotor current of the machine by Clarke and Park transformations. Once the reactive component current is calculated then the fixed dc voltage connected to stator circuit is estimated by eqn.3.6.

$$V_{dc} = R_s I_{dr} \tag{3.6}$$

$$I_{dr} \cong I_s \cong I_{dc} \tag{3.7}$$

Alternatively, fixed dc voltage is calculated based on dc link voltage source characteristics (Fig. 3.31) drawn between fixed dc voltage and torque component current/reactive component current of the machine.

3.6. 4 Power and Control Circuit Faults during Energy Efficient Starting

3.6. 4. 1 DC Link Voltage Sensor Gain Fault in rotor side VSC

Gain fault is modelled by connecting a gain block in series with sensor signal [193]. DC link voltage sensor gain fault (1.5 p.u) is injected in back-to-back VSC at 175 s and results are shown in Fig. 3.32 (i). During the fault, dc link voltage controller reads input as more than the desired value and decreases proportional gain of the controller results to decreases the dc link voltage of the back-to-back converter as 0.66 p.u. From the test results, it is summarized as: (i)grid side rotor currents decreases in all phases, (ii) dc link voltage of the back-to-back power converter decreases with respect to the faulty gain value, (iii) power factor of the grid side system

is maintained unity, (iv) rotor current of the machine increases during the faulty period as shown in Fig 3.32(i)a, (v) reactive power is delivered from the machine (shown in Fig 3.32(i)b), (ii)speed of the machine is fluctuated initially and gradually increases as se by the RSC control system (shown in Fig. 3.32(i) (c)), (vi) total power consumption from the grid increases. In case of omission fault, dc link voltage increases and results to more reactive power consumption from the grid.

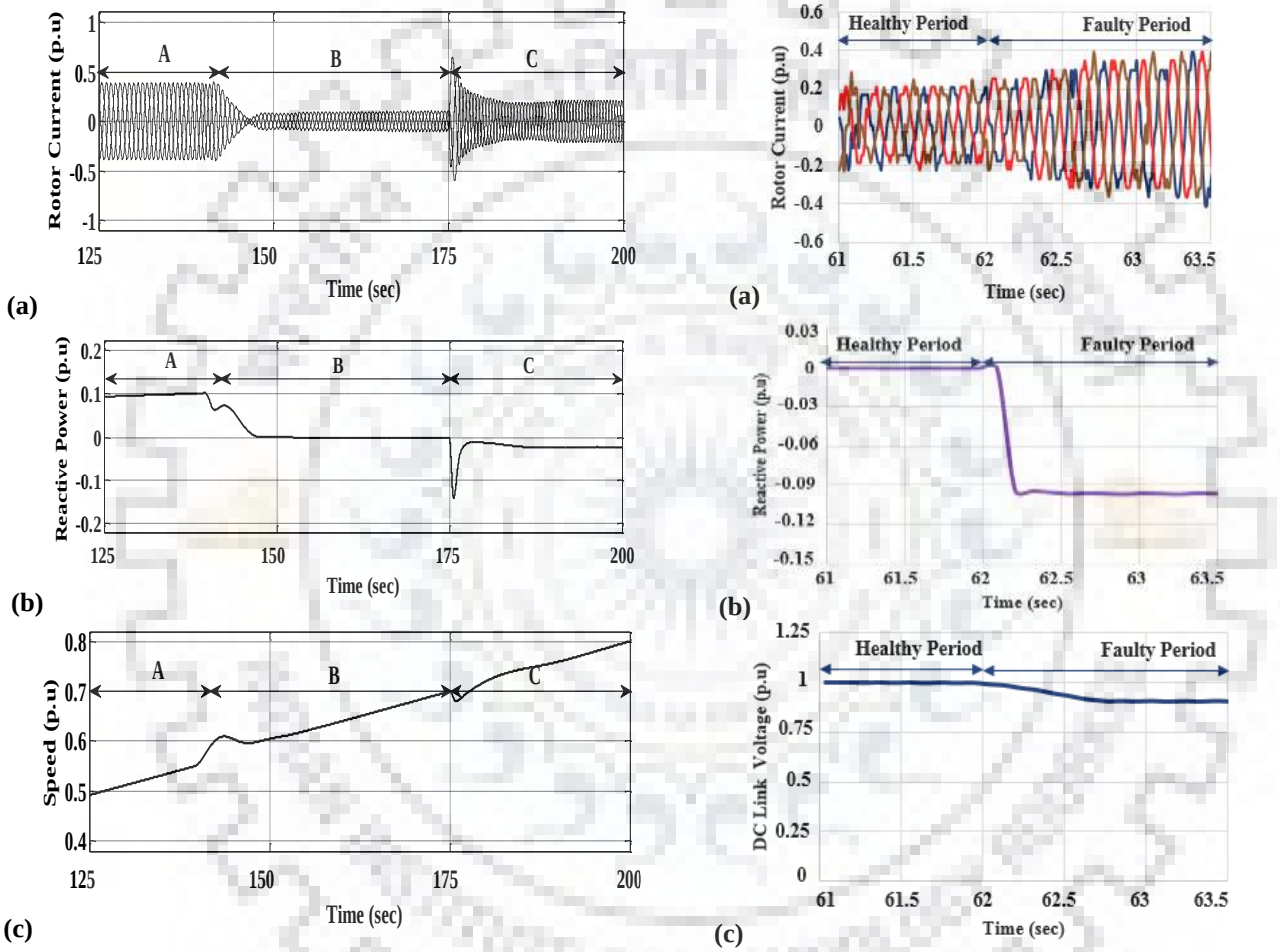

(i) Simulation Results (250 MW) (ii) Experimental Results (2.2 kW)

Fig. 3.32. DC link voltage sensor gain fault in VSC 250 MW DFIM: A - Stator short Circuited; B - Stator Connected to FDC; C - Fault Period

3.6. 4. 2 DC Link Voltage Sensor Gain Fault in DC Chopper

DC link voltage sensor gain fault (1.5 p.u) is injected in dc chopper at 175 s and results are shown in Fig. 3.33(i) c. During the fault, value of fixed dc voltage connected to the stator circuit is decreased with respect to the gain fault. From the test results, it is summarized as: (i) reactive power consumption of the machine increases as shown in Fig. 3.33(i)b, (ii) rotor current

of the machine increases as shown in Fig 3.33(i)a, (iii) speed of the machine is unchanged (shown in Fig. 3.33(i)c). In case of omission fault, FDC is increased and results to reactive power is delivered to the grid.

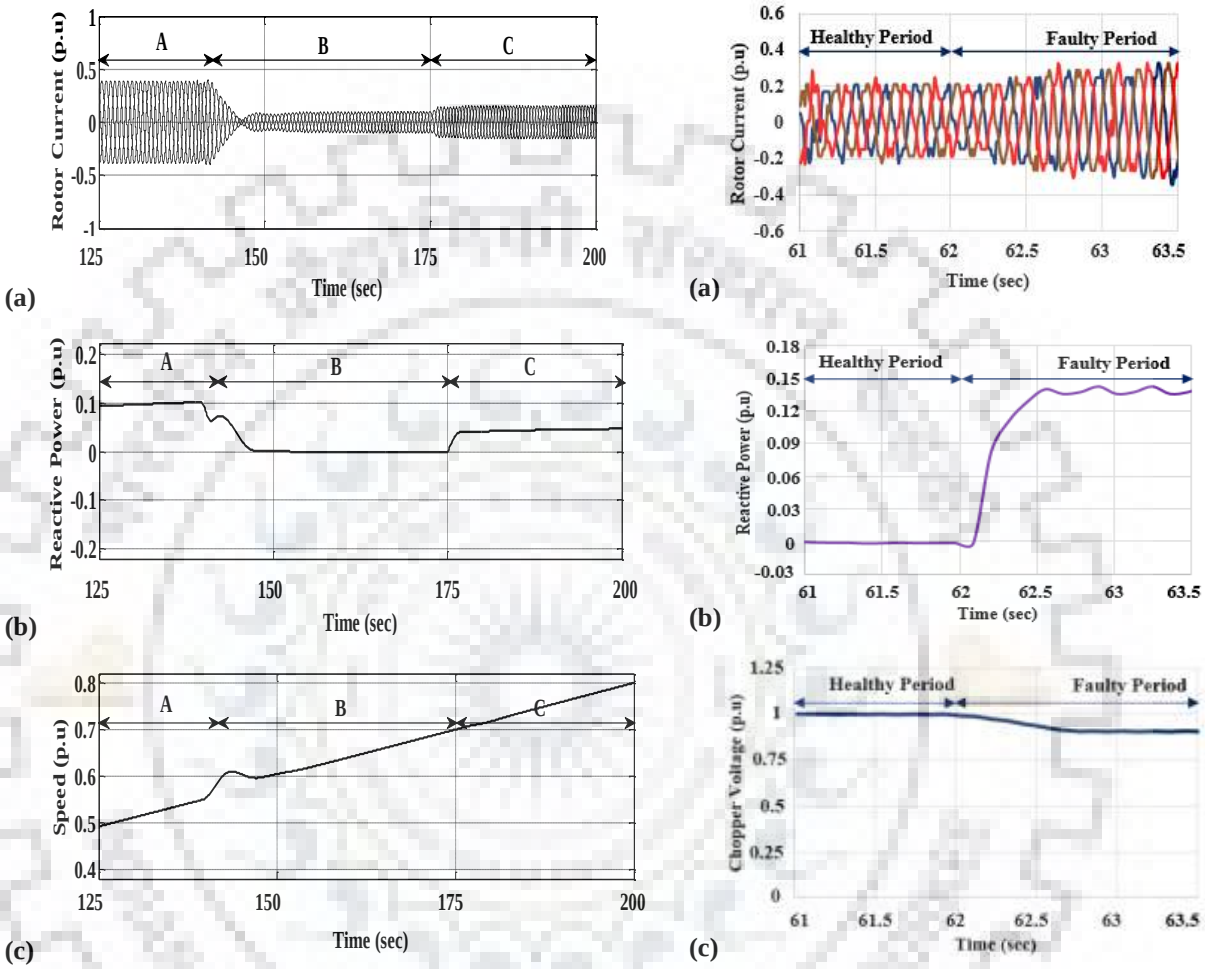

Fig. 3.33. DC link voltage sensor gain fault in dc chopper: A - Stator short Circuited; B - Stator Connected to FDC; C - Fault Period

A 2.2 kW DFIM is tested in the laboratory to validate the power and control circuit faults. Faults are injected at 62s and test results are shown in Fig. 3.32(ii) and Fig. 3.33(ii). In case of dc link voltage sensor gain fault (1.2 p.u) in VSC, rotor current increases about 2 times than normal value as shown in Fig. 3.32(ii). During the fault, dc link voltage of the VSC is decreased (shown in Fig. 3.32(ii)) and reactive power is delivered from the machine (shown in Fig. 3.32(ii)). In case of dc link voltage sensor gain fault (1.2 p.u) in dc chopper, machine absorbing reactive power from the grid as shown in Fig. 3.33(ii) c. When comparing with

simulation results, rise/reduction in rotor current, reactive power, dc link voltage and speed of the machine are similar to the experimental test results.

3.7 Conclusion of the Chapter

This chapter has presented dynamic performance of a 250 MW hydrogenerating unit operating with smooth starting and regenerative braking. Faults in power and control circuits were injected during starting and braking and the results were analyzed comprehensively. Survival of machine drive was tested for each fault case. From the test results, it was observed that the drive survived during single device and single leg gate drive open circuit faults, upper/lower two switches short circuit faults through pulses and not in short circuit faults with devices (internal short circuits). The drive survived during all kinds of single grid current sensor faults and failed in grid voltage sensors and dc link voltage sensor faults. In addition, a suitable fault tolerance in open circuit fault at power converter was proposed and it brought an additional storage of 2.49% electrical energy compared to the operation of DFIM without power redundancy. It has presented the detailed analysis of energy efficient starting of DFIM which saved about 35% of electrical energy compared to conventional smooth starting. Key elements of the energy efficient starting were identified and importance of such elements were well discussed.

Chapter IV

Dynamic Performance of Generation Mode of a Large Variable Speed PSPP

[This chapter discusses the expected benefits of generation mode of operation of DFIM based variable speed PSPP in comparison with fixed speed PSPP in consideration of head variation from 130 m to 230 m. In addition, dynamic behavior of a hydrogenerating unit subjected to power converter and control circuit faults are analyzed. Survivability status of DFIM operating in generating mode during excitation faults is assessed based on performance measures: (i) current, (ii) speed, (iii) reactive power consumption. The economic analysis on power and control circuit faults are discussed. Also, it discusses the fault tolerant operation during single converter open circuit fault in generating mode to increase the continuity of operation of the unit.]

4.1 Introduction

Electrical energy plays an important role in the development of country's economy. Sustained economic growth, rise in income level, and modernization over the past years at developing countries assured to face substantial increase in electrical energy demand. Many countries are reduced to use fossil fuel generation due to its negative impacts and renewable energy projects increases to ensure energy security. With the addition of renewables like wind, solar etc. in the grid, which are highly unpredictable and highly variable, the stability of grid is becoming of a great concern. This has shifted the focus toward employing energy storage technology particularly the pumped storage power plant. The PSPP is a mature energy storage technology (shown in Figure 4.1) available in MW range which provides flexibility and stability to power system.

4.2 Variable Speed Hydrogenerating Unit

Hydrogenerating units are designed to operate at maximum efficiency with the considerations of water head, turbine speed and water discharge. The efficiency of hydro turbine varies according to the water head and water discharge. Further, speed of the turbine is a function of water head. Machine rotating at fixed speed over the entire range of water head results in reduction in turbine performance. Therefore, the speed of the turbine adjusted to get maximum efficiency for an available water head, called as variable speed PSPP. Generator efficiency for the fixed and variable speed hydrogenerating unit is shown in Fig 4.2a and Fig. 4.2b.

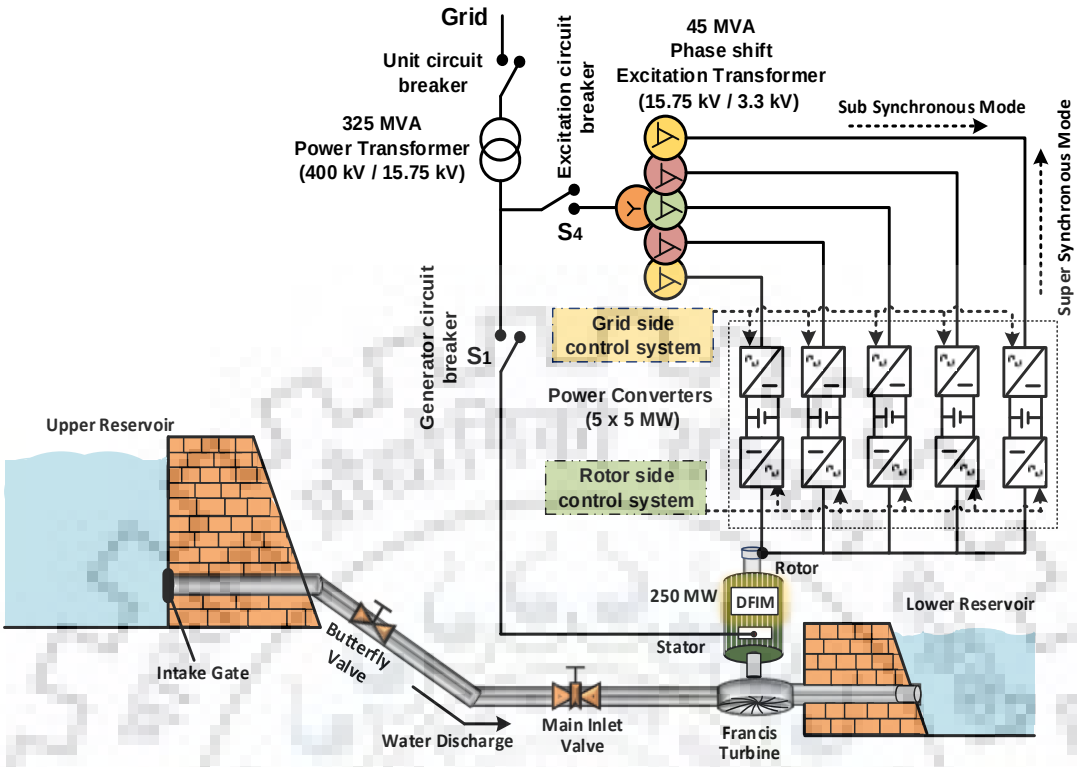

Fig. 4.1. Hydrological and electrical depiction of a 250 MW DFIM variable speed hydrogenerating unit – generation Mode
(This figure is reproduced from chapter 3 for ease reference)

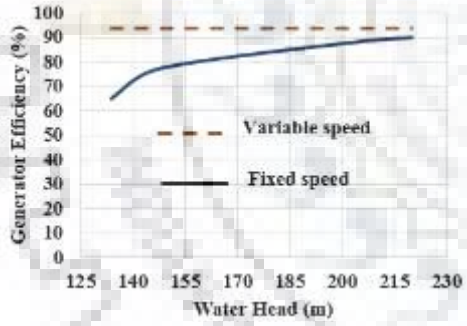

(a) efficiency versus water head at fixed power delivery (250 MW)

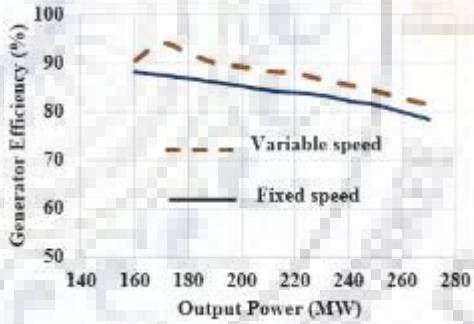

(b) efficiency versus output power at fixed water head (200 m)

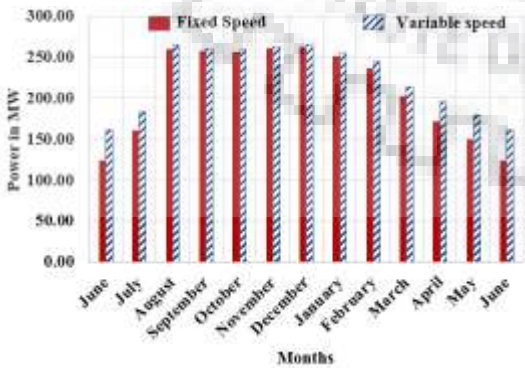

(c) Power generation at various water heads

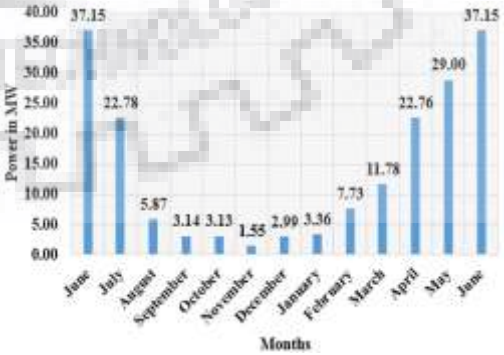

(d) Additional power generation during variable speed mode

Fig. 4.2. Comparison of a typical fixed speed and variable speed PSPP schemes

Table 4.1. Comparison of typical fixed and variable speed PSPP schemes at generation mode

Month	Water Head (m)	Input Power (MW)	Base Input Power (MW)	Input Power (P.U)	Peripheral Velocity Factor	Peripheral Velocity Factor		Efficiency		Output Power (MW)		Additional Output Power (MW)
						Fixed Speed	Variable Speed	Fixed Speed	Variable Speed	Fixed Speed	Variable Speed	
June	133.66	190.52	268.00	0.71	98.21	1.17	83.97	0.65	0.85	123.84	160.99	37.15
July	148.00	210.96	268.00	0.79	93.33	1.11	83.97	0.76	0.87	160.33	183.11	22.78
August	206.00	293.63	268.00	1.10	79.11	0.94	83.97	0.89	0.91	259.86	265.74	5.87
September	220.00	313.59	268.00	1.17	76.55	0.91	83.97	0.82	0.83	257.14	260.28	3.14
October	219.50	312.87	268.00	1.17	76.64	0.91	83.97	0.82	0.83	256.56	259.69	3.13
November	217.00	309.31	268.00	1.15	77.08	0.92	83.97	0.85	0.85	261.37	262.91	1.55
December	209.66	298.85	268.00	1.12	78.41	0.93	83.97	0.88	0.89	262.99	265.97	2.99
January	196.66	280.32	268.00	1.05	80.96	0.96	83.97	0.90	0.91	251.73	255.09	3.36
February	180.66	257.51	268.00	0.96	84.47	1.01	83.97	0.92	0.95	236.91	244.64	7.73
March	165.33	235.66	268.00	0.88	88.30	1.05	83.97	0.86	0.91	202.67	214.45	11.78
April	155.00	220.94	268.00	0.82	91.20	1.09	83.97	0.78	0.88	172.33	195.09	22.76
May	145.33	207.15	268.00	0.77	94.18	1.12	83.97	0.73	0.87	150.19	179.19	29.00
June	133.66	190.52	268.00	0.71	98.21	1.17	83.97	0.65	0.85	123.84	160.99	37.15

Input Power = $\frac{9.81 * \text{Rated Discharge} * \text{Water Head}}{1000}$ Peripheral Velocity Factor = $\frac{\text{Rotational Speed} * \text{Diameter of Turbine Vanes}}{\sqrt{\text{Water Head}}}$

Total Energy Generated at Fixed Speed PSPP = 1894.73 MU (8760 hours/year) Rated Discharge = 145.3 m^3/sec

Total Energy Generated at Variable Speed PSPP = 2005.15 MU (8760 hours/year) Rated Head - 188 m

% of Additional Energy saving = $\left(\frac{2005.15 - 1894.73}{1894.73}\right) \times 100\% = 6.1\ \%$

A typical 250 MW DFIM unit (Tehri PSPP, India) is considered to evaluate the effects of fixed and variable speed operation for a site with wide water head variation. The rated head and turbine speed are chosen as 188m and 234 rpm respectively. Nevertheless, gross water head

may vary over the year between 130m and 230m. In generation mode, the output power generation depends on water head. i.e., availability of minimum water head in dam provides less electrical power generation for the rated discharge. Reversible Francis turbine hill curves have been used for estimating the turbine efficiency at fixed and variable speed operation [194]. Subsequently, power generation for the various head level is calculated and is graphically presented (shown in Fig. 4.2c.). from the graph (Fig. 4.2d), it can be inferred that maximum power generation variation between variable and fixed speed operation (161 -124 = 37 MW at the water head level of 134m in June) is obtained at minimum water head (i.e. efficiency of variable speed operation is much higher than fixed speed at minimum water head). For the whole year analysis, variable speed mode brings additionally 6.1% power generation than fixed speed operation leads to an additional generation of 441.6 MU/year for a 1000 MW plant.

4.3 Real and Reactive Power Control of DFIM

Stator circuit of DFIM is directly connected to grid and rotor circuit (three phase cylindrical winding) is also connected to the grid through power converters and excitation transformers. Voltage source back-to-back power converters are connected in rotor circuit of the machine is responsible for real and reactive power control of the machine. Allowable speed variation of the machine depends on voltage rating of power converter connected in rotor circuit of the machine (slip voltage). Grid voltage oriented vector control is employed in grid side converter (GSC) to ensure the decoupled control of dc link voltage and unity power factor at grid side (rotor); stator flux oriented vector control is implemented in RSC to ensure the decoupled control of real and reactive power of the machine. Due to the limitation in the semiconductor device rating, it becomes difficult to design a single converter for large current ratings. In such a situation parallel converters can be adopted to share high current in rotor circuit of the machine. Active Current Sharing (ACS) method is most suitable for the parallel converters in large rated variable speed PSPP. In ACS, three control loop can be employed namely voltage control loop, current control loop and inner current sharing control loop. In addition, current sharing bus is employed to share the equal current distribution to the converters. For this dynamic control, three grid voltage sensors, three grid current sensors, dc link voltage sensor, encoder, three rotor current sensors are used. Detailed d-q modelling and control equations of DFIM are explained in Chapter 2. However, essential equations are considered here for a clear

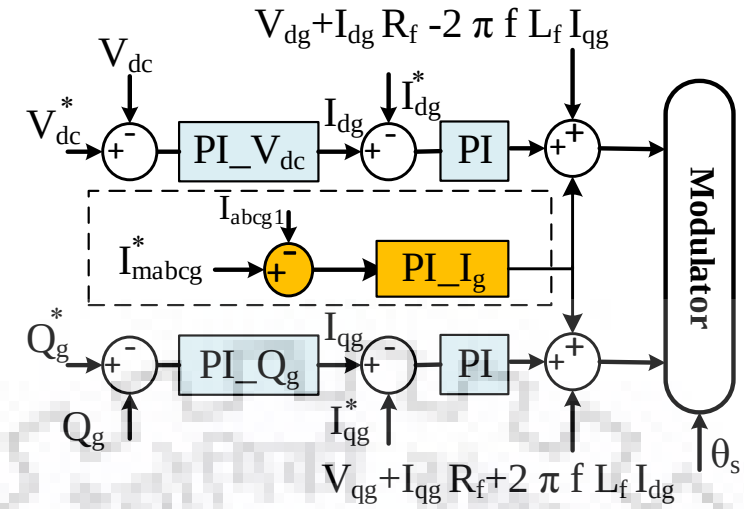

(a) GSC control system

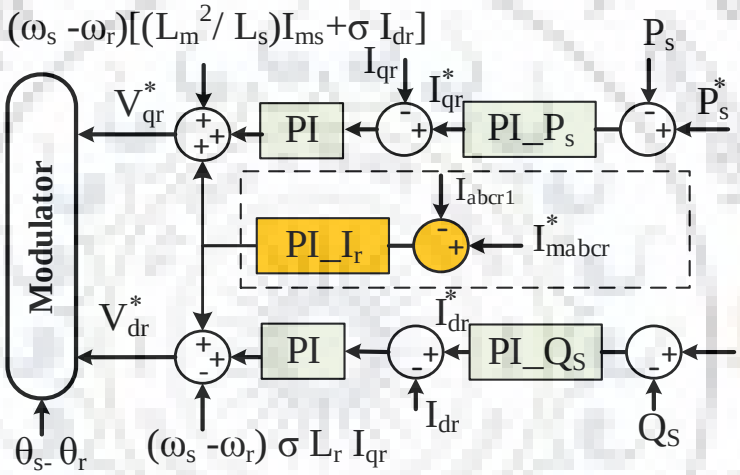

(b) RSC control system

Fig. 4.3. Vector control of DFIM with parallel converters

understanding of fault analysis. Control systems used for real, and reactive power control of DFIM is shown in Fig.4.3.

4.3.1 Grid Voltage Oriented Vector Control

In grid side system, (i) angular speed of ω_a is chosen as angular speed of the grid voltage ω_s, (ii) d-axis rotating frame is aligning with grid voltage space vector. Hence,

$$\vec{V}^a_{dg} = \left|\vec{V}^a_g\right| \quad ; \quad \vec{V}^a_{qg} = 0; \quad \omega_a = \omega_s \tag{4.1}$$

Active (P_g) and reactive (Q_g) power are calculated as

$$P_g = \frac{3}{2}\left|\vec{V}^a_g\right| \vec{I}^a_{dg} \tag{4.2}$$

$$Q_g = -\frac{3}{2}\left|\vec{V}_g^{\,a}\right| \vec{I}_{qg}^{\,a} \tag{4.3}$$

4.3.2 Stator flux Oriented Vector Control

With the stator flux orientation, decoupled control between electro-magnetic torque and stator reactive power control is achieved. In stator flux oriented vector control, d-axis stator flux is aligning with stator flux space vector $\vec{\psi}_s^{\,a}$ in synchronously rotating reference frame.

$$\vec{\psi}_{ds}^{\,a} = \vec{\psi}_s^{\,a} \qquad \vec{\psi}_{qs}^{\,a} = 0 \qquad \vec{\psi}_s^{\,a} = L_m \vec{I}_{ms}^{\,a} \tag{4.4}$$

The expression of electro-magnetic torque and reactive power equations can be derived as

$$T_{em} = -\frac{3}{2} p \frac{L_m}{L_s} \frac{\vec{V}_s^{\,a}}{\omega_s} \vec{I}_{qr}^{\,a} \tag{4.5}$$

$$Q_s = \frac{3}{2}\left(\frac{\vec{V}_s^{\,a^2}}{\omega_s L_s} - \vec{V}_s^{\,a} \frac{L_m}{L_s} \vec{I}_{dr}^{\,a} \right) \tag{4.6}$$

4.4 Results and Discussion

The performance bounds of the 250MW DFIM drive during generation mode is considered as follows (i) allowable reactive power variation is ± 0.05 p.u, (ii) allowable speed variation is ± 0.03 p.u, (iii) dc link voltage variation is ± 0.1 p.u, (iv) rotor side grid current variation up to 0.05 p.u, (v) stator current variation up to 0.05 p.u, (vi) machine rotor current variation up to 0.05 p.u, (vii) controller settling time is less than 250ms. The real and reactive powers of a 250 MW DFIM at normal operating condition are given in Fig. 4.4. From figure, it is inferred that the rotor current of the machine varies when real and reactive power of the machine changes. In addition, it is noted that the magnitude of the rotor voltage is depends on the slip of the machine. In case of faulty cases, machine is instructed to operate at 0.96 p.u (221.5rpm) speed and shaft power is considered as 240MW. Further, power factor of the machine is set as 0.95 through reactive power control system. From the tests, it is observed that: (i) magnitude of line current in stator winding is 10060A (0.894 p.u), (ii) voltage (P-P) applied to rotor winding by rotor side converter is 1255V (0.38 p.u), (iii) line current in rotor winding is 10360A (0.893 p.u), (iv) reactive power consumption of the machine is 15.3 MVAr (0.05 p.u), (v) frequency of rotor current is 2 Hz.

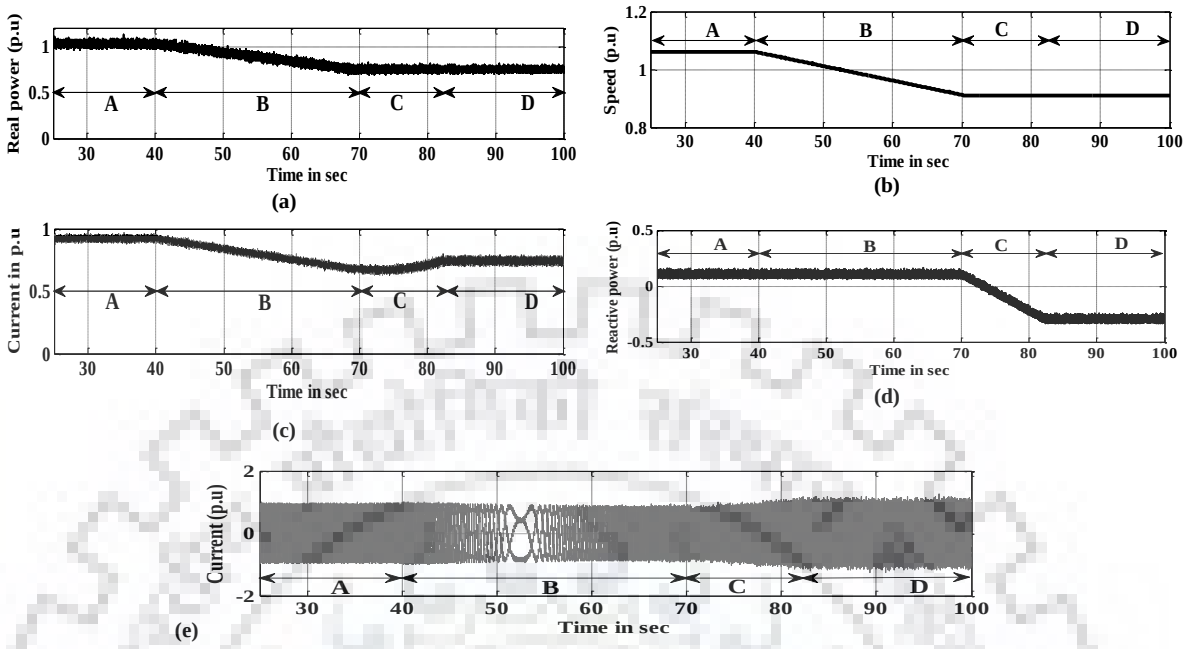

A – 260 MW, 30.6 MVar (consumption), 240 rpm; B – Transition from 260 to 195 MW, 240 to 210 rpm, 30.6 MVar (consumption); C- Transition from 30.6 MVar (consumption) to 91.8 MVar (Deliver to grid); D – 195 MW, 91.6 MVar (Deliver to grid)

Fig.4.4. Real and reactive power control of 250 MW DFIM: (a) real power, (b) speed, (c) stator current, (d) reactive power, (e) rotor current

4.4.1 Simulation Results (250 MW DFIM)

4.4.1.1 Power Converter Failure in a Single Converter

4.4.1.1.1 GSC Single Switch Open Circuit Fault

Single switch gate drive open circuit fault (upper switch) is injected in one of the parallel connected GSC at 160s and results are given in Fig. 4.5. During the fault, phase current corresponding to the faulty leg is distorted in upper half cycle and negative half cycle is omitted, results in variation in phase and magnitude of other two phase currents (shown in Fig. 4.5a). However, current flowing through the other healthy converters are not affected as shown in Fig. 4.5b. From the test results, it is inferred that: (i) dc link voltage marginally fluctuated in the faulty converter as shown in Fig. 4.5c (oscillation in the rate of grid frequency), (ii) variation in capacitor dc link voltages, faulty switch connected to the dc link capacitor voltage (Vd_1) gets marginally reduced and other dc link capacitor voltage (Vd_2) increases to regulate the dc link voltage, (iii) Fluctuation in power factor at grid side (rotor) due to the variation in reactive power consumption. (iv) speed of the machine is constant as set by machine side control system. In case of open circuit fault in lower switch, results are similar to the upper switch fault. However,

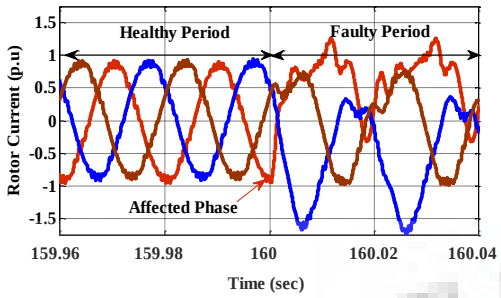

(a) Rotor Current (Grid Side) – Faulty Converter

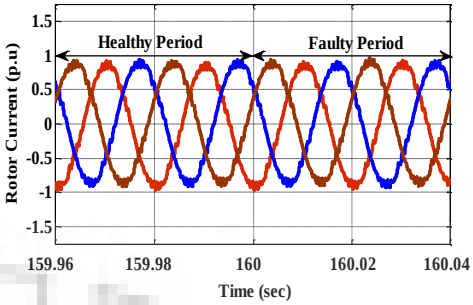

(b)Rotor Current (Grid Side) – Healthy Converter

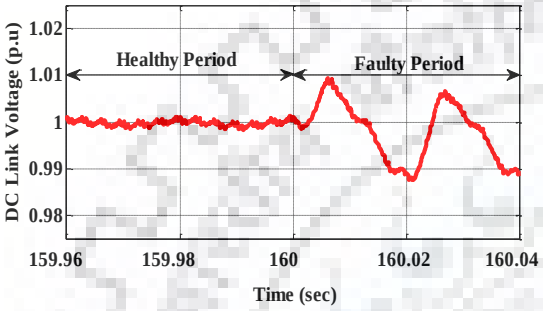

(c) DC Link Voltage – Faulty Converter

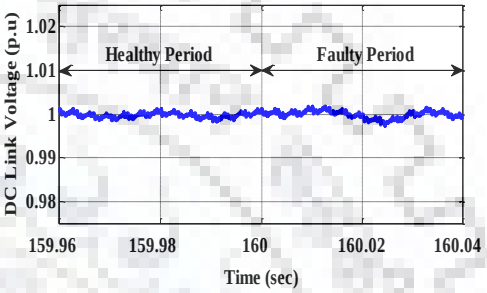

(d) DC Link Voltage- Healthy Converter

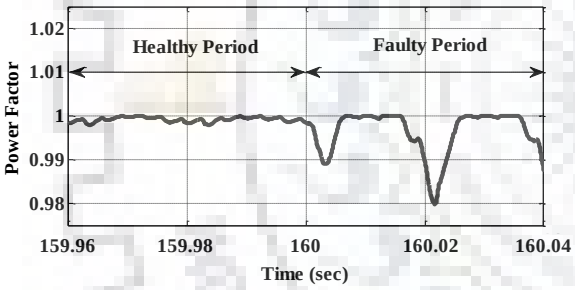

(e) Power Factor

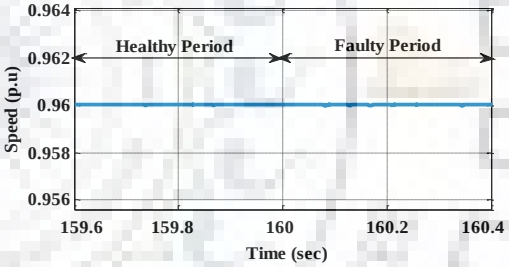

(f) Speed

Fig. 4.5. GSC upper single switch OCF (250 MW DFIM) at generation

it is observed that (i) Faulty leg phase current is disturbed in lower half cycle and omitted in upper half cycle, (ii) variation in capacitor dc link voltages are reversed when compared to upper switches short circuit fault. The test results are similar to starting mode where magnitude of the fluctuation in current and power profile is changed since converters are carrying large current than no-load condition.

4.4.1.1.2 RSC Single Leg Open Circuit Fault

Single leg gate signal open switch fault is injected in one of the parallel connected RSC at 160s and results are given in Fig. 4.6. During the fault, the rotor current in one of the phase of faulty converter goes to zero (Fig. 4.6a) whereas the other two phases are carrying as equal

currents. However, the same phase current in other parallel converters increases by 1.286 times of the regular value (Fig. 4.6b) to maintain required rotor phase current. It is seen from the test results that: (i) during the fault the healthy power converters are overloaded and this results in stopping of the unit, (ii) speed of the machine is maintained at desired level through RSC control system, (iii) dc link voltage of the faulty and healthy converters are fluctuated as shown in Fig. 4.6c and Fig. 4.6d, respectively. Reactive power and speed of the machine maintained as constant as shown in Fig. 4.6e and Fig. 4.6f respectively.

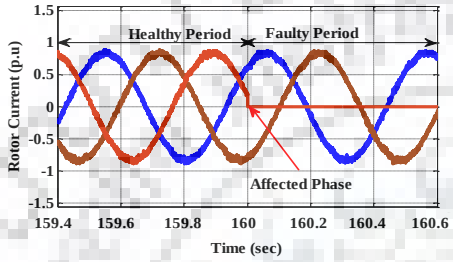

(a) Rotor Current (Grid Side) – Faulty Converter

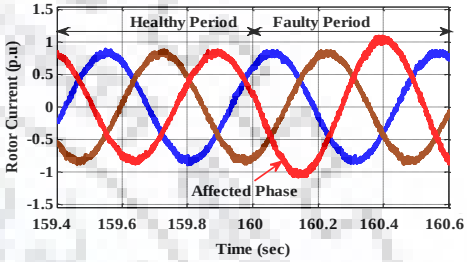

(b)Rotor Current (Grid Side) – Healthy Converter

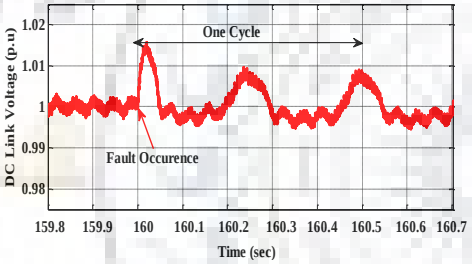

(c) DC Link Voltage – Faulty Converter

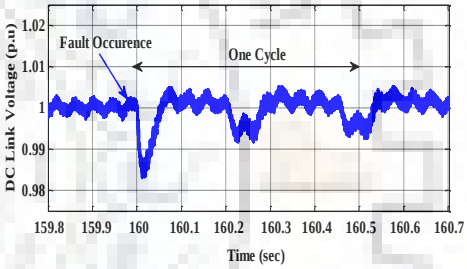

(d) DC Link Voltage- Healthy Converter

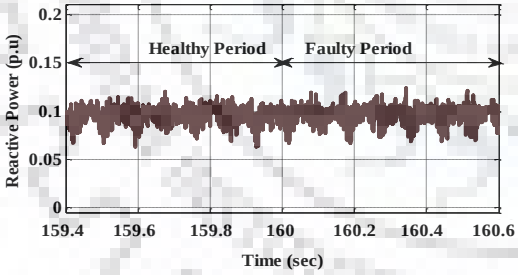

(e) Power Factor

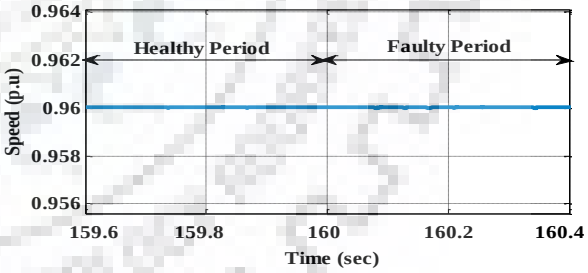

(f) Speed

Fig. 4.6. RSC single leg OCF (250 MW DFIM) at generation

In summary, open switch fault in GSC results to distort the current waveform in the same converter and does not affects the healthy converters connected in parallel. On the other hand, open switch fault in inverter results to affect the healthy converters current value and also distort the dc link voltages of all the converters connected in parallel. From the results, open switch fault in both GSC and RSC results to stopping of the unit. Detailed survivability status of the DFIM unit for the converter fault is reported in Table 4.2.

4.4.1.2 Power Converter Failure in All Channels (Five Converters)

Open and short circuit failures in all grid side converters are similar to the faults in any one of the parallel connected grid side converters. Nonetheless, variation in dc link voltage and power factor (rotor side) is higher as compared to faults occur in only one converters. But, faults in rotor side converters are different form the single converter fault and it is discussed here.

4.4.1.2.1 RSC Single Switch Open Circuit Fault

The fault is injected at 410s and results are shown in Fig. 4.7. When fault occurs, one of the rotor phase currents is discontinuous and other two phases are carrying currents which are altered during discontinuous period of faulty phase current as shown in Fig. 4.7a. Change in rotor currents affect stator currents and consequently speed, real and reactive power consumption of the machine is troubled. During fault, magnitude of stator and rotor phase transient currents reach to 4.15 p.u (shown in Fig. 4.7b) and 2.9p.u (shown in Fig. 4.7a),

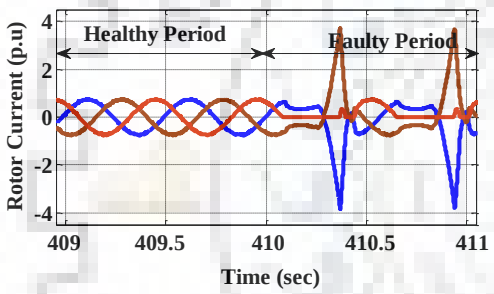

(a) Rotor Current (Machine side)

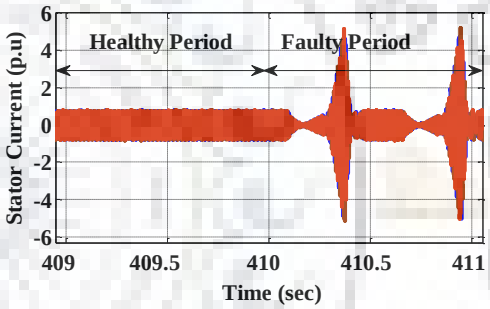

(b)Stator Current

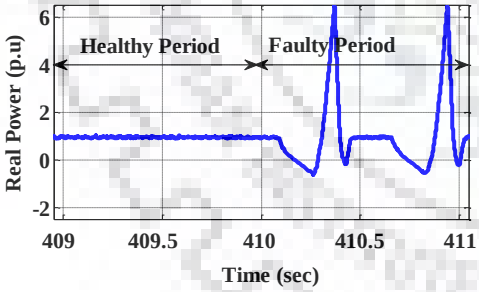

(c) Real Power - DFIM

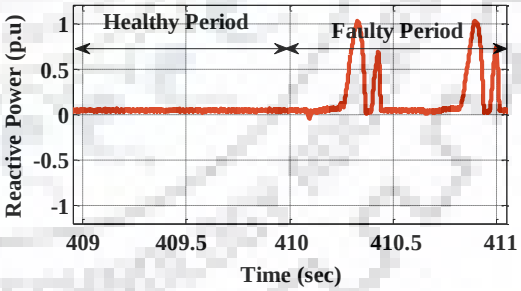

(d) Reactive Power - DFIM

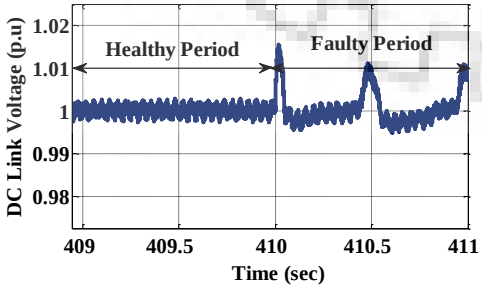

(e) DC Link Voltage

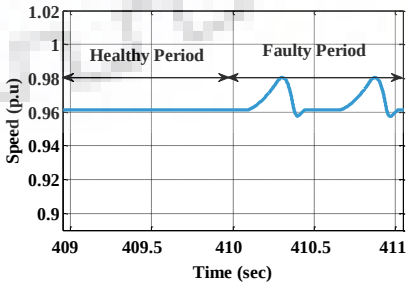

(f) Speed

Fig. 4.7. RSC single switch OCF (250 MW DFIM) at generation

respectively. From the test results, it is observed that: (i) healthy phase rotor currents are deviations in phase and produce transients at meeting point of these two phase currents, (ii) both stator and rotor currents reach to above the rated value, (iii) fluctuation in speed of the machine (shown in Fig. 4.7f), (iv) instability in real and reactive power consumption of the machine as shown in Fig 4.7c and Fig. 4.7d, respectively, (v) RSC control system is out of action.

4.4.1.2.2 RSC Single Leg Gate Drive Open Circuit Fault

Single leg gate drive open circuit fault is injected in RSC at 410s and results are shown in Fig. 4.8. When fault occurs, one of the rotor phase current goes to zero (Fig. 4.8a) and the conduction mode is equivalent to the single phase converter with other two healthy legs. During fault, magnitude of both stator and rotor currents reach to the high value as similar to fault in single device fault. However, rotor currents transient repeatedly occurs two times per interval

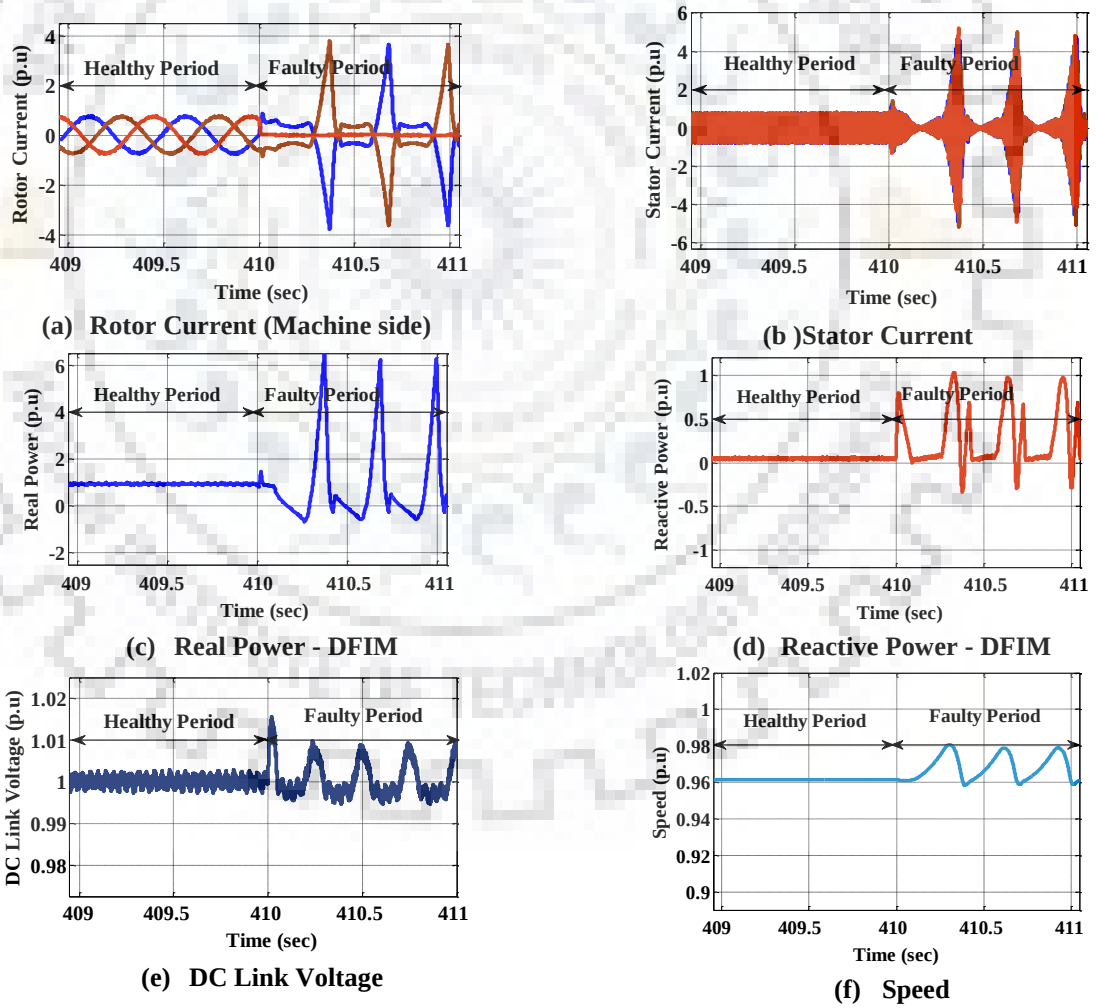

Fig. 4.8. RSC Single Leg OCF (250 MW DFIM) at Generation

more than single device fault, consequently stator current (shown in Fig. 4.8b), speed, real power and reactive power of the machine are affected (shown in Fig. 4.8c, Fig. 4.8d and Fig. 4.8f). From the test results, it is observed that the results are similar to single device fault except the number of times of transients at specific time period.

4.4.1.3 Control Circuit (Sensor) Failure

4.4.1.3.1 Single Rotor Current Sensor Omission Fault

Fault is undergone at 365 s and results are shown in Fig. 4.9. During a fault, one of the sensor reads zero value and results to change in I_{dr} and I_{qr}. The change in both I_{dr} and I_{qr} distorts the current controller output results in fluctuations in the speed. From the results it is observed that: (i) Speed of the machine is marginally fluctuated (shown in Fig. 4.9f) and results to change in real power delivery (shown in Fig. 4.9c), (ii) variation in rotor and stator currents (shown in Fig. 4.9a and 4.9b). However, machine is in continuous operation and Idr maintains the

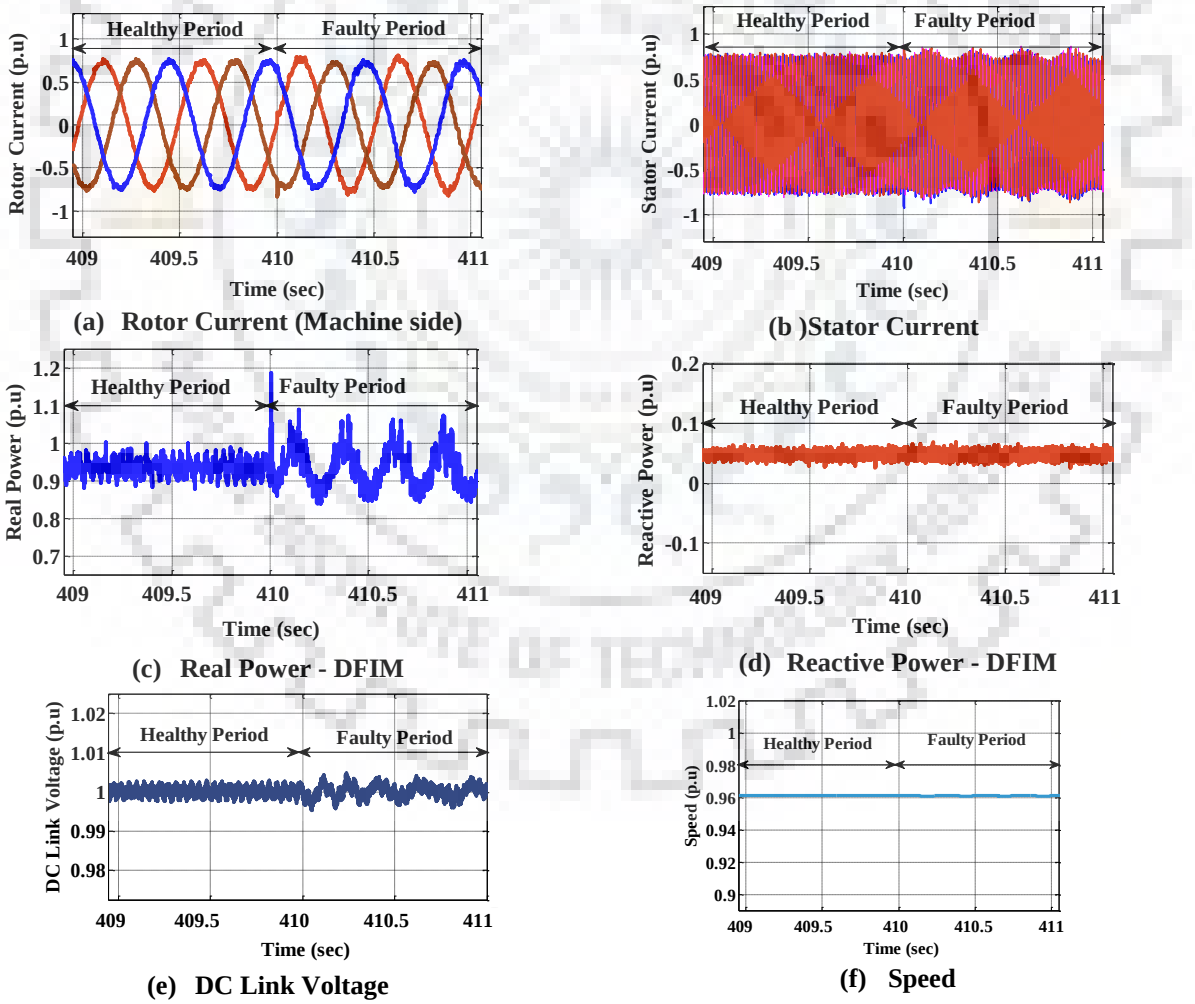

(a) Rotor Current (Machine side)

(b)Stator Current

(c) Real Power - DFIM

(d) Reactive Power - DFIM

(e) DC Link Voltage

(f) Speed

Fig. 4.9. Single rotor current sensor omission fault (250 MW DFIM) at generation

controlled reactive power at grid (stator side). In observation, all controllers are in regular operation at grid side converters and maintains the dc link voltage.

Table 4.2: DFIM drive status and economic analysis of converter and sensor failure at generation mode [165], [166]

System	Mode of operation	Faults		Fault Status	No. of Failures/year	250 MW DFIM				
						U Period/ year	Generation Losses* (MU)	Financial Losses**/ year (M$)	Fault Tolerant Status	Fault Tolerant Benefits (M$)
Power Converter	Sub synchronous	Rotor side converter	Open Circuit Fault (SDOC, SLOC)	F	1.9940	151.77	34.76	3.82	Yes	3.17***
			Short Circuit Fault (SDSC,PPSC,PGSC)	F	0.6646	50.59	11.59	1.27	NA	-
		Grid side converter	Open Circuit Fault (SDOC, SLOC)	S	0.3025	35.48	8.12	0.89	Yes	0.74
			Short Circuit Fault (SDSC,DCSC,PPSC,PGSC)	F	0.1008	11.83	2.71	0.30	NA	-
	Super synchronous	Rotor side converter	Open Circuit Fault (SDOC, SLOC)	S	1.9940	151.77	34.76	3.82	Yes	3.17
			Short Circuit Fault (SDSC,PPSC,PGSC)	F	0.6646	50.59	11.59	1.27	NA	-
		Grid side converter	Open Circuit Fault (SDOC, SLOC)	F	0.3025	35.48	8.12	0.89	Yes	0.74***
			Short Circuit Fault (SDSC,DCSC,PPSC,PGSC)	F	0.1008	11.83	2.71	0.30	NA	-
		DC Link	Open circuit/Short circuit	F	0.007	6.57	1.50	0.17		

Total Energy Generated at Fixed Speed PSPP = 1421.0475 MU (18 hours/day)

Total Energy Generated at Variable Speed PSPP = 1503.86 MU (18 hours/day)

Unavailability period of VSC over the year is 256.23 hours

Total Energy Generated without Power Redundancy = 1445.21 MU

% of Additional Energy saving of Variable Speed PSPP considering Power Redundancy Issue = $\left(\frac{1445.21 - 1421.05}{1421.05}\right) \times 100\% = 1.7\ \%$

Table 4.2: DFIM drive status and economic analysis of converter and sensor failure at generation mode (contd.) [165], [166]

System	Mode of operation	Faults		Fault Status	No.of Failures/year	250 MW DFIM				
						U Period/year	Generation Losses* (MU)	Financial Losses**/year (M$)	Fault Tolerant Status	Fault Tolerant Benefits (M$)
Control Circuit faults	Sub and super synchronous	Omission/ saturation	Speed sensor	F	0.247	16.23	3.72	0.41	NA	-
			DC link voltage sensor	F	0.247	16.23	3.72	0.41	NA	-
			Reactive power signal	F	0.247	16.23	3.72	0.41	NA	-
			Single rotor Current Sensor	S	0.247	16.23	3.72	0.41	Yes	0.41
			Single grid current sensor	S	0.247	16.23	3.72	0.41	Yes	0.41
			Single grid voltage sensor	F	0.247	16.23	3.72	0.41	NA	-
		Gain	Speed sensor	F	0.355	23.32	5.34	0.59	NA	-
			DC link voltage sensor	F	0.355	23.32	5.34	0.59	NA	-
			Reactive power signal	S	0.355	23.32	5.34	0.59	Yes	0.59
			Single rotor Current Sensor	S	0.355	23.32	5.34	0.59	Yes	0.59
			Single grid current sensor	F	0.355	23.32	5.34	0.59	NA	-
			Single grid voltage sensor	S	0.355	23.32	5.34	0.59	Yes	0.59

* Average generation is 229 MW/year/unit for a 250 MW DFIM ** Financial losses are considered as $ 0.11/kWh
*** Fault tolerant proposed in this paper with reduced power generation (190 MW) U - unavailability
SDOC - single device open circuit fault SLOC - single leg open circuit fault SDSC - Single device short circuit DCSC - DC link short circuit
PPSC - Phase to phase SC PGSC - Phase to ground SC S - Survived F - Failed

In multi-channel three level converter, short circuit faults in power converter switches leads to short circuit the dc link capacitors and seriously damage the overall system. To avoid this, unit has to be stopped with the aid of fuses or circuit breakers. On the contrary, open switch fault cause a changes in the rotor current pattern and oscillate the dc link voltages, degrade the performance of the system. Also, continuous operation of the unit with open switch fault result in severe harms to the healthy switches/converters.

4.4.1.4 Economic Analysis on Power and Control Circuit Faults

Consider a plant (TEHRI PSPP) having 4 units with each unit rated at 250MW. The average energy generation is considered as 18 hours/day. The probability of operational state of a back-to-back power converter without redundancy per year is 96.10%. Therefore, the unavailability of the back-to-back power converter per year is projected as 256.23 hours/year. The average generation to each unit is estimated as 229 MW over the year considering water head and efficiency and it is estimated that the generation loss of about 58.677 MU/year/unit due to the inadequate power and control redundancy. Further, considering four units in a plant, the estimated generation losses of the plant will be 234.70 MU/year. The selling price of a unit of energy (kWh) is considered in hydropower plant in India as $ 0.11. Therefore, it is noted that about $25,817,835/year/plant financial losses are estimated due to the inadequate redundancy in power and control circuits. Detailed financial losses are given in Table 4.2. The cost of extra converter module is about $ 4,445,705/- which is retrieved within 2 to 3 months, if redundancy is designed. In addition, employing redundant converter in a unit is also beneficial in pumping mode of operation.

4.4.1.5 Open Switch Fault Diagnostic Method for Multi-Channel VSI

Condition monitoring and fault diagnosis of the power converter is essential in the drive to detect the failures and also avoid catastrophic consequences. Detection of open switch fault in multi-channel VSI is essential to prevent the destruction of other switches/converters and improve the reliability of the system. In this paper, open switch fault is detected based on variation in rotor phase currents and dc link voltage variation. Open switch faults in both inverter and rectifier are performed simultaneously. Three diagnostic variables are considered in this study to detect and find the location of the faults. Diagnostic variables are derived from, (i) normalized phase currents using park vector's technique (D_1), (ii) average value of the phase

currents (D_2), (iii) dc link voltage variation (D_3). Block diagram for the fault detection and localization is shown in Fig.4.10.

Three phase currents are normalized in order to endow a diagnostic technique. Normalized quantity is derived from the park vectors approach. In ideal conditions, Park's vector components are given in eqn. 4.7, the value of Park's vector modules under ideal condition is equals to 1.2247, given in eqn. (4.8).

$$I_{dr} = I_m \frac{\sqrt{6}}{2} \sin \omega t \qquad I_{qr} = I_m \frac{\sqrt{6}}{2} \cos \omega t \tag{4.7}$$

$$I_s = \sqrt{I_{dr}^{\ 2} + I_{qr}^{\ 2}} = I_m \text{ x } 1.2247 \tag{4.8}$$

Normalization is performed by dividing the rotor phase current with Park's vector modules (I_s). In a balanced three phase system, normalized rotor currents are given by,

$$i_{aN} = \frac{I_m \sin(\omega t + \varphi)}{|I_s|} \qquad i_{bN} = \frac{I_m \sin\left(\omega t + \varphi - \frac{2\pi}{3}\right)}{|I_s|} \qquad i_{cN} = \frac{I_m \sin\left(\omega t + \varphi + \frac{2\pi}{3}\right)}{|I_s|} \tag{4.9}$$

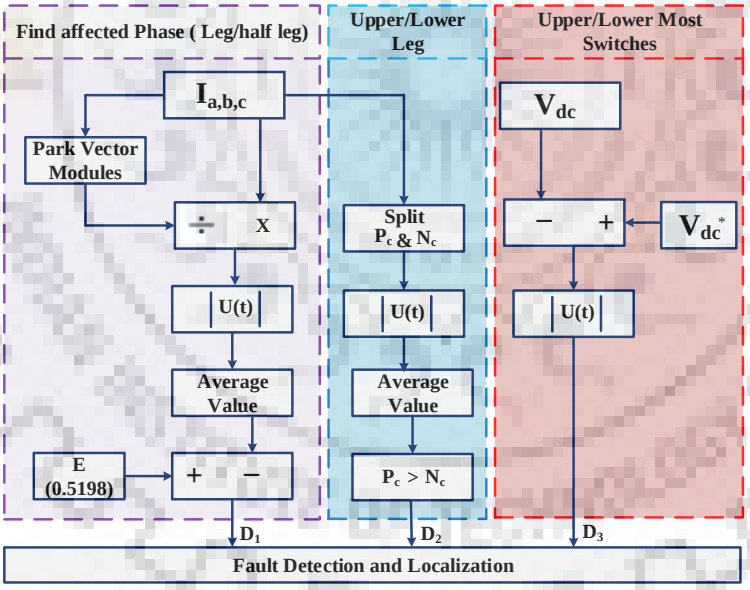

(a) Generalized block diagram of open switch fault diagnostics

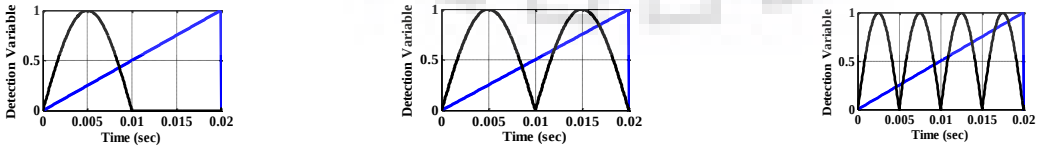

Outer Switches Inner Switches Single leg

(b) DC link voltage oscillation during open switch fault in GSC

Fig. 4.10. open switch fault diagnosis of grid side and rotor side converter

Under ideal conditions, the average absolute value of three phase normalized rotor currents is given by eqn. (4.10).

$$E=\left|i_{aN}+i_{bN}+i_{cN}\right|=0.5198 \quad (4.10)$$

Then the diagnostic variable (D) is obtained by finding the errors between the average value and the corresponding normalized phase value.

$$D = E - |i_{nN}| \quad (4.11)$$

From the equations, when the drive is operating under normal conditions, diagnostic values (D_1) are equals to zero. However, if open switch fault occurs diagnostic variable will not be zero, and it provides a positive value, consequently corresponding affected phase is located. Threshold value of the diagnostic value (D_1) is empirically set to 0.09, to allow sudden load changes, large transients and operating conditions. Mean value of the each phase current (D_2) be responsible for the information about the fault in upper/lower switches. The location of the faulty switch is observed from the oscillation of dc link voltage (D_3). Faults in grid side converter leads to oscillate the dc link voltage with respect to the grid frequency. On the other hand, slip frequency oscillation in dc link voltages due to rotor side converter faults.

4.4.1.5.1 GSC Single Switch Open switch Fault

Open switch fault is injected at 160 s and results are shown in Fig. 4.11. When fault occurs, diagnostic variable (D_1) corresponding to the affected phase increase to the positive value of 0.21 (shown in Fig 4.11a). The other two healthy phases value are decreased to the negative values of 0.056 and 0.14 (shown in Fig. 4.11b). Diagnostic value (D_2) is estimated from the mean value of the phase current. When fault occurs, diagnostic value (D_2) decreases to the negative value of 0.35 (shown in Fig. 4.11c), it is assumed that the fault occurred in the upper switches. Further, diagnostic variable (D_3) shows the variation in dc link voltage (shown in Fig. 4.11d), it is inferred that the fault occurred in the lower part of the upper switches (S_{G2}), since the dc link voltage oscillation was double the grid frequency. In case of fault in lower switches, mean value of the affected phase current (D_2) results in positive value. Further, fault detection in outer switches (S_{G1}, S_{G4}) can be evaluated from diagnostic variable D_2 and D_3, since the affected phase current remains zero only for a very short duration. From the results, it is inferred that open switch fault is detection at 0.016s after the fault occurrence when fault occurred in GSC.

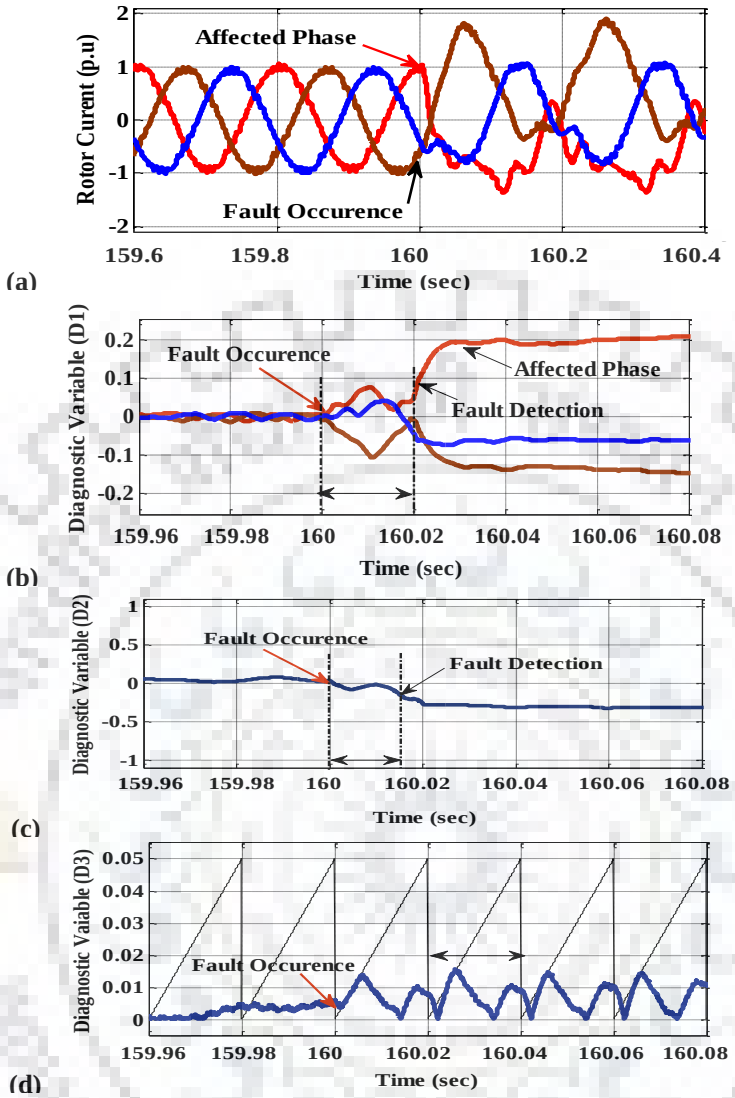

Fig. 4.11. Diagnostic variables for GSC single open switch fault

4.4.1.5.2 RSC Single Leg Open Fault

Fig. 4.12 shows the waveforms of the diagnostic variables for the single leg fault. The frequency of the rotor phase current is 2 Hz. Fault is injected at 160 s, as a result, affected phase of the diagnostic variable (D_1) increases to the positive value of 0.5 (shown in Fig. 4.12a) and other two healthy phase values are decreased and reach a negative value of about 0.21 (shown in Fig. 4.12b). Average value of the affected phase current (D_2) is continually measured as zero. Further, dc link voltage variation (D_3) as shown in Fig. 4.12c occurred two times in a cycle. From the test results it is concluded that fault detection period in rotor side converter is quite high since the phase current frequency is very low, typically it takes to detect 40 ms after the fault occurrence.

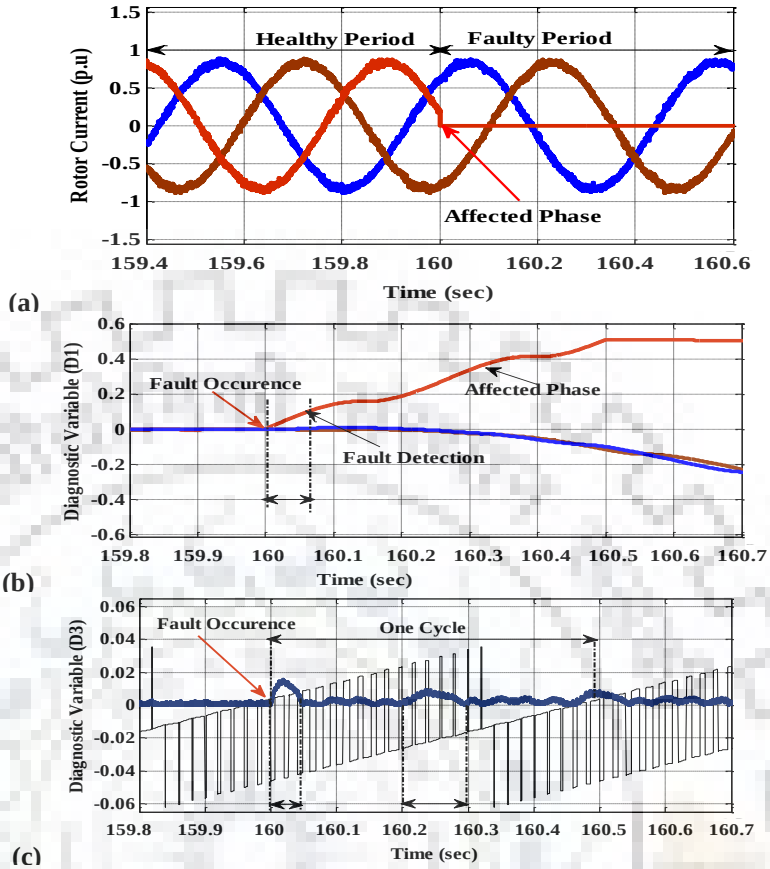

Fig. 4.12. Diagnostic variables for RSC single leg Fault

4.4.1.6 Fault Tolerant Operation of RSC Open Circuit Fault

As discussed in section 4.4, open switch fault in RSC during generation mode affected the continuous operation of the unit. To continue the operation of the unit, fault tolerance or converter redundancy need to be provided in the parallel converters. However, there is no full converter redundancy/fault tolerant operation available in variable speed PSPP (DFIM) unit due to the operational challenges.

This section presents the fault tolerant operation in parallel converter fed DFIM without the contactors connected in series with each channels. By doing so, risk of over voltages in rotor winding can be avoided during operations (ON/OFF) of the contactors. It is planned to stop the PWM pulses of faulty converters (for open circuit and other faults, except short circuit fault in a whole leg) and operate the machine with other healthy converters with reduced power delivery. The fault detection techniques of RSC is discussed in section 4.4.1.5. On detection of fault, the faulty converter is isolated from the converter units and then the power delivery is set to reduce

to adaptable power generation as given by master control system based on healthy converters unit.

In hydropower plant, reduction of power delivery from rated power to amendable power takes about 20s to 30s. During this period, healthy rotor side converters should not carry the current above-rated limit. In order to achieve this, during transition period (i.e. 30s), the reactive power of the machine is adjusted through reactive power control system. In simulation, 4 units rated of 250 MW variable speed PSPP is developed and a unit is chosen for the fault tolerant operation. DFIM is assigned to deliver the rated power 0.96 p.u (240 MW) at 0.96 p.u rpm with the aid of three level back-to-back with five parallel connected converter system. The power factor of the unit is set as 0.9, stator and rotor circuits are carrying current as 0.854 p.u and 0.894 p.u, respectively. Single leg gate drive open switch fault is injected at anyone of the parallel converter module at 160s and the fault is detected through rotor phase currents and dc link voltage variation.

The corresponding faulty converter is isolated/inactivated from the parallel converter system through removing pulses (i.e. modulation index as zero) by master controller as shown in Fig. 4.13a. Subsequently, fault diagnostic control system gives the faulty signal (shown in Fig. 4.13b) to the master control system and it inactivates the faulty converter then reduces the power delivery to 0.76 p.u (190 MW) which is adaptable with the remaining healthy converter current limit and the unit is in continuous operation. Transition period from rated power 1 p.u (250 MW) to reduced power generation 0.76 p.u (190 MW) takes about 25s as shown in Fig. 4.13d.

During the period, reactive power controller adjust the reactive power consumption of the machine as shown in Fig.4.13e, in which the healthy power converters are not carrying above the rated limit of the current as shown in Fig. 4.13c. Stator current of the machine at time of fault increases to 0.95 p.u and then gradually decreases to 0.67 p.u during the transition period as shown in Fig. 4.13f. Further, reactive power consumption of the unit from the power grid during transition period is adjusted by healthy converter units in the plant through coordinated control system. From the simulation results, it is inferred that the current in stator winding and rotor currents in healthy power converter are below the rated value and it is harmless for the continuous operation of the unit.

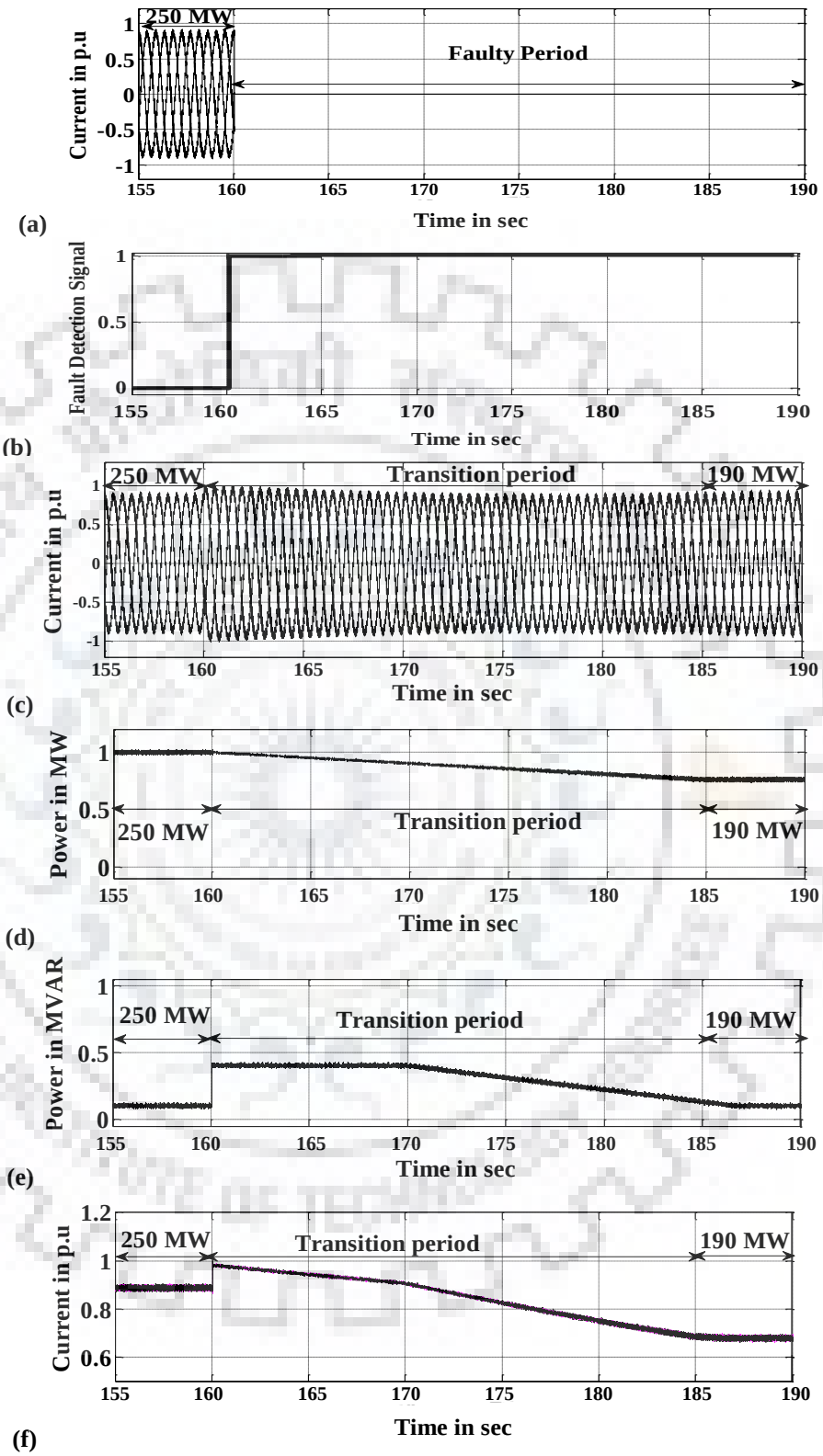

Fig. 4.13. Fault tolerant operation of converter open circuit fault at generation mode for a 250 MW DFIM: (a) Rotor current – faulty converter, (b) Faulty signal, (c) Rotor current –healthy converter, (d) Real power, (e) Reactive power, (f) Stator current

A typical 250MW DFIM unit is operated in between 206 rpm (shaft power of 116.4 MW) and 250 rpm (shaft power of 280 MW) for the consideration of available speed variation. The rated current of the each power converter is 2400 A and the required rotor current during the partial operation of 190 MW is about 8345A. Therefore, four power converters are enough to handle the required current during this partial generation. Hence, when open circuit fault in a power converter during rated generation occurs then the faulty converter is inactivated by removing gate pulses and the machine is in continuous mode with reduced power delivery.

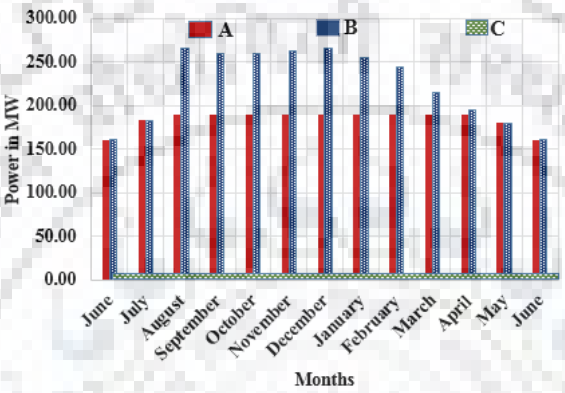

A – With fault tolerant operation B – Normal operation C – Without power redundancy

Total Energy Generated at Variable Speed PSPP = 1503.86 (18 hours/day)

Total Energy Generated without Power Redundancy = 1445.21 MU

Total Energy Generated considering Fault Tolerant Operation = 1473.1 MU

Benefit of fault tolerant operation = $\left(\frac{1473.1 - 1445.21}{1445.21}\right) \times 100\% = 1.93\ \%$

Fig. 4.14. Power generation of 190 MW at various water heads

The amount of power generation with respect to the variation in head (Shown in Fig. 4.14). It shows that the proposed fault tolerant operation in open circuit fault provides considerable amount of power generation through four parallel connected healthy converters. In addition, the incorporation of fault tolerant operation in power converter open circuit fault improves operational state of the power converter to 98.04%. It shows that the proposed fault tolerance during single leg/single device brings additional generation of 1.93 % electrical energy compared to the DFIM without power redundancy operation.

4.4.2 Experimental Validation (2.2 kW DFIM)

4.4.2.1 Power Converter Failure in All Channels (Five Converters)

4.4.2.1.1 RSC Single Leg Open Circuit Fault

DFIM is made to deliver 0.91 p.u (2 kW) power to grid at 0.9 p.u (1350 rpm) speed. Single leg open circuit fault at RSC is injected at 160 s and results are shown in Fig. 4.15. the magnitude of rotor current in healthy legs reach to 2.75 p.u (Fig 4.15a) and stator phase currents

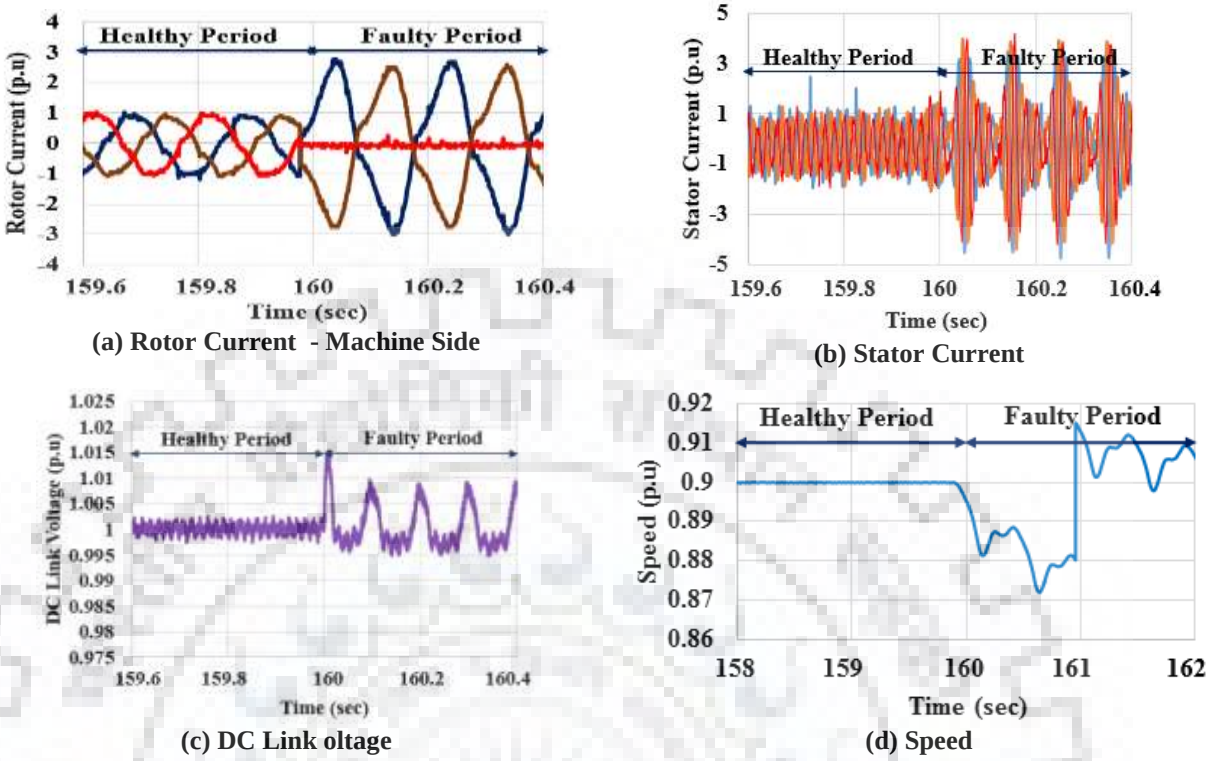

(a) Rotor Current - Machine Side

(b) Stator Current

(c) DC Link oltage

(d) Speed

Fig. 4.15. RSC single leg open circuit fault (2.2 kW DFIM) at generation

reach to 4 p.u (Fig. 4.15b). Both current transients are repeatedly occurring two times per interval more than single device open circuit fault. Reactive power and speed of the machine is significantly affected and results to stopping of the unit.

4.4.2.2 Power Converter Failure in Single Converter

4.4.2.2.1 RSC Single Leg Open Circuit Fault

Single leg open switch fault is injected at 80s at any one of the converter and results are shown in Fig. 4.16. During the fault, one of the phase currents in the faulty converter is omitted (shown in Fig. 4.16a) and same phase current in other healthy converter (shown in Fig. 4.16b) increases to two times than its regular value. Further, dc link voltage of the both converters are disturbed (shown in Fig. 4.16c) and speed of the unit is continually constant (shown in Fig. 4.16d) as set by control system. From the experimental results, it is seen that rise in rotor current is similar to simulation results.

4.4.2.3 Fault Tolerant Operation of RSC Open Circuit Fault

For fault tolerant operation, the machine is made to deliver 0.91 (2 kW) power to grid at 0.9 p.u (1350 rpm) speed through RSC/GSC control system. Single leg open switch fault is injected in any one of the converters at 80s. Fig. 4.17, shows the experimental results of the fault

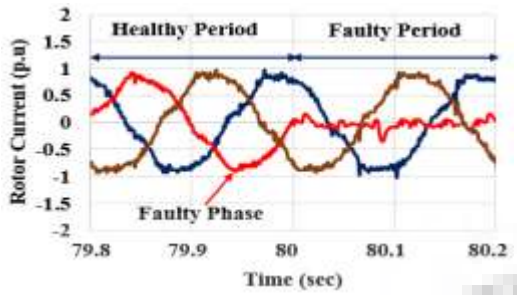

(a) Rotor Current - Faulty Converter

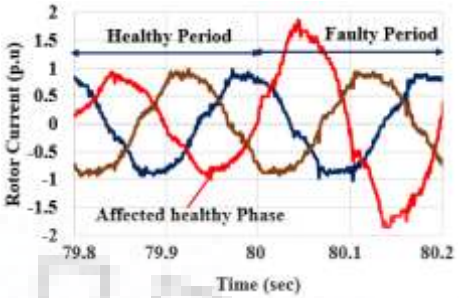

(b) Rotor Current – Healthy Converter

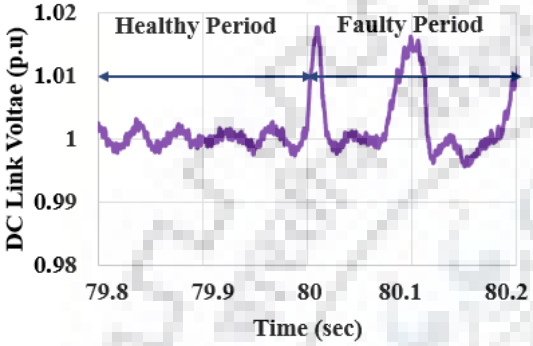

(c) DC Link Voltage

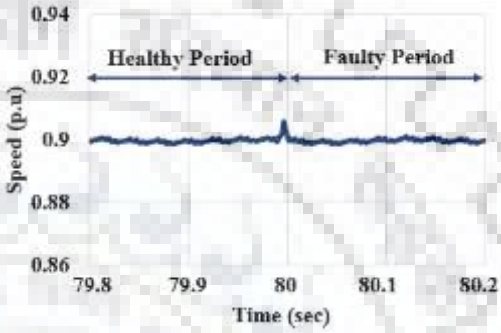

(d) Speed

Fig. 4.16. RSC single leg open circuit fault (2.2 kW DFIM) at generation

diagnostic method, where rotor current (machine side) is rotating at slip frequency of 5 Hz. Under normal conditions, diagnostic variables are equals to zero value. When a single leg fault is introduced in one of the multi-channel machine side VSI at 80s, diagnostic variables are increases to show the value similar to the simulation results. Considering the threshold value, fault is detected at 80.04 s, i.e. 0.04 s after the fault occurrence. Once the fault is detected and it sends the faulty signal to the real time controller as shown in Fig. 4.18b, faulty MSC is isolated from the system at 80.04s (shown in Fig. 4.18a). It is noted that the acceptable power delivery through only one converter is 0.35 p.u (0.77 kW) for a 2.2 kW DFIM. Therefore, power delivery of the machine is reduced to 0.35 p.u (shown in Fig. 4.18d) through controller and it takes about

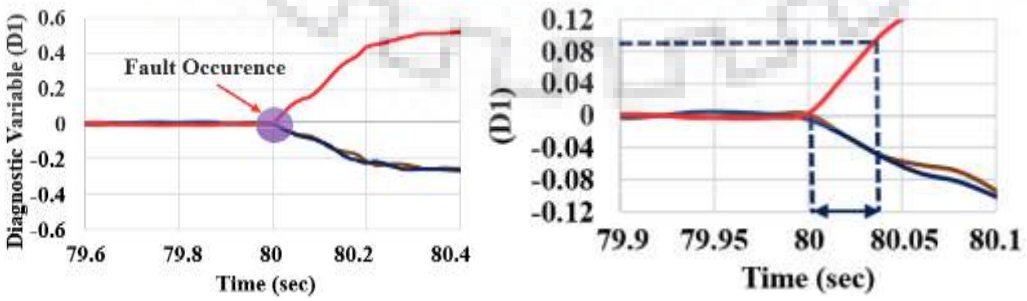

Fig. 4.17. Experimental results of fault diagnosis in RSC single leg fault

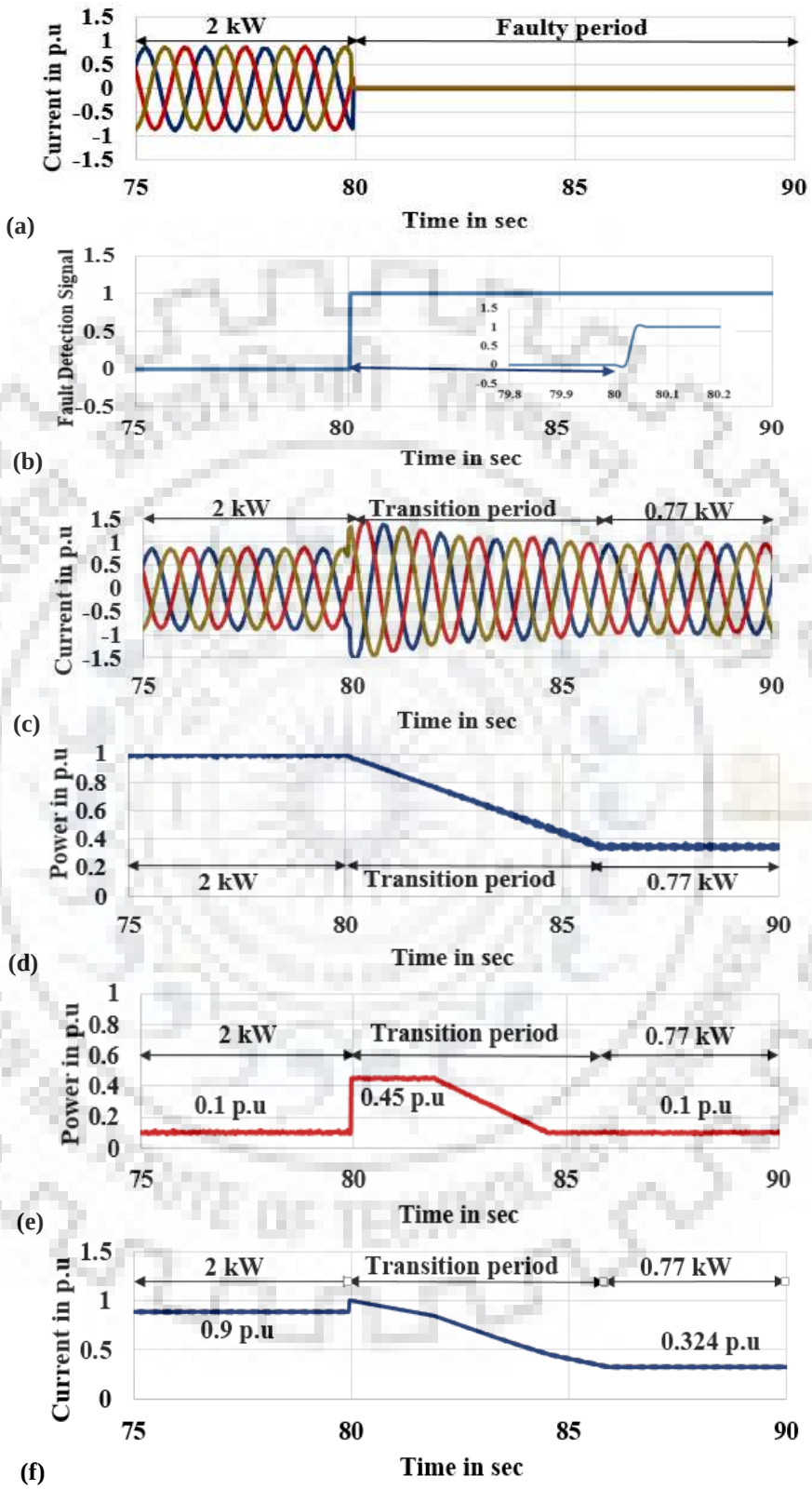

Fig 4.18. Fault tolerant operation of converter open circuit fault at generation mode for a 2.2 kW DFIM (a) Rotor current – faulty converter, (b) Faulty signal, (c) Rotor current –healthy converter, (d) Real power, (e) Reactive power, (f) Stator current

6s to reach the set value. During the transition period, reactive power controller increases reactive power consumption (shown in Fig. 4.18e) of the machine (0.45 p.u) to control the rotor current as shown in Fig. 4.18c. Stator current of the machine increases to 1 p.u (shown in Fig. 4.18f) at initial transition period due to reactive power consumption and it gradually reduces based on the reduced power delivery.

4.5 Conclusion of the Chapter

The dynamic performance of a 250MW DFIM of PSPP operating in generation mode has presented in this chapter. The power and control circuits were subjected to different faults during the operation and the output results were analyzed comprehensively. At each fault case, the survivability of the machine drive was tested. It can be seen from the test results that the drive survived during RSC single device/leg open circuit faults at super synchronous generation mode, but not in sub-synchronous mode. The drive survived during all kind of single current sensor faults, gain fault in reactive power signals at both sub and super synchronous speeds. It is noted that a 1000MW plant shall have financial losses up to $25,817,835/year/plant due non availability of full redundancy in power and control circuits of Converter. In addition, fault tolerant operation during single converter open circuit fault is proposed and it provides additional generation of 1.93 % electrical energy compared to without fault tolerant operation.

Chapter V

Dynamic Performance of Pumping Mode of a Large Variable Speed PSPP

[This chapter discusses the expected benefits of pumping mode of DFIM based variable speed PSPP in comparison with the synchronous machine based fixed speed PSPP in accordance with the head variation from 130 m to 230 m. In addition, dynamic behavior of a large rated DFIM hydrogenerating unit operating in pumping mode subjected to power converter and control circuit faults are discussed. Survivability status of DFIM operating in pumping mode during excitation faults is also assessed. Also, it discusses the fault tolerant operation of hydrogenerating unit during single converter open circuit fault.]

5.1 Variable Speed Pumping Unit

Hydrogenerating units are designed to operate at maximum efficiency with the considerations of water head, turbine speed and water discharge. The efficiency of pump turbine varies according to the water head and volume of water pumped back to the upper reservoir (dam) from the lower one. Further, the speed of the turbine is a function of water head. Variable vane settings is used for partial pumping mode at fixed speed PSPP. The efficiency of the synchronous unit with variable vane setting is reduced due to: (i) changing water head level in dam over the year, (ii) varying surplus power availability in grid. The efficiency of the synchronous unit with variable vane setting is shown in Fig. 5.2. It shows that the efficiency of the unit is varying when water head and surplus power available in grid changes. Therefore, the speed of the turbine is adjusted to get maximum efficiency for an available water head, called as variable speed PSPP.

A typical 250 MW DFIM unit (Tehri PSPP, India) is considered to evaluate the effects of fixed and variable speed operation for a site with wide water head variation. The rated head and turbine speed are chosen as 188m and 230.77rpm, respectively. Nevertheless, gross water head may vary over the year between 130m and 230m, shown in Fig. 5.3a. In pumping mode, the requirement of input power of the machine depends on water head. i.e., availability of minimum water head level in dam requires less input power for the rated discharge. Reversible Francis turbine hill curves [shown in Appendix] have been used for estimating the turbine efficiency at fixed and variable speed operation. Subsequently, water pumped back to the dam for the various

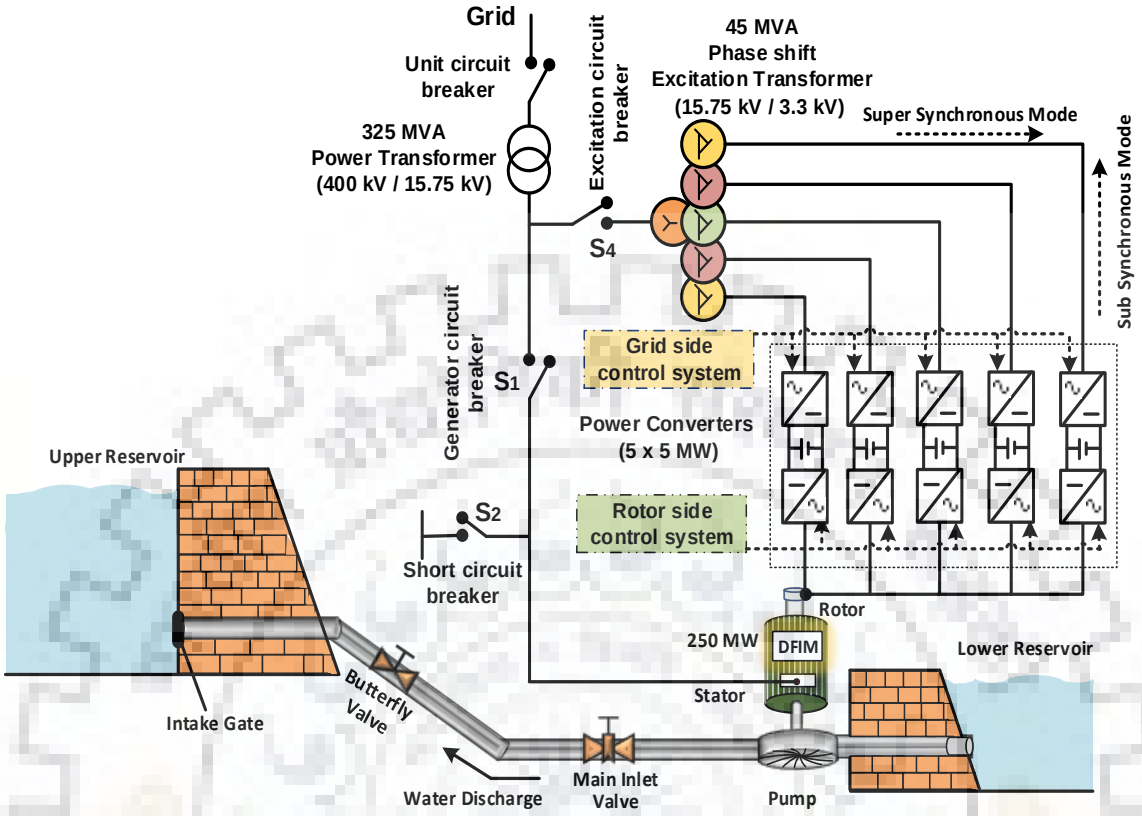

Fig. 5.1. Hydrological and electrical depiction of a 250 MW DFIM variable speed hydrogenerating unit – pumping Mode
(This figure is reproduced from chapter 3 for ease reference)

head level is calculated and is graphically presented in Fig. 5.3b. From the graph, it can be inferred that maximum water discharge variation between variable and fixed speed operation (109 - 89 = 20 m^3/s at the water head level of 134m in June) is obtained at minimum water head

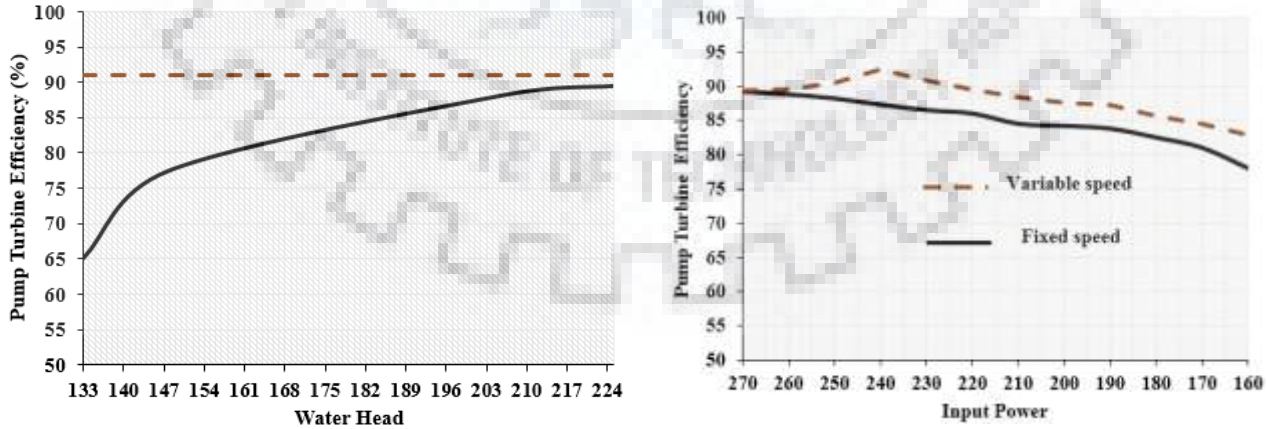

(a) **efficiency versus water head at fixed input power (250 MW)**

(b) efficiency versus input power at fixed water head (200 m)

Fig. 5.2 Pump turbine efficiency at variable vane settings of fixed speed PSPP

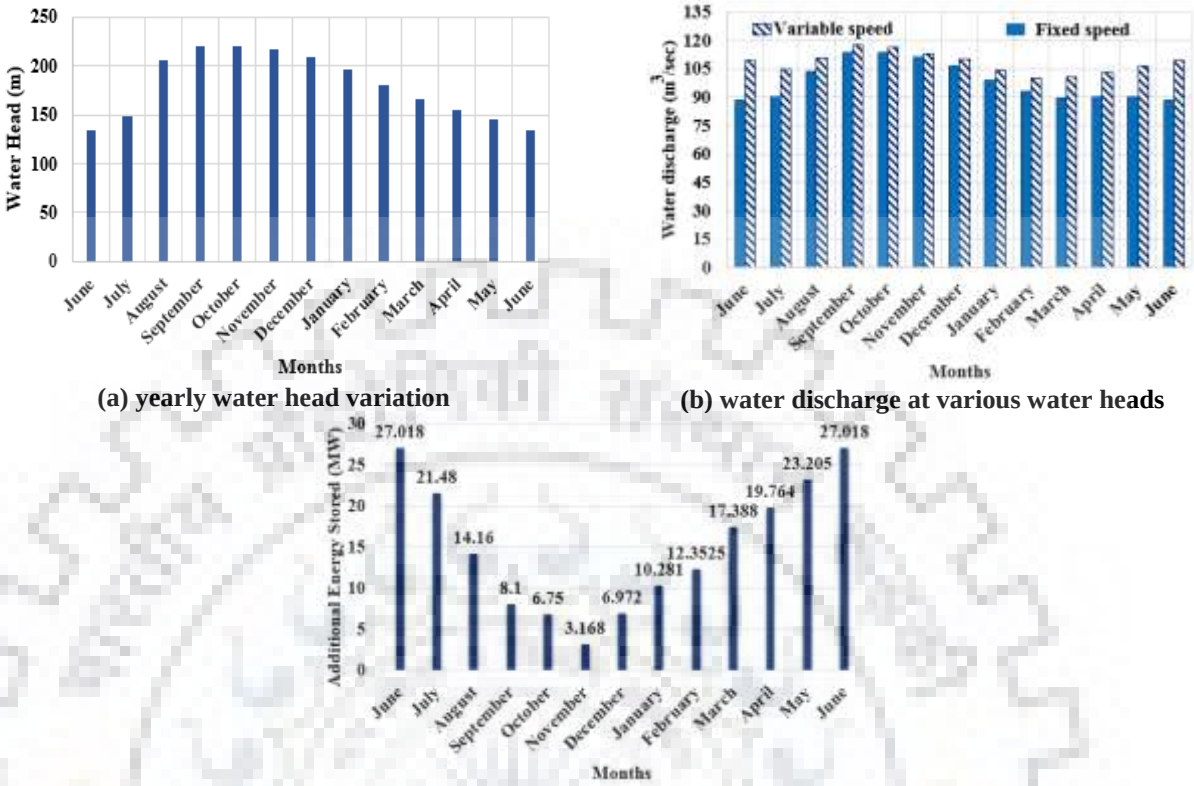

(a) yearly water head variation

(b) water discharge at various water heads

(c) additional power stored during variable speed mode

Fig. 5.3. Comparison of a typical fixed speed and variable speed PSPP schemes

level (i.e. efficiency of variable speed operation is much higher than fixed speed at minimum water head). For the analysis of whole year, variable speed mode brings additionally 336 MCM (Million Cubic Meter) of water pumped back to the dam from the lower reservoir which leads to an additional storage of 7.87 % electrical energy than the fixed speed of operation, shown in Fig. 5.3c.

5.2 Speed and Reactive Power Control of DFIM

Voltage source back-to-back power converters are connected in rotor circuit of the machine is responsible for controlling speed and reactive power of the machine. Grid voltage oriented vector control is employed in grid side converter (GSC) to ensure the decoupled control of dc link voltage and unity power factor at grid side (rotor). Stator flux oriented vector control is implemented in RSC to ensure the decoupled control of speed and stator reactive power of the DFIM. For this dynamic control, three grid voltage sensors, three grid current sensors, dc link voltage sensor, encoder, three rotor current sensors are used. Detailed d-q modelling and control equations of DFIM are explained in chapter 2. However, essential equations are considered here

Table 5.1. Comparison of typical fixed and variable speed PSPP schemes at pumping mode

Month	Water Head (m)	Input Power (MW)	Base Input Power (MW)	Input Power (P.U)	Peripheral Velocity Factor	Peripheral Velocity Factor		Efficiency		Water Pumped (m^3/sec)		Additional Power Stored (MW)
						Fixed Speed	Variable Speed	Fixed Speed	Variable Speed	Fixed Speed	Variable Speed	
June	133.66	171	255	0.67	98.21	1.19	82.81	0.68	0.84	88.68	109.29	27.02
July	148	179	255	0.70	93.33	1.13	82.81	0.73	0.85	90.00	104.80	21.48
August	206	240	255	0.94	79.11	0.96	82.81	0.87	0.93	103.44	110.45	14.16
September	220	270	255	1.06	76.55	0.92	82.81	0.91	0.94	113.84	117.60	8.10
October	219.5	270	255	1.06	76.64	0.93	82.81	0.91	0.93	113.48	116.61	6.75
November	217	264	255	1.04	77.08	0.93	82.81	0.90	0.91	111.37	112.85	3.17
December	209.66	249	255	0.98	78.41	0.95	82.81	0.88	0.91	106.78	110.17	6.97
January	196.66	224	255	0.88	80.96	0.98	82.81	0.85	0.90	98.70	104.03	10.28
February	180.66	203	255	0.79	84.47	1.02	82.81	0.82	0.88	93.35	100.32	12.35
March	165.33	189	255	0.74	88.30	1.07	82.81	0.77	0.86	89.73	100.45	17.39
April	155	183	255	0.72	91.20	1.10	82.81	0.75	0.86	90.26	103.26	19.76
May	145.33	179	255	0.70	94.18	1.14	82.81	0.72	0.85	90.15	106.42	23.21
June	133.66	171	255	0.67	98.21	1.19	82.81	0.68	0.84	88.68	109.29	27.02

Power Stored = $\frac{9.81*\text{Additional Water Pumped}*\text{Water Head}}{1000}$ Rated Discharge = 145.3 m^3/sec Rated Head = 188 m

Total Energy Storage at Fixed Speed PSPP = 1584.82 MU (8760 hours/year) Total Energy Storage at Variable Speed PSPP = 1709.49 MU (8760 hours/year)

% of Additional Energy saving = $\left(\frac{1709.49 - 1584.82}{1584.82}\right) \times 100\% = 7.87\ \%$

for a clear understanding of fault analysis. Control systems used for real, and reactive power control of DFIM is shown in Fig. 5.4.

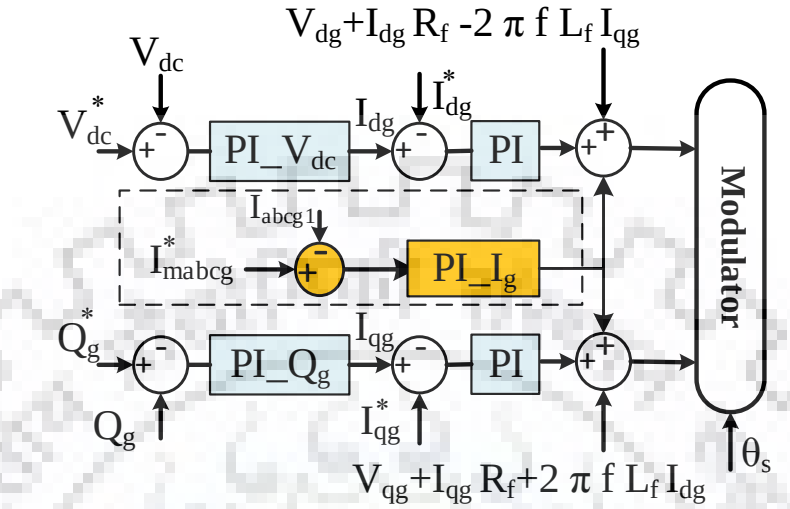

(b) GSC control system

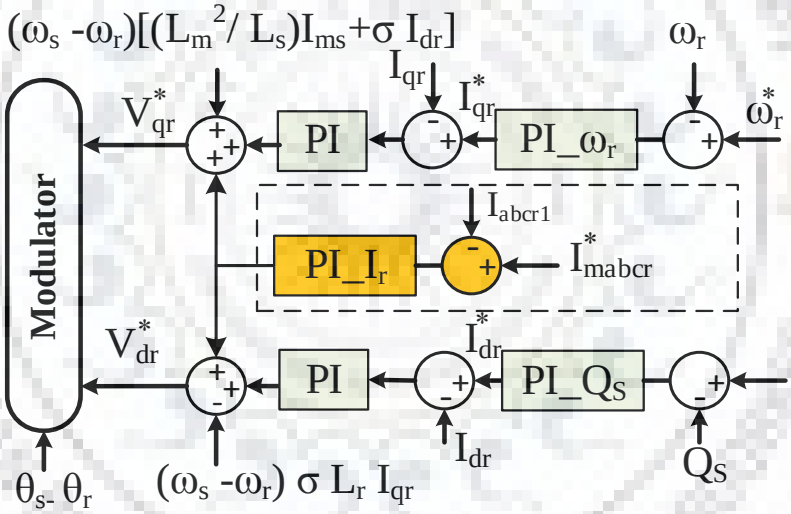

(b) RSC control system

Fig. 5.4. Vector control of DFIM with parallel converters at pumping mode

5.2.1 Grid Voltage Oriented Vector Control

In grid side system, a synchronous rotating reference frame with angular speed 'ω_a'is chosen during conversion of three phase quantities into rotating two phase quantity. In grid voltage oriented control: (i) angular speed of ω_a is chosen as angular speed of the grid voltage ω_s, (ii) d-axis rotating frame is aligning with grid voltage space vector. Hence,

$$\vec{V}^{a}_{dg} = \left|\vec{V}^{a}_{g}\right| \quad ; \quad \vec{V}^{a}_{qg} = 0 \quad ; \quad \omega_a = \omega_s \tag{5.1}$$

Active (P_g) and reactive power (Q_g) are calculated as

$$P_g = \frac{3}{2}\left|\vec{V}_g\right|\vec{I}_{dg} \quad ; \quad Q_g = -\frac{3}{2}\left|\vec{V}_g\right|\vec{I}_{qg} \tag{5.2}$$

5.2.2 Stator Flux Oriented Vector Control

With the stator flux orientation, decoupled control between electro-magnetic torque and stator reactive power control is achieved [13] - [15]. In stator flux oriented vector control, d-axis stator flux is aligning with stator flux space vector $\vec{\psi}_s$ in synchronously rotating reference frame.

$$\vec{\psi}_{ds} = \vec{\psi}_s \quad ; \quad \vec{\psi}_{qs} = 0 \quad ; \quad \vec{\psi}_s = L_m \vec{I}_{ms} \tag{5.3}$$

The expression of electro-magnetic torque and reactive power equations can be derived as

$$T_{em} = -\frac{3}{2} p \frac{L_m}{L_s} \frac{\vec{V}_s}{\omega_s} \vec{I}_{qr} \tag{5.4}$$

$$Q_s = \frac{3}{2}\left(\frac{\vec{V}_s^{\,2}}{\omega_s L_s} - \vec{V}_s \frac{L_m}{L_s} \vec{I}_{dr} \right) \tag{5.5}$$

Allowable speed variation of the machine depends on voltage rating of power converter connected in rotor circuit of the machine (slip voltage). Vector control of 250 MW DFIM (parameters are given in Chapter II) is simulated in MATLAB/Simulink environment. Power transfer of the machine during starting, pumping mode at super and sub synchronous speeds are shown in Fig. 5.5. Electrical quantities noted in figures are obtained through Simulation tests. From the tests, it is observed that, (i) real power consumption in both stator and rotor circuits is based on speed reference, (ii) slip power of the machine is delivered to the grid in case of sub synchronous speed, (iii) rotor voltage and frequency of rotor current are adjusted in accordance

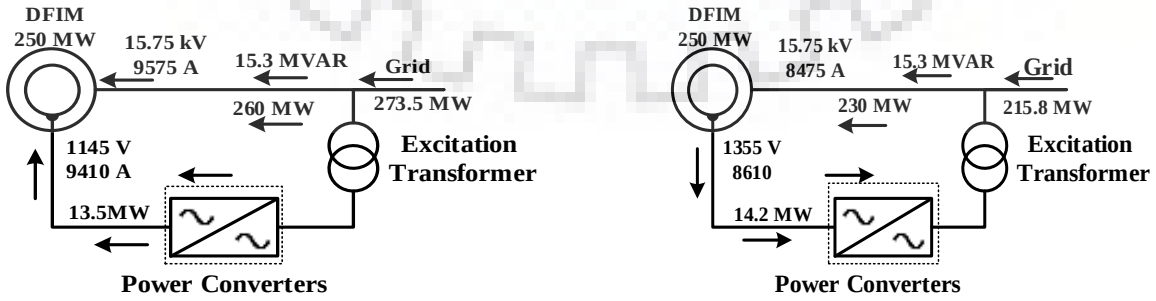

(a) super synchronous speed (240 rpm) (b) subsynchronous speed (220 rpm)

Fig. 5. 5 Power flow diagram of 250 MW DFIM at part load operation

with the machine speed and power factor, (iv) net active power taken from the grid is less in sub synchronous mode.

Rotor voltage of the machine depends on slip speed of the machine. However, rotor current highly varies with respect to load and power factor of the machine. In a typical 250MW DFIM, it is observed that, (i) rotor voltage varies about 50 volts from no load to full load, (ii) rotor current changes from 4200A to 10500A between no-load and full load, respectively.

5.3 Results and Discussions

The performance bounds of the 250MW DFIM drive during pumping mode is considered as follows: (i) allowable reactive power variation is ± 0.05 p.u, (ii) allowable speed variation is ± 0.03 p.u, (iii) dc link voltage variation is ± 0.1 p.u, (iv) rotor side grid current variation up to 0.05 p.u, (v) stator current variation up to 0.05 p.u, (vi) machine rotor current variation up to 0.05 p.u, (vii) controller settling time is less than 250ms. In simulation, machine is instructed to operate at 1.04 p.u (240rpm) speed and shaft power is considered as 260MW. Further, power factor of the machine is set as 0.95 through reactive power control system. From the tests, it is observed that: (i) magnitude of line current in stator winding is 9575A (0.85 p.u), (ii) voltage (P-P) applied to rotor winding by rotor side converter is 1145V (0.35 p.u), (iii) line current in rotor winding is 9410A (0.81 p.u), (iv) reactive power consumption of the machine is 15MVAr (0.05 p.u), (v) frequency of rotor current is 2Hz.

5.3.1 Simulation Results (250 MW DFIM)

5.3.1.1 Power Converter Failure in a Single Converter

5.3.1.1.1 GSC Single Switch Open Circuit Fault

Single switch gate drive open circuit fault (upper switch) is injected in one of the parallel connected GSC at 160s and results are given in Fig. 5.6. During the fault, phase current corresponding to the faulty leg is distorted in upper half cycle and negative half cycle is omitted, results in variation in phase and magnitude of other two phase currents (shown in Fig. 5.6a). However, current flowing through the other healthy converters are not affected as shown in Fig. 5.6b. From the test results, it is inferred that: (i) dc link voltage marginally fluctuated in the faulty converter as shown in Fig. 5.6c (oscillation in the rate of grid frequency), (ii) variation in capacitor dc link voltages, faulty switch connected to the dc link capacitor voltage (Vd1) gets marginally reduced and other dc link capacitor voltage (Vd2) increases to regulate the dc link voltage, (iii) Fluctuation in power factor at grid side (rotor) due to the variation in reactive power

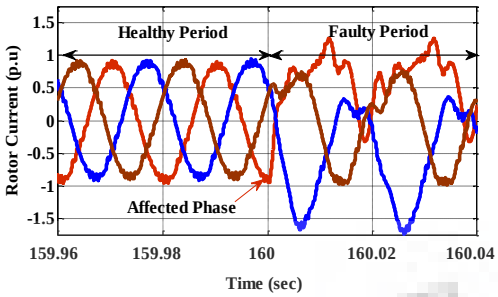

(b) Rotor Current (Grid Side) – Faulty Converter

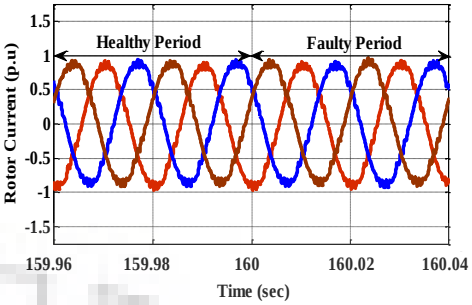

(b)Rotor Current (Grid Side) – Healthy Converter

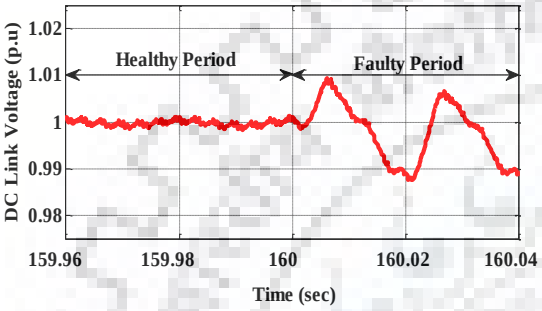

(g) DC Link Voltage – Faulty Converter

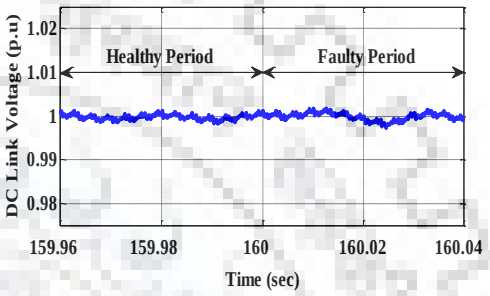

(h) DC Link Voltage- Healthy Converter

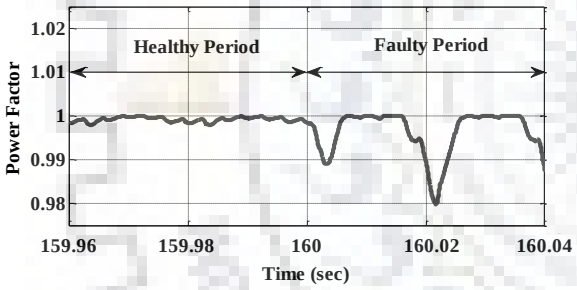

(i) Power Factor

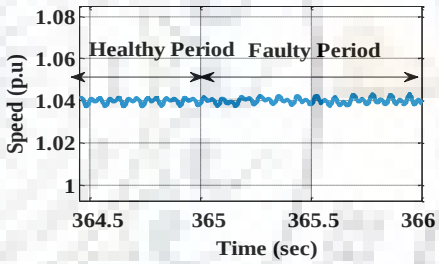

(j) Speed

Fig. 5.6. GSC upper single switch OCF (250 MW DFIM) at pumping

consumption. (iv) speed of the machine is constant as set by machine side control system. In case of open circuit fault in lower switch, results are similar to the upper switch fault. However, it is observed that (i) Faulty leg phase current is disturbed in lower half cycle and omitted in upper half cycle, (ii) variation in capacitor dc link voltages are reversed when compared to upper switches short circuit fault. When GSC is acting as rectifier, rotor current profile is similar in starting, generation, pumping and condenser mode of operation.

5.3.1.1.2 RSC Single Leg Open Circuit Fault

Single leg gate signal open switch fault is injected in one of the parallel connected RSC at 160s and results are given in Fig. 5.7. During the fault, the rotor current in one of the phase

of faulty converter goes to zero (Fig. 5.7a) whereas the other two phases are carrying as equal currents. However, the same phase current in other parallel converters increases by 1.286 times of the regular value (Fig. 5.7b) to maintain required rotor phase current. It is seen from the test results that: (i) during the fault the healthy power converters are overloaded and this results in stopping of the unit, (ii) speed of the machine is maintained at desired level through RSC control system, (iii) dc link voltage of the faulty and healthy converters are fluctuated as shown in Fig. 5.7c and Fig. 5.7d, respectively. Likewise, all open and short circuit faults in converters were done and survivability status of the DFIM unit operating in pumping mode for the said faults are reported in Table 5.2.

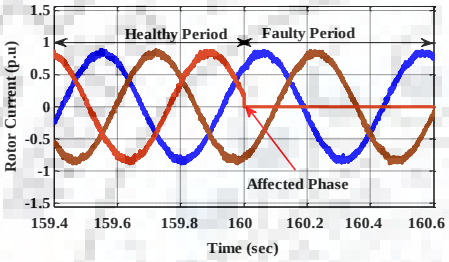

(a) Rotor Current (Grid Side) – Faulty Converter

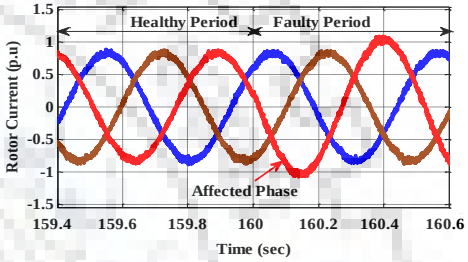

(b)Rotor Current (Grid Side) – Healthy Converter

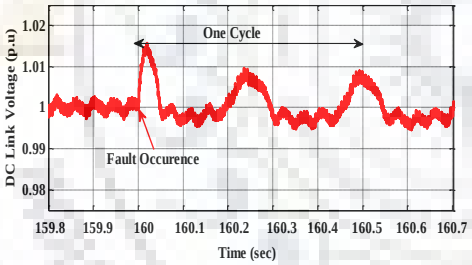

(c) DC Link Voltage – Faulty Converter

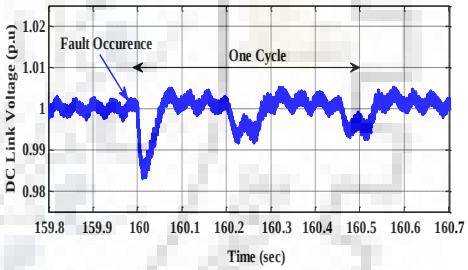

(d) DC Link Voltage- Healthy Converter

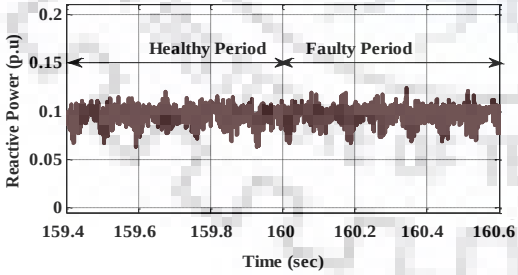

(e) Power Factor

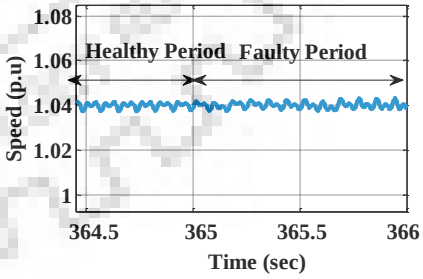

(f) Speed

Fig. 5.7. RSC single leg OCF (250 MW DFIM) at pumping

5.3.1.2 Power Converter Failure in All Channels (Five Converters)

Open and short circuit failures in all grid side converters are similar to the faults in any one of the parallel connected grid side converters. Nonetheless, variation in dc link voltage and

power factor (rotor side) is higher as compared to faults occur in only one converters. But, faults in rotor side converters are different from the single converter fault and it is discussed here.

5.3.1.2.1 RSC Single Switch Open Circuit Fault

The fault is injected at 365s and results are shown in Fig. 5.8. When fault occurs, one of the rotor phase currents is discontinuous and other two phases are carrying currents which are altered during discontinuous period of faulty phase current as shown in Fig. 5.8a. Change in rotor currents affect stator currents and consequently speed, real and reactive power consumption of the machine is troubled. During fault, magnitude of stator and rotor phase transient currents reach to 5.05 p.u (shown in Fig. 5.8b) and 4.1 p.u (shown in Fig. 5.8a) respectively. From the test results, it is observed that: (i) healthy phase rotor currents are deviations in phase and produce transients at meeting point of these two phase currents, (ii) both stator and rotor currents reach to above the rated value, (iii) fluctuation in speed of the machine,

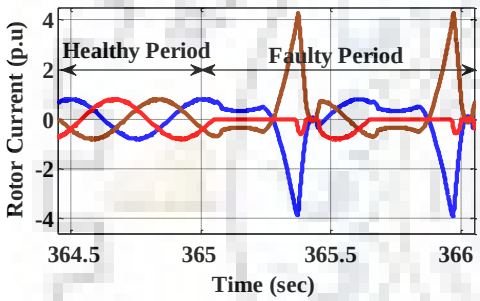

(a) Rotor Current (Machine side)

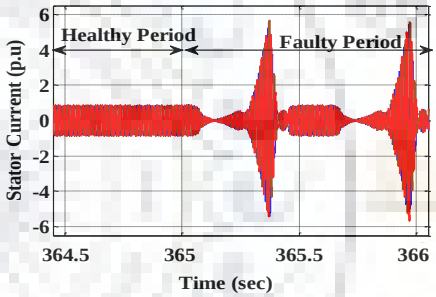

(b)Stator Current

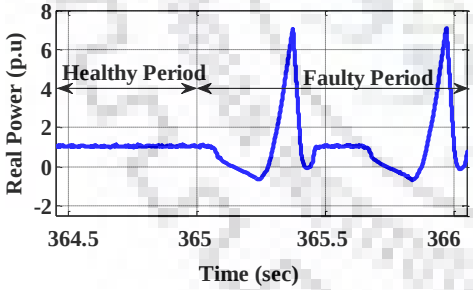

(c) Real Power - DFIM

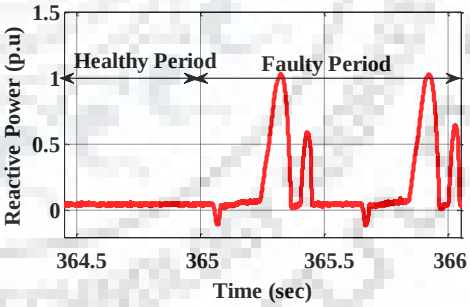

(d) Reactive Power - DFIM

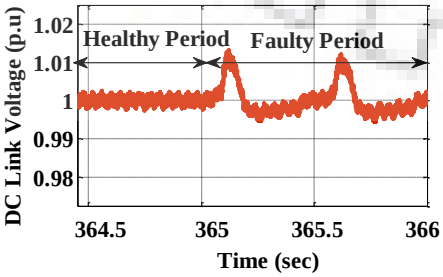

(e) DC Link Voltage

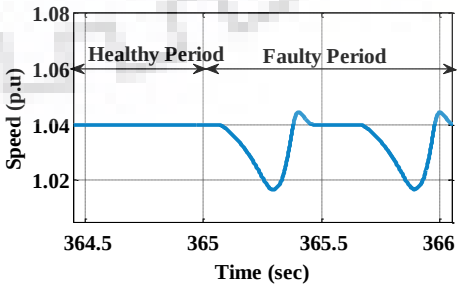

(f) Speed

Fig. 5.8. RSC single switch OCF (250 MW DFIM) at pumping

(iv) instability in real and reactive power consumption of the machine, (v) RSC control system is out of action.

5.3.1.2.2 RSC Single Leg Open Circuit Fault

Single leg gate drive open circuit fault is injected in RSC at 365s and results are shown in Fig. 5.9. When fault occurs, one of the rotor phase current goes to zero (Fig. 5.9a) and the conduction mode is equivalent to the single phase converter with other two healthy legs. During fault, magnitude of both stator and rotor currents reach to the high value as similar to fault in single device fault. However, rotor currents transient repeatedly occurs two times per interval more than single device fault, consequently stator current (shown in Fig. 5.9b), speed, real power and reactive power of the machine are affected. From the test results, it is observed that the

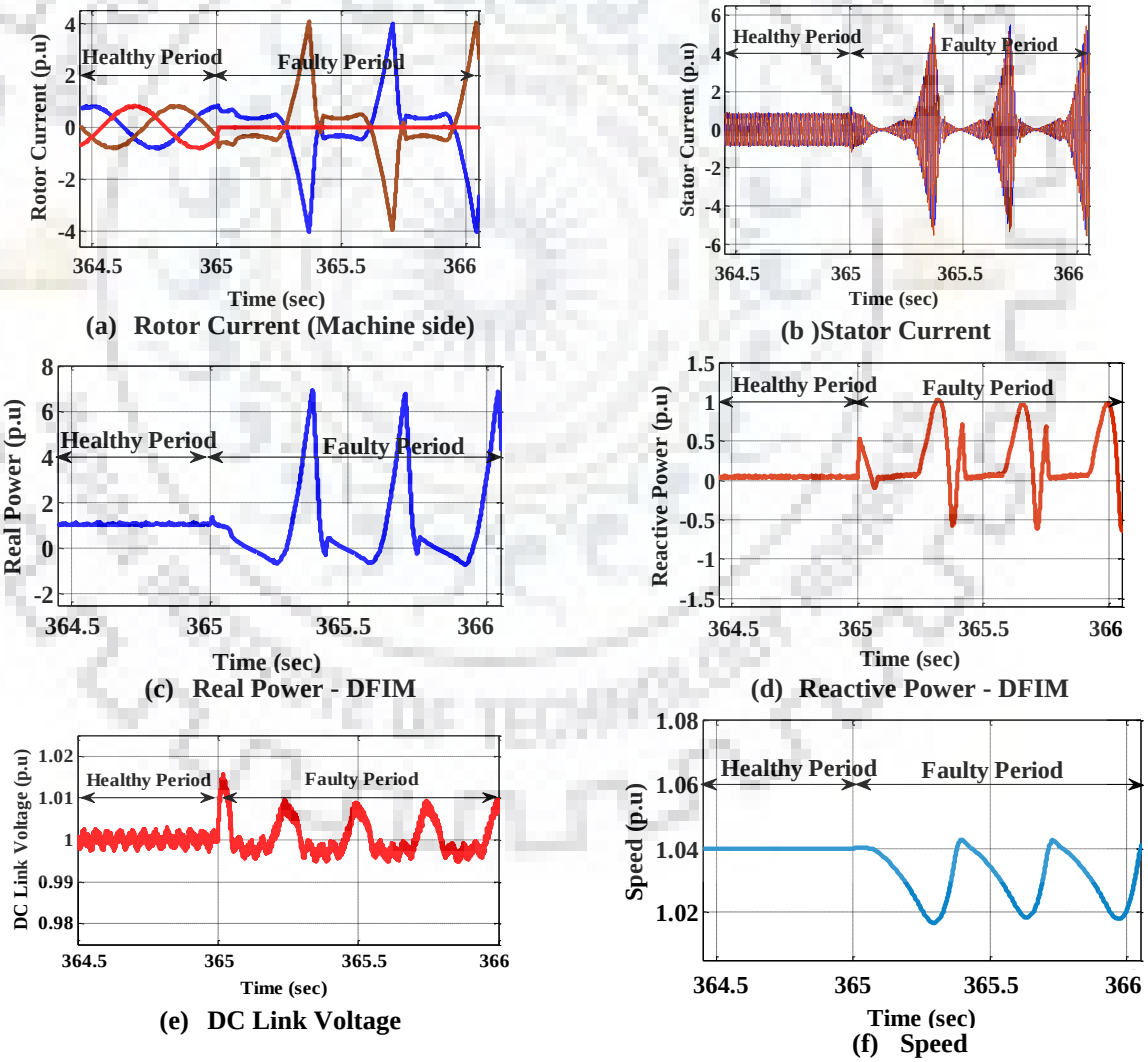

Fig. 5.9. RSC single leg OCF (250 MW DFIM) at pumping

results are similar to single device fault except the number of times of transients at specific time period.

5.3.1.3 Control Circuit (Sensor) Failure

5.3.1.3.1 Encoder Omission Fault

Encoder omission fault is injected at 365s in all converters and the results are shown in Fig. 5.10. When fault occurs, speed controller reads input as zero and increases proportional gain of the speed controller which increase the q-axis rotor current, frequency of rotor current increases as shown in Fig. 5.10a. Consequently, machine speed increases (shown in Fig. 5.10f) until the speed gets saturated. From the test results, it is summarized as: (i) speed of the machine increases until the q-axis rotor current (Iqr) gets saturated, (ii) increase in Idg (direct axis current - grid) to maintain the dc link voltage, (iii) reactive power delivery during encoder fault is

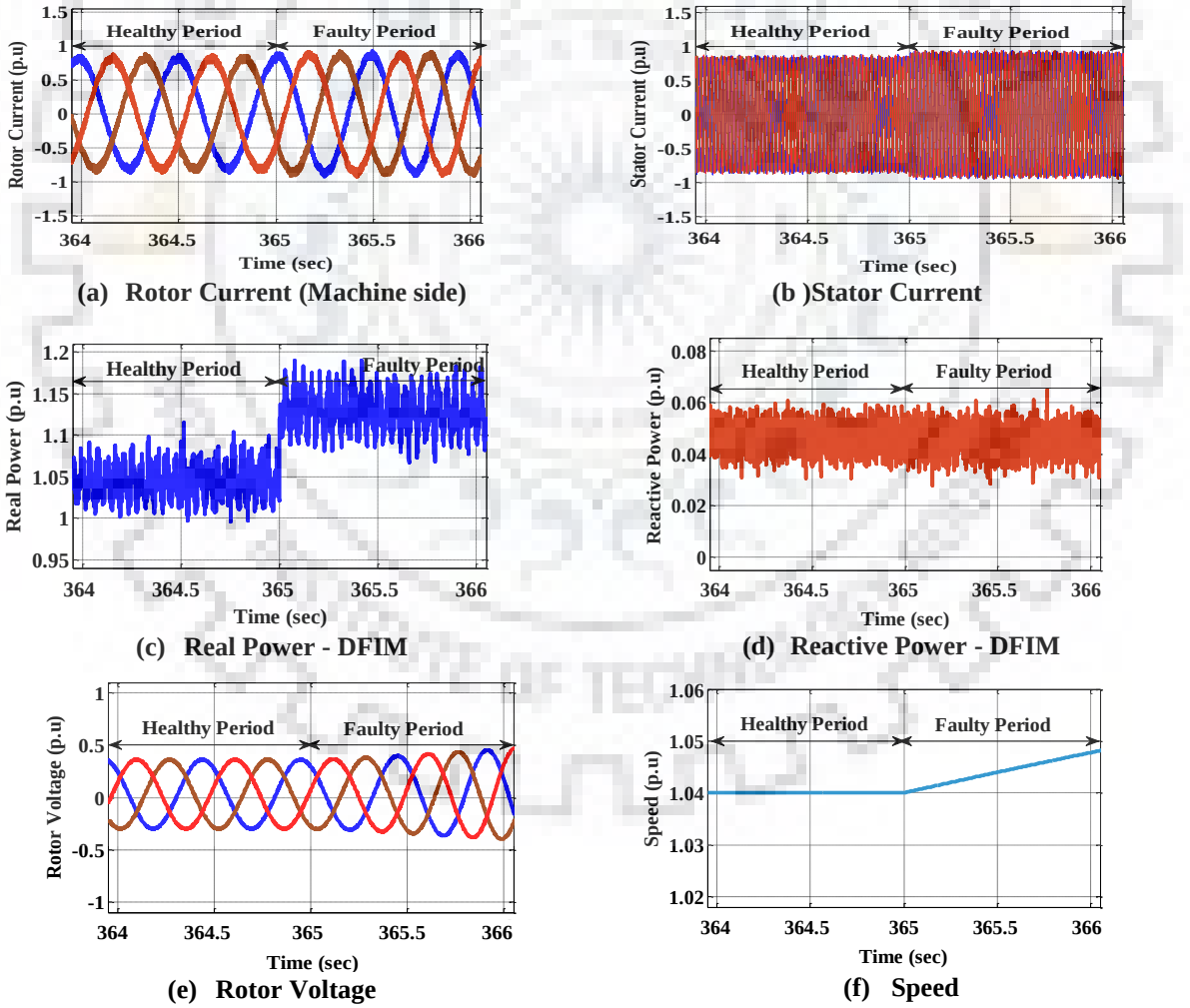

Fig. 5.10. Encoder omission fault (250 MW DFIM) at pumping

unchanged. Likewise, Reactive power signal omission fault and Single rotor current sensor omission Fault are injected and results are summarized in Table 5.2.

Table 5.2: DFIM drive status and economic analysis of converter and sensor failure at pumping mode [165], [166]

System	Mode of operation	Faults	Fault Status	250 MW DFIM					
				No.of Failures/year	U Period/ year	Energy Storage Losses* (MU)	Financial Losses** /year (M$)	Status	Fault Tolerant Benefits (M$)
Power Converter	Sub synchronous	Rotor side converter	Open Circuit Fault (SDOC, SLOC)	S	1.9940	50.59	9.87	0.59	Yes	0.51
			Short Circuit Fault (SDSC,PPSC,PGSC)	F	0.6646	16.86	3.29	0.20	NA	-
		Grid side converter	Open Circuit Fault (SDOC, SLOC)	F	0.3025	11.83	2.31	0.14	Yes	0.12***
			Short Circuit Fault (SDSC,DCSC,PPSC, PGSC)	F	0.1008	3.94	0.77	0.05	NA	-
	Super synchronous	Rotor side converter	Open Circuit Fault (SDOC, SLOC)	F	1.9940	50.59	9.87	0.59	Yes	0.51***
			Short Circuit Fault (SDSC,PPSC,PGSC)	F	0.6646	16.86	3.29	0.20	NA	-
		Grid side converter	Open Circuit Fault (SDOC, SLOC)	S	0.3025	11.83	2.31	0.14	Yes	0.12
			Short Circuit Fault (SDSC,DCSC,PPSC, PGSC)	F	0.1008	3.94	0.77	0.05	NA	-
		DC Link	Open circuit/Short circuit	F	0.007	2.19	0.43	0.03	NA	-

Total Energy Storage at Fixed Speed PSPP = 396.205 MU (6 hours/day) Unavailability period of VSC over the year is 85.4 hours

Total Energy Storage at Variable Speed PSPP = 427.373 MU (6 hours/day) Total Energy Storage without Power Redundancy = 410.71 MU

% of Additional Energy saving of Variable Speed PSPP considering Power Redundancy Issue = $\left(\frac{410.71 - 396.21}{396.21}\right) \times 100\% = 3.66\ \%$

Table 5.2: DFIM drive status and economic analysis of converter and sensor failure at pumping mode (contd.) [165], [166]

System	Mode of operation		Faults	Fault Status	No.of Failures /year	250 MW DFIM U Period/ year	Energy Storage Losses* (MU)	Financial Losses** /year (M$)	Fault Tolerant Status	Benefits (M$)
Control Circuit faults	Sub and super synchronous	Omission/ saturation	Speed sensor	F	0.247	5.41	1.05	0.063	NA	-
			DC link voltage sensor	F	0.247	5.41	1.05	0.063	NA	-
			Reactive power signal	F	0.247	5.41	1.05	0.063	NA	-
			Single rotor Current Sensor	S	0.247	5.41	1.05	0.063	Yes	0.063
			Single grid current sensor	S	0.247	5.41	1.05	0.063	Yes	0.063
			Single grid voltage sensor	F	0.247	5.41	1.05	0.063	NA	-
		Gain	Speed sensor	F	0.355	7.77	1.52	0.091	NA	-
			DC link voltage sensor	F	0.355	7.77	1.52	0.091	NA	-
			Reactive power signal	S	0.355	7.77	1.52	0.091	Yes	0.091
			Single rotor Current Sensor	S	0.355	7.77	1.52	0.091	Yes	0.091
			Single grid current sensor	F	0.355	7.77	1.52	0.091	NA	-
			Single grid voltage sensor	S	0.355	7.77	1.52	0.091	Yes	0.091

* Average energy storage is 195MW//year/unit for a 250 MW DFIM ** Financial losses are considered as $ 0.06/kWh

*** Fault tolerant proposed in this paper with reduced power generation (168 MW) U - unavailability

SDOC - single device open circuit fault SLOC - single leg open circuit fault SDSC - Single device short circuit

DCSC - DC link short circuit PPSC - Phase to phase SC PGSC - Phase to ground SC

S - Survived F - Failed

5.3.1.4 Economic Analysis on Power and Control Circuit Faults

Consider a plant (TEHRI PSPP) having 4 units with each unit rated at 250MW. The average pumping period is considered as 6 hours/day. The probability of operational state of a back-to-back power converter without redundancy per year is 96.10%. Therefore, the unavailability of the back-to-back power converter per year is 85.4 hours/year. The average surplus power availability to each unit is estimated as 195 MW over the year considering water head and efficiency and it is estimated that the energy storage loss is about 16.653 MU/year/unit due to the inadequate power and control redundancy. Further, considering four units in a plant, the estimated energy storage losses of the plant will be 66.61 MU/year. The selling and purchase price of a unit of energy (kWh) are considered in hydropower plant in India as $ 0.11 and $ 0.05, respectively. Hence, per unit cost of stored electrical energy is $ 0.06. Therefore, it is noted that about $999,180/year/unit ($0.06 per kWh) financial losses are estimated due to the inadequate redundancy in power and control circuits. The cost of extra converter module is about $4,445,705/- which is retrieved within 4 years and 6 months, if redundancy is designed. The effect of variation in selling and purchasing prices in payback period is shown in Fig. 5.11. In addition, employing redundant converter in a unit is also beneficial in generating mode of operation.

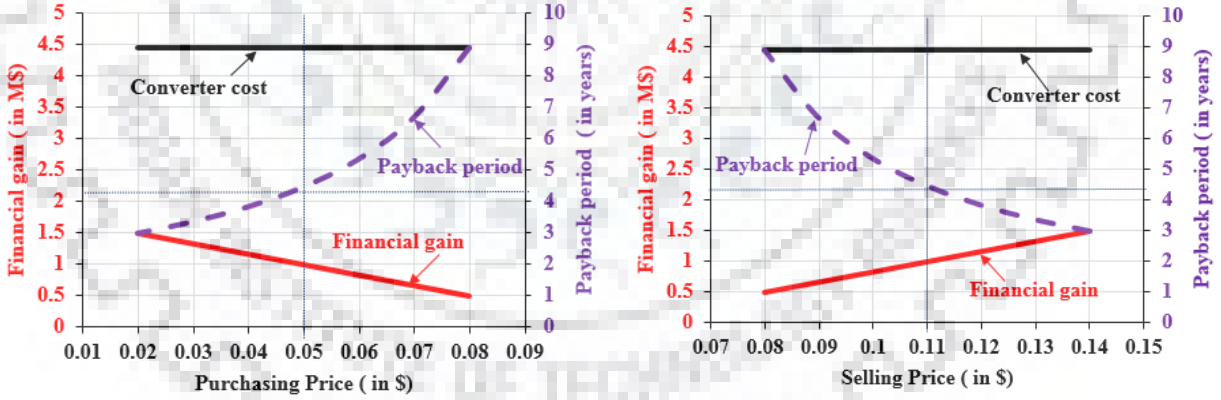

(a) Variation in purchasing prices (b) Variation in selling prices

Fig. 5.11 Payback period in redundancy converter

5.3.1.5 Fault Tolerant Operation of RSC Open Switch Fault

A typical 250MW DFIM unit is operated at pumping mode in between 206 rpm (shaft power of 168 MW) and 250 rpm (shaft power of 280 MW) for the consideration of available speed variation. The rated current of the each power converter is 2400 A. During open circuit fault in a converter, the corresponding converter unit is isolated/inactivated from the parallel

converter system and remaining four units are in continuous operation. However, power handling of the unit with the aid of four converter is limited to 168 MW. Therefore, shaft power of the unit is fixed at 168 MW during fault tolerant operation.

Open circuit faults in power converter are diagnosed with the help of rotor side currents and dc link voltage variation as well discussed in chapter 4. Further, the similar methodology is used for isolating the faulty converter and fault tolerant operation, i.e. faulty converter is inactivated by removing gate pulses and the machine is in continuous mode with reduced power delivery. Fig. 5.12b shows the amount of water discharge from lower to upper reservoir at fixed input power (168 MW) considering variable water heads (shown in Fig. 5.12a). It shows that the proposed fault tolerant operation in open circuit fault provides considerable amount of water pumped back to the upper reservoir through four parallel connected healthy converters. It provides an additional storage of 2.49% electrical energy compared to the operation of DFIM without power redundancy operation. Table 5.2 shows the outcomes of the fault tolerant operation.

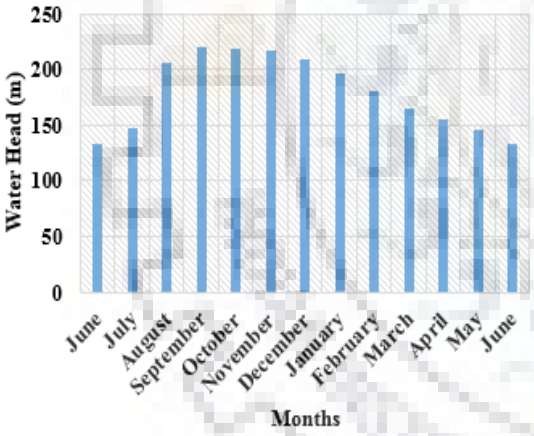

(a) Yearly water head variation (reproduced)

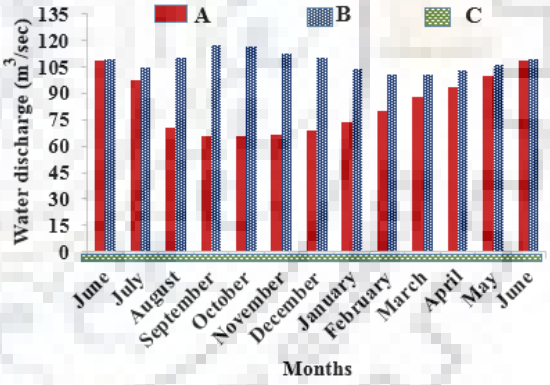

(b) Discharge at various water heads at 168 MW input power

A – With fault tolerant operation B – Normal operation C - Without power redundancy

Total energy storage year is 427.37 MU (Considering 6 hours/day)

Total energy storage considering fault tolerant operation is 420.92 MU

Total energy storage considering power redundancy problem is 410.71 MU

Benefit of fault tolerant operation = $\frac{420.92 - 410.71}{410.71}$ =2.49 %

Fig. 5.12. Fault tolerant operation of a 250 MW DFIM variable speed PSPP

5.3.2 Experimental Validation (2.2 kW DFIM)

Machine is instructed to operate at super synchronous speed of 1.1 p.u (1650 rpm) and shaft power is considered as 0.81 p.u (1800 W). Further, reactive power consumption is

considered as 0.05 p.u (110 VAR). The various faults are injected at pumping mode operation and discussions are given below.

5.3.2.1 RSC Single Switch Drive Open Circuit Fault in All Converters

The fault is injected at 190 s and results are shown in Fig. 5.13. the magnitude of rotor current in healthy legs reach to 2.5 p.u (Fig 5.13a) and stator phase currents reach to 3.2 p.u (Fig. 5.13b). The speed and reactive power of the machine is considerably affected.

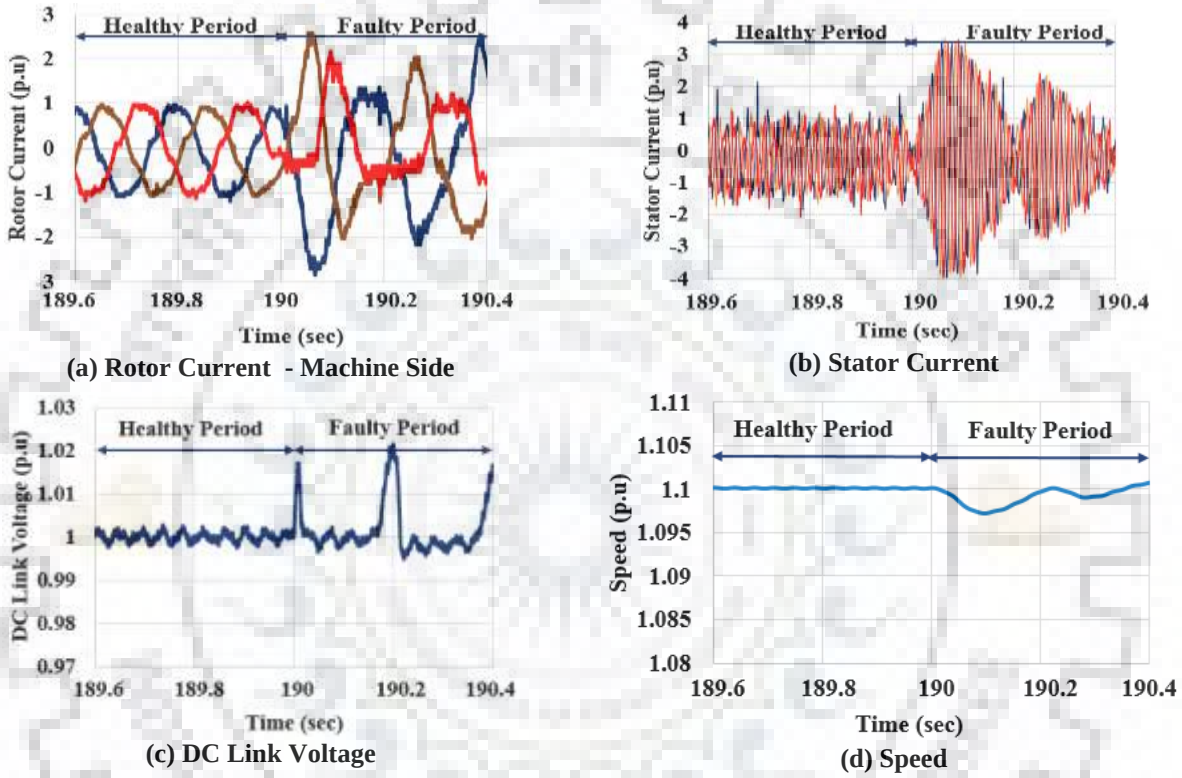

(a) Rotor Current - Machine Side

(b) Stator Current

(c) DC Link Voltage

(d) Speed

Fig. 5.13. RSC single switch open circuit fault (2.2 kW DFIM) at pumping

5.3.2.2 RSC Single Leg Open Circuit Fault in All Converters

The fault is injected at 190 s and results are shown in Fig. 5.14. The magnitude of rotor current in healthy legs reach to 2.75 p.u (Fig 5.14a) and stator phase currents reach to 4 p.u (Fig. 5.14b). Both current transients are repeatedly occurring two times per interval more than single device open circuit fault and speed of the machine is significantly affected. When comparing with simulation (250MW) results, rise/transients in current at stator and rotor circuits and speed are nearly similar to experimental machine. Further, survivability of the machine during open circuit power converter fault and control circuit fault is identified and is similar to the simulation

results. Short circuit faults are excluded during experimentation for the safety to the experimental set-up.

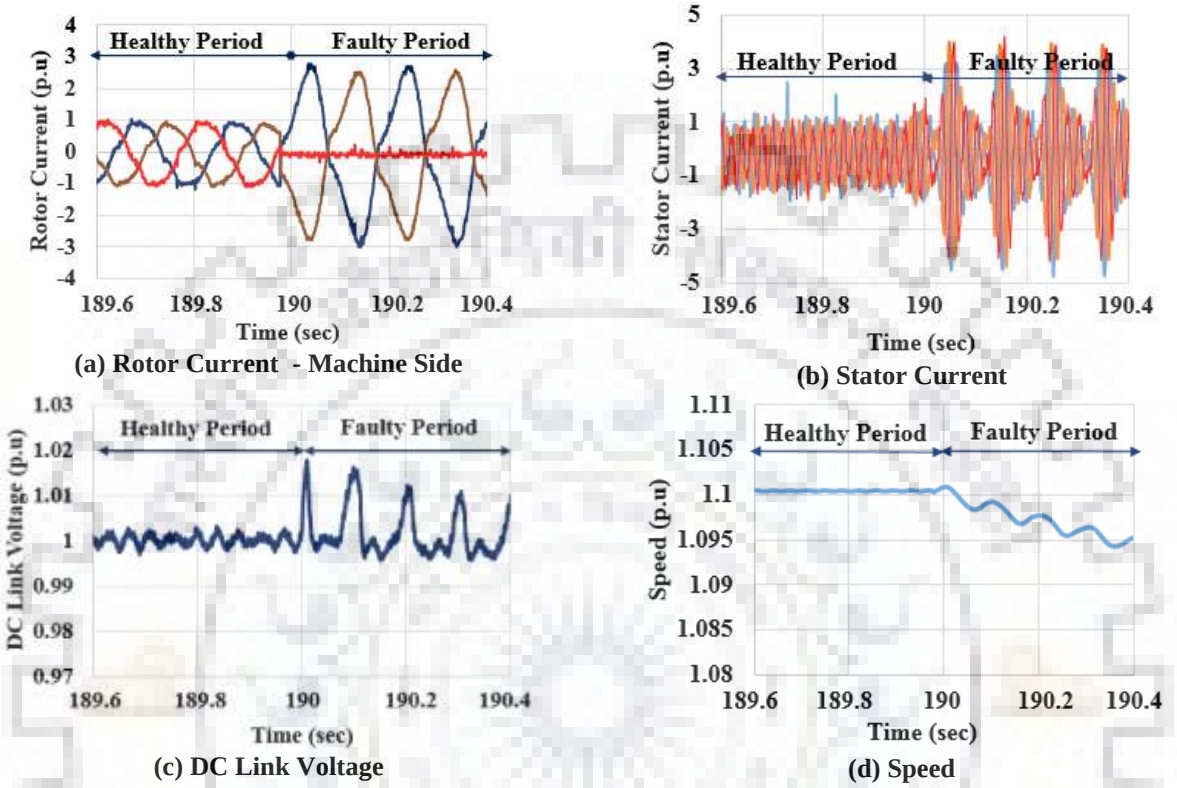

(a) Rotor Current - Machine Side

(b) Stator Current

(c) DC Link Voltage

(d) Speed

Fig. 5.14. RSC single leg open circuit fault (2.2 kW DFIM) at pumping

5.3.2.3 Encoder Omission Fault

The fault is injected at 160s and results are shown in Fig. 5.15. At encoder omission fault, frequency of the rotor current is gradually increased from 5Hz and saturates at 6.66 Hz (shown in Fig. 5.15a) as set by the control system. The speed of the machine gradually increases

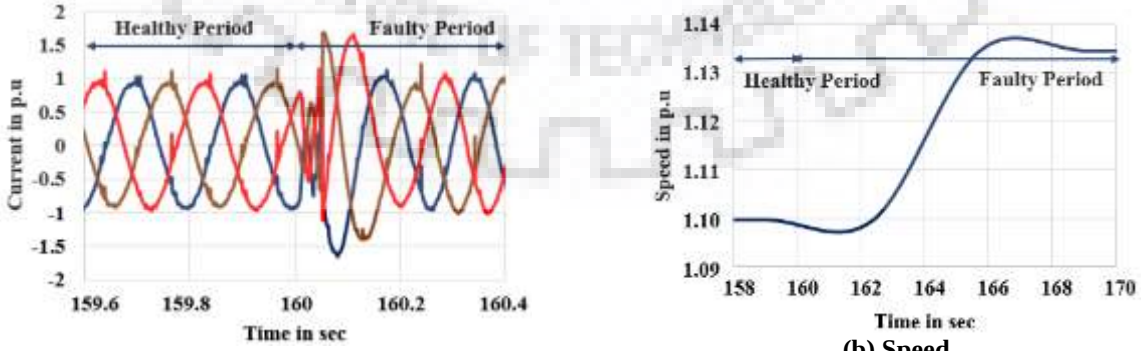

(a) Rotor Current- Machine Side

(b) Speed

Fig. 5.15. Encoder omission fault (2.2 kW DFIM) at pumping

from 1.1 p.u to 1.1325 p.u (shown in Fig.5.15b) and consumes power from the grid. Further, rotor voltage increases to 1.35 times of regular value.

5.4 Conclusion of the Chapter

This chapter has presented the dynamic performance of a 250MW hydrogenerating unit during pumping mode. Faults in power and control circuits were injected during the operation and the results were analyzed comprehensively. Survivability of machine drive was tested at each fault case. From the test results, it was observed that the drive survived during RSC single device/leg gate drive open circuit faults at sub-synchronous pumping mode, but not in super-synchronous mode. The drive survived during all kind of single current sensor faults, gain fault in reactive power signals at both sub and super synchronous speeds. In addition, a 1000MW plant shall undergo 66.61 MU/year energy storage losses due to inadequate redundancy in power and control circuits. Further, fault tolerant operation with reduced power delivery during converter open circuit fault brings additional storage of 2.49% electrical energy compared to the operation of DFIM without power redundancy operation.

This Page is Intentionally Left Blank

Chapter VI

Dynamic Performance of Condenser Mode of a Large Variable Speed PSPP

[This chapter presents the dynamic behavior of DFIM at variable speed condenser mode under normal and abnormal (faults in power and control circuit) operating conditions and persevere ability of the machine is also analyzed. Further, it present the condenser operation of variable speed doubly fed induction machine]

6.1 Introduction

Power factor of the grid system tends to drop when it is highly loaded. The solution to this problem requires the use of capacitive elements as a load to compensate for the power factor drop. Since the use of large capacitor banks is uneconomical, an alternative solution is to run the generator itself as a capacitive load by running it as a motor at no load condition, called as condenser mode of operation[195] - [198]. Hydro power plants are typically used in condenser mode of operation as compared to other power plants due to flexibility in its operation. In India, the electricity authority i.e. Central Electricity Authority, has made it mandatory to have condenser operation in 50 MW and above rated fixed speed hydro power plants [132]. Doubly fed induction machine (DFIM) is capable to operate as a condenser by varying flux in rotor windings through variable rotor voltage [199], [200]. However, DFIM is not made to operate at synchronous speed due to the challenges in machine stability and unequal power losses in rotor side power converters. Reactive power delivery is controlled by rotor side power converter (RSC) employing stator flux oriented vector control resulting in high dynamic performance of the DFIM.

6.2 DFIM Operation as Condenser Mode

The reliability and flexibility of pumped-hydropower condenser mode is exceptional. The time required during the transition of generation/pumping to condenser mode in a large rated DFIM unit plays an important role in power grid stable operation. Hydraulic diagram with the electrical circuit of a 250 MW variable speed hydro generating unit is given in chapter III of this paper (shown in Fig. 3.1). A flowchart indicating the transition of generation to condenser mode with timing diagram is shown in Fig.6.1. Water conductor system has three locations where valves/gate are located. At the intake, the gate is provided followed by a butterfly valve at

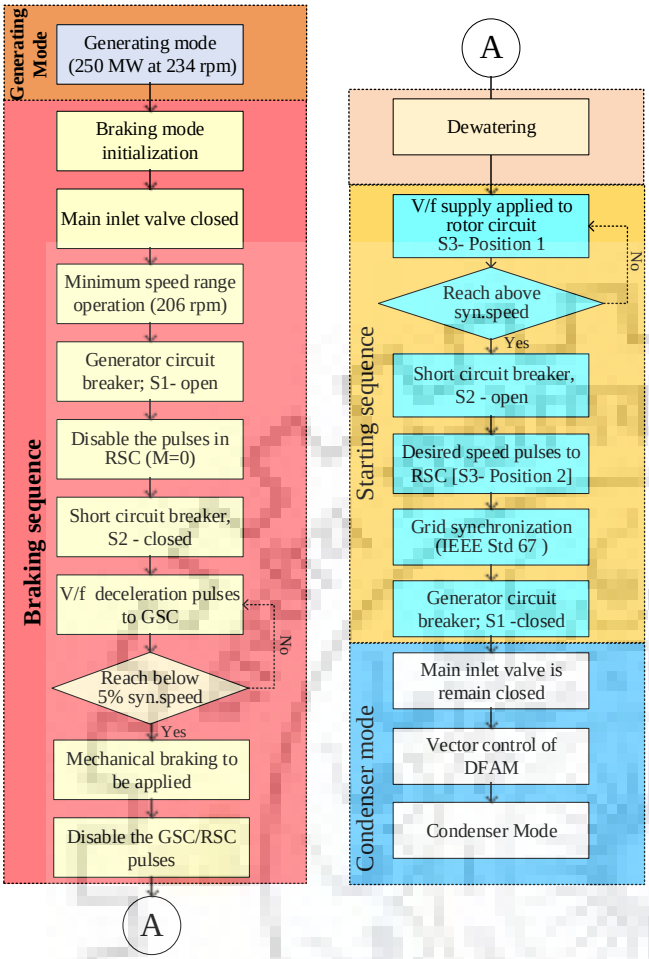

(a) Flowchart for transition of generation to condenser mode sequences

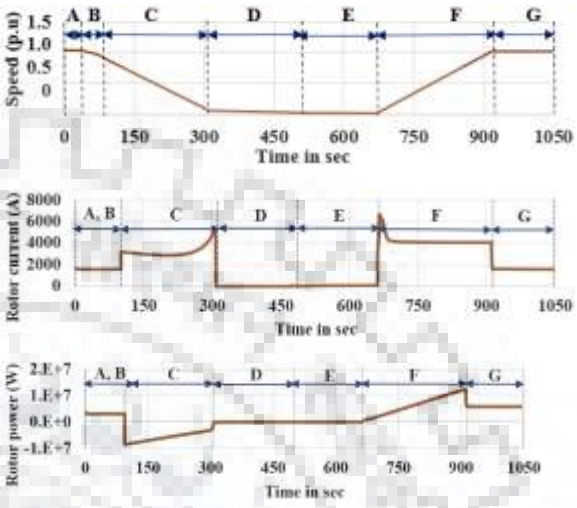

A - generation mode, B - minimum speed range at generation mode, C- regenerative braking mode, D - mechanical braking, E - Dewatering , F – smooth starting, G- condenser mode

(b) Timing diagram during mode changeovers

Fig.6.1 Transition of generation to condenser mode of a 250 MW DFIM unit

penstock. Right at the entry of spiral casing main inlet valve (MIV) is provided. All control and protection related sequences make use of MIV. Other valves are used to facilitate maintenance activities of water conductor system. From figures, it is inferred that the total time required to change over from generation to condenser mode is about 15 minutes for a 250 MW DFIM unit.

In DFIM the Stator circuit is directly connected to grid whereas the rotor which has three phase cylindrical winding is also connected to grid through power converter and excitation transformer. Controlling rotor supply via power converter of the machine results in adjusting the speed and reactive power delivery of the machine [201]. Analytical equations for real (P_s) and reactive power (Q_s) delivery are given below,

$$P_s = 3\frac{V_S}{Z^2}R_s + 3\frac{V_S V_R}{Z}\sin(\delta - \alpha) \qquad (6.1)$$

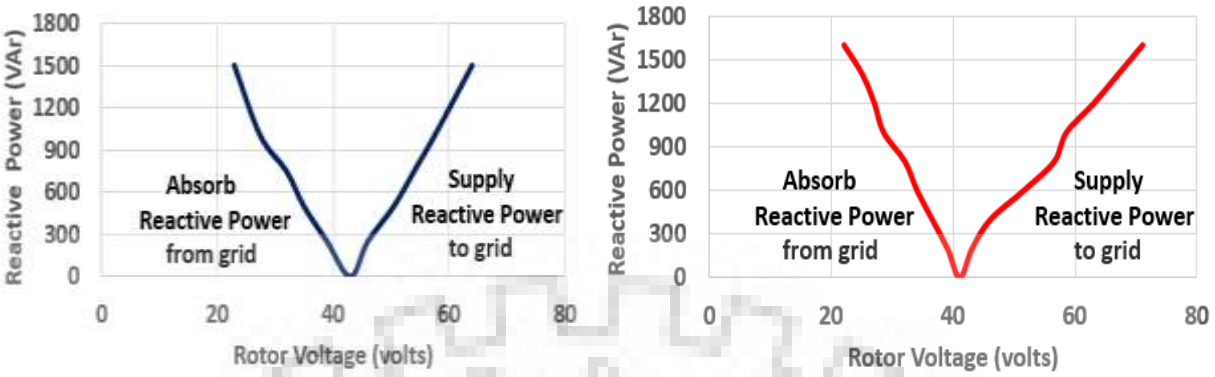

(a) Simulation Test **(b) Experimental Test**

Fig. 6.2 Reactive power transfer between grid and DFIM Vs Rotor Voltage (2.2 kW DFIM)

$$Q_s = 3\frac{V_S}{Z^2}X_s - 3\frac{V_S V_R}{Z}\cos(\delta-\alpha) \quad ; \qquad \alpha = 90-\theta \tag{6.2}$$

From Eqn.6.2, it is seen that stator reactive power depends on rotor side voltage. Increase in rotor voltage provides the negative value of the reactive power, which means the machine is supplying reactive power to the grid (called as condenser). Also, a decrease in rotor voltage results in positive reactive power, i.e. the machine is absorbing reactive power from the grid. Equations for stator current, rotor current and flux during condenser mode are given as below:

$$I_S = \frac{Q_{s\_ref}}{3V_s} + j\frac{\omega_s T_{e(no-load)}}{3pV_s}; \qquad \psi_s = \frac{|V_s|}{\omega_s} \tag{6.3}$$

$$\left.\begin{aligned} I_r &= \frac{V_s}{\omega_s}\cdot\frac{1}{L_m} - \frac{Q_{s\_ref}}{3V_s}\cdot\frac{L_s}{L_m} - j\frac{\omega_s T_{no-load}}{3pV_s}\cdot\frac{L_s}{L_m} \\ \psi_r &= \frac{V_s}{\omega_s}\cdot\frac{L_r}{L_m} - \frac{Q_{s\_ref}}{3V_s}\cdot\frac{\sigma L_s L_r}{L_m} - j\frac{\omega_s T_{no-load}}{3pV_s}\cdot\frac{\sigma L_s L_r}{L_m} \end{aligned}\right\} \tag{6.4}$$

$$I_s + I_r = \frac{V_s}{\omega_s}\frac{1}{L_m} \tag{6.5}$$

Eqns. between 6.3 and 6.5, implies that, (i) magnetization current is provided by only rotor circuit when Q_{s_ref} is zero, (ii) When, $Q_{s\_ref} \cong \frac{3V_s^2}{L_s\omega_s}$ magnetization current is provided by only stator circuit, and (iii) During condenser mode, amplitude of rotor flux linkage should be higher than stator flux linkage and hence maximum magnetization current is shared by rotor current.

Maximum reactive power support to the the grid during condenser mode depends on capability curve of the specific machine. In practice, hydrogenerating unit is operated at

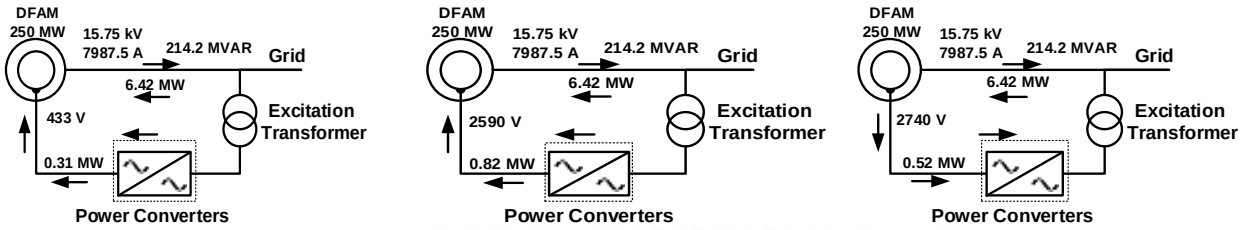

(a) nearby synchronous speed (234 rpm) **(b) super synchronous speed (250 rpm)** **(c) subsynchronous speed (210 rpm)**

Fig: 6.3. Power flow diagram of 250 MW DFIM delivering 0.7 p.u reactive power to grid

maximum of 0.8 p.u MVAR rating. Power transfer of a 250 MW DFIM (parameters given in Chapter II) operating at 0.7 p.u reactive power delivery to grid at different speeds are shown in Fig.6.3 as per MATLAB/ Simulink simulation. It is seen from the tests that real power consumption in stator side intended for respective reactive power support for different speeds are similar. However, real power transfer through rotor side changes with respect to the speed of the machine. In case of sub synchronous speed, the slip power through rotor is delivered to the grid. The voltage and frequency of rotor current are adjusted in accordance with the machine speed and the amount of reactive power delivery. The net active power consumed from the grid during condenser mode, is lesser in sub synchronous speed.

Vector control of 306 MVA DFIM is simulated in MATLAB/ Simulink environment. The DFIM is operated speed of 234 rpm near to synchronous speed, results are shown in Fig.6.4. Results show that the increase in rotor current (d-axis current) results in increase in d-axis component of stator current and consequently reactive power delivered to the grid.

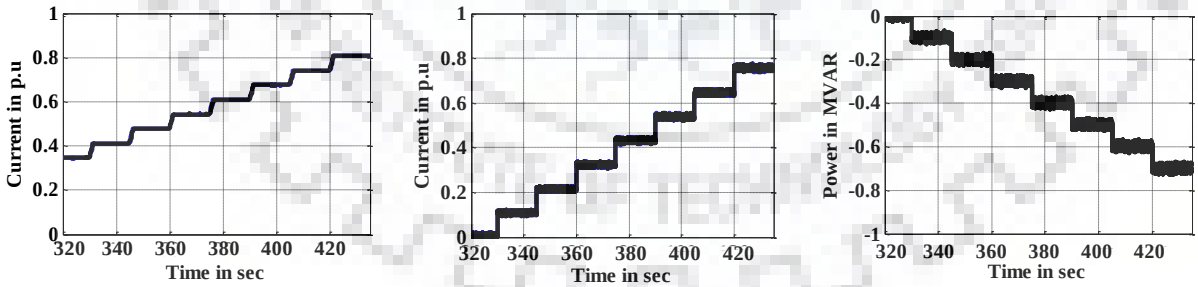

(a) **(b)** **(c)**

Fig.6.4. Reactive power delivery of a 250 MW DFIM (a) Rotor current (b) Stator current (c) Reactive power

6.3 Results and Discussions

DFIM is simulated to provide 0.6 p.u reactive power support to the grid at supersynchronous speed of operation (1.04 p.u). From the simulation results it is seen that: (i)

line current in stator winding is 7256A (0.645 p.u), (ii) phase to phase voltage applied to rotor winding by rotor side converter is 1385V (0.42 p.u), (iii) rotor winding line current is 10300A (0.891 p.u), (iv) frequency of rotor current at machine side is 2 Hz. Waveforms for selected faults are given with discussion and survivability of drive under each fault is summarized in Table 6.1.

6.3.1 Simulation Results (250 MW DFIM)

6.3.1.1 Power Converter Failure in a Single Converter

6.3.1.1.1 GSC Single Switch Open Circuit Fault

Single switch gate drive open circuit fault (upper switch) is injected in one of the parallel connected GSC at 410s and results are given in Fig. 6.5. During the fault, rotor current and dc link profiles are fluctuated as similar to the other modes of operation. However, magnitude of rotor current and dc link voltage variation is marginally varied as compare to other modes. From

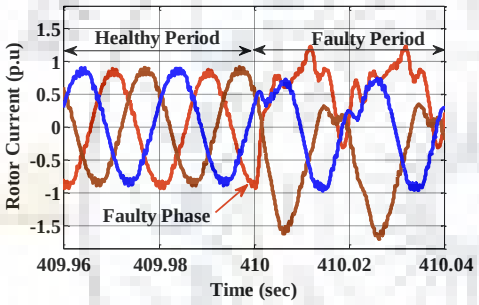

(a) Rotor Current (Grid Side) – Faulty Converter

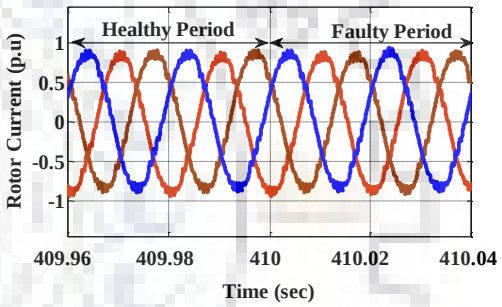

(b)Rotor Current (Grid Side) – Healthy Converter

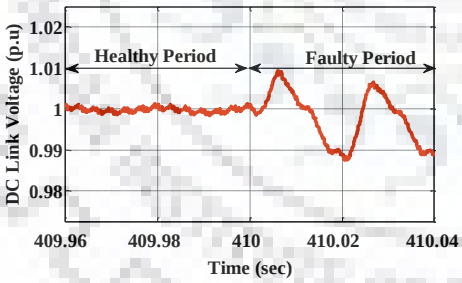

(c) DC Link Voltage – Faulty Converter

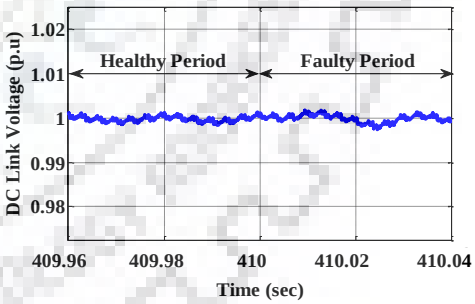

(d) DC Link Voltage- Healthy Converter

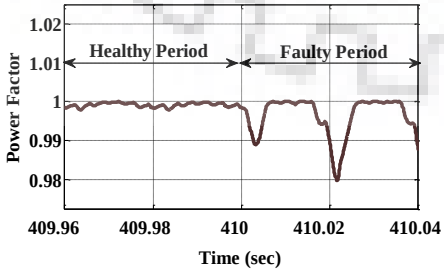

(e) Power Factor (Rotor Side)

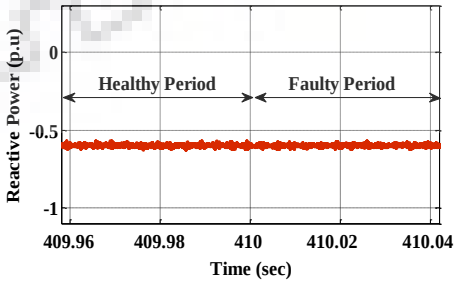

(f) Reactive Power (Stator Side)

Fig. 6.5. GSC upper single switch OCF (250 MW DFIM) at condenser

the results it is inferred that the reactive power delivery from the machine is not affected during the open circuit fault in grid side converters.

6.3.1.1.2 RSC Single Leg Open Circuit Fault

Single leg gate signal open switch fault is injected in one of the parallel connected RSC at 410s and results are given in Fig. 6.6. During the fault, the rotor current in one of the phase of faulty converter goes to zero (Fig. 6.6a) whereas the other two phases are carrying as equal currents. However, the same phase current in other parallel converters increases by 1.286 times of the regular value (Fig. 6.6b) to maintain required rotor phase current as like as other modes of operation. It is seen from the test results that the reactive power delivery (shown in Fig. 6.6e) from the machine is not affected as it is controlled by master control system.

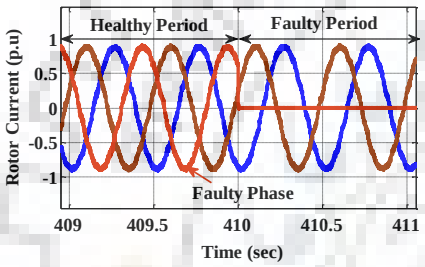

(a) Rotor Current (Machine Side) – Faulty Converter

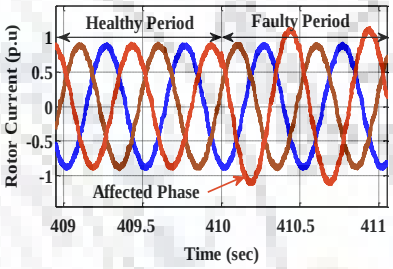

(b)Rotor Current (Machine Side) – Healthy Converter

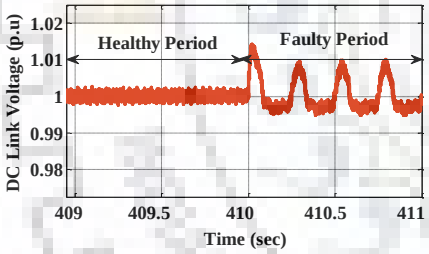

(c) DC Link Voltage – Faulty Converter

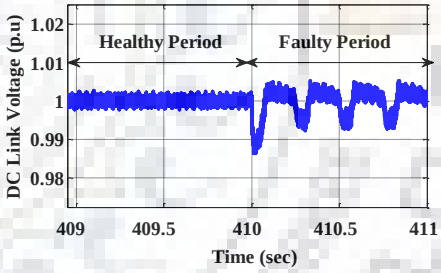

(d) DC Link Voltage- Healthy Converter

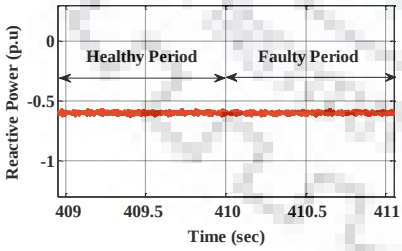

(e) Reactive Power

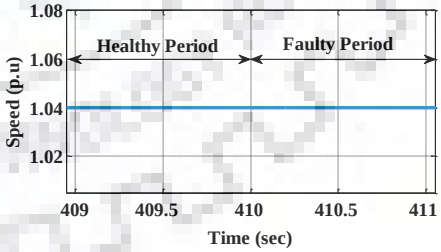

(f) Speed

Fig. 6.6. RSC single leg OCF (250 MW DFIM) at condenser

6.3.1.2 Power Converter Failure in All Channel (Five Converter)

Open and short circuit failures in all grid side converters are similar to the faults in any one of the parallel connected grid side converters. Nonetheless, variation in dc link voltage and

power factor (rotor side) is higher as compared to faults occur in only one converters. But, faults in rotor side converters are different form the single converter fault and it is discussed here.

6.3.1.2.1 RSC Single Switch Open Circuit Fault

The fault is undergone at 410 s and results are shown in Fig.6.7. During fault, negative half cycle of the single phase rotor current is omitted and other two phases are carrying the current. However, the stator current gets disturbed (reach about 3.2 p.u transient current) due to compensating the half cycle rotor current results to disturbance in the rotor current. Consequently, fluctuation is followed in speed of the machine results to disturbance in the real power consumption. Also, d-axis rotor current (Idr) is distorted results in disturbance to the reactive power (grid- stator side) support to the grid. In observation, both grid voltage oriented controllers and stator flux oriented controllers were disturbed. In general, single switch open

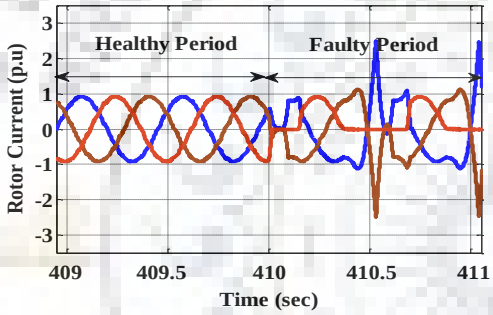

(a) Rotor Current (Machine side)

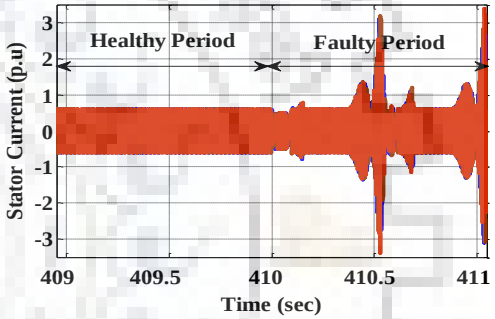

(b)Stator Current

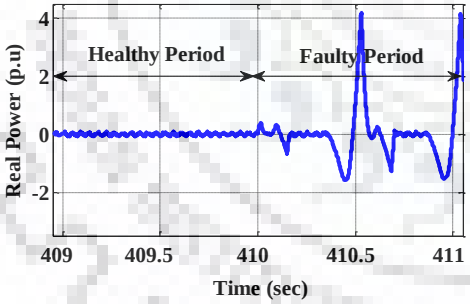

(c) Real Power - DFIM

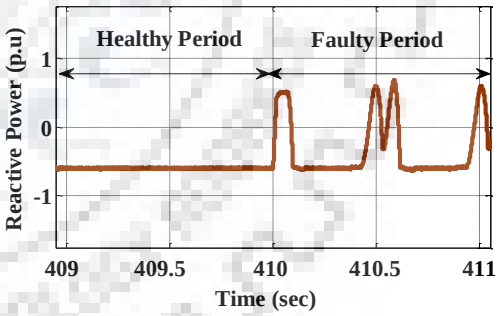

(d) Reactive Power - DFIM

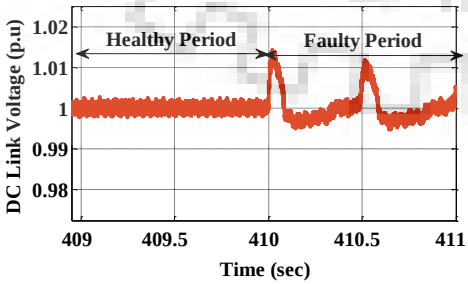

(e) DC Link Voltage

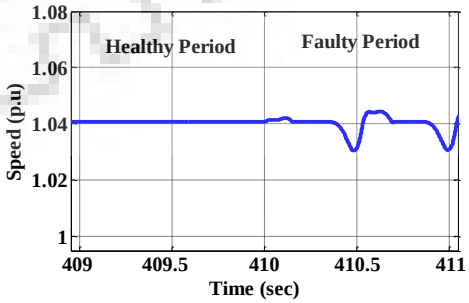

(f) Speed

Fig. 6.7. RSC single switch OCF (250 MW DFIM) at condenser

circuit fault in RSC is affecting the regular operation of the machine, also it leads to further faults in the power converter switches.

6.3.1.2.2 RSC Single Leg Open Circuit Fault

Single leg open circuit fault in RSC is undergone at 410s and results are shown in Fig. 6.8. During the fault, one of the phases connected to machine is carrying zero current, other two phases carrying current as higher than acceptable limit. Also the stator current is disturbed (reach about 3 p.u transient current) due to compensating the single phase current in the rotor results to more fluctuation in speed of the machine and rotor current (shown in Fig. 6.8a). Further, transients in rotor current is affects the dc link voltage and results to more fluctuation. In

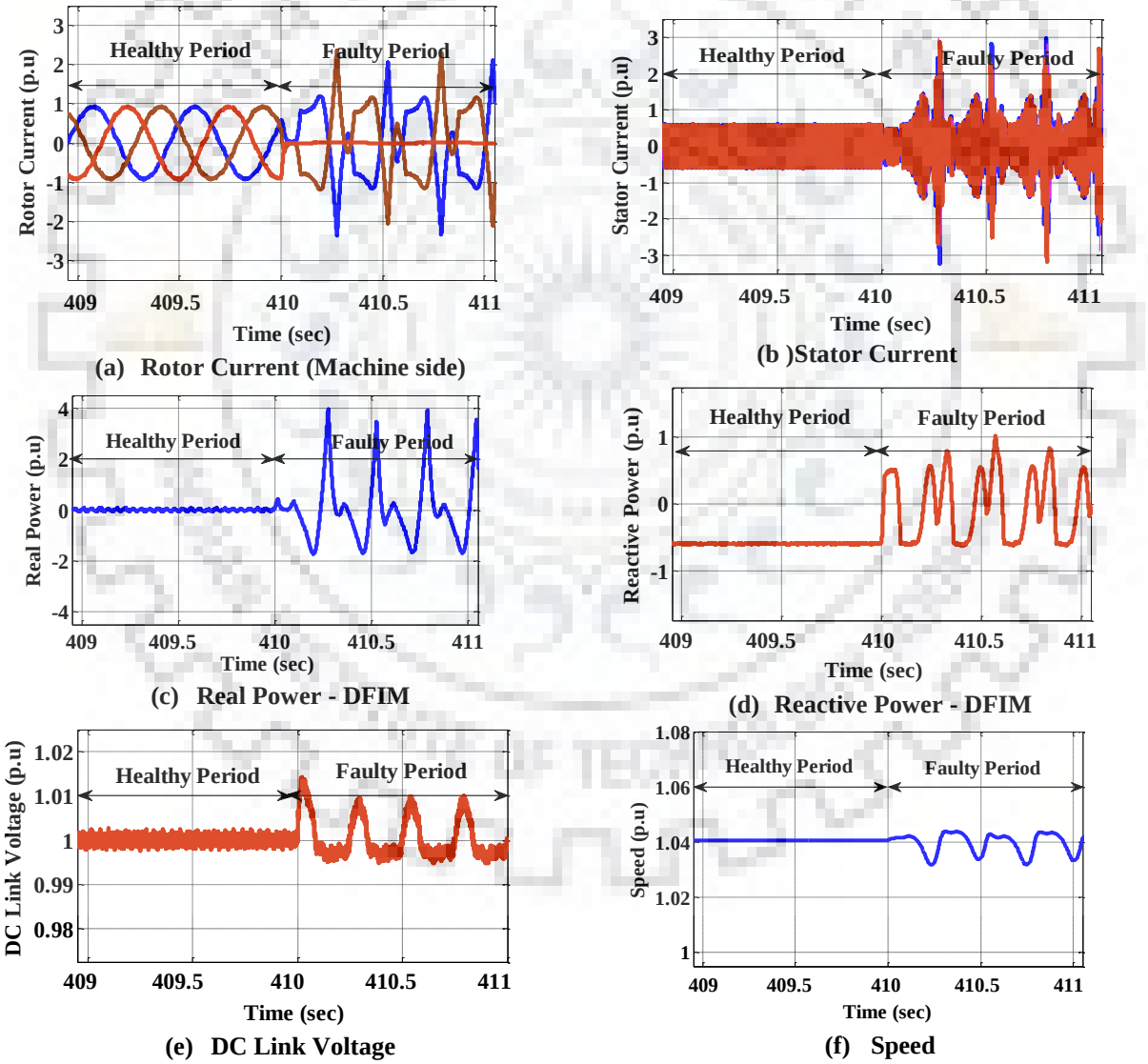

Fig. 6.8. RSC single leg OCF (250 MW DFIM) at condenser

observation, real power consumption and reactive power support to the grid gets disturbed. Also both grid voltage oriented and stator flux oriented controllers get distorted and out of control.

6.3.1.3 Control Circuit (Sensor) Failure

6.3.1.3.1 Reactive Power Signal Gain Fault

The reactive power signal gain fault is injected at 410s and the results are shown in Fig. 6.9. When the fault occurs, reactive power controller reads input as higher than the set value and decreases the proportional gain of the reactive power controller which decreases the d-axis rotor current, consequently, the reactive power delivery of the machine decreases (shown in Fig. 6.9d) until the set value is reached. It can be summarized from the test results that: (i) reactive power delivery of the machine decreases until the d-axis rotor current (Idr) reaches the set value, (ii)

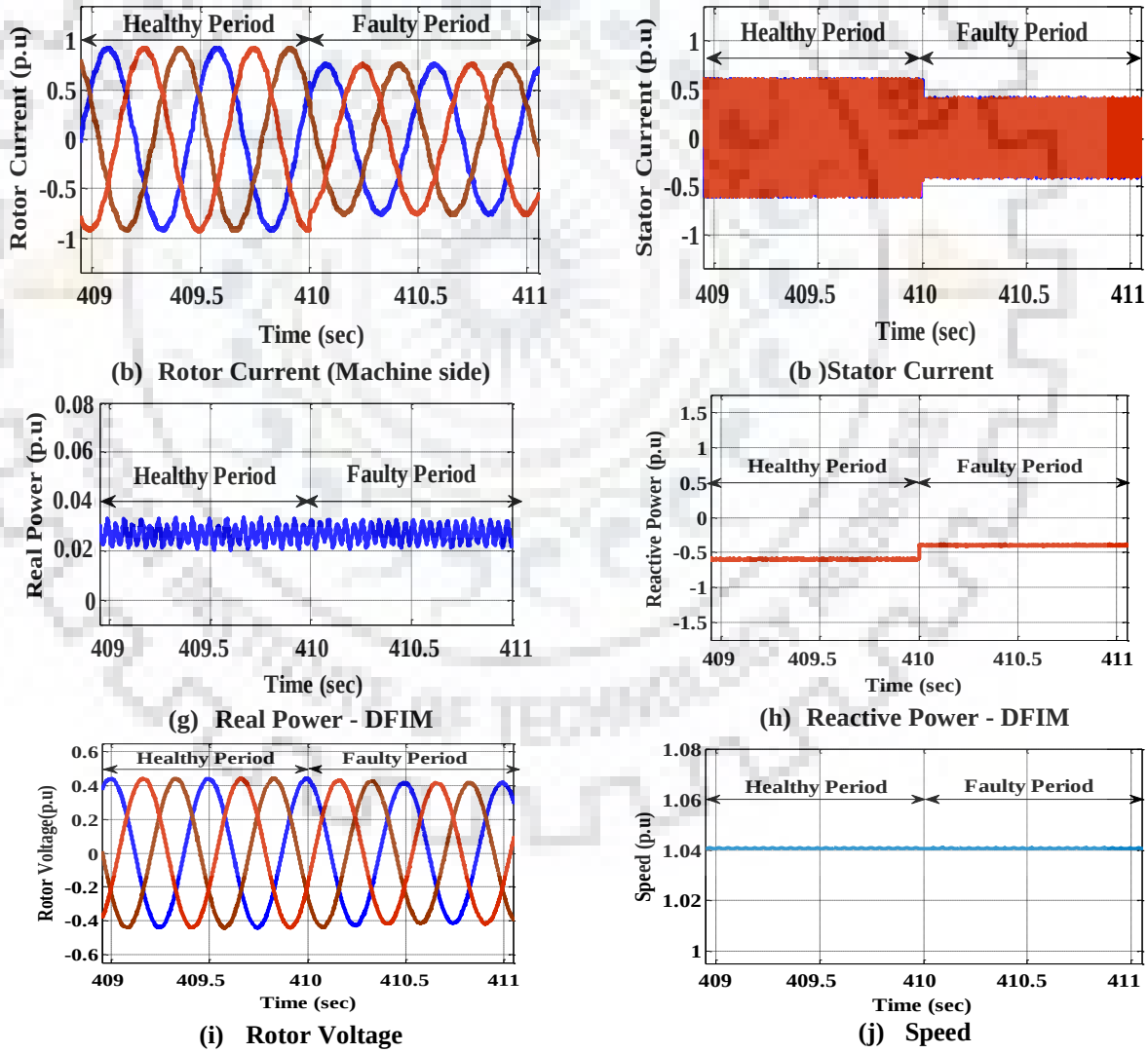

Fig. 6.9. Recative power signal gain fault (250 MW DFIM) at condenser

decrease in Idg (direct axis current - grid) to maintain the dc link voltage, (iii) speed and real power consumption of the machine during reactive power signal gain fault remains unchanged.

Table 6.1: DFIM drive status and economic analysis of converter and sensor failure at condenser mode [165], [166]

System	Mode of operation	Faults	Fault Status	No. of Failures/ year	250 MW DFIM					
					'U' Period/ year	Reactive power Losses* (MU)	Financial Losses**/ year (M$)	Status	Fault Tolerant Benefits (M$)
Power Converter	Sub synchronous	Rotor side converter	Open Circuit Fault (SDOC, SLOC)	S	1.9940	16.83	3.60	0.2	Yes	0.162
			Short Circuit Fault (SDSC,PPSC,PGSC)	F	0.6646	1.78	0.38	0.02	NA	-
		Grid side converter	Open Circuit Fault (SDOC, SLOC)	F	0.3025	1.25	0.27	0.015	Yes	0.012***
			Short Circuit Fault (SDSC,DCSC,PPSC,PGSC)	F	0.1008	0.41	0.09	0.005	NA	-
	Super synchronous	Rotor side converter	Open Circuit Fault (SDOC, SLOC)	F	1.9940	16.83	3.60	0.2	Yes	0.162***
			Short Circuit Fault (SDSC,PPSC,PGSC)	F	0.6646	1.78	0.38	0.02	NA	-
		Grid side converter	Open Circuit Fault (SDOC, SLOC)	S	0.3025	1.25	0.27	0.015	Yes	0.012
			Short Circuit Fault (SDSC,DCSC,PPSC,PGSC)	F	0.1008	0.41	0.09	0.005	NA	-

Table 6.1: DFIM drive status and economic analysis of sensor failure at condenser mode (contd.) [165], [166]

System	Mode of operation		Faults	Fault Status	No.of Failures/ year	250 MW DFIM				
						'U' Period/ year	Reactive power Losses* (MU)	Financial Losses**/ year (M$)	Fault Tolerant Status	Fault Tolerant Benefits (M$)
Control Circuit faults	Sub and super synchronous	Omission/ saturation	Speed sensor	F	0.247	0.82	0.18	0.01	NA	-
			DC link voltage sensor	F	0.247	0.57	0.12	0.005	NA	-
			Reactive power signal	F	0.247	0.57	0.12	0.005	NA	-
			Single rotor Current Sensor	S	0.247	0.57	0.12	0.005	Yes	0.005
			Single grid current sensor	S	0.247	0.57	0.12	0.005	Yes	0.005
			Single grid voltage sensor	F	0.247	0.57	0.12	0.005	NA	-
		Gain	Speed sensor	F	0.355	0.57	0.12	0.005	NA	-
			DC link voltage sensor	F	0.355	0.82	0.18	0.01	NA	-
			Reactive power signal	S	0.355	0.82	0.18	0.01	Yes	0.01
			Single rotor Current Sensor	S	0.355	0.82	0.18	0.01	Yes	0.01
			Single grid current sensor	F	0.355	0.82	0.18	0.01	NA	-
			Single grid voltage sensor	S	0.355	0.82	0.18	0.01	Yes	0.01

* Average real power delivery is 214 MVAr for a 250 MW DFIM ** Financial losses are considered as $ 0.055/kWh (half of the real power cost).

*** Fault tolerant proposed in this paper with reduced reactive power delivery (175 MVAr) U - unavailability

SDOC - single device open circuit fault SLOC - single leg open circuit fault SDSC - Single device short circuit DCSC - DC link short circuit

PPSC - Phase to phase SC PGSC - Phase to ground SC S - Survived F - Failed

6.3.1.4 Fault Tolerant Operation of RSC Open Switch Fault for a 250 MW DFIM

The maximum reactive power support to the grid is estimated as 214 MVAR considering rotor current and unit capability for a 306 MVA unit. The average reactive power support to the grid is considered as 2 hours/day. Open circuit fault in RSC during condenser mode affects the continuous operation of the unit. To continue the operation of the unit, fault tolerant or converter redundancy needs to be provided in the parallel converters. This section discusses a fault tolerant operation in condenser mode due to single converter open circuit fault. The technique applied is similar to the fault tolerant operation in generator/pumping mode modes.

It is planned to remove the PWM pulses to faulty converters (during open circuit and other faults except for short circuit fault in a whole leg) and operate the machine with other healthy converter with reduced reactive power support to the grid. DFIM is assigned to deliver the

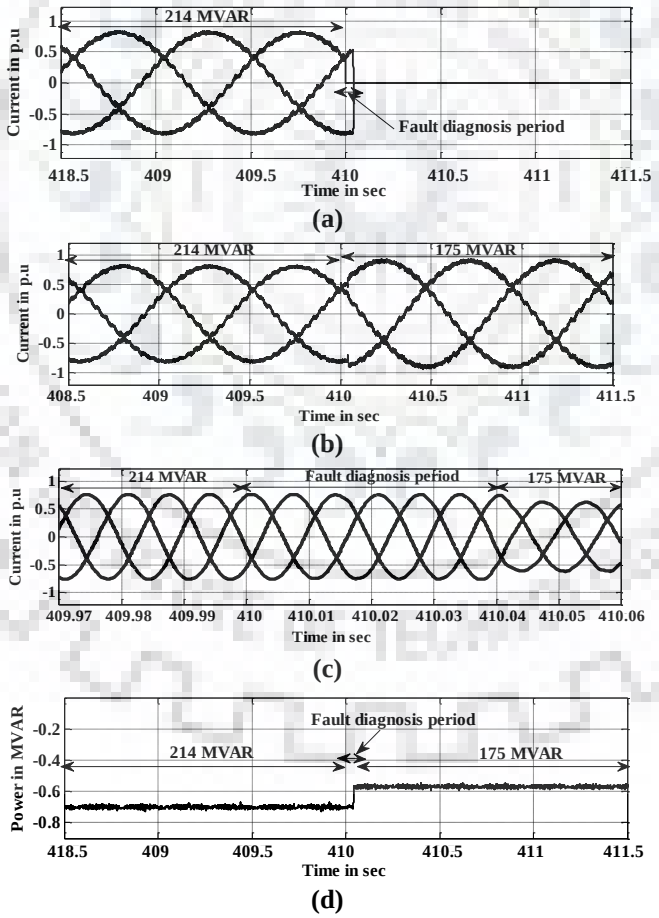

Fig 6.10. Fault tolerant operation of converter open circuit fault at condenser mode (a) Rotor current – faulty converter, (b) Rotor current –healthy converter, (c)) Stator current, (d) Reactive power

reactive power to the grid as 0.7 p.u (214 MVAR) at 1.014 p.u rpm (234 rpm) with the aid of three level back-to-back five parallel converter system. The stator and rotor circuits are carrying current as 0.755 p.u and 0.92 p.u respectively. Single leg gate drive open circuit fault is injected at any one of the parallel converter module at 410s and the fault is detected through rotor currents and dc link voltage variation as discussed in chapter IV. The corresponding faulty converter is isolated/inactivated from the parallel converter system through removing pulses (i.e. modulation index as zero) by the master controller as shown in Fig.6.10a. Subsequently, the master controller reduces the power delivery to 0.57 p.u (175 MVAR) which is adaptable with the remaining healthy converter current limit and the unit is in continuous operation. Stator current of the machine decreases to 0.615 p.u during the fault tolerant operation as shown in Fig. 6.10c. From the simulation results, it is inferred that the current in stator winding and rotor currents in healthy power converter are below the rated value and it is harmless for the continuous operation of the unit.

6.3.2 Experimental Validation (2.2 kW DFIM)

During the laboratory experiment, a 2.2 kW DFIM is operated to deliver 0.5 p.u (1100 kVar) of the reactive power to the grid at the speed of 1.04 p.u rpm (1560 rpm). Further, it consumes about 0.14 p.u (300 W) real power during the operation.

6.3.2.1 RSC Single Switch Drive Open Circuit Fault in All Converters

The fault is injected at 180 s and results are shown in Fig. 6.11. the magnitude of rotor current in healthy legs reach to 1.3 p.u (Fig 6.11a) and stator phase currents reach to 2.2 p.u (Fig. 6.11b). From the test results it is observed that the reactive power support to the grid and real

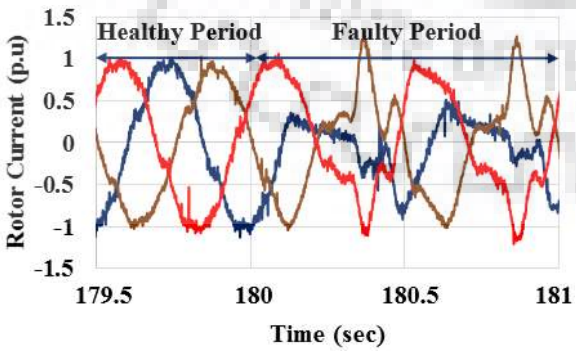

(a) Rotor Current - Machine Side

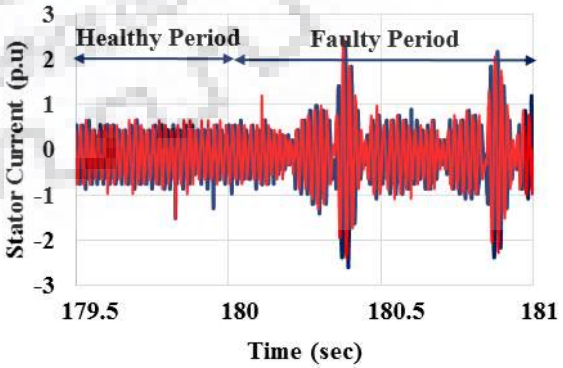

(b) Stator Current

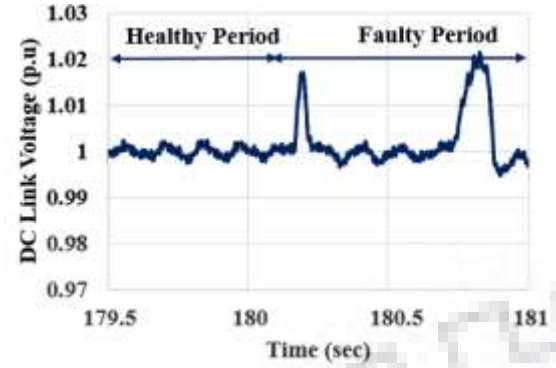

(c) DC Link Voltage

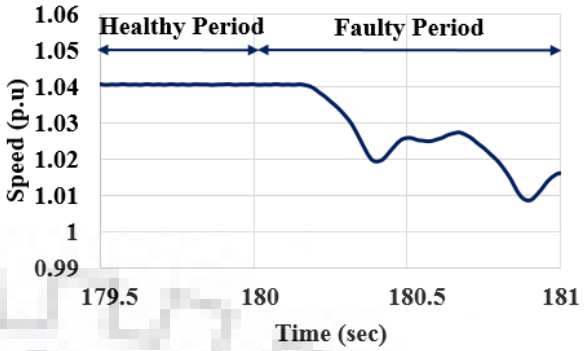

(d) Speed

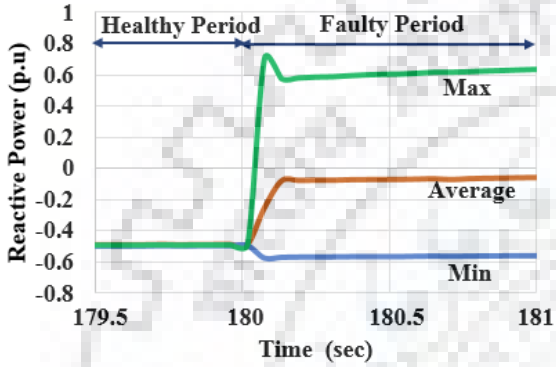

(e) Reactive Power – Machine Side

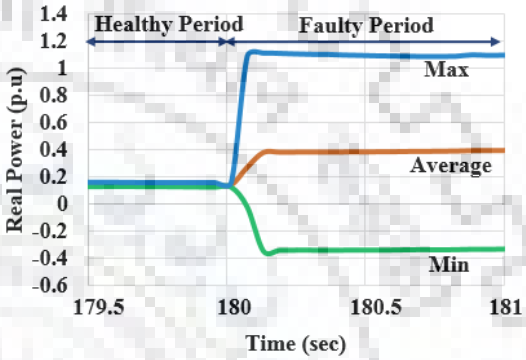

(f) Real Power

Fig. 6.11. RSC single switch open circuit fault (2.2 kW DFIM) at condenser

power is fluctuated as shown in fig. 6.11e and fig.6.11f. Further, speed of the machine and dc link voltage of the back-to-back power converter is considerably affected.

6.3.2.2 RSC Single Leg Open Circuit Fault in All Converters

The fault is injected at 180 s and results are shown in Fig. 6.12. The magnitude of rotor current in healthy legs reach to 1.1p.u (Fig 6.12a) and stator phase currents reach to 3.1 p.u (Fig.

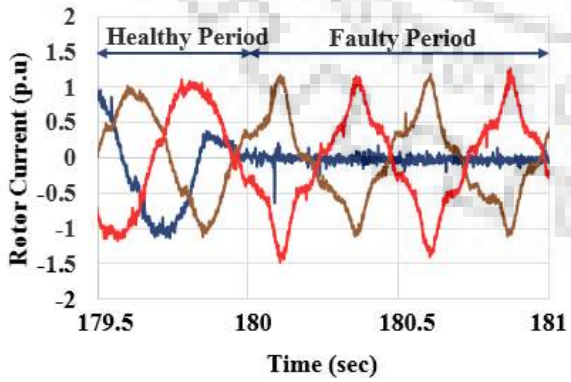

(a) Rotor Current - Machine Side

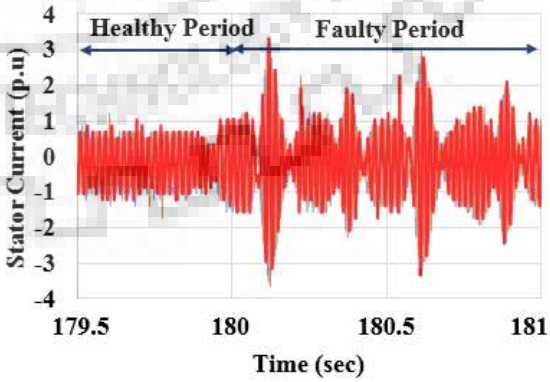

(b) Stator Current

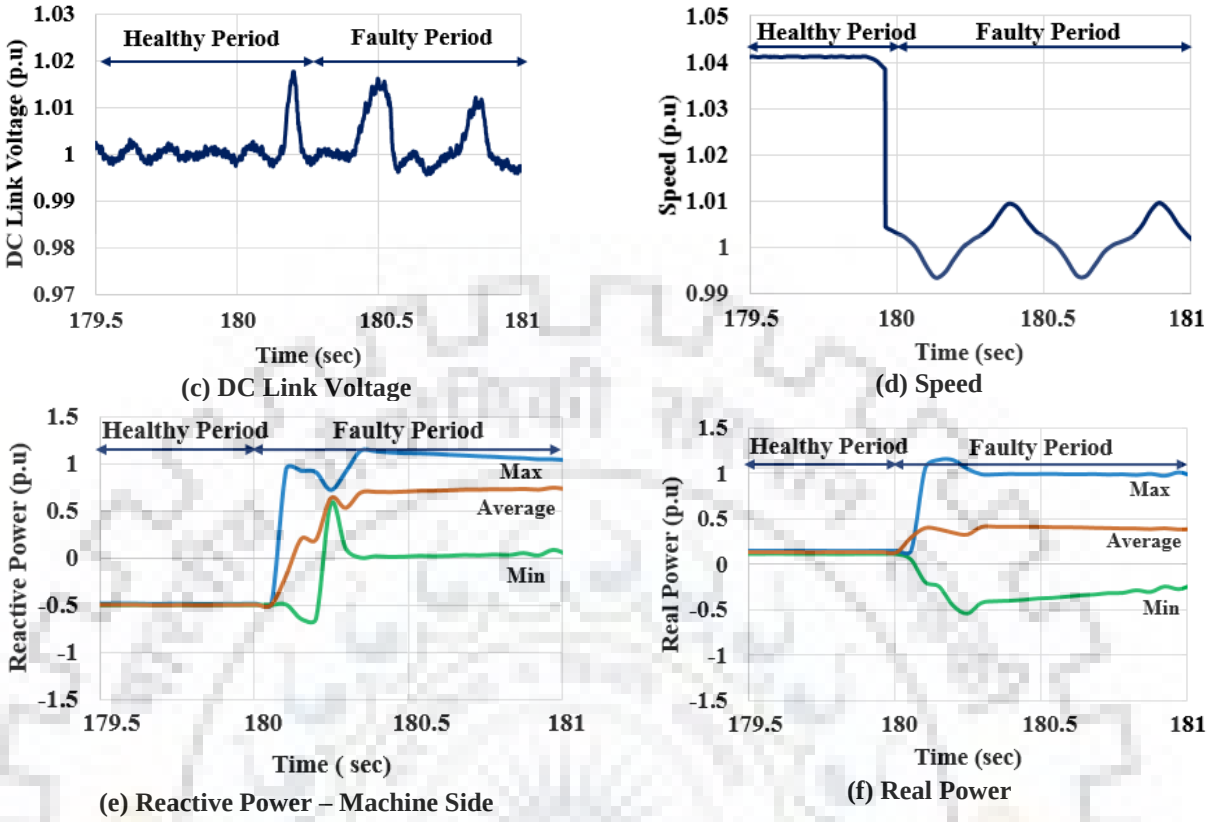

(c) DC Link Voltage (d) Speed

(e) Reactive Power – Machine Side (f) Real Power

Fig. 6.12. RSC single leg open circuit fault (2.2 kW DFIM) at condenser

6.12b). Reactive power and real power fluctuation is observed from Fig. 6.12e and Fig.6.12f respectively. It is noted that the fluctuation in parameters are two times more than the single device fault.

6.3.2.3 RSC Single Switch Open Circuit Fault in Single Converter

The fault is injected at 180 s and results are shown in Fig. 6.13. From the test results, current in healthy converter reaches to two times of its regular value (upper half cycle) as shown in

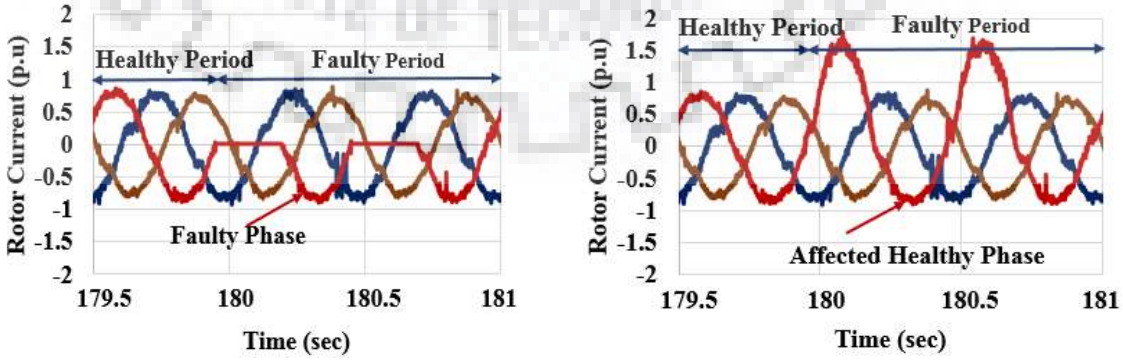

(a) Rotor Current - Faulty Converter (b) Rotor Current – Healthy Converter

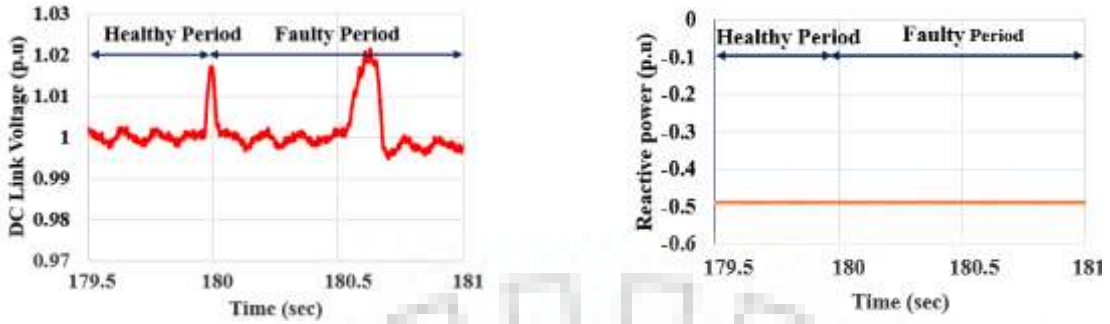

(c) DC Link Voltage **(d) Reactive Power (Machine Side)**

Fig. 6.13. RSC single switch open circuit fault (2.2 kW DFIM) at condenser

Fig. 6.13b since only two converters are connected in parallel. Based on experimental results, it is inferred that the rise or decrease in rotor current is similar to simulation results with the consideration of number of converters connected in parallel, turns ratio and inertia.

6.3.2.4 Fault Tolerant Operation of RSC Open Circuit Faults for a 2.2 kW DFIM

Single leg open circuit fault is injected at 180 s and the faulty converter is isolated from the system at 180.04 s (shown in Fig. 6.14a) with the aid of fault diagnosis techniques as discussed in chapter IV. It is noted that the acceptable reactive power delivery with the healthy converter is 0.28 p.u for a 2.2 kW DFIM. Therefore, the reactive power delivery of the machine is reduced to 0.28 p.u (shown in Fig. 6.14c) from 0.5 p.u by real time controller and stator current of the machine is reduced to 0.34 p.u (shown in Fig. 6.14d).

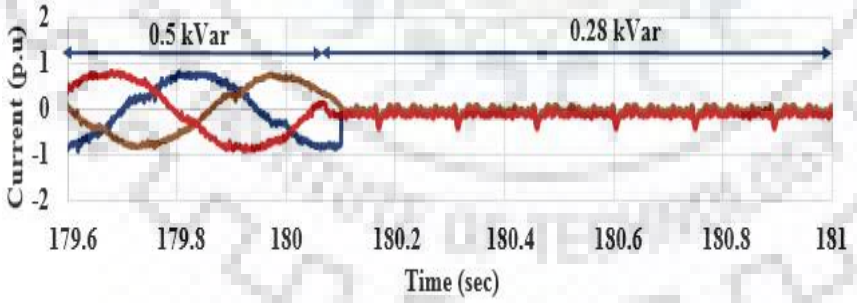

(a)

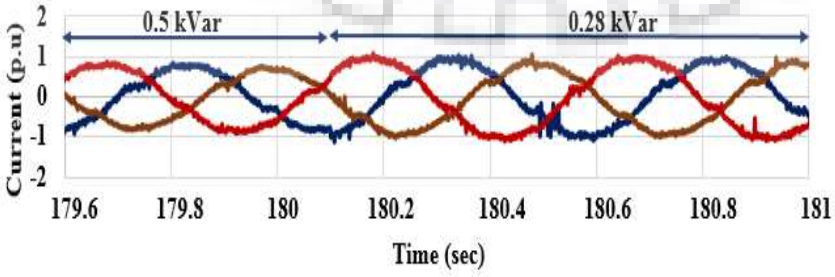

(b)

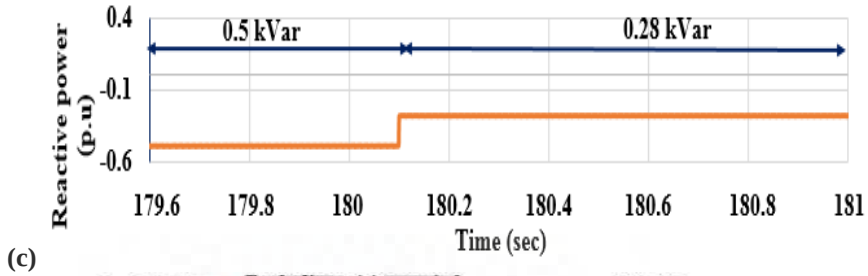

(c)

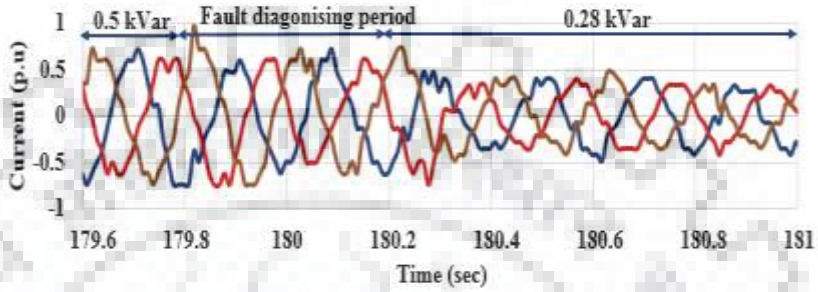

(d)

Fig 6.14. Fault tolerant operation of converter open circuit fault at Condenser mode for a 2.2 kW DFIM (a) Rotor current – faulty converter, (b) Rotor current –healthy converter, (c) Reactive power, (d) Stator current

6.4 Conclusion of the Chapter

This chapter has presented the dynamic performance of a 250 MW DFIM hydrogenerating unit operating in condenser mode. The converter power and control circuit faults were injected during the operation and the comprehensive analysis of the results were undertaken. Survivability of machine drive was tested at each fault case. It was observed from the test results, that the drive survived during single device/leg open circuit faults at sub-synchronous condenser mode, but failed during super-synchronous condenser mode. The drive survived during gain faults in encoder and reactive power signals at both sub and super synchronous speeds. In addition, fault tolerant operation during single converter open circuit fault is discussed and it provides a considerable amount of reactive power delivery to the grid, while the machine is in continuous operation with healthy converters.

This Page is Intentionally Left Blank

Chapter VII

Conclusion and Future Scope

[This chapter provides concluding remarks of present work with future research scopes of large rated variable speed hydrogenerating unit.]

7.1 Conclusion

This thesis has presented the advantages of variable speed PSPP over fixed speed PSPP in terms of power generation and energy storage in generation and pumping mode, respectively. It is reported that a 250 MW variable speed hydrogenerating unit shall be able to bring additional 6.1% power generation than fixed speed PSPP. Likewise, it shall bring more than 7.87 % energy storage in comparison with fixed speed PSPP at pumping mode. Further, comprehensive review in the area of variable speed pumped storage and the usage of power electronic converters were presented including converter topologies, modulation techniques, and power sharing schemes for parallel converters.

This thesis has also presented the dynamic performance of a 250MW hydrogenerating unit during generation, pumping and condenser modes of operation. Faults in power and control circuits were injected during the operation and the results were analyzed comprehensively. Survivability of machine drive was tested at each fault case. From the test results, it was observed that: (a) pumping mode: the drive survived during RSC single device/leg gate drive open circuit faults at sub-synchronous pumping mode, but not in super-synchronous mode, (b) generation mode: the drive survived during RSC single device/leg open circuit faults at super synchronous generation mode, but not in sub synchronous mode, (c) the drive survived during single device/leg open circuit faults at sub-synchronous condenser mode, but failed during super-synchronous condenser mode. In case of sensor faults, the drive survived during all kind of single current sensor faults, gain fault in reactive power signals at both sub and super synchronous speeds of operation. Further, the drive survived during gain faults in encoder at condenser mode of operation. A 2.2 kW DFIM is experimented at laboratory level to support the simulation results.

In addition, operational issues of parallel converter fed large rated asynchronous generators were pointed out with the help of simulation and experimental results. It is clearly mentioned that the power converter redundancy is not recommended in DFIM based variable speed PSPP due to: (i) possibilities of over voltage in rotor windings during the operation of

breakers/contactors in power converter redundant process, (ii) detection of dc component rotor current and dynamic variation of rotor frequency during converter short circuit fault. Therefore, the extra power potential of the DFIM fed variable speed PSPP is reduced to 1.7 % from 6.1% due to the inadequate power converter and control circuit redundancy. In a similar way, energy storage is reduced to 3.66% from 7.87 % in case of pumping mode. The economic analysis for all modes of operation has been analyzed in view of probability of operational state of a back-to-back power converter without redundancy per year is 96.10%.

The present research has proposed the fault tolerant operation (FTO) of DFIM during open circuit fault in RSC which is considered as higher probability of occurrence. It has provided fault tolerant operation in multichannel converter fed DFIM without the contactors connected in series with each channel. It is planned to be isolated the faulty converter (remove the PWM pulses to faulty converters (open circuit and other faults except short circuit fault in a whole leg)) and operate the machine with other healthy converters with reduced power delivery. It is noted that the acceptable power delivery at generation and pumping mode during FTO are identified as 190 MW and 168 MW, respectively, for a 250 MW unit in consideration of handling current capability of the healthy converters. In hydropower plant, reduction of power delivery from rated power to amendable power (reduced power delivery) has been taken about 20 to 30s. During the transition period, rotor current is limited with the help of reactive power control system to safeguard the healthy converters. The proposed fault tolerance method during single leg/single device fault has brought additional generation of 1.93 % electrical energy compared to the DFIM without power redundancy operation. In case of pumping mode, it brought an additional storage of 2.49% electrical energy.

7.2 Future Scopes

(i) The significant advantages of improved dynamic performance, unity power factor, reduction in THD are the main reasons that multi-level voltage source converters are applied in variable speed PSPP. However, inventions in power semiconductor devices, modulation schemes, and converter topologies will intensely influence the future growth of power electronics serving in large rated variable speed PSPP.

(ii) In view of operational issues in variable speed PSPP such as insufficient converter redundancy, lack of fault tolerant control, the following research opportunities are identified:

(a) Design and development of redundancy system in power and control circuits of large variable speed hydrogenerating equipments.

(b) Design of suitable control system for fault tolerant operation of back-to-back power converters fed DFIM in case redundancy could not be designed.

(iii) In case of sensor faults, the practice of secondary control system (v/f control) shall be instructed to coordinate with the primary control (vector control) to reduce the stoppage of hydrogenerating unit.

(iv) Design of two-stage protection circuit for multi-channeled power electronic converter fed large hydro generators to improve the fault ride-through capability and continuous operation of the plant.

(v) Analyse the dynamic performance of asynchronous generator in the presence of phase hardware in loop (PHIL) simulation tools.

This Page is Intentionally Left Blank

PUBLICATIONS FROM THE WORK

Patent

1. T. R. Chelliah, **Anto Joseph**, R. Raja Singh, Karthik Desingu, and Deepak Khare, "Energy Efficient Starting of Pump Turbine Equipped with Doubly Fed Induction Machine" submitted to IPR agencies through IIT Roorkee.

International Peer Reviewed Journals

1. **Anto Joseph** and T. R. Chelliah, "A Review of Power Electronic Converters for Variable Speed Pumped Storage Plants: Configurations, Operational Challenges and Future scopes"***, IEEE Journal of Emerging and Selected Topics in Power Electronics,*** vol. 6, no. 1, pp. 103-119, March 2018. (SCI Impact Factor: 4.269).
   URL: http://ieeexplore.ieee.org/stamp/stamp.jsp?tp=&arnumber=7932839&isnumber=8277196
2. **Anto Joseph**, K. Desingu, R.R. Semwal, T. R. Chelliah, and D. Khare "Dynamic Performance of Pumping Mode of 250 MW Variable Speed Hydro-Generating Unit Subjected to Power and Control Circuit Faults," ***IEEE Transactions on Energy Conversion***, vol. 33, no. 1, pp. 430-441, March 2018. (SCI Impact Factor : 3.808)
   URL: http://ieeexplore.ieee.org/stamp/stamp.jsp?tp=&arnumber=8010321&isnumber=8294002
3. **Anto Joseph**, Raghu Selvaraj, T. R. Chelliah, and Appa Sarma "Starting and Braking of a Large Variable Speed Hydro-Generating Unit Subjected to Converter and Sensor Faults," ***IEEE Transactions on Industry Applications***, Accepted (Early Access), DOI: 10.1109/TIA.2018.2816904. (SCI Impact Factor: 2.937)
   URL: https://ieeexplore.ieee.org/stamp/stamp.jsp?tp=&arnumber=8318704

International Conferences

1. **Anto Joseph**, and T. R. Chelliah, "Starting performance of Doubly Fed Induction Machine drive serving to pumped storage plants subjected to faults in power and control circuits," in Proc. ***IEEE 1st International Conference on Power Electronics, Intelligent Control and Energy Systems (ICPEICES)***, Delhi, July 2016.
2. **Anto Joseph**, and T. R. Chelliah, " Analysis of Doubly Fed Asynchronous Machine Based Variable Speed Pumped Storage Plants Subjected to Converter and Sensor Faults"

in Proc. ***19th Vienna Hydropower Conference***, Austria, ISBN 978-3-9504338-0-7, pp. 729-739, November 2016.

3. **Anto Joseph** and T. R. Chelliah, "Analysis of Doubly Fed Asynchronous Machine operating at condenser mode subjected to power converter faults," in Proc. ***IEEE International Conference on Power Electronics, Drives and Energy Systems (PEDES)***, Trivandrum, pp. 1-6, December 2016.
4. R.R. Semwal, **Anto Joseph**, and T. R. Chelliah, "Two-Stage Protection Circuit for Multi-Channeled Power Electronic Converter Fed Large Asynchronous Hydrogenerating Unit," in Proc. ***IEEE International Power Electronics Conference (IPEC)***, Niigata, Japan, Delhi, May 2018 (Presented).
5. Raghu Selvaraj, Karthik Desingu, **Anto Joseph**, and T. R. Chelliah, "Design Challenges on Redundancy in Power and Control Circuit of Large Variable Speed Hydro Generating Unit," ***International R&D Conclave on Emerging Opportunities and Challenges of R&D in Indian Power Sector***, Central Electricity Authority, Ministry of Power, Government of India, New Delhi, February 2018.

BIBLIOGRAPHY

[1] J.P. Deane, B.P. Gallachóir, and E.J. McKeogh, "Techno-economic review of existing and new pumped hydro energy storage plant," *J. Renew. Sustain. Energy Rev*, vol.14, no.4, pp. 1293-1302, May 2010.

[2] M. Swain, "Pumped storage hydropower plant," *Electrical India*, pp. 127-136, November 2013.

[3] R. Rajasingh, T.R. Chelliah, and P. Agarwal, "Power electronics in hydroelectric energy systems – A review," *J. Renew. Sustain. Energy Rev*, vol.32, pp. 944–959, April 2014.

[4] G.Cavazzini, and J. I. Pérez-Diaz, "Technological developments for pumped hydro energy storage," *European energy research alliance*, Tech. Rep, pp. 1-128, May 2014.

[5] N. Lefebvre, M. Tabarin, and O. Teller, "A solution to intermittent renewables using pumped hydropower," *Renew. Energy World Magazine*, pp. 1-6, May 2015.

[6] T. S. Kuwabara, A. Furuta, H. Kita, and E. Mitsuhashi, "Design and dynamic response characteristics of 400MW adjustable speed pumped storage unit for Ohkawachi power station," *IEEE Trans. Energy Convers*, vol. 11, no.2, pp. 376-384, June 1996.

[7] M. Harris, "Switzerland's 1000-MW Linthal pumped-storage plant connected to grid", *Hydro Review*, Zurich, pp. 1-4, January 2016.

[8] F. Barati, R. McMahon, S. Shao, E. Abdi and H. Oraee, "Generalized vector control for brushless doubly fed machines with nested loop rotor," *IEEE Trans. Ind. Electron*, vol. 60, no. 6, pp. 2477-2485, June 2013.

[9] S. Basak, and C. Chakraborty, "Dual stator winding induction machine: problems, progress, and future scope," *IEEE Trans. Ind. Electron*, vol. 62, no. 7, pp. 4641-4652, July 2015.

[10] R. Joseph, and L. Umanand, "A brushless wound rotor induction generator for variable speed micro hydel plants without ballast load," *IEEE Trans. Sustain. Energy*, vol. 6, no. 1, pp. 20-27, January 2015.

[11] A. Bocquel, and J. Janning, "Analysis of a 300MW variable speed drive for pump storage plant applications," in Proc. *14th Eur. Conf. Power Electron. Appl*., pp. 56-64, Dresden, September 2010.

[12] N. K. S. Naidu and B. Singh, "Experimental implementation of a doubly fed induction generator used for voltage regulation at a remote location," *IEEE Trans. Ind. Appl*, vol. 52, no. 6, pp. 5065-5072, Nov.-Dec. 2016.

[13] J.I. Pérez-Diaz, M.Chazarra, J.G. González, G. Cavazzini, and A.Stoppato, "Trends and challenges in the operation of pumped-storage hydropower plants," *J. Renew. Sustain Energy Rev*, vol.44, pp. 767-784, April 2015.

[14] R. Pena, J.C. Clare, and G. M. Asher, "Doubly fed induction generator using back-to-back PWM converters and its application to variable speed wind-energy generation," *IEEE Proc. Electric. Power Appl.*, vol. 143, no. 3, pp. 231- 241, May 1996.

[15] Balogun, O. Ojo, F. Okafor and S. Karugaba, "Determination of steady-state and dynamic control laws of doubly fed induction generator using natural and power variables," *IEEE Trans. Ind. Appl*, vol. 49, no. 3, pp. 1343-1357, May-June 2013.

[16] Bharat Singh and S.N Singh, "Development of grid connection requirements for wind power generators in India", *Renew. Sustain. Energy Rev*. Vol. 15, No. 3, pp. 1669-1674, April 2011.

[17] N. K. S. Naidu and B. Singh, "Grid-interfaced DFIG-based variable speed wind energy conversion system with power smoothening," *IEEE Trans. Sustain. Energy*. vol. 8, no. 1, pp. 51-58, Jan. 2017.

[18] Bharat Singh Rajpurohit, S.N Singh, Performance analysis of unified doubly-fed induction generator for wind power application," *Wind Engg. Journal*. Vol. 39, No. 5, pp.533-548, October 2015.

[19] J. K. Lung, Y. Lu, W.L. Hung, and W.S. Kao, "Modeling and dynamic simulations of doubly fed adjustable-speed pumped storage units," *IEEE Trans. Energy Convers*, vol. 22, no.2, pp. 250-258, June 2007.

[20] N. K. Swami Naidu and B. Singh, "Experimental implementation of doubly fed induction generator-based standalone wind energy conversion system," *IEEE Trans. Ind*. Appl, vol. 52, no. 4, pp. 3332-3339, July-Aug. 2016.

[21] M. Pronin, O. Shonin, A. Vorontsov, and G. Gogolev, "A pumped storage power plant with double-fed induction machine and cascaded frequency converter," in Proc.*14th Eur. Conf. Power Electron Appl*., pp.1-9, Birmingham, September 2011.

[22] I. Erlich, and U. Bachmann, "Dynamic behavior of variable speed pump storage units in the German electric power system," in Proc. *15th Triennial World Congress Conf*., pp. 1-6, Spain, July 2002.

[23] M. Nawaz, and K. Ilves, "On the comparative assessment of 1.7 kV, 300 A full SiC-MOSFET and Si-IGBT power modules," in Proc. *IEEE Applied Power Electron. Conf. and Exposition*, pp. 276 – 282, USA, May 2016.

[24] S. Linder, "High-power semiconductor devices, review and comparative assessment," *J. Russian Electrical Engg*., vol. 78, no. 10, pp. 509–514, October 2007.

[25] X. Yuan, J. Chai, and Y. Li, "A converter-based starting method and speed control of doubly fed induction machine with centrifugal loads," *IEEE Trans. Ind. Appl*., vol. 47, no. 3, pp. 1409- 1418, June 2011.

[26] J. Lanese, A. Powers, and H. Naeff, "Selection of large variable speed pumps for the Domenigoni valley reservoir project," in Proc. *Intl. Conf. Hydropower*, vol. 2, pp. 1902-1912, USA, 1995.

[27] J.J. Simond, A. Sapin, M. T. Xuan, R. Wetter, and P.Burmeister, "12-pulse LCI synchronous drive for a 20MW compressor – modelling, simulation and measurements," In Proc. *IEEE Conf. Ind. Appl.*, vol. 4, pp. 2302-2308, Hong Kong, October 2005.

[28] Sangshin Kwak and H. A. Toliyat, "A hybrid solution for load-commutated-inverter-fed induction motor drives," *IEEE Trans. Ind. Appl*, vol. 41, no. 1, pp. 83-90, Jan.-Feb. 2005.

[29] S. Bal, A. K. Rathore, and D. Srinivasan, "Naturally commutated current-fed three-phase bidirectional soft-switching dc-dc converter with 120o modulation technique," *IEEE Trans. Ind. Appl*, vol 52, no 5, pp 4354-4364, Oct 2016.

[30] G. K. Kulothungan, A. Edpuganti*, A. K. Rathore, and D. Srinivasan, "Current-fed multilevel converters: an overview of circuit topologies, modulation techniques, and application," *IEEE Trans. Power Electron*., vol.32, no. 5, pp. 3382-3401, May 2017.

[31] S. Mondal, and D. Kastha, "Improved direct torque and reactive power control of a matrix converter fed grid connected doubly fed induction generator," *IEEE Trans. Ind. Electron*., vol. 62, no. 12, pp. 7590-7598, December 2015.

[32] R. Cardenas, R. Pena, G. Tobar, J. Clare, P. Wheeler, and G. Asher, "Stability analysis of a wind energy conversion system based on a doubly fed induction generator fed by a matrix converter," *IEEE Trans. Ind. Electron*., vol. 56, no. 10, pp. 4194-4206, October 2009.

[33] M. A. Cruz, and M. Ferreira, "Comparison between back-to-back and matrix converter drives under faulty conditions," in proc. *IEEE 13th Eur. Conf. Power Electron. Appl*., pp. 1-10, Barcelona, October 2009.

[34] O. Ojo and I. E. Davidson, "PWM-VSI inverter-assisted stand-alone dual stator winding induction generator," *IEEE Trans. Ind. Appl*, vol. 36, no. 6, pp. 1604-1611, Nov/Dec 2000.

[35] T. Friedli, J. Kolar, J. Rodriguez, and W. Patrick, "Comparative evaluation of three-phase AC-AC matrix converter and voltage dc-link back-to-back converter systems," *IEEE Trans. Ind. Electron*., vol. 59, no.12, pp. 4487-4510, December 2012.

[36] B.Wu, J. Pontt, J. Rodríguez, S. Bernet, and S. Kouro, "Current-source converter and cycloconverter topologies for industrial medium-voltage drives," *IEEE Trans. Ind. Electron*., vol. 55, no. 7, pp. 2786 – 2797, July 2008.

[37] Y. K. Pannatier, B. Nicolet, C. Simond, J.J. Schwery, and A. Allenbach, "Investigation of control strategies for variable speed pump turbine units by using a simplified model of the converters," *IEEE Trans. Ind. Electron*., vol. 57, no.9, pp. 3039-3049, September 2010.

[38] H. Stemmler, and A. Omlin, "Converter controlled fixed frequency variable speed motor/generator," in Proc. *IEEE Intl. Conf. Power Eng*., pp.1-6, vol.1, Japan, February 1995.

[39] H. Abu-Rub, J. Guzinski, Z. Krzeminski and H. A. Toliyat, "Predictive current control of voltage-source inverters," *IEEE Trans. Ind. Electron*., vol. 51, no. 3, pp. 585-593, June 2004.

[40] G. Dong and O. Ojo, "Current regulation in four-leg voltage-source converters," *IEEE Trans. Ind. Electron*, vol. 54, no. 4, pp. 2095-2105, Aug. 2007.

[41] K. Basu, J. S. S. Prasad and G. Narayanan, "Minimization of Torque Ripple in PWM AC Drives," *IEEE Trans. Ind. Electron*, vol. 56, no. 2, pp. 553-558, Feb. 2009.

[42] Sangshin Kwak and H. A. Toliyat, "Design and performance comparisons of two multi-drive systems with unity power factor," *IEEE Trans. Power Deliv*ery., vol. 20, no. 1, pp. 417-426, Jan. 2005.

[43] Anzalchi, A. Sarwat, and A. K. Rathore, "A new topology of higher order power filter for single-phase grid-tied voltage source inverters," *IEEE Trans. Ind. Electron*., vol 63, no 12, pp. 7511-7522, Dec 2016.

[44] E. Levi, R. Bojoi, F. Profumo, H. A. Toliyat and S. Williamson, "Multiphase induction motor drives - a technology status review," *IET Electric Power Appl*, vol. 1, no. 4, pp. 489-516, July 2007.

[45] N. K. Swami Naidu and B. Singh, "Doubly fed induction generator for wind energy conversion systems with integrated active filter capabilities," *IEEE Trans. Ind. Inform*., vol. 11, no. 4, pp. 923-933, Aug. 2015.

[46] Sangshin Kwak and H. A. Toliyat, "A hybrid converter system for high-performance large induction motor drives," *IEEE Trans. Ener. Convers*. vol. 20, no. 3, pp. 504-511, Sept. 2005.

[47] S Khomfoi, and L. Tolbert, "Power electronics handbook", 2nd ed., *Academic Press, USA*, 2007.

[48] E Ghiani, S Mocci, G Celli, and F Pilo, "Increasing the flexible use of hydro pumping storage for maximizing the exploitation of RES in Sardinia," in proc. *IEEE 3rd Renew. Power Gen. Conf*., pp.1-6, Naples, September 2014.

[49] J. Koutnik, "Frades II - variable speed pumped storage project and its benefit to the electrical grid," in Proc. *Intl. Conf. Renew. Energy*, pp.1-7, Orlando, January 2012.

[50] A. Sapin, A. Hodder, J.J. Simond, and D. Schafer, "Doubly fed asynchronous machine with 3-level VSI for variable speed pump storage," in Proc. *Intl. Conf. Elect. Machines*, pp.1-6, Finland, August 2000.

[51] K. Krüger, and J. Koutnik, "Dynamic simulation of pump-storage power plants with different variable speed configurations using the Simsen tool," In proc. *Intl J. Fluid Machinery and Sys*., vol. 2, no. 4, pp. 334- 345, December 2009.

[52] E. E. Schmidt, J. Preiss, A. Zensch, R. Schurhuber, and R., J. Hell, “Simulation of steady-state and transient operational behavior of variable-speed motor-generators of hydro power plants,” in Proc. *IEEE Intl. Conf. Elect. Machines & Drives*, pp. 607-611, Canada, May 2011.

[53] R. K. Behera, S. P. Das and O. Ojo, "Utility friendly three-level neutral point clamped converter-fed high-performance induction motor drive," *IET Power Electron*., vol. 5, no. 7, pp. 1196-1203, August 2012

[54] G. K. Kulothungan, A. Edpuganti*, A. K. Rathore, D. Srinivasan, C. Cecati,and C. Buccella, “Optimal low switching frequency pulse width modulation of current-fed three-level converter for solar power integration,” *IEEE Trans. Ind. Electron*., vol. 63, no. 11, Nov 2016, pp. 6877-6886.

[55] J. Rodriguez, J.S. Lai, Z. Fang, and Peng, “Multilevel inverters: a survey of topologies, controls and applications,” *IEEE Trans. Ind. Electron*., vol. 49, no 4, pp. 724-738, August 2002.

[56] TA. Meynard, and H. Foch, “Multi-level conversion: high voltage choppers and voltage-source inverters,” in Proc. *IEEE Conf. Power Electron. Specialist*, pp. 21-26, Spain, 1992.

[57] D. Krug, S. Bernet, and S. Saeed Fazel, “Comparison of 2.3-kV medium-voltage multilevel converters for industrial medium-voltage drives,” *IEEE Trans. Ind. Electron*., vol. 54, no. 6,pp. 2979- 2992, December 2007.

[58] F. Wang, and J. Jiang, “A novel static frequency converter based on multilevel cascaded H-bridge used for the startup of synchronous motor in pumped-storage power station,” *J. Energy Convers Manage*, vol. 52, pp.2085-2091, May 2011.

[59] L. Xu, and VG. Agelidis, “Active capacitor voltage control of flying capacitor multilevel converter,” in Proc. *IEEE Electric Power Appl*., vol.151, no.3, pp. 1179–1184, May 2004.

[60] Edpuganti and A. K. Rathore, “A Survey of low switching frequency modulation techniques for medium-voltage multilevel converters," *IEEE Trans. Ind. Appl*., vol. 51, no. 5, pp.4212-4228, Sept 2015.

[61] Radha Thangaraj, Millie Pant, Pascal Bouvry and Ajith Abraham, “Solving stochastic programming problems using modified differential evolution algorithms”, *The Logic Journal, Oxford University Press*, UK, 20(4):732-746, August 2012.

[62] A. Rajasekhar, R. K. Jatoth, A. Abraham and V. Snasel, "A novel hybrid ABF-PSO algorithm based tuning of optimal FOPI speed controller for PMSM drive," in Proc. *IEEE Conf. 12th Intl. Carpathian Control Conference (ICCC)*, Velke Karlovice, pp. 320-325, 2011.

[63] J. I. Leon, S. Kouro, G. Leopoldo, G. Franquelo, J. Rodriguez, and B. Wu, “The essential role and the continuous evolution of modulation techniques for voltage-source inverters in the past, present, and future power electronics,” *IEEE Trans. Ind. Electron.* vol. 63, no. 5, pp.2688- 2701, May 2016.

[64] C. Binoj Kumar, B. Saritha and G. Narayanan, "Experimental Comparison of Conventional and Bus-Clamping PWM Methods Based on Electrical and Acoustic Noise Spectra of Induction Motor Drives," in *IEEE Trans. Ind. Appl*, vol. 52, no. 5, pp. 4061-4073, Sept.-Oct. 2016.

[65] V. S. S. Pavan Kumar Hari and G. Narayanan, "Theoretical and experimental evaluation of pulsating torque produced by induction motor drives controlled with advanced bus-clamping pulse width modulation, "*IEEE Trans. Ind. Electron*., vol. 63, no. 3, pp. 1404-1413, March 2016.

[66] S. Madishetti, B. Singh and G. Bhuvaneswari, "Three-level NPC-inverter-based SVM-VCIMD with feed forward active PFC rectifier for enhanced ac mains power quality," *IEEE Trans. Ind. Appl*., vol. 52, no. 2, pp. 1865-1873, March-April 2016.

[67] C. B. Kumar and G. Narayanan, "Variable-switching frequency pwm technique for induction motor drive to spread acoustic noise spectrum with reduced current ripple," *IEEE Trans. Ind. Appl*, vol. 52, no. 5, pp. 3927-3938, Sept.-Oct. 2016.

[68] P. Xuewei, A. K. Rathore, and U. R. Prasanna, "Novel soft-switching snubber less naturally clamped current-fed full-bridge front-end converter based bidirectional inverter for renewables, microgrid and ups applications," *IEEE Trans. Ind. Appl*, Vol. 50, no. 6, pp. 4132-4141, Dec 2014.

[69] P. R. Rakesh and G. Narayanan, "Analysis of sine-triangle and zero-sequence injection modulation schemes for split-phase induction motor drive," *IET Power Electron*., vol. 9, no. 2, pp. 344-355, 2 10 2016.

[70] TH. Abdelhamid, and KM. El-Naggar, "Optimal PWM control of a new generalized family of multilevel inverters," *J. Electric. Power Comp. Sys*, vol.36, no.1, pp.73–92, July 2008.

[71] O. Ojo, "The generalized discontinuous PWM scheme for three-phase voltage source inverters," *IEEE Trans. Ind. Electron*., vol. 51, no. 6, pp. 1280-1289, Dec. 2004.

[72] Y.X. Gao, and D. Sutanto, "A method of reducing harmonic contents for SPWM," in Proc. *IEEE Conf. Power Electron. Drive Systems*," vol.1, pp.150-160, Hong Kong, July 1999.

[73] B. Ismail, S. Taib, RM. Saad, M. Isa, and Hadzer, "Development of a single phase SPWM microcontroller-based inverter," in Proc. *IEEE Conf.1st Intl Power and Energy*, pp.423-430, Malaysia, November 2006.

[74] R. K. Saiju, and J. Krueger, "Dynamic analysis of start-up strategies of AC excited double fed induction machine for pumped storage power plant," in Proc.*13th Eur. Conf. Power Electron. Appl*., pp. 11-18, Spain, September 2009.

[75] Y.Pannatier, B.Kawkabani, C.Nicolet, A.Schwery, and J. Simond, "Optimization of the start-up time of a variable speed pump-turbine unit in pumping mode," in Proc. *20th Intl. Conf. on Electrical Machine*, pp. 2126 – 2132, France, September 2012.

[76] S. Karugaba and O. Ojo, "A carrier-based pwm modulation technique for balanced and unbalanced reference voltages in multiphase voltage-source inverters," *IEEE Trans. Ind. Appl*, vol. 48, no. 6, pp. 2102-2109, Nov.-Dec. 2012.

[77] RS. Kanchan, K. Gopakumar, and R. Kennel, "Synchronized carrier-based SVPWM signal generation scheme for the entire modulation range extending up to six-step mode using the sampled amplitudes of reference phase voltages," *IET Electric Power Appl*., vol.3, no.3, pp. 407-415, May 2007.

[78] AR. Beig, G. Narayanan, and VT. Ranganathan, "Modified SVPWM algorithm for three level VSI with synchronized and symmetrical waveforms," *IEEE Trans. Ind. Electron*., vol.54, no.1, pp.486–493, February 2007.

[79] K. Gupta, and AM. Khambadkone, "A space vector PWM scheme for multilevel inverters based on two level space vector PWM," *IEEE Trans. Ind. Electron*. vol.53, no. 5, pp.1631–1639, October 2006.

[80] V. S. S. P. K. Hari and G. Narayanan, "Space-vector-based hybrid pulse width modulation technique to reduce line current distortion in induction motor drives," *IET Power Electron*., vol. 5, no. 8, pp. 1463-1471, September 2012.

[81] H. Hu, W. Yao, and Z. Lu, "Design and implementation of three-level SVPWM IP core for FPGAs," *IEEE Trans. Power Electron*., vol.22, no.6, pp.2234–2244, November 2007.

[82] D. Zhao, V. S. S. P. K. Hari, G. Narayanan and R. Ayyanar, "Space-vector-based hybrid pulse width modulation techniques for reduced harmonic distortion and switching loss," *IEEE Trans. Power Electron*., vol. 25, no. 3, pp. 760-774, March 2010.

[83] HS. Patel, and RG. Hoft, "Generalized harmonic elimination and voltage control in thyristor converters: part I – harmonic elimination," *IEEE Trans. Ind. Appl*., vol. 9, no.3, pp.310–317, May 1973.

[84] C. Buccella, C. Cecati, M. G. Simoroni, G. K. Kulothungan, A. Edpuganti, and A. K. Rathore, " A selective harmonic elimination method for five-level converters for distributed generation," *IEEE J. Emerg. Select Topic. Power Electron.*, vol 5, no 2, June2017, pp. 775-783.

[85] D. Ahmadi, K. Zou, C. Li, Y. Huang, and J. Wang, "A universal selective harmonic elimination method for high-power inverters," *IEEE Trans. Power Electron*., vol. 26, no. 10, pp. 2743-2752, August 2011.

[86] L. Li, D. Czarkowski, Y.Liu, and P. Pillay, "Multilevel selective harmonic elimination PWM in series connected voltage inverters," *IEEE Trans. Ind. Appl*., vol. 36, no. 1, pp. 160–170, February 2000.

[87] L. Matakas, and E. Masada, "Analysis of the parallel connection of 3-phase VSC converters," in Proc. *Intl. Conf. Power Electron*., pp. 854-859, Yokohama, July 1995.

[88] J Hou, Q Chen, S.C. Wong, C. K. Tse, and X. Ruan, "Analysis and control of series/series-parallel compensated resonant converter for contactless power transfer," *IEEE J. Emerg. Sel. Topics Power Electron*, vol. 3, no. 1, pp. 124-136, March 2015.

[89] O. V. Kulkarni, S. Doolla and B. G. Fernandes, " Mode transition control strategy for multiple inverter based distributed generators operating in grid-connected and standalone" *IEEE Trans. Ind. Appl*, Vol. 53(6), pp. 5927-5939, Nov/Dec 2017.

[90] Seethalekshmi K., S.N Singh and S.C Srivastava, "An adaptive scheme for minimal load shedding utilizing synchrophasor measurements to ensure frequency and voltage stability", *Electric Power Components and Systems*, Vol. 38, No. 11, pp. 1211 -1227, August 2010.

[91] J. S. S. Prasad, R. Ghosh and G. Narayanan, "Common-mode injection pwm for parallel converters, "*IEEE Trans. Ind. Electron.*, vol. 62, no. 2, pp. 789-794, Feb. 2015.

[92] Ingalalli, H. Satheesh and M. Kande, "Platform for hardware in loop simulation," in Proc. *IEEE Conf. on Power Electronics, Electrical Drives, Automation and Motion (SPEEDAM),* pp. 41-46, Anacapri, 2016.

[93] R. Gore, H. Satheesh and M. Kande, "Platform analysis in embedded systems," in Proc. *IEEE Conf. Emerging Technology Trends in Electronics, Communication and Networking*, pp. 1-6 Surat, 2014.

[94] CK. Sao, and PW. Peter, "Control and power management of converter fed micro grids," *IEEE Trans. on Power Sys.*, vol. 23, no. 3, pp,1088–1098, July 2008.

[95] Varghese, H. Satheesh, S. Valsan and G. Sekharan, "Performance analysis of Zigbee for energy transmission monitoring in smart grids," in Proc. *IEEE Conf. on Computing and Network Communications* (CoCoNet), pp. 85-89, Trivandrum, 2015.

[96] R. Majumder, B. Chaudhuri, A. Ghosh, G. Ledwich, and F. Zare, "Improvement of stability and load sharing in an autonomous Microgrid using supplementary droop control loop," *IEEE Trans. Power Sys*, vol. 25, no. 2, pp.796- 808, March 2010.

[97] T. S. Sreeram, D. K. Dheer, S. Doolla, and S. Singh, "Hopf bifurcation analysis in droop controlled islanded microgrids" *Intl. J. Electric. Power and energy Systems, Elsevier*, Vol 90, pp. 208-224, Sep 201.

[98] D. K. Dheer, S. Doolla, S. Bandyopadhyay, and J. M. Guerrero, "Effect of placement of droop based generators in distribution network on small signal stability margin and network loss" *Intl. J. of Electric. Power and Energy Sys, Elsevier,* Vol 88, June 2017, pp. 108-118.

[99] S. Augustine, M.K. Mishra, and N. Lakshminarasamma, "Adaptive droop control strategy for load sharing and circulating current minimization in low-voltage standalone dc microgrid," *IEEE Trans. on Sustain. Energy*, vol.6, no. 1, pp.132 – 141, January 2015.

[100] N. Soni, S. Doolla and M. C. Chandorkar, "Analysis of frequency transients in isolated micro grids", *IEEE Trans. Ind. Appl*, Vol 53(6), pp. 5940-5951, Nov/Dec 2017.

[101] J.C. Vasquez, J.M. Guerrero, and A. Luna, "Adaptive droop control applied to voltage-source inverters operating in grid-connected and islanded modes," *IEEE Trans. on Ind. Electron*., vol.56, no.10, pp.4088-4096, October 2009.

[102] D. K. Dheer, O. V. Kulkarni, S. Doolla and A. K. Rathore, "Effect of reconfiguration and mesh on small signal stability margin of a droop-based islanded microgrid" *IEEE Trans. Ind. Appl*., (Accepted)

[103] H. S. V. S. Kumar Nunna and S. Doolla, "Energy management in microgrids using demand response and distributed storage- a multi-agent approach", *IEEE Trans. on Power Delivery*, Vol. 28(2), pp. 939-947, April 2013.

[104] B. Ehrman, "Passive current sharing boosts power and reliability," *Power Electron. Tech. Magazine*, pp.58-59, January 2005.

[105] B. Telles, A.L. Guilherme, T. Bauer, and I. Barbi. "A control strategy for parallel operation of single-phase voltage source inverters: analysis, design and experimental results," *IEEE Trans. Ind. Electron*., vol.60, no. 6, pp.2194–2204, June 2013.

[106] Kanthaphayao, Y. Kamnarn, U. Chunkag, and Viboon, "Redundant operation of a parallel ac to dc converter via a serial communication bus," *J. of Power Electron*., vol.11, no. 4, pp.533-541, July 2011.

[107] J.F.Chen, C.L. Chu, and Y.C. Liou, "Modular parallel three-phase inverter system," in Proc. *IEEE Intl. Symp. Ind. Electron.*, vol.1, pp.237-242, July 1995.

[108] T.F. Wu, K. Siri, and C.Q. Lee, "Reliability improvement in parallel connected converter systems," in Proc. *Conf. Ind. Electron. Control and Instrumentation*, vol.1, pp. 429 – 434, Kobe, November 1991.

[109] T.-F. Wu, Y.-H. Huang, Y.-K. Chen, and Z.R. Liu, "A 3C strategy for multi-module inverters in parallel operation to achieve an equal current distribution," in Proc. *IEEE Conf. Power Electron. Specialists*, vol.1, pp.186-192, Fukuoka, May 1998.

[110] W. Tsai-Fu, and C. Yu-Kai, "3C strategy for inverters in parallel operation achieving an equal current distribution," *IEEE Trans. Ind. Electron*., vol.7, no. 2, pp.273–281, April 2000.

[111] X. Sun, YS. Lee, and D. Xu, "Modelling, analysis, and implementation of parallel multi-inverter system with instantaneous average-current-sharing scheme," *IEEE Trans. Power Electron*., vol.18, no. 3, pp.844-856, May 2003.

[112] R. Gore, H. Satheesh, M. Varier and S. Valsan, "Analysis of an IEC 61850 based electric substation communication architecture," in Proc. *IEEE Conf. Intelligent Systems, Modelling and Simulation (ISMS)*, pp. 388-393, Bangkok, 2016.

[113] W. Jiang, and B. Fahimi, "Active current sharing and source management in fuel cell battery hybrid power system," *IEEE Trans. Ind. Electron.* vol. 57, no. 2, pp. 752 - 761, February 2010.

[114] C.T. Pan, and Y.H. Liao, "Modeling and coordinate control of circulating currents in parallel three-phase boost rectifiers," *IEEE Trans. Ind. Electron*., vol. 54, no. 2, pp. 825- 838, April 2007.

[115] B. Chen, Y. Chen, C. Tian, J. Yuan, and X. Yao, "Analysis and suppression of circulating harmonic currents in a modular multilevel converter considering the impact of dead time," *IEEE Trans. Power Electron*., vol.30, no.7, pp. 3542-3552, July 2015.

[116] F. Wang, Y. Wang, Q. Gao, C. Wang, and Y. Liu, "A control strategy for suppressing circulating currents in parallel-connected PMSM drives with individual dc links," *IEEE Trans. Power Electron*., vol.31, no.2, pp. 1680-1691, February 2016.

[117] J. S. Siva Prasad and G. Narayanan, "Minimization of Grid Current Distortion in Parallel-Connected Converters Through Carrier Interleaving," *IEEE Trans. Ind. Electron*., vol. 61, no. 1, pp. 76-91, Jan. 2014.

[118] S.K Jain and S.N Singh, "Harmonics estimation in emerging power system: key issues and challenges", *Electric Power Systems Research*, Vol. 81, No. 9, pp. 1754-1766, September 2011.

[119] J.J. Verboomen, D.V. Hertem, P. H. Schavemaker, W. L. Kling, and R. Belmans, "Phase shifting transformers: principles and applications," in proc. *IEEE Intl. Conf. Future Power Sys*. pp 1-6, Amsterdam, November 2005.

[120] J.G. Boudrias, "Power factor correction and energy saving with proper transformer, phase shifting techniques and harmonic mitigation," in proc. *IEEE Intl. Conf. Large Engg. Sys. Power Engg*. pp. 98-101, Jordan, July 2004.

[121] K. Xing, F.C. Lee, D. Borojevic, Z. Ye, and S. Mazumder, "Interleaved PWM with discontinuous space-vector modulation," *IEEE Trans. Power Electron*., vol. 14, no. 5, pp.906-917, September 1999.

[122] Z. Ye, D. Boroyevich, J.Y. Choi, and F.C. Lee, "Control of circulating current in two parallel three-phase boost rectifiers," *IEEE Trans. Power Electron*., vol. 17, no. 5, pp.609-605, September 2002.

[123] C. Wen, J. Li, X. Zhu, and H. Xu, "Research on circulation of parallel three-phase converters in MW wind power system," *Workshop Power Electron. Intelligent Transportation Sys*, pp. 349-354, Guangzhou, August 2008.

[124] P.C. Tsai P, and L.Y. Hung, "Modelling and control of circulating currents for parallel three-phase boost rectifiers with different load sharing," *IEEE Trans. Ind. Electron*., vol.55, no. 7, pp.2776–2785, July 2008.

[125] Y. Song, and B. Wang, "Survey on reliability of power electronic systems," *IEEE Trans. Power Electron*., vol. 28, no. 1, pp.591-604, January 2013.

[126] R.R. Errabelli, and P. Mutschler, "Fault-tolerant voltage source inverter for permanent magnet drives," *IEEE Trans. Power Electron*., vol. 27, no. 2, pp. 500-508, February 2012.

[127] B. Lu, and S.K. Sharma, "A literature review of IGBT fault diagnostic and protection methods for power inverters," *IEEE Trans. Ind. Appl.*, vol. 45, no. 5, pp. 1770-1777, September 2009.

[128] H.H. Memon, and M.M. Alam, "Reliability, maintainability, availability and failure rate analysis of IGBT triggering system designed for marine environment," in Proc. *IEEE 13th Intl. Conf. Applied Sciences Tech*., pp.1-5, Bhurban, March 2016.

[129] P.W. Wheeler, J.C. Clare, L. de Lillo, K.J. Bradley, M. Aten, C. Whitley, and G. Towers, "A comparison of the reliability of a matrix converter and a controlled rectifier-inverter," in Proc. *IEEE Eur. Conf. Power Electron. Appl*., pp.1-7, Dresden, September 2005.

[130] Mitsubishi Electric Corporation, "Power module reliability: products- semiconductors," *Tech. Report*, pp. 1-13, 2013.

[131] S.A Yang, P.T. Bryant, A.D. Mawby, D. Xiang, L. Ran, and P. Tavner, "An industry-based survey of reliability in power electronic converters," *IEEE Trans. Power Electron*., vol. 25, no.3, pp. 2734-2752, November 2010.

[132] Central Electricity Authority of India, "Technical standards for connectivity to the grid – Hydropower plant," *CEA – Tech. Rep., India*- 2007.

[133] C. An, G. J. Lloyd, B. Smith, L. Zou, E. Girardot, A. Schwery, A. Wechsler, G. Perugini, and B. Kawkabani, "Design and testing of a new protection relay for variable speed DFI motor generators," in Proc. *12th IET Int. Conf. Developments in Power System Protection*, pp. 1-6, Denmark, April 2014.

[134] D. Dufournet, and R.W. Alexander, "Transient recovery voltage for high voltage circuit breakers," *Tech. Rep*. pp- 1-41, 2013.

[135] D.L. Swindler, P. Schwartz, P.S. Hamer, and S.R. Lambert, "Transient recovery voltage considerations in the application of medium-voltage circuit breakers," *IEEE Trans. Ind. Appl.*, vol.33, no.2, pp.383-388, March 1997.

[136] IEEE application guide for transient recovery voltage for AC high-voltage circuit breakers, *IEEE Std C37.011-2005*, vol.1, no.1, pp. 01-62, 2006.

[137] D. Braun, and G. Koeppl, "Transient recovery voltages during the switching under out-of-phase conditions," in Proc. *IEEE Intl. Conf. Power Sys. Transients*, pp.1-5, USA, September 2003.

[138] D. Dufournet, "Transient recovery voltages for high-voltage circuit breakers – Part 1," *Alstom Grid – Tech. Rep*. , pp. 1- 186, San Antnoia, USA, Sep 2013.

[139] K. Kadriu, A. Gashi, I. Gashi, A. Hamiti, and G. Kabashi, "Influence of dc component during inadvertent operation of the high voltage generator circuit breaker during mis-synchronization," *J. Energy and Power Engg.*, vol. 5, pp. 225-235, March 2013.

[140] IEEE standard for ac high-voltage generator circuit - breaker rated on a symmetrical current basis, revision of *IEEE Std. C37.013-1993*.

[141] J. Machowski, J. W. Bialek, and J. R.Bumby, "Power system dynamics and stability," *2nd Edition, Jon Wiley & Sons Ltd*., Hoboken, 2008.

[142] N. Ahmed, S. Norrga, H. P. Nee, A. Haider, D. V. Hertem, L. Zhang, and L. Harnefors, "HVDC super grids with modular multilevel converters - the power transmission backbone of the future," in Proc. *Int. Conf. Syst., Signals Devices*, pp. 1–7, Germany, March 2012.

[143] J. Candelaria, J.D. Park, "VSC–HVDC system protection: A review of current methods," in Proc. *IEEE Power Syst. Conf. Expo*., pp. 1–7, USA, March 2011.

[144] C. Franck, "HVDC circuit breakers: are view identifying future research needs," *IEEE Trans. Power Del*., vol. 26, no. 2, pp. 998–1007, April 2011.

[145] O. Noureldeen, "Behavior of DFIG wind turbines with crowbar protection under short circuit," *Intl. J. Electric. Comp. Sciences*, vol. 12, no. 3, pp. 32-37, June 2012.

[146] J.H. Liu, C.C. Chu, and Y.Z. Lin, "Applications of nonlinear control for fault ride-through enhancement of doubly fed induction generators," *IEEE J. Emerg. Sel. Topics Power Electron*, vol. 2, no. 4, pp. 749-763, December 2014.

[147] G. Pannell, D. Atkinson, and B. Zahawi, "Minimum-threshold crowbar for a fault-ride-through grid-code-compliant DFIG wind turbine," *IEEE Trans. Energy Convers*, vol.25, pp.750-759, September 2010.

[148] M. M. Baggu, B. H. Chowdhury, and J. W. Kimball, "Comparison of advanced control techniques for grid side converter of doubly-fed induction generator back-to-back converters to improve power quality performance during unbalanced voltage dips," *IEEE J. Emerg. Sel. Topics Power Electron*, vol.3, no.2, pp. 516-524, June 2015.

[149] S. R. Kalantarian, and H. Heydari, "A new crowbar protection method for improvement in performance of doubly fed induction generator under fault conditions," in Proc. *IEEE Intl. Conf. Environment and Electric.* Eng., pp. 1-4, Rome, May 2011.

[150] R. Zhu, Z. Chen, Y. Tang, F. Deng, and X. Wu, "Dual-loop control strategy for DFIG-based wind turbines under grid voltage disturbances," *IEEE Trans. Power Electron*., vol. 31, no. 3, pp. 2239-2253, March 2016.

[151] R. Maheshwari, G. Gohil, L. Bede, and S. Munk-Nielsen, "Analysis and modelling of circulating current in two parallel-connected inverters," *IET Power Electron*, vol. 8, no. 7, pp. 1273–1283, July 2015.

[152] M.H. Ravanji, N.A. Ashtiani, M. Parniani, and H. Mokhtari, "Modeling and control of zero-sequence circulating current in parallel converters with space vector modulation," *IEEE J. Emerg. Sel. Topics Power Electron*, vol. 5, no. 1, March 2017.

[153] M. Bruns, B. Rabelo, and W. Hofmann, "Investigation of doubly-fed induction generator drives behavior at synchronous operating point in wind turbines," in Proc. *13th Eur. Conf. Power Electron. Appl*. pp. 1-10, Spain, September 2009.

[154] L. Wei, J. McGuire, and R. A. Lukaszewski, "Analysis of PWM frequency control to improve the lifetime of PWM inverter," *IEEE Trans. Ind. Appl*., vol. 47, no. 2, pp. 922-929, April 2011.

[155] M. Z. Sujod, I. Erlich, and S. Engelhardt, "Improving the reactive power capability of the DFIG-based wind turbine during operation around the synchronous speed," *IEEE Trans. Energy Convers*., vol. 28, no. 3, pp. 736-745, September 2013.

[156] ABB: HVDC Fundamentals tutorial, Mar 2013, Available: *http://www.ercot.com/ meetings/rpg-crez/keydocs/2007/RPG CREZ 20071008/HVDC.pdf.*

[157] V. Yaramasu, B. Wu, P.C. Sen, S. Kouro, and M. Narimani, "High-power wind energy conversion Systems: State-of-the-art and emerging technologies," *Proc. IEEE*, vol. 103, no. 5, pp. 740-788, May 2015.

[158] N. K. Swami Naidu and B. Singh, "Sensorless control of single voltage source converter-based doubly fed induction generator for variable speed wind energy conversion system," *IET Power Electron*., vol. 7, no. 12, pp. 2996-3006, 12 2014.

[159] F. Blaabjerg, and K. Ma, "Future on power electronics for wind turbine systems," *IEEE J. Emerg. Sel. Topics Power Electron*. vol. 1, no.3, pp. 139-152, September 2013.

[160] Energy efficiency in energy & environment, "National energy policy", *IEEE-USA*, 2011.

[161] B. K. Bose, "Global energy scenario and impact of power electronics in 21st century," in *IEEE Trans. on Ind. Electron*., vol. 60, no. 7, pp. 2638-2651, July 2013.

[162] S.S. Williamson, F. Musavi, and A. K. Rathore, "Industrial electronics for electric transportation: current state-of-the-art and future challenges," *IEEE Trans. Ind. Electron*., vol. 62, no. 5, pp. 3021-3032, May 2015.

[163] Todayoshi Mukai, Izumi Otsu, and Akira Yoshino, Seto," Induction Motor Control System", *Matsushita Electric Works Ltd, U.S. Patent: 5010287*, Apr.23, 1991.

[164] R. Rajasingh, T.R.Chelliah, "Energy saving start-up strategy of pumped storage power plant equipped with doubly-fed asynchronous machine", *IEEE Intl. Conf. Power Electronics, Intelligent Control and Energy Systems (ICPEICES)*, pp 1-6, New Delhi, June 2016.

[165] K. Xie, Z. Jiang, and W. Li, "Effect of Wind Speed on Wind Turbine Power Converter Reliability", *IEEE Trans. Energy Convers*, vol. 27, no. 1, March 2012

[166] J Carroll J, A McDonald, and D McMillan, "Failure Rate, Repair Time and Unscheduled O&M Cost Analysis of Offshore Wind Turbines", *Wind Energy*, vol.19,no.6, pp.1107-1119, June 2016

[167] J. S. Lee, K.B. Lee, and F. Blaabjerg, "Open-switch fault detection method of a back-to-back converter using NPC topology for wind turbine systems," *IEEE Trans. Ind. Appl.*, vol. 51, no. 1, pp. 325-335, February 2015.

[168] D.G. Giaourakis, and A.N. Safacas, "Effect of short-circuit faults in the back-to-back power electronic converter and rotor terminals on the operational behavior of the doubly-fed induction generator wind energy conversion system," *J. Machines*, vol.5, no.1, pp. 1-26, February 2015.

[169] Z. Yang, and Y. Chai," A survey of fault diagnosis for onshore grid connected converter in wind energy conversion systems" *J. Renew. Sustain Energy Rev*, vol.66, pp. 345-359, December 2016.

[170] T. A. Najafabadi, F. R. Salmasi, and P. J.Maralani, "Detection and isolation of speed-, DC-link voltage-, and current-sensor faults based on an adaptive observer in induction-motor drives," *IEEE Trans. Ind. Electron*., vol. 58, no. 5, pp. 1662-1672, May 2011.

[171] B. Akin, S. Choi, U. Orguner and H. A. Toliyat, "A simple real-time fault signature monitoring tool for motor-drive-embedded fault diagnosis systems," *IEEE Trans. Ind. Electron*., vol. 58, no. 5, pp. 1990-2001, May 2011.

[172] S. Choi, B. Akin, M. M. Rahimian and H. A. Toliyat, "Implementation of a fault-diagnosis algorithm for induction machines based on advanced digital-signal-processing techniques," *IEEE Trans. Ind. Electron*. vol. 58, no. 3, pp. 937-948, March 2011.

[173] C. Chakraborty, and V. Verma, "Speed and current sensor fault detection and isolation technique for induction motor drive using axes transformation," *IEEE Trans. Ind. Electron*., vol. 62, no. 3, pp. 1943-1954, March 2015.

[174] A. Gaillard, S. Karimi, P. Poure, S. Saadate and E. Gholipour, "A fault tolerant converter topology for wind energy conversion system with doubly fed induction generator", In Proc. *IEEE European Conf. on Power Electron and Appl*, pp. 1-6, Sep. 2007.

[175] B. Lu and S. K. Sharma, "A literature review of IGBT fault diagnostic and protection methods for power inverter," *IEEE Trans. Ind. Appl*., vol. 45, no. 5, pp. 1770–1777, Sep./Oct. 2009.

[176] W. Yang, P. J. Tavner and M. R. Wilkinson, "Condition monitoring and fault diagnosis of a wind turbine synchronous generator drive train", *IET Renewable Power Generation*, vol. 3, no. 1, pp. 1-11, Mar. 2009.

[177] Jorge O. Estima and Antonio J. Marques Cardoso, "A new approach for real-time multiple open-circuit fault diagnosis in voltage-source inverters", *IEEE Trans. Ind. Appl*., vol. 47, no. 6, pp. 2487-2484, December 2011.

[178] Nuno M. A. Freire, Jorge O. Estima, and António J. Marques Cardoso, "Open-circuit fault diagnosis in PMSG drives for wind turbine applications", *IEEE Trans. Ind. Electron*., vol. 60, no. 9, pp. 3957-3967, September 2013.

[179] W. Sleszynski, J. Nieznanski and A. Cichowski, "Open-transistor fault diagnostics in voltage-source inverters by analyzing the load currents", *IEEE Trans. Ind. Electron*., vol. 56, pp. 4681-4688, Nov. 2009.

[180] S. Nandi, H. A. Toliyat and X. Li, "Condition monitoring and fault diagnosis of electrical motors-a review," *IEEE Trans. Ener. Convers*. vol. 20, no. 4, pp. 719-729, Dec. 2005.

[181] W. Zhang, D. Xu, P.N. Enjeti, H. Li, J. T. Hawke, and H.S. Krishnamoorthy, "Survey on fault-tolerant techniques for power electronic converters", *IEEE Trans. on Power Electron*., vol. 29, no.12, pp. 6319-6331, December 2014.

[182] A. Karthikeyan, C. Nagamani, A. B. Ray Chaudhury, and G. S. Ilango, "Implicit position and speed estimation algorithm without the flux computation for the rotor side control of doubly fed induction motor drive," *IET Electric Power Appl*., vol. 6, no. 4, pp.243 – 252, April 2012.

[183] J. Guzinski, H. Abu-Rub and H. A. Toliyat, "An advanced low-cost sensor less induction motor drive," *IEEE Trans. Ind. Appl*., vol. 39, no. 6, pp. 1757-1764, Nov.-Dec. 2003.

[184] Radha Thangaraj, Thangaraj Chelliah, Millie Pant, Ajith Abraham and Crina Grosan, "Optimal gain-tuning of pi speed controller in induction motor drives using particle swarm optimization", *The Logic Journal, Oxford University Press*, UK, 19(2): 343-356, 2011.

[185] Thanga Raj, Radha Thangaraj, Millie Pant, Pascal Bouvry and Ajith Abraham, "Design optimization of induction motors with differential evolution algorithms with an application in textile spinning," *J. of Applied Artificial Intelligence, Taylor and Francis*, 26(9), pp. 809-831, September 2012.

[186] Radha Thangaraj, Thanga Raj Chelliah, Pascal Bouvry, Millie Pant and Ajith Abraham , "Optimal design of induction motor for a spinning machine using population based metaheuristics" , in Proc *IEEE Intl. Conf. on Computer Information Systems and Industrial Management Applications (CISIM 2010),* pp. 341-346, 2010.

[187] S. Owais, V. Snasel, P. Kromer and A. Abraham, "Survey: using genetic algorithm approach in intrusion detection systems techniques," in Proc. *IEEE 7th Computer Information Systems and Industrial Management Applications*, pp. 300-307, Ostrava, 2008.

[188] Ajith Abraham and Baikunth Nath, "Connectionist models for intelligent reactive power control, "In Proc. *The Australasian MATLAB Users Conference 2000*, Published by Ceanet Pty Ltd, Australia, 2000.

[189] Allen Bradley, "Power flex adjustable frequency ac drive", *Rockwell Automation Publication* 20A-UM001O-EN-P, pp.1-126, July 2014.

[190] A. Banerjee, M. S. Tomovich, S. B. Leeb, and J. L. Kirtley, Jr., "Power converter sizing for a switched doubly fed machine propulsion drive," *IEEE Trans. Ind. Appl*., vol. 51, no. 1, pp. 248–258, Jan./Feb. 2015.

[191] Arijit Banerjee, Michael S. Tomovich, Steven B. Leeb, James L. Kirtley, "Control Architecture for a Switched Doubly Fed Machine Propulsion Drive", *IEEE Trans. Ind. Appl*., vol. 51, no. 2, pp. 1538–1550, Mar/ April. 2015.

[192] B. C. Rabelo, W. Hofmann, J. L. da Silva, R. G. de Oliveira and S. R. Silva, "Reactive power control design in doubly fed induction generators for wind turbines," *IEEE Trans. Ind. Electron*., vol. 56, no. 10, pp. 4154-4162, Oct. 2009.

[193] A. M. Bazzi, A. D. Garcia, and P.T. Krein, "Markov reliability modeling for induction motor drives under field-oriented control", *IEEE Trans. Power Electron*., vol. 27, no. 2, pp.534-546, February 2012.

[194] C. Carunaiselvane, and T. R. Chelliah, "Present trends and future prospects of asynchronous machines in renewable energy systems," *J. Renew. Sustain Energy Rev,* vol.74, pp: 1028-1041, July 2017.

[195] C. Sankaran, "Power Quality," *CRC Press LLC*, USA, 2002.

[196] S.K Parida, S.N Singh and SC Srivastava, "A review on reactive power management in electricity markets," *International Journal of Energy Sector Management*, Vol. 5, No.2, pp. 201 – 214, August 2011.

[197] R. Niwas and B. Singh, "Solid-state control for reactive power compensation and power quality improvement of wound field synchronous generator-based diesel generator sets," *IET Electric Power Appl.*, vol. 9, no. 6, pp. 397-404, 7 2015.

[198] Sangshin Kwak and H. A. Toliyat, "Design and rating comparisons of PWM voltage source rectifiers and active power filters for AC drives with unity power factor," *IEEE Trans. Power Electron*., vol. 20, no. 5, pp. 1133-1142, Sept. 2005.

[199] Sercan Teleke, Tarik Abdulahovic, TorbjÖrn Thiringer, and Jan Svensson, "Dynamic Performance Comparison of Synchronous Condenser and SVC", *IEEE Trans. on Power Delivery*, vol.23, no.3, pp.1606-1612, 2008.

[200] A C Ferreira, L M Souza, and E H Watanabe, "Improving power quality with a variable speed synchronous condenser", in proc. *IEEE Intl. Conf. Power Electron. Machines & Drives*, pp. 456-461, 2002.

[201] A C Ferreira, L M de Souza, and E H. Watanabe, "Variable speed synchronous condenser using doubly-fed induction machine", *Revista Controle & Automation*, vol.15, no.2, pp.172- 180,June 2004.

This Page is Intentionally Left Blank

Hill Curve: This curve is plotted between input power (p.u) vs peripheral velocity factor (p.u). For variable speed operation, various efficiency points can be obtained corresponding to the input power and peripheral velocity factor. The peripheral velocity factor for Francis turbine can be obtained as follows.

Peripheral velocity factor = $N*D/(H)^{1/2}$

where,

N= Synchronous speed

D= Diameter of the turbine

H= Pumping head

Fig.A1 shows the variable nature of efficient point with respect to variable peripheral velocity factor. Hence, pump efficiency can be optimized in accordance with available surplus power in the grid and water level availability in the dam.

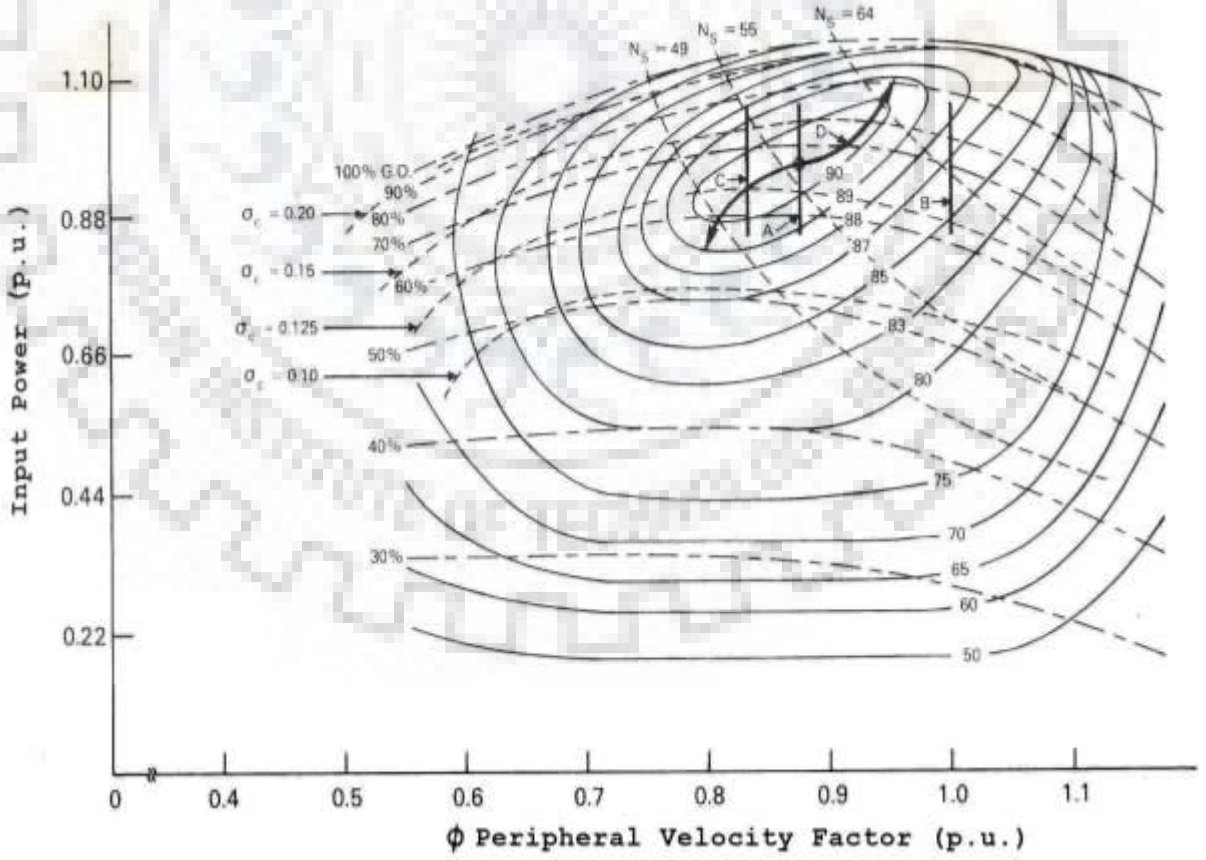

Fig. A1. Hill curve (unit dimension Francis model turbine)